School of Chemical and Petroleum Engineering

Department of Petroleum Engineering

Sub-Sea Gas Processing

David William Parks

This thesis is presented for the Degree of

Doctor of Philosophy

of

Curtin University

July 2011

Declaration

This thesis contains no material, which has been accepted for the award of any other degree or diploma in any university

To the best of my knowledge and belief, this thesis contains no material previously published by other person except where due acknowledgement has been made.

Signature ……..

Date ……

Abstract

To meet the demands of deeper and more remote reservoirs, subsea processing has been poised as one of the most potentially promising technology developments in the offshore development.

Natural Gas usually contains significant quantities of water vapour, which must be removed for gas processing and transmission. A pipeline transporting natural gas at a pressure of 10 Mega Pascals at equilibrium with seawater at 4 C must have water content lower than around 144 parts per million (by volume) to ensure water will not condense within the pipeline. Failure to sufficiently reduce the water content can lead to condensation of liquid water and the formation and accumulation of gas hydrates into pipe blocking plugs. This is particularly important for subsea pipelines with the high pressure and low temperatures conditions that exposes the gas to hydrate formation conditions.

This research investigates a novel dehydration solution that is applicable for subsea installation. The technique is based on technology that was trialled in an above ground implementation by Cool Energy with significant system modifications to make it applicable to a subsea environment. The ultimate objective of this research is to develop a sea bed dehydration solution that will reduce the water content of the gas to pipeline quality standard.

The solution utilises the concepts of gas cooling through expansion and the controlled formation and management of gas hydrates to reduce the water content of a saturated gas stream to levels suitable for gas transport in subsea pipelines. A pilot plant was implemented to test the solution design at pressures up to 10 Mega Pascals and flow rates of 35 standard cubic meters per hour. The experiments successfully demonstrated gas dehydration to below -40 degrees C, performance that meets the pipeline water specification requirements for subsea transportation of natural gas.

This thesis presents the current status of implemented subsea technology, reviews current dehydration technologies and discusses their applicability to subsea implementation. It describes the iterative dehydration process development and presents the achieved dehydration results. A production scenario is defined and a modelled solution presented together with novel approaches in management of the system.

Acknowledgements

I should like to thank my supervisor, Professor Robert Amin for the opportunity to perform this research and for his assistance and guidance during the project.

The support and friendship provided by Dr David Pack was greatly appreciated, his constant guidance and willingness to act as a sounding board really made the studying a thoroughly enjoyable experience.

My thanks also go to the support staff at the Woodside Research Facility, in particular Saif Ghadbhan who helped out a lot in the lab while I was recovering from my back surgery and Dr Ahmed Barifcani for his support.

Without the support of my wife Terri and children Alex and William, the ability to dedicate my time to this endeavour would not have been possible, so my love and thanks to them.

Finally, I must also thank Woodside for providing the funding for the research project.

Table of Contents

List of Figures

List of Tables

List of symbols and abbreviations

Upper case letters

Symbol	Description	Units
A	Area	m^2
C_d	Drag coefficient	
C_{ml}	Longmuir constant	
C_p	Specific heat at constant pressure	J/(kg.K)
C_v	Specific heat at constant volume	J/(kg.K)
D	Diffusion coefficient	
D_H	Hydraulic diameter	m
E_{cv}	Energy of controlled volume	J
G	Gibbs energy per mol	J/mol
K	Souders Brown coefficient	
L	Length	m
M	Mach number	
Nu	Nusselt number	
P	Pressure	Pa
P_{br}	Reduced normal boiling point pressure	
P_c	Critical pressure	Pa
P_m	Pressure	MPa
P_{pc}	Pseudo critical pressure	Pa
P_0	Atmospheric pressure	Pa
P_v	Vapour pressure	Pa
Pr	Prandtl number	
$\dot{Q}_{cv}$	Heat added to controlled volume	W
R	Universal gas constant	J/(mol.K)
R^*	Gas constant	J/(kg.K)
R_c	Cell cavity radius	m
Re	Reynolds number	
R_s	Droplet size ratio	
S	Super saturation	
T	Absolute temperature	K
T_{br}	Reduced normal boiling point temperature	
T_c	Critical temperature	K
T_{pc}	Pseudo critical temperature	K
T_r	Reduced temperature	
T_{st}	Steam point temperature	K

Symbol	Description	Units
T_0	Ice point temperature	K
U	Overall heat transfer coefficient	J/m^2.K.s
W_{xx}	Water content of component xx	
$\dot{W}_{cv}$	Work added to control volume	W
V	Velocity	m/s
Z	Compressibility factor	

Lower case letters

Symbol	Description	Units
a	Core radius	m
a_s	Speed of sound	m/s
$\dot{e}_{st}$	Saturation water pressure at steam point pressure	atm
$\dot{e}_{i0}$	Saturation water vapour pressure at ice point pressure	atm
f	Fugacity	Pa
g	Gravity	m/s^2
g_v	Gibbs energy per unit volume	J/m^3
h	Enthalpy	J/kg
h	Thermal convection coefficient	J/K.m^2.s
k	Boltzmann's constant	
k_x	Thermal conductivity coefficient of material x	J/K.m.s
$\dot{m}$	Rate of mass transfer	kg/s
n	Number of mols	
n_h	Hydration number	
p	Pressure	MPa
q	Heat flux	J/s
r	Radius	m
s	Entropy	J/K
t	Time	s
t_f	Temperature	F
v	Specific volume	m^3
x	Mole fraction in liquid phase	
y	Mole fraction in gas phase	
z	Height	m
z_c	Coordination number	

Greek Letters

Symbol	Description	Units
μ	Dynamic viscosity	Pa.s
μ_{jt}	Joule Thomson coefficient	K/MPa
μ_w	Chemical potential of water	J/mol
π	Pi	
α	Binary interaction parameter	
ε	Characteristic energy	J
σ	Surface tension	N/m
Φ	Fugacity coefficient	
ρ	Density	kg/m^3
ω	Acentric factor	
v	Kinematic viscosity	m^2/s
γ	Ratio of specific heats	
λ	Gas gravity	
θ	Contact angle	degrees

Abbreviations

ANSI	American national standards institute
BSP	British standard pipe
BTEX	Benzene, toluene, ethylbenzene, xylenes
DC	Direct current
DEG	Diethylene glycol
JT	Joule Thomson
LTS	Low temperature separation
MMSCFD	Million standard cubic feet per day
MSCFD	Thousand standard cubic feet per day
NPS	Nominal pipe size
NPT	National pipe thread
ppmv	Parts per million by volume
PREOS	Peng-Robinson equation of state
PVC	Polyvinyl chloride
TCF	Trillion cubic feet
TEG	Triethylene glycol
WA	Western Australia

1 Introduction to the Research

Of the Australian gas reserves estimated to be in the order of 90 TCF most located offshore in Western Australia's North West shelf some 70 TCF are in stranded resources[1]. Some experts estimate that worldwide stranded resources may exceed 4,000 TCF.[2]

With stranded gas fields the large capital and operating costs experienced with platform based processing solutions cannot be economically justified so to exploit these resources cheaper solutions such as subsea completions and processing will be required with pipelines utilised to transport the gas to shore or centralised platforms.

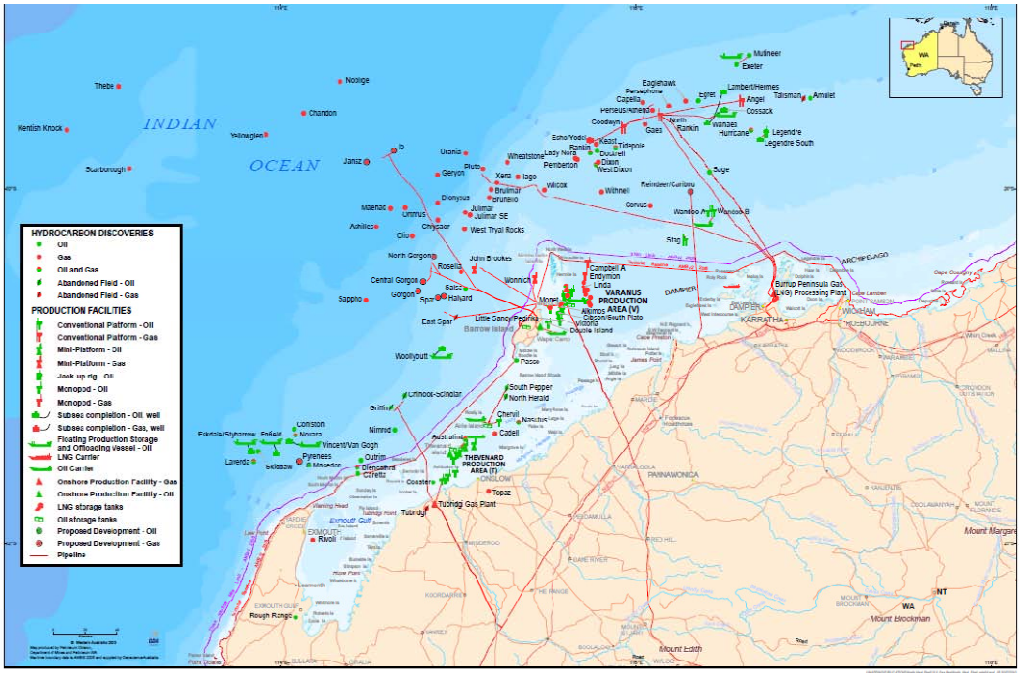

Figure 1-1 North West shelf gas resources

1.1 Subsea Gas Processing Systems

A typical gas production system comprises of a number of gas wells, a gas processing plant and duplicate transportation mechanisms between wells and processing plant and from processing plant to the end customers. The gas processing plant will accept the fluid stream from the well, separate the stream into gas, liquid hydrocarbon, effluent streams and condition the gas stream so that it is suitable for transport in pipelines.

The presence of liquid water in gas pipelines can cause blockages through the formation of gas clathrate and corrosion though formation of acids with acid gasses in the gas stream. To ensure efficient operation of pipelines the gas stream must have a moisture content low enough to ensure that condensation of liquid water will not occur at the operational conditions experienced by the pipeline.

Clathrate hydrates are crystalline structures consisting of a shell or cage made up of multiple water molecules surrounding a single guest gas molecule. Many natural gas components including Methane, Ethane and Propane can act as the host molecule and allow stable hydrates to form under suitable temperature and pressure conditions. Once formed hydrates can grow and accumulate, typically at low points of the pipeline, around valves and at bends, then aggregate to form an impervious plug which causes a pipeline to block. Pipe line blockages are difficult and expensive to remove and can be potentially dangerous.

Depending on the depth, subsea water temperatures experienced by gas pipelines can be below 4 C which at typical pipeline operating pressures is well within the hydrate formation region for both lean and rich natural gases. A typical profile of water temperature is shown in Figure 1-2.

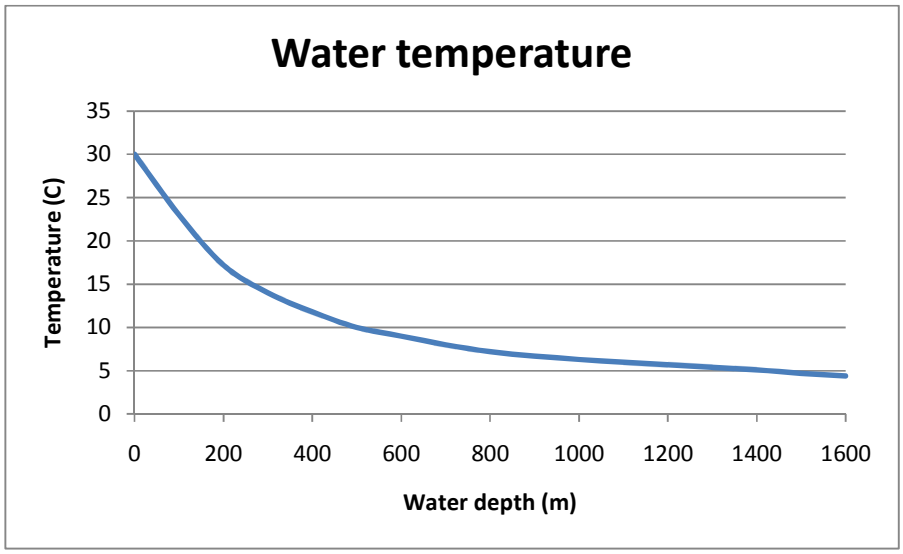

Figure 1-2 Typical seawater temperatures at different water depths[3]

Various techniques can be utilised to prevent the pipeline reaching hydrate formation conditions such as insulation, heating and burying of the pipeline. An alternative commonly used approach is lower the hydrate formation temperature through the injection of chemicals such as Methanol or Gylcol. These techniques however are expensive and an alternative potentially cheaper method to prevent hydrate formation is to reduce the dew point of the gas stream to a low level so that liquid water will not condense in the pipeline at the low subsea temperatures experienced.

The production stream from a gas well will typically consist of water saturated natural gas together with hydrocarbons and connate water and some fines from the producing formation. The temperature, pressure and composition of the production stream may vary from well to well depending on the producing formation, the size and depth of the reservoir, the production techniques and production history. This is typical of most oil fields but less so with

gas fields. A subsea gas processing system must be able to accept the variable production stream for the full lifecycle of the well.

Due to the remoteness of stranded reserves and the ocean depths encountered the costs and practical difficulties of interventional operations mean that subsea systems must have maximised reliability to minimise interventions and be designed to facilitate easy intervention when required.

The principle functions of a subsea system are to interface with a well bore, separate the various inlet stream components, condition and feed the gas stream to a gas pipeline and safely handle or dispose of the hydrocarbon and effluent streams. To achieve this functionality the following separate subsystems can be identified:

- Subsea completion of the wellhead
- Separation subsystem to separate the inlet stream into a gas stream, liquid hydrocarbon stream and effluent stream (connate water and formation fines/sand)
- Gas conditioning subsystem to dehydrate the gas stream from the separator subsystem to required pipeline conditions
- Power generation subsystem to generate sufficient power to operate the subsea system
- Disposal subsystem to provide an environmentally acceptable method of disposing of non-required well stream components
- System monitoring and control system to automatically manage and report subsea processing operations
- Subsea tiebacks from wellhead to processing system and from processing system to ground based facilities for further processing

The following subsections will provide a high level description of the subsystems required for a subsea gas production system, introduce the current development status and define the scope of this research to progress towards a practical subsea processing solution.

1.1.1 Subsea completions

A Subsea completion will include the fitting of a wet or dry subsea tree (commonly referred to as a Christmas tree) to the well on the sea floor. The tree includes various operational and safety valves and is controlled by an umbilical connected to the monitoring and control subsystem. Well fluids pass up the well bore, through a control choke in the tree and into a pipeline for transport to the proceeding system.

The controls for subsea trees may be manual via divers, hydraulic, electrical or a combination. An all electrical wet tree has been implemented in The Netherlands[4], a solution driven by direct current that requires no batteries or accumulators. The improved

reliability, controllability and speed of operations compared to previous electro/hydraulic solutions will be of significant benefit to remote deep sea installations.

Subsea completions have been used since 1961 and to date completions in water depths of over 3 km have been implemented in the Gulf of Mexico.[5]

1.1.2 Subsea separation

The first stage of a subsea processing system is the subsea separator whose purpose is to separate the constituent parts of the well stream for further processing downstream.

There are three physical principles used to achieve the physical separation of gas from liquids or solids, momentum, gravity settling, and coalescing. Different separator types use these principles to varying degrees with some such as hydro-cyclone separators primarily using momentum characteristics whilst others such as large tank separators rely primarily on gravity characteristics to cause phase separation.

The configuration of the separator will depend on the lifecycle characteristics of the well fluids and the intended handling of the effluent stream. In a well with low amounts of hydrocarbon fluid the separator may simply separate gas from liquid and dispose of any liquid hydrocarbons with the connate water. When economically significant quantities of hydrocarbon liquids are present in the well stream a three phase separator may be utilised allowing the hydrocarbon liquid to be captured and dealt with separately from the gas and water streams.

The outlet gas stream from the separator is saturated with water at the operating pressure and temperature conditions of the separator and may also include a small amount of water and hydrocarbon liquid carryover.

Subsea projects generally use gravity based separators and for gas projects a vertical separator will most likely be used. Vertical separators are considered easier to deploy in deep water.[6, 7]

Several subsea separator trials have been performed around the world, including the Pazflor project at 800 m depth in Angola[8] and the VASPS project at 400 m depth in Brazil[9, 10].

The first commercial scale subsea separation system was implemented in 2007 with a three-phase separator solution in 200 m of water at the Tordis field in the North Sea.[4, 6]

An extreme depth separation system is currently being implemented for the Perdido[11] project in the Gulf of Mexico with water depths of around 2,400 m. This uses a vertical Caisson separator to separate gas and liquid and an electrical submersible pump to boost the liquid pressure.

Figure 1-3 Tordis subsea separator[12]

Significant development in industry to improve subsea separation is being performed by a number of companies looking for more compact and efficient techniques, including inline separation using high G-forces, separation in pipe segments rather than large vessels and use of electrostatic coalescence.

1.1.3 Subsea power system

The power requirement of a subsea system varies significantly depending on the specifications of the system. Power is required for all subsea subsystems to monitor and control system operations. In many solutions, high power demands will be present when systems require pressure boosting through use of high power pumps for effluent disposal or boosting stream pressures to pipeline requirements.

Current subsea systems utilise umbilicals either to adjacent surface platform facilities or to shore for provision of power. Power losses experienced in long umbilicals limit the length that a subsea system can be separated from the surface power source. As the power requirements increase the maximum step out distance decreases. A 120 km long umbilical supplying 65 MW of power is currently being implemented for the Ormen Lange natural gas field off Norway.[6, 13]

Localised power generation has the potential to lower the high costs of high power umbilicals and major surface installations. Potential techniques for subsea power generation include exploiting subsea currents, utilising Stirling cycle engines or thermoelectric generators and the temperature differentials between well fluids and seawater, and Buoys with wind/wave power generation facilities.[14] Power generated by these techniques is relatively low,

sufficient to power control systems but unable to provide sufficient power to operate subsea compressors or pumps that typically require megawatts of power.

Small floating generator platforms have been studied and may offer a cost effective solution for powering remote subsea installations that require a few megawatts.[15]

1.1.4 Subsea disposal system

All well production streams contain some water and sand with oil wells typically producing significantly more water than gas wells. The separator will separate most of the water and sand from the gas and hydrocarbons streams and will pass it onto the disposal system that is responsible for disposing of it in an environmentally acceptable manner. The separated water will include some hydrocarbons in solution and in emulsion form. The levels of hydrocarbons that can be disposed of into the Ocean is controlled by International bodies with the most significant being the Oslo-Paris Commission (OSPAR) and the United States Environmental Protection Agency (USEPA)[16]. Australian regulatory requirements require the oil content to be below 50 mg/l and average below 30 mg/l over a 24 hour period.[17]

Of the produced water, ninety percent is reinjected into injection wells to enhance production by sustaining the formation pressure, seven percent is cleaned to the required standards and released into surface water and the balance is disposed of as waste.[18] Water is typically cleaned using gas flotation techniques or hydro-cyclones.[16]

In subsea systems water is typically disposed of in suitable subsurface formations. In some systems (e.g. Tordis project) the effluent water is pressure boosted and reinjected into the producing formation. In other projects the water is injected into a lower pressure formation alleviating the requirement to boost the pressure of the effluent stream.

Alternative methods for subsea disposal of produced water have been studied, including the water treatment system proposed by Nazhat at the Woodside Research Facility of Curtin University[19]. This system proposes to use large floating gravity separation system to separate hydrocarbon residues from the water at atmospheric conditions, disposing of the cleaned water in the ocean and the hydrocarbons through evaporation to the atmosphere and physical collection. The laboratory experiments performed suggest that the approach has merit when the amount of water to be disposed off is relatively small and is unlikely to be appropriate for disposing of bulk water from a separator. It may however be an appropriate method to support a processing system downstream of the separator, where the water quantity to be handled is smaller and reinjection techniques are inappropriate.

Sand typically collects in the bottom of the separator and is periodically removed, either manually with a shovel or automatically with built in water jets. The removed sand is oil-contaminated and unsuitable for dumping at sea.[20] In most platform based operations the sand once removed from the separator is shipped to land for processing and disposal. In

subsea projects the sand is removed automatically from the separator and either sent with the fluid stream to the surface for treatment, e.g. Pazflor project or is reinjected with the effluent water stream e.g. Tordis project.

1.1.5 Subsea control system

A subsea control system monitors the operational status and controls the operation of a subsea production system. Correct operation of the control system is critical to ensure safe and reliable operations.[21]

A typical platform based control system comprises topside control equipment, subsea control equipment and an umbilical to connect the topside and subsea components. Topside equipment may include electronic and hydraulic power units and a well control panel. Subsea equipment controls the operation of the production and safety valves and chokes on the wellhead (tree and down-hole) and may be operated hydraulically or electro-hydraulically. The umbilical provides the connections for hydraulic power and electronic control signals as required by the implemented configuration. The length of the required umbilical limits the type of control system that can be implemented. With hydraulic systems the lag time from the surface command to the subsea valve operation is affected by the pressurisation of the hydraulic fluid. A lag time of 8 minutes is typical of a 10 km umbilical. In an electro-hydraulic system the umbilical carries electrical signals from the surface control system to the subsea system to command the control systems, so the delay experienced with hydraulic systems is alleviated and longer umbilicals can be implemented. Electro-hydraulic systems tend to be less field-serviceable and more costly than hydraulic systems but the benefits of faster operations, better control, ability to monitor operations and smaller umbilicals have made this today's preferred solution.

The current development trend for subsea control is to remove the need for umbilicals and topside equipment by placing more of the system on the seabed. Two systems that have been developed are the Subsea Powered Autonomous Remote Control System (SPARCS) and the Integrated Control Buoy.

The SPAR[22] solution includes subsea power generation using turbines on the well injection stream or thermo-generators on the well production stream together with subsea hydraulic power generation, control circuits and communications to a surface unit via an acoustic transponder. The SPARCS system was trialled in 1998 and further systems were proposed, such as APAC[23]. Today there is little ongoing development or implementation of self-powered wellhead systems.[24]

The Integrated Control Buoy[25] solution installs all control and monitoring equipment in a small 6m diameter, 6m high buoy immediately above the wellhead and uses a short vertical hydraulic and signal riser to connect to the subsea tree. Electrical and hydraulic power is

generated within the buoy, thereby requiring periodic resupply of fuel (annual). The control systems in the buoy are supervised via a radio link by a master control system on a remote platform or production facility. This solution also has the ability to provide a level of chemical injection to the production line.

In 1996, the East Spar gas and condensate field in Western Australia came into production without an umbilical, using a control buoy connected by radio to the Varanus Island processing facility, 63 km away.[24, 26]

Umbilicals can provide control communications using dedicated control wires within the umbilical construction. Other techniques that are used include “Signal on Power” and Fibre optic connections.

1.1.6 Subsea tiebacks

Subsea tiebacks are used to connect wells to existing platform based or onshore production facilities and are critically required to make stranded fields economically viable. They typically consist of the pipelines for production fluids and an umbilical that provides power and control cables for subsea operational processes and may also include flow lines for chemical injection purposes.[27] Distances of over 100 km have been covered by subsea tiebacks.

As subsea projects get deeper and tiebacks get longer the temperature of gas in gas pipelines will cool to the seabed temperature which at depth can be between 4 and 7 C.[27] With typical pipeline gas pipeline pressures of between 9 and 14 MPa the natural gas falls well within the hydrate formation region as illustrated in Figure 1-4.

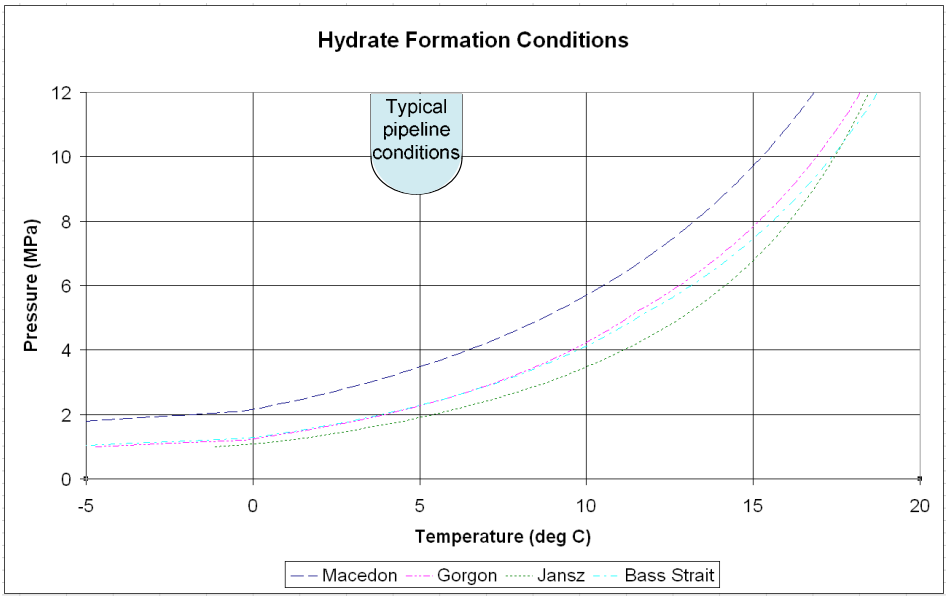

Figure 1-4 Hydrate formation curves vs. subsea gas pipeline conditions[28]

Under these pressure and temperature conditions and the presence of liquid water, gas hydrates may form, accumulate at low lying points and produce hydrate plugs that can completely block the pipeline. The safety and cost implications of hydrate pipe blockage and its removal are significant[29], so pipeline operations must be designed to ensure that this situation is prevented.

1.2 Pipeline hydrate prevention

Various methods can be used to prevent hydrates forming in pipelines. These include:

- Ensuring that the gas never reaches the hydrate formation conditions by:
  - Insulation of pipelines
  - Pipe in Pipe construction
  - Burying pipelines
  - Heating pipelines
- Changing the hydrate thermodynamic or formation characteristics of the gas by injection of kinetic and thermodynamic inhibitors or anti-agglomerates
- Removal of water from pipeline by:
  - Round trip pigging to remove water and hydrate build up
  - Subsea separation and dehydration.

Piping design and installation techniques tend to be very expensive particularly with long tiebacks.

Thermodynamic modification techniques are commonly used in systems with local platforms where storage and injection of chemicals is relatively straight forward. Long tie-back projects, such as the Dolphin gas project in the Middle East[30] utilise the umbilical to transport chemicals for injection in the pipeline. The purchase, handling and recycling costs of using chemicals can be significant particularly when significant quantities of chemicals are required. For stranded fields the additional capital costs in additional umbilical complexity and subsea injection pumps must also be considered.

Round trip pigging for stranded fields will typically require looped flow-lines meaning a doubling up of the pipeline length which at long offsets makes the cost prohibitive. The speed of pig travel is also such that time to perform a long loop, when production is typically stopped is excessively long.

Subsea separation as discussed in section 1.1.2 removes most of the free water from the gas but leaves the gas saturated at the exit conditions of the separator. As the temperature

in the pipeline drops liquid water will condense from the gas. Consequently separation alone is not sufficient to prevent down-pipe hydrate formation to occur. Performing dehydration of the gas stream to a dewpoint below the temperature conditions encountered in the pipeline will prevent the condensation of water in the pipeline and has the potential to be an efficient and cost effective method of preventing hydrate formation and blockages.

It is the subsea dehydration of the gas stream that is the principle research topic of this Thesis.

1.3 Objectives of the Research

The primary objective of this sub-sea dehydration research is to define a dehydration system concept that will be suitable for sea-bed operation independent from a nearby platform and to test the concept and limits of operation of the concept through experimentation.

The dehydration method proposed and being researched is a continuous process using Joule Thomson cooling and hydrate formation to reduce the dewpoint of the inlet gas stream. At subsea temperature conditions of 4 C and a pipeline pressure of 10 MPa a dewpoint of below -38.9 C (water content of 144 parts per million by volume (ppmv)) will be required to ensure no condensation of liquid water occurs from the gas stream.

The research has the following objectives:

a) To design a highly reliable gas dehydration system suitable for operation in deep sub-sea environments for at least 10 years in a predictable manner and requiring minimal maintenance. The key element of the dehydration system will be a pressure and temperature controlled reactor vessel in which clathrate hydrates will be encouraged to form and from which they can be removed in a controlled manner separate from the outlet gas stream. Formation of hydrates will allow the removal of water from the gas stream beyond what could be achieved through equivalent chilling alone. The system must include a hydrate management system that can monitor, control and dispose of hydrates built up by the process.
b) Determine the operational boundaries of the reactor vessel conditions that will successfully reduce the dew point of the gas stream to a value suitable for transport of the processed gas through long sub-sea pipelines.

   Reactor conditions that will be investigated will include:

   i. Inlet gas stream temperature and pressure
   ii. Gas stream composition
   iii. Inlet gas water content
   iv. Gas stream flow rate
   v. Outlet gas stream pressure

vi. Outlet gas stream water content
vii. Heat exchange rate of sea water and reactor vessel
viii. Heat exchange rate between flow-line and sea water
ix. Insulation of the flow-line and reactor vessel

c) Investigate mechanisms for continuous monitoring of the operational state of the reactor vessel and controlling the capture and safe disposal of the removed process water and hydrocarbons from the input gas stream. To ensure the solution meets the reliability requirements solutions should ideally has no mechanically moving parts or parts that need replacing on a regular basis.

It is recognized that Joule-Thomson cooling requires the well stream to undergo a significant pressure drop which can have undesirable implications. If the gas stream existing the dehydration system has a lower than optimal pressure, additional costs due to increased pipeline diameters or subsea gas compression may make the subsea dehydration process uneconomic.

1.4 Significance of the Research

The system is the first to attempt to utilise Low Temperature Separation (LTS) technology combined with controlled hydrate formation in a subsea environment for gas dehydration.

The sequence of process steps used in this design will make the system more efficient and less reliant on mechanical or moving parts. More importantly the system will be less power dependent as compared to surface separating systems, thereby permitting a more compact size and reduced maintenance requirements as is desirable for sub-sea operation.

Areas of research undertaken lead to significant new knowledge in the following:

a) Optimum hydrate formation conditions for a flowing gas stream
b) Methods to monitor hydrate build up and control dissociation in a reactor vessel
c) Dew point suppression of a gas stream through a combination of water condensation and hydrate formation due to cooling and pressure drop for a continuous process
d) Definition of the operational bounds for a dehydration reactor vessel under varying sea temperatures

1.5 Thesis Outline

This thesis describes subsea gas processing and the current development status of the various subsystems. It identifies that subsea dehydration has the potential to improve subsea processing and determines that using LTS techniques and controlled hydrate formation is a potentially beneficial technique from both a cost and practicality viewpoint. The

thesis describes the system concept, the science behind the approach and the experimentation performed and results obtained.

The thesis consists of 7 chapters, laid out in a manner to guide the reader through the research. Chapter 1 provides a high level introduction to the research and how it fits with current subsea processing initiatives. Chapter 2 reviews current dehydration techniques, their suitability for implementation subsea and presents the low temperature hydrate formation technique investigated in this research. Chapter 3 describes the known science behind the proposed dehydration technique. Chapter 4 describes the dehydration experiments providing a detailed description of the test equipment, the commissioning tests and the experiments performed to identify the operating parameters for successful dehydration. Chapter 5 presents the results of the experiments Chapter 6 describes a production well scenario and provides details on a practical method for the management and control of the hydrates created by the dehydration process. Chapter 7 provides the conclusions of the research and recommendations including further work.

All literature referenced in the various chapters of this thesis are listed in Chapter 8.

Appendices provide additional detail on system configuration, calculations, published papers, experimental run data and other relevant technical data.

2 Subsea Dehydration

2.1 Introduction

Natural Gas usually contains significant quantities of water vapour, which must be removed for gas processing and transmission. A pipeline transporting natural gas at a pressure of 10MPa at equilibrium with seawater at 4C must have water content lower than 144ppmv to ensure water will not condense within the pipeline. Failure to sufficiently reduce the water content can lead to condensation of liquid water and the formation and accumulation of gas hydrates into pipe blocking plugs.

To prevent hydrate formation in subsea pipelines, liquid water must be prevented from both entering the pipeline and from condensing out from the gas stream as the gas cools during its passage through the pipeline. To achieve this, the production gas stream needs to be dehydrated to a dewpoint that is below the lowest temperature that the pipeline will be exposed to.

Implementation of a dehydration process in a subsea environment has the potential to make viable many smaller or geographically isolated gas fields that are currently uneconomic to bring into production.

2.2 Gas well production

All gas coming from a subsurface formation is at equilibrium with its surroundings including the connate water so will be saturated with water vapour at the formation conditions. A well production stream includes this water saturated gas, an amount of liquid water that varies with well history, some sand and fines from the formation and often also some liquid hydrocarbons. As the production stream travels up the well bore to the well head the well stream will depressurise due to hydrostatic changes and will cool due to reducing formation temperatures at shallower depths.[31] At the wellhead the well stream passes through the production chokes in the subsea tree that are used to control the production rate. These chokes will further reduce the pressure and temperature of the stream. The well stream is then passed to a separator at a lower temperature and pressure that will capture most of the liquids from the well stream but will pass on a small amount of liquid water (liquid carry over) with the separated gas.

As a gas stream temperature decreases or the pressure increases the amount of equilibrium water vapour that can be carried in the gas decreases, the gas stream becomes super-saturated with water vapour and water will condense out from the gas stream. The chart (Figure 2-1) developed by McKetta and Wehe[32] and extended by Wichert provides a simple and reasonably accurate way of predicting the equilibrium water vapour content of natural gases.

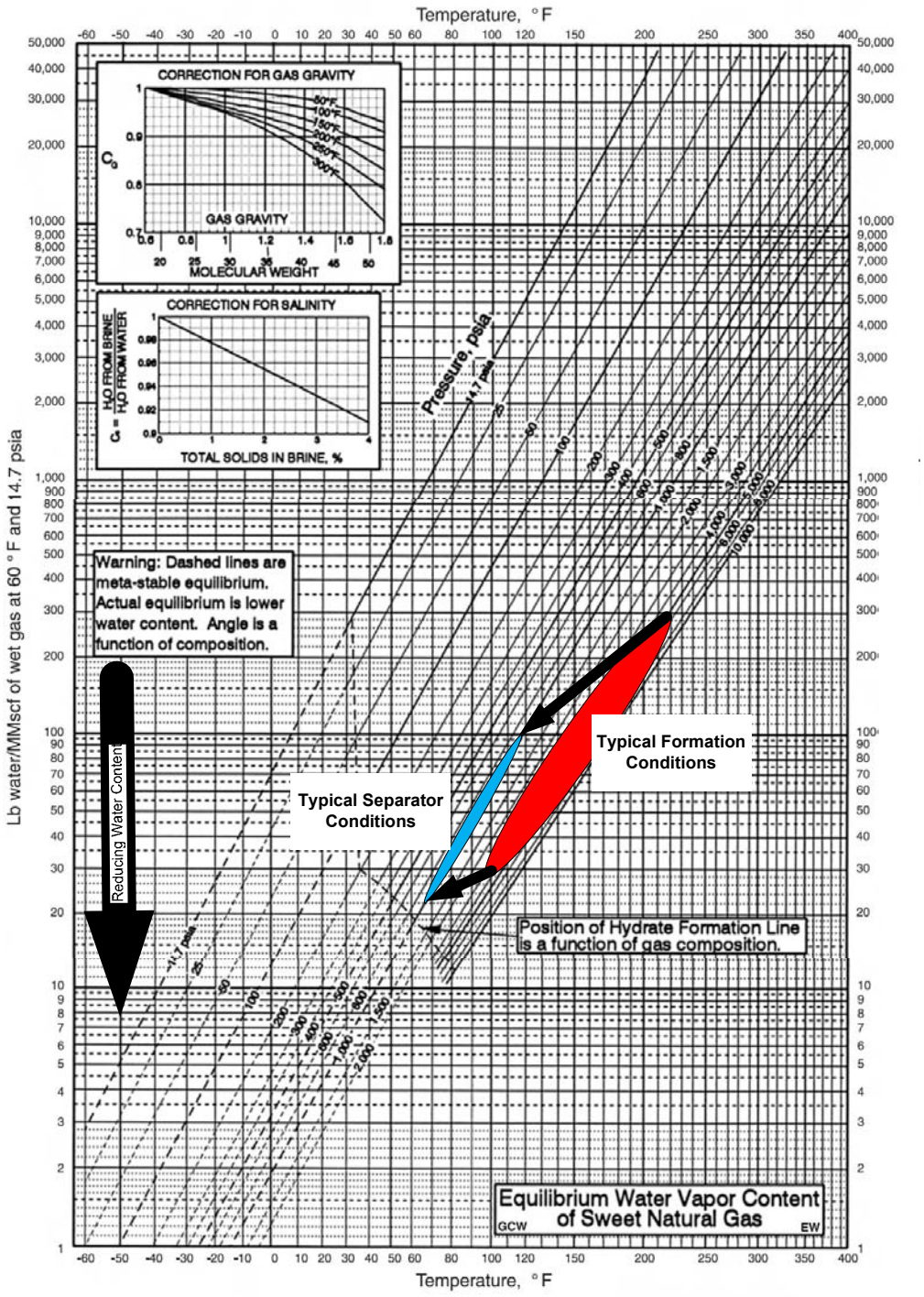

Figure 2-1 Water vapour content prediction using Gorden Wichert extension to the McKetta and Wehe chart[32]

If we consider the typical pressure and temperature conditions of a gas formation and at the separator and plot them on the chart, see Figure 2-1, we can clearly see that the water vapour content decreases as we move from the formation to the separator. This excess

water will condense from the gas and most will be captured in the separator. The gas leaving the separator will be fully saturated with water vapour.

If the gas leaving the separator cools to subsea pipelines conditions where 4 to 7 C is fairly common the water vapour content of the gas will drop and water will condense in the pipeline. Water in pipelines can lead to both hydrate blockage and corrosion problems so must be avoided. A solution to this is to dehydrate the gas stream coming from the separator before it is sent to the pipeline. The water vapour content of the dehydrated gas stream must be low enough so that condensation of liquid water in the pipeline will not occur at the temperature and pressure conditions experienced in the pipeline.

For a pipeline operating at 10 MPa in water temperatures down to 4 C the water vapour content must be less than 144 ppmv[1] to ensure that condensation will not occur. This is an equivalent dewpoint of -38.9 C measured at atmospheric pressure

The following sections of this chapter review the dehydration techniques that are currently used to dehydrate natural gas and assess their potential applicability to subsea operations.

2.3 Dehydration techniques

There are many ways that a gas stream can be dehydrated. The following list includes techniques that are widely used today and some new techniques that are in earlier stages of their development:

- Commercial techniques in gas production today:
  - Absorption with recyclable liquid desiccants such as glycols
  - Adsorption with solid desiccants such as recyclable silica gel or disposable calcium chloride
  - Membrane permeation
  - Refrigeration with methanol
- New experimental techniques
  - Hydrate crystallisation
  - Conversion of water to dry hydrate
  - Vortex tubes
  - Supersonic processes
  - Low temperature separation

[1] Gas composition dependent

2.3.1 Absorption with liquid desiccants

Dehydration using absorption uses a physical phenomenon where water molecules are taken up by the bulk volume of a desiccant. Liquids that are typically used as desiccants include the various glycols with diethylene glycol (DEG) and triethylene glycol (TEG) the most commonly used. Glycols absorb water due to their hydroxyl (OH) group hydrogen bonding with hydrogen atoms in the water molecules. The glycol dehydration process can reduce the water content of natural gas down to around 10 ppmv with enhanced regeneration.[33]

Glycol based dehydration is the most widely applied process[34] with around 40,000 plants (95% of natural gas dehydration plants[18]) at gas wellheads in the US alone. A typical system capable of dehydrating 10 MMSCF of gas a day can be purchased for US$100,000 and run for a few cents per MSCF of gas processed.[35]

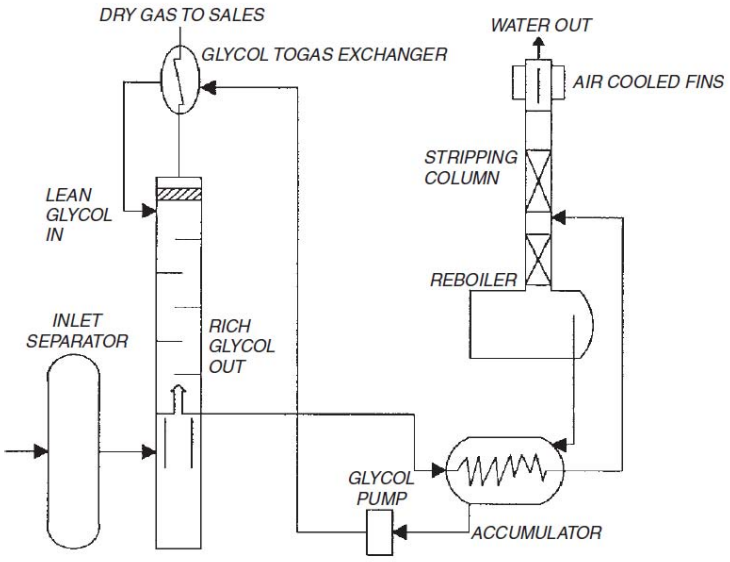

Figure 2-2 Simplified Adsorption based dehydration system using Glycol[36]

In a glycol-based dehydration system a lean stream of the glycol desiccant is sprayed from the top of a dehydration vessel whilst wet gas is passed up the vessel. The glycol passing down the vessel absorbs the water vapour from the counter-flow of gas drying the gas in the process. The dried gas exits from the top of the vessel via a mist extractor that is designed to reduce the amount of glycol carry over in the gas stream. The water-rich glycol leaves from the bottom of the vessel and is passed to a regeneration system to remove the captured water. In the regeneration system the rich desiccant undergoes a number of processes including heating to around 190 C and often gas stripping. The regenerated lean-glycol can then be reused in the dehydration process. A simplified diagram of the glycol dehydration process is shown in Figure 2-2.

The process typically loses around 3.3 litres of glycol in the outgoing gas stream for every million standard cubic meters of gas processed. To ensure continuous operation of the glycol dehydration process constant replenishment of the lost glycol is required.

A glycol based dehydration system operates effectively on shore and on offshore platforms but is not suited for subsea operations for the following major reasons:

1. A glycol dehydration plant is rather large and complex with a typical offshore regeneration skid 12.5 m x 5 m x 6 m and 54 tons and a glycol contactor 3 m in diameter, 9 m high and over 37 tons.(BP/AIOC, 350 MMSCFD, Offshore Azerbaijan[37])
2. Operation of a reboiler at the high temperatures needed to regenerate the glycol to the required concentration will require significant electrical power to power the heaters and fully insulated reboiler vessels.
3. The need for continuous replenishment of lost glycol is undesirable
4. Subsea disposal of removed water with the BTEX components stripped from the natural gas by glycol may prove environmentally difficult.

2.3.1.1 Vortex tube technology

An alternative to the traditional tray based dehydration vessel used in most glycol plants is the vortex tube technology.

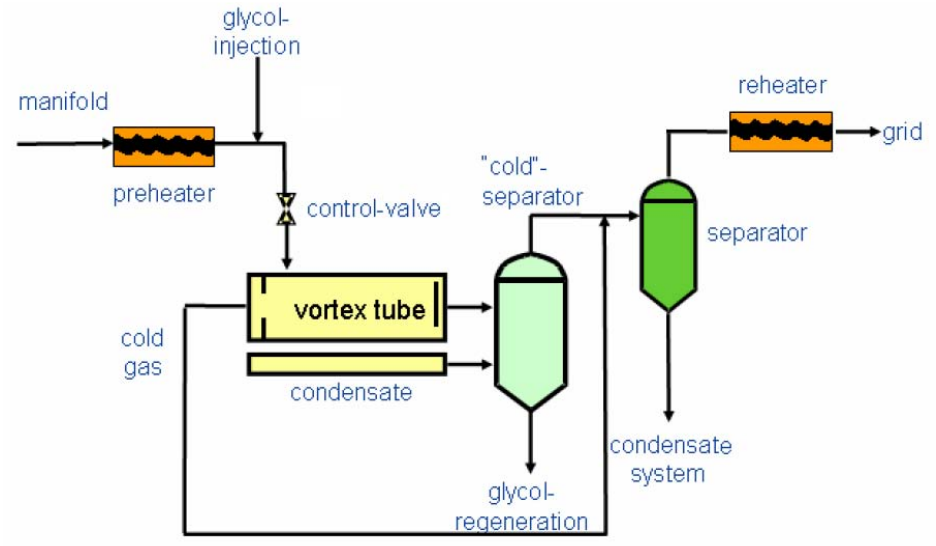

Figure 2-3 Vortex tube dehydration solution[38]

To dehydrate a gas stream a mixture of gas and water-adsorbing glycol is injected tangentially into the vortex tube through an expansion nozzle. Through the JT effect the expansion causes the gas to cool. The vortex tube spins the cooled gas at near sonic

speeds and with G-forces up to 100,000g which causes condensed droplets to move to the walls of the tube thereby separating from the gas stream.[38]

Within the vortex tube the Ranque-Hilsch effect splits gas into a warm outer stream and cool inner stream. The cool stream will be below the gas temperature caused by the JT expansion nozzle which will improve the glycol adsorption equilibrium and consequently the dehydration process.

The separated fluids are removed from the wall of vortex tube together with some entrained gas. The water rich glycol is removed from the gas using a separator and is then sent to a regenerator to recover the glycol.

The vortex tube dehydration technique requires a glycol flow rate of typically half what is required in conventional glycol absorption gas dehydration units. It has no moving parts but requires a 25-35% pressure drop for optimal operation.

A vortex tube system has been successfully used with glycol (TEG) to dehydrate a gas stream for a cavern storage unit in Epe, Germany.[38, 39]

2.3.2 Adsorption with solid desiccants

In an Adsorption process the water is captured on the surface of the desiccant material by van der Waal forces. Desiccant materials typically consist of highly porous spheres or beads that provide a high surface area to volume ratio thereby maximising the adsorption property. Adsorbing desiccants that are used include silica gel, activated alumina and molecular sieves.

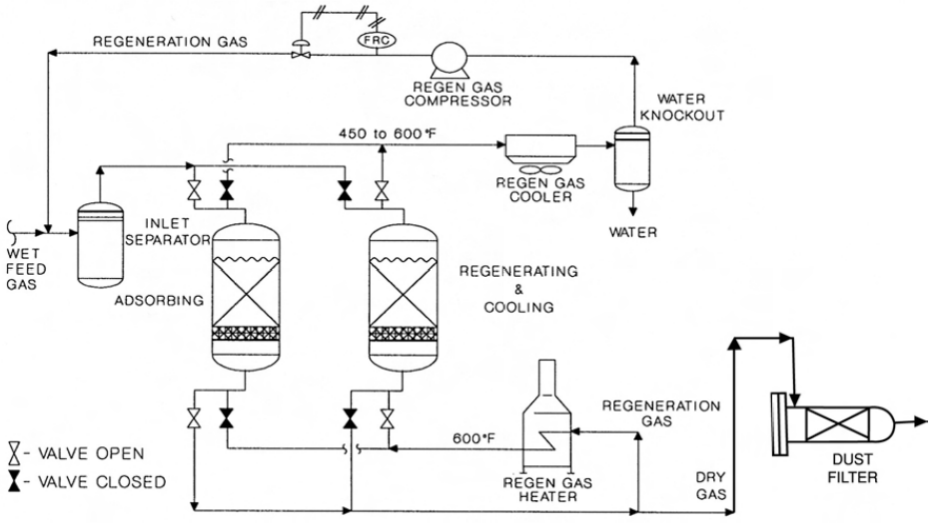

Figure 2-4 Simplified adsorption dehydration system using solid desiccant[40]

Adsorption techniques generally produce a lower water vapour content than absorption techniques[37] with levels down to 0.1ppmv possible using molecular sieves[41]. The technique is however more expensive than absorption processes to achieve the same water

content specifications[38] so typically are only used in applications such as high hydrogen sulphide or oxygen content gases or where a very low dewpoint is required.[40]

Solid desiccant absorptions systems account for around 5% of natural gas dehydration systems in the United States.[18]

For continuous operation adsorption systems typically comprise of two adsorption beds one operating in a drying mode whilst the other is in regeneration mode. Some systems may have 3 or more beds, some performing dehydration while others are regenerating or cooling. During regeneration the adsorption bed is heated to remove the captured water. A dust filter is normally used to capture any small particles of the desiccant.

During drying operations the gas passes down the beds gradually giving up its water content to the desiccant. This process sets up a moving water concentration gradient, the “Mass transfer zone”, down the bed with high concentrations at the top and a low section at the bottom as illustrated below in Figure 2-5. As dehydration operations continue the gradient front moves down the bed and the “Active zone” shrinks. To ensure dehydration operations meet specifications the bed dehydration operations must stop before breakthrough of the gradient front at the bottom of the bed. At this time the bed is switched over to regeneration mode where a dry gas flow passes up the beds and removes the water from the desiccant. The drying ability of the system is limited by the water content of the regeneration gas flow.

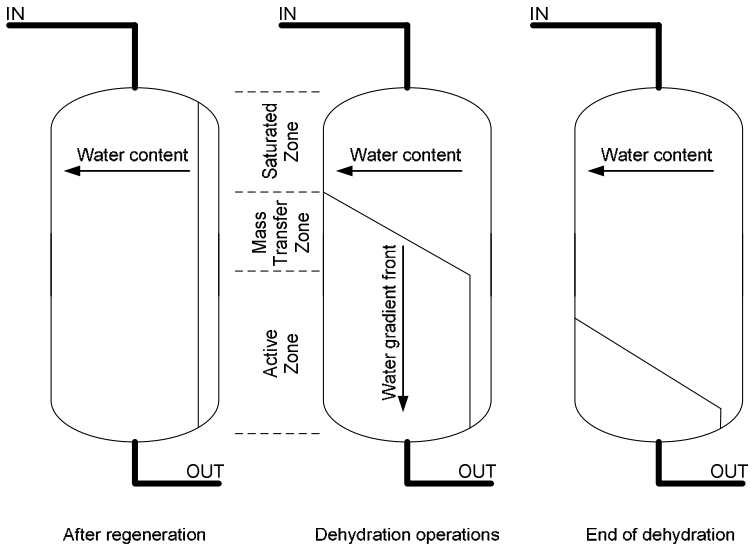

Figure 2-5 Adsorption operations

During desorption of water from the desiccant in the regeneration cycle dry gas is heated to between 200 and 315 C, depending on desiccant type and is passed up the adsorption bed removing the water and saturating the hot gas. The gas is then cooled, separated and recompressed to the input pressure. Approximately 5 to 10% of the throughput gas is used in the regeneration cycle. The regenerated bed is cooled with cool gas before going back into

drying operations. The cycling between adsorption and regeneration is normally set up to occur automatically with timers.

The major operating costs of adsorption are the significant energy required to regenerate the wet adsorption beds.

The adsorbent desiccant degrades over time due to carbon and sulphur fouling and failure of desiccant binding materials with a typical 35% decrease over 3 to 5 years. To maintain efficient operations the desiccant requires periodic replacement.

Solid desiccant based dehydration systems are typically larger than equivalent glycol plants and are not found in offshore facilities where size is a major consideration.

Their large size, high power requirements and need for periodic desiccant replacement make solid desiccant dehydration plants undesirable for subsea operation.

2.3.3 Desiccant dehydration with calcium chloride

An alternative to the use of recycled solid desiccant via regeneration cycles is to use a deliquescent desiccant such as calcium chloride that absorb large quantities of water and form a liquid solution. The system can reduce the water vapour content down to 20 ppmv.

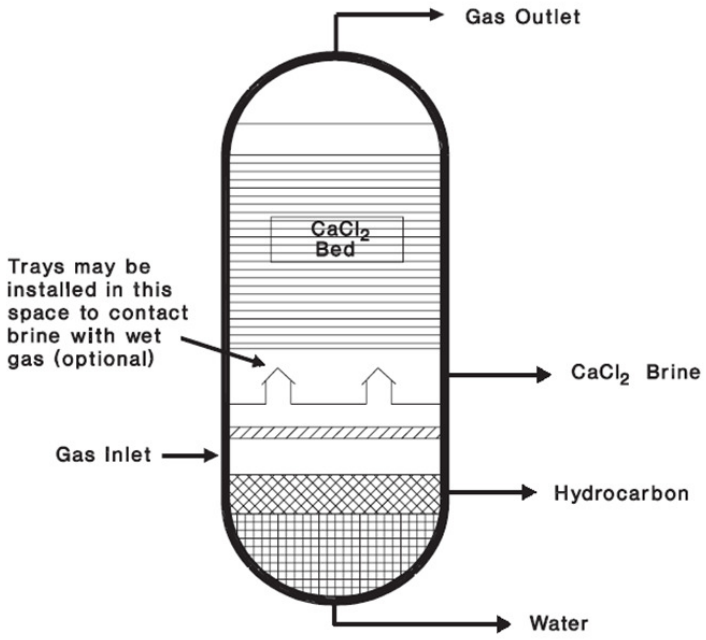

Figure 2-6 Typical calcium chloride dehydration bed[40]

Calcium chloride pellets are placed into a fixed bed similar to an adsorption bed and gas is flowed up the bed. Dry gas exits from the top of the bed and calcium chloride brine, hydrocarbons and water from the bottom of the bed as illustrated in Figure 2-6. Deliquescent

desiccants and generally only economically viable at gas temperatures less than 25 C as their effectiveness reduces at higher temperatures.[42]

The calcium chloride desiccant is a consumable item that must be replenished as it is used up. Around three kilograms of water can be removed by a kilogram of calcium chloride. In a gas well producing 10 MMSCFD around 90 kg of calcium chloride would be required each day to dry saturated gas to subsea pipeline requirements

The simplicity of a deliquescent based dehydration system is attractive for subsea operations but the constant replenishment of significant quantities of desiccant and the need to dispose of the brine in an environmentally acceptable way make it impractical for subsea dehydration.

2.3.4 Membrane permeation

Dehydration with membranes utilises the different permeability rates of gases through polymeric membranes. Fast gases such as water vapour, carbon dioxide and hydrogen sulphide are more permeable and will transfer through the membrane faster than slow gases such as hydrocarbon gases. The permeate stream of gases that have passed through the membrane will then have a high concentration of the fast gases and a low concentration of the slow gases. The residual gas that passes out at the high pressure side will as a consequence have much lower concentrations of the fast gases. Water vapour is considered super fast so the residual gas will have been dehydrated.[43]

The permeation rate through the membrane is proportional to the difference in the partial pressures across the membrane. During the process of removing water vapour around 5 to 10 percent of the feed gas volume also passes through the membrane[40], though this can be reduced to under 1 percent by lowering the permeate pressure or using a sweep gas.[35]] The permeate gas leaves at a low pressure so has to be either recompressed and recycled or used as a fuel gas. The dry gas leaves at a small pressure drop to the input feed.

To prevent membrane blockage, all free solids and droplets larger than 3 microns need to be removed from the feed gas before entering the membrane. Condensation in the membrane must also be prevented, so a saturated gas stream needs to be heated prior to entry to membrane and the membrane temperature must be controlled.

Figure 2-7 Membrane system for dehydrating 3.2 MMSCFD gas feed[44]

Units can operate at pressures of up to 8 MPa with feed gases containing up to 2,000 ppmv of water. Dehydration down to 20 ppmv can be obtained with membranes.

Membranes systems are fairly small compared to glycol plants (approximately 15% of the size), provide a low maintenance method for dehydrating gas streams and are able to easily handle changes in gas flow rate. The technology is hampered by performance degradation of the membrane requiring that the membranes are replaced every 10 years or so to ensure dehydration standards are maintained.[45]

Membranes are relatively expensive for large gas flow rates and are prone to fouling by contaminants.

The small size and low maintenance requirements make membrane permeation a possible method for subsea dehydration operations. Issues that need to be resolved before further consideration include:

1. How to minimise and deal with the gas lost in the permeate stream, e.g. use by power generators in a buoy or compress and reprocess
2. Operations of gas stream pre-processing systems that filter and warm the feed upstream from the membrane
3. Controlling membrane temperature to ensure condensation of water does not occur in the membrane
4. Periodic subsea replacement of membranes
5. Capital expense of membranes

2.3.5 Methanol - refrigeration process

In the methanol refrigeration process, methanol is added to the gas stream and the mixture is refrigerated to very low temperature that causes the water and methanol to drop out from

the feed. The methanol/water liquid is sent to a stripper column where heat is used to recover the methanol, which is then recycled by the process.

The methanol refrigeration process can produce very low dew points in the -70 to -100 C range.[33]

An improvement to this process, the IFPEX-1 process, was developed by Institut Français du Pétrole (IFP) that replaces the heated stripper column with a contactor column where the methanol is stripped from the water-methanol liquid by a counter-current of the incoming saturated gas feed.[46]

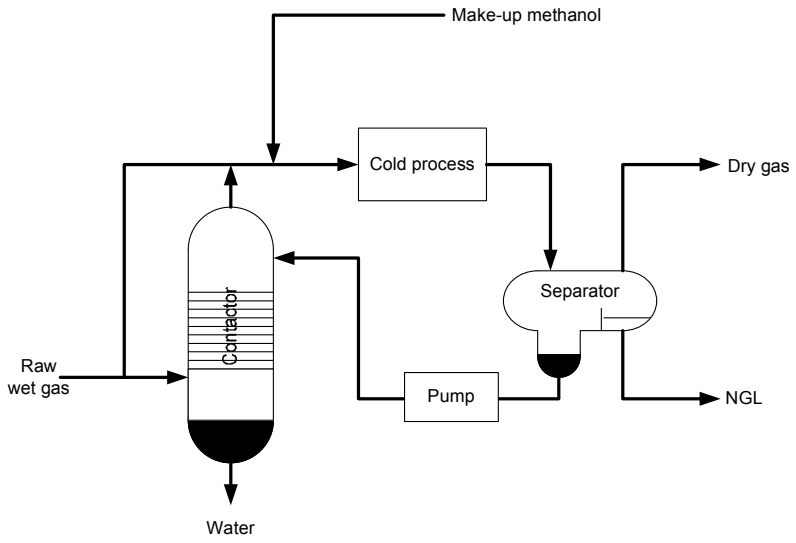

Figure 2-8 IFPEX-1 methanol refrigeration dehydration process

The cold process must reduce the feed temperature to the required dewpoint temperature. Any cold process can be used in the IFPEX-1 system from a simple JT expansion valve to an elaborate turbo-expander process.

Both the dry gas and the water collected in the contactor will contain a small amount of methanol carry-over. With sufficient trays in the contactor the methanol content of the water can be reduced to a low enough level that the water can be disposed off with no further processing in the ocean. Methanol losses of the process are around 0.3 ml/sm^3 (2 gallons/MMSCF) of gas processed.[47]

For dewpoint lower than -30 C the IFPEX-1 system is competitive with glycol plants and has a claimed 30% lower CAPEX. The first commercial installation was in Canada 1992 and in 2006 there were 15 IFPEX-1 plants in operation with capacities up to 350 MMSCFD.[48]

The simplicity of the system and the ability to use simple cooling methods suggest that the IFPEX-1 process may be suitable for subsea operations provided a continual supply of

methanol can be made available for injection at the gas feed pressures and the feed pressure is high enough to allow sufficient JT cooling to take place.

2.3.6 Twister technology

The Twister technology uses a combination of gas expansion and centrifugal force to dehydrate a gas stream. It is a technology that was developed in 1997, has been used for a number of field trials in Holland, Nigeria and Norway and had its first commercial implementation installed in Malaysia during 2004. The technology is claimed to be able to dehydrate a gas stream down to pipeline conditions of 50 ppmv.[49]

A cross-section diagram of the Twister technology is shown in Figure 2-9.

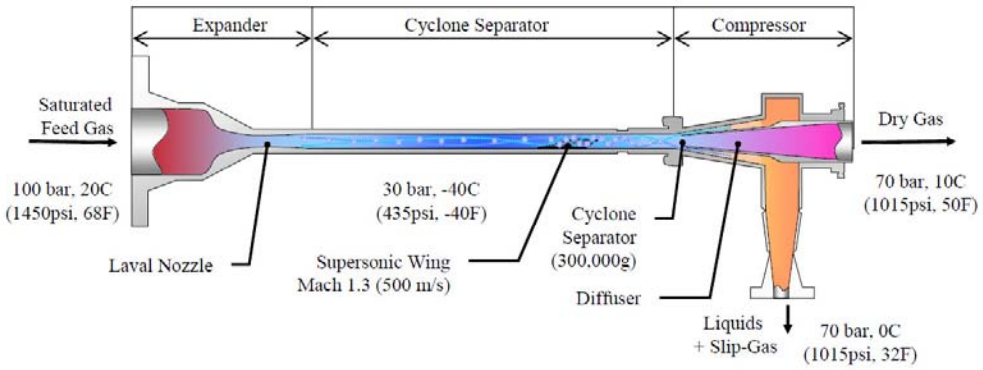

Figure 2-9 Cross sectional diagram of the Twister technology[49]

The inlet gas stream is passed through a Laval nozzle that accelerates the gas to supersonic speed thereby cooling the gas. This cooling causes nucleation of water and hydrocarbon and their growth into droplets. A wing is fitted after the nozzle that causes the gas stream to spin creating large centrifugal forces resulting in the denser droplets collecting on walls of the vessel. The dried gas is removed from the centre of the vortex where it is slowed down by diffusers thereby recovering between 60% and 85% of the initial pressure. The liquids separated by the process together with some slip gas (20-30% of input gas) are removed via a second path, recovering the pressure and is sent to a de-gassing vessel to separate the liquids and recover the gas. The operating region of the degassing vessel is typically within the hydrate formation region so heating coils are used to melt the hydrates.

The Twister tube is a fixed volumetric flow device designed so that the speed at Laval nozzle throat is always Mach 1. Variation in flow regime can be adjusted to some extent by changing the inlet pressure but to provide better variability banks of Twister tubes that can be switched in and out of operation are typically used. The technology is susceptible to solids in the gas flow and to provide reliable operation filtering is required to remove any particles larger than 15 microns.

The Twister technology has no moving parts and is small in size compared to glycol based dehydration plants. A Twister tube capable of 35 MMSCFD is only 2 m long and fits within a 150 mm diameter casing.

A study performed in 2002 found it was a suitable technology for subsea dehydration operations and development of a subsea trial system has been completed. A subsea trial is planned for Petrobras, Brazil in 2010.[50]

The Twister technology and that proposed and trialed by this work both utilise JT cooling but there are some significant differences between the techniques. The Twister technology advantageously requires less pressure drop to obtain the required dehydration performance due to its use of supersonic gas velocities and the pressure recovery stage. Laval nozzle could potentially be used with the proposed technique and this may improve system performance. Laval nozzles were not however trialed due to the small nozzle sizes required for the trial system and the ease by which they became blocked with hydrates.

The Twister technology requires very low particulate content to prevent wear and has the drawback of having a significant amount of slip gas removed from the gas stream with the captured fluids, The proposed technique is likely to be relatively immune to moderate amounts of particulates and does not lose gas through slippage.

2.3.7 Experimental dehydration techniques

2.3.7.1 Pass through hydrate crystalliser

Tatro et al.[51] reported in 2007 of using a cooled porous membrane with a pressure differential as a dehydration mechanism. Hydrate forms on the cooled membrane on the high pressure side and dissociates on the low pressure side thereby capturing water from the high pressure side and dehydrating the gas stream.

The concept has been demonstrated in the laboratory but no detailed results or indications of commercial trials have been found.

2.3.7.2 Low temperature separation

The principle that "*as a gas cools the amount of water vapour it can contain decreases*" is the basis for using the low temperature separation method to dehydrate a gas stream. There are a number of ways that a gas can be industrially cooled including:

- Refrigeration of the vessels or pipe work (cooling jackets, heat exchangers etc.)
- Expansion through a choke (at conditions when the gases JT coefficient is positive)
- Expansion through a turbo-expander

Dehydration using refrigeration and expansion through a JT valve have both been successfully demonstrated. Turbo-expanders have been used extensively to liquefy

hydrocarbon fractions through cooling but due to their susceptibility to impaired operations in the presence of hydrates they are not suitable for dehydration processes.

Aly[52] at the Woodside Research Facility of Curtin University performed dehydration tests in a laboratory test system comprising a refrigerated vessel and utilising a fixed JT choke at the inlet. The operating conditions for Aly's experiments were as follows:

- Gas composition: lean domestic gas supply with 85% methane.
- Flow rate: 0.078 sm^3/min (4 MSCFD)
- Pressure drop across choke: 0.7 MPa (100 psia)
- Dehydration vessel operating pressure: 2.7 to 8.2 MPa (400 to 1200 psia)
- Dehydration vessel operating temperature: -15 to 5 C
- Inlet gas feed temperature: 25 to 50 C
- Dehydration vessel volume: 24 litres (0.85 cubic ft.)
- Typical gas residence time: 9 to 31.5 minutes

Dehydration was achieved by cooling the gas to a temperature below the hydrate formation temperature at the experimental pressure. Cooling was achieved through the 0.7 MPa pressure drop across the nozzle and by refrigerating the dehydration vessel using an external cooling jacket. The nozzle contributed around 3 C of cooling due to the Joule Thomson effect and the refrigeration the balance. The gas residence time ensured that the gas was in the vessel for sufficient time for the gas to cool, water vapour to condense, hydrates to form and water droplets and hydrates to separate out via gravity.

The key observations of this research were that the lower the vessel temperature, the lower the achieved dewpoint with less change in dewpoint achieved with temperatures below -5 C.

His experiments demonstrated that a saturated gas stream could be successfully dehydrated using expansion and vessel refrigeration down to water content of less than 20 ppmv.

2.3.8 Suitability of existing methods for subsea operations

2.3.8.1 Subsea Equipment constraints

Subsea components must have a weight limit of around 150 tons to ensure they can be installed with rig and support ship cranes.[53]

The costs involved with the servicing of subsea components are very high so equipment must have high design reliability and require minimal interventional maintenance during its service life.

The depths of installation impose additional temperature and pressure requirements on subsea components. With target depths of 1,000 m and more, pressures of over 10 MPa and temperatures under 4 C may be experienced.

2.3.8.2 Drivers for selecting suitable dehydration technology

Beyond the constraints required for subsea operations, there are other drivers for the selection of suitable dehydration technology including environmental, cost and safety.

Environmental considerations include:

- issues relating to the toxicity of components
  - Polymer membranes are highly toxic[54] and use toxic catalysts during manufacture
  - Ethylene glycol is relatively non-toxic but it can oxidise to the poisonous compound formate and some of its metabolites are toxic and can be fatal[55] Triethylene and diethylene glycol are less toxic but ingestion can cause damage to kidneys and the nervous system and can be fatal.
- The reduction of undesirable effluent emissions such as the BTEX emissions typically found with glycol plants

The total capital and running costs of dehydration solutions must be evaluated.

2.4 Subsea dehydration research

The research performed and described in this thesis investigates the suitability of a system that utilises the Joule Thomson cooling effect to dehydrate a gas stream and is a viable solution for subsea operations.

2.4.1 Background

This research revisits the approach taken by Aly[52] at Curtin University, modifying the technique to make the solution more applicable to subsea operations. The research performed by Aly utilised a combination of Joule Thomson cooling and an external closed cycle refrigeration system with the requisite compressor. To reduce the complexity of the system and increase system reliability external refrigeration was removed and Joule Thomson cooling was used as the sole mechanism for cooling the gas stream. Overall system weight and costs are also reduced by removing the external refrigeration system.

2.4.2 Process

Gas stream pre-conditioning Prior to the gas being passed into the dehydration reactor the water saturated gas from the subsea separator is passed through an adjustable heat exchanger designed to cool it to a temperature just above the hydrate region.[56] A combination of ambient sea water and the cold dehydration process outlet gas can be utilised to cool the inlet gas stream.

The inlet temperature is set as close as is possible to the hydrate formation temperature to allow the minimum possible pressure drop during the Joule Thomson expansion whilst avoiding hydrate blockage of the expansion nozzle.

Gas stream cooling by Joule Thomson expansion The inlet gas stream is expanded by passing through a nozzle which cools the gas through the Joule Thomson effect. The pressure and temperature conditions in the dehydration vessel that results from the expansion are such that the saturated water content is lower than the inlet stream so water condenses out as a mist.

An alternative method for cooling the gas is the use of turbo-expanders which can give better cooling for the same pressure drop. These devices are complex machines requiring significant maintenance so were discounted as a viable alternative in the subsea environment.

Hydrate formation on walls of the dehydration vessel After the gas expansion the conditions in the dehydration reactor are suitable for the formation of gas hydrates which can potentially grow in two locations:

- Within the condensed water droplets formed within the bulk gas phase
- In the condensed water film on surface of the dehydration vessel which during normal operations is likely to be previously formed sheets of hydrate

Natural gas in equilibrium with gas hydrates has lower water content than when no hydrates are present. This phenomenon causes the gas stream to dehydrate to a lower dewpoint than would occur through cooling alone.

The combination of water condensing out from the gas stream and hydrate depression of water content dehydrates the gas stream.

Mist eliminator at gas exit A mist eliminator is fitted to the exit port of the dehydration reactor to capture mist from the gas before it leaves minimising carry over and ensuring the dehydration process effectiveness is not compromised.

3 Process model

3.1 Equation of State selection

Equations of state are formulas that provide a mathematical relationship between two or more state functions. Equations of state typically take the form of polynomial equations with constants that are gas specific and are selected to provide the best fit for the experimental data. They are very useful in describing many properties of fluids and mixtures of fluids.

There are many equations of state, but in the gas industry today the Peng-Robinson equation of state is the most commonly used. It has been widely reviewed against other equations of state and found to provide reliable results[57].

There are three recognised shortcomings of the Peng-Robinson equation of state (PREOS)[58]:

1. it is poor at describe the saturated vapour pressure at low temperatures
2. it becomes unreliable in fluids with large acentric factors ($\omega > 0.5$)
3. it is unreliable at predicting liquid and vapour phase volumes along the saturation curve

Each of these shortcomings need to be reviewed in relation to where we will be utilising the Equation of State. This is sole the purpose of sections 3.1.1 through 3.1.3.

3.1.1 Critical temperature consideration

For the purpose of calculating the pseudo critical temperature (T_{pc}) and pressure (P_{pc}) the molar averaging technique is appropriate:

$$T_{pc} = \sum_i y_i T_{c_i} \quad \text{... 1}$$

and

$$P_{pc} = \sum_i y_i P_{c_i} \quad \text{... 2}$$

where T_{c_i}, P_{c_i} and y_i are the critical temperature, critical pressure and mole fraction for component *i*.

The characteristics of studied gas compositions have the following range of values:

- The pseudo critical temperatures vary between 188 K and 217 K
- The pseudo critical pressure vary between 4.5 MPa and 4.9 MPa

The critical Temperature of the fluids we are looking at is in the range between 188 K and 217 K. With operating temperatures around 277 K, the reduced temperatures therefore range between 1.25 and 1.5. This is outside the low temperature region where the PREOS is considered unreliable.

3.1.2 Acentric factor consideration

The acentric factor for the major Natural gas components, methane is 0.0115 and ethane is 0.0994. The heavier components up to C_6 all have values of less than 0.3. The acentric factors of non-hydrocarbon components N_2 and CO_2 are 0.0372 and 0.2239 respectively[40].

For the purpose of calculating an approximate acentric factor for natural gas mixtures a molar average calculation will again suffice:

$$\omega = \sum_i y_i \omega_i \qquad \text{... 3}$$

where ω is the calculated acentric factor for the mixture and ω_i and y_i are the acentric factor and mole fraction of component *i*.

The acentric factors for the studied gas compositions vary between 0.014 and 0.049.

The maximum acentric factor for the fluids is 0.049 well below 0.5 and within the region where the PREOS is reliable.

3.1.3 Vapour phase volume consideration

The inaccuracies in volume determination are not of great concern to the uses to which we require a reliable equation of state.

To summarise, none of the recognised shortcomings of the Peng-Robinson equation of state are of concern so for this research the Peng-Robinson equation of state shall be used.

3.1.4 Peng-Robinson equation of state definition

The Peng-Robinson equation of state is as follows[59]:

$$P = \frac{RT}{v-b} - \frac{a(T)}{v(v+b)+b(v-b)} \qquad \text{... 4}$$

where $a = \Omega_a \left(R^2 T_c^2 / P_c\right)\alpha(T_r, \omega)$, $\quad b = \Omega_b \dfrac{RT_c}{P_c}$, $\quad \alpha(T_r, \omega)^{0.5} = 1 + m\left(1 - T_r^{0.5}\right)$,

$m = 0.37464 + 1.54226\,\omega - 0.26992\,\omega^2$, $\Omega_a = 0.45724$ and $\Omega_b = 0.07880$

P, P_c, *R*, *T*, T_r, T_c, *v* and ω are the pressure, critical pressure, universal gas constant, temperature, reduced temperature, critical temperature, specific volume and acentric factor.

The default values for the Binary Interaction Parameters used by the HYSYS implementation of the PREOS were used for all calculations.

3.2 Operational region of dehydration process

Classical gas wells typically have a gas composition that does not change significantly with time. Some gas wells do show a variation with time that is thought to be due to non classical mechanisms such as adsorption in the rock matrix caused possibly by shales and Knudsen diffusion due to small pore sizes and variation in diffusion characteristics of gas components.[60]

From well to well there is significant variation in the gas composition from some wells which are almost entirely methane, e.g. WA's Macedon field where methane comprises 99.5% of the hydrocarbon content[28], to wells with significant heavier components, e.g. some Bass Straight fields with around 15% of heavier hydrocarbon components. Details of the various gas compositions are provided in the Appendix.

3.3 Water content of natural gas

Natural gas in a subsurface reservoir is in a thermodynamic equilibrium state, so will be fully saturated with the formation connate water at the subsurface conditions of temperature and pressure.

During production, the natural gas enters the well bore and travels to the surface, where the gas stream pressure and temperature conditions are lower due to reduced hydrostatic forces and temperature decrease with reduced depth.

3.3.1 Prediction of natural gas water content

The water content of a gas depends on the pressure and temperature conditions and the composition of the gas.

The various common methods used to predict the water content of Natural gases are discussed below[61]:

3.3.1.1 Partial pressure and fugacity relationships

Raoult's law can be applied to water vapour within a gas leading to the equation:

$$y_w = P_v / P \qquad \text{... 5}$$

where P_v is the vapour pressure of water at the system conditions and *P* is the system pressure. As Raoult's law is applicable only to ideal gases so this relationship is valid only at low system pressures including atmospheric pressure..

Raoult's law can be used for the calculation of the water content of a gas if one knows the saturation water vapour pressure at the temperature. Goff and Gratch[62] developed a method for determining the saturation water vapour pressure as a function of temperature which is widely used in Industry. The method is expressed as two equations, one for the vapour pressure over water and the other over ice. The equations are:

$$\begin{aligned}\log \dot{e} \; &= -7.90928\left(\frac{T_{st}}{T-1}\right)+5.02808\log\left(\frac{T_{st}}{T}\right) \\ &\quad -1.3816E-7\left(10^{11.344(1=T/T_{st})}-1\right) \\ &\quad +8.1328E-3(10^{=3.49149(T_{st}/T-1)}-1)+\log \dot{e}_{st}\end{aligned} \qquad \text{... 6}$$

over water, and

$$\log \dot{e}_i = -9.09718\left(\frac{T_0}{T-1}\right)-3.56654\log\left(\frac{T_0}{T}\right)+0.876793\left(\frac{1-T}{T_0}\right)+\log \dot{e}_{i0} \qquad \text{... 7}$$

over ice. Where T is the temperature of interest, $\dot{e}, \dot{e}_i$ are the saturation water vapour pressure over water and ice, T_{st} is the steam point temperature at 1 atmosphere, T_0 is the ice point temperature, $\dot{e}_{st}$ is saturation water vapour pressure at the steam point pressure and $\dot{e}_{i0}$ is saturation water vapour pressure at the ice point pressure.

The combination of Goff-Gratch and Raoult's Law is utilised in this project to convert dewpoint temperature measured at atmospheric pressure to water content in parts per million (by volume).

3.3.1.2 Empirical plots

Dewpoint plots have been used for many years to predict the water content of natural gases with the most used plot being the one created in 1958 by McKetta and Wehe[32]. This plot allows an estimate of the saturated water content to be obtained for a gas given the pressure and temperature conditions. It also provides corrections for gas relative density and water salinity.

This method is typically accurate to within 10 percent for sweet natural gases but is less accurate in the presence of carbon dioxide or hydrogen sulphide. With compensation techniques however this method may be extended for use with sour gases.

3.3.1.3 PVT equations of state

An equation of state can also be used to predict the water content of natural gases both sweet and sour. The Peng Robinson equation is a cubic equation of state that is an enhancement of the Soave, Redlich, Kwong equation of state to provide improved fluid property prediction around the critical point. For the calculation of water content of

hydrocarbon gases the Peng Robinson Equation of state demonstrates excellent agreement with experimental data.[63]

Due to the relative difficulty in taking accurate readings from the McKetta and Wehe chart and the availability of suitable software, the Peng Robinson EOS will be utilised in this research to predict the saturated water content of the inlet gas stream to the dehydration process.

3.3.2 Effect of acid gases on water content

At high pressures (above 5 MPa) and at temperatures of interest to this project, the presence of acid gases, carbon dioxide and hydrogen sulphide significantly increase the amount of water present in a saturated gas stream. If less than 40% acid gases are present water content can be calculated using correction charts or the following equation:

$$W = y_{HC}W_{HC} + y_{CO_2}W_{CO_2} + y_{H_2S}W_{H_2S} \quad \text{... 8}$$

where y_{xx} is the mol fraction of hydrocarbon, carbon dioxide or hydrogen sulphide and W_{xx} is the water content for hydrocarbon, pure carbon dioxide or pure hydrogen sulphide gases typically taken from available industry charts for the applicable conditions.

For this research, all gas required for experiments will be a dry, sweet gas drawn from the gas main which contains no significant quantity of any sour gas.

3.3.3 Effect of hydrates on water content

A number of experimental studies have been performed on the water content of natural gases when the gas is in equilibrium with hydrates [56, 64, 65]. This experimental data was used by Chapoy[66] to develop a correlation that can be used to predict the water content of natural gases in equilibrium with hydrates (refer to section 3.4.2.5 for more information)

n all cases the water content of the gas in equilibrium with gas hydrates was found to be lower than when in equilibrium with the metastable liquid. The suppression of water content was found to be dependent on the gas composition, a result that was explained as being due to the different hydrate structures formed by different gas mixtures.

The scarcity of water content data in the hydrate region poses some question marks as to the validity of empirical charts and commonly applied Equations of State for accuracy of predictions in the hydrate region.

A useful consequence of these findings is that it will be beneficial to the dehydration process if hydrates are encouraged to form within the dehydration vessel.

3.4 Analysis of the dehydration process

The two natural phenomena being exploited by the proposed natural gas dehydration process are the cooing of natural gases when they expand through a nozzle, the Joule Thomson effect and the depression of water vapour content of natural gases when they are in contact with gas hydrates.

3.4.1 Joule Thomson Cooling

The following sections describe the calculation methods for determining the change in temperature for a gas as it is expanded through a nozzle. This is used to allow the comparison of experimentally measured cooling with that predicted by theory.

3.4.1.1 Expansion of gas through a nozzle in a controlled volume

When we look at the process of expanding a gas through a nozzle where no phase change occurs (i.e. steady state) and consider a controlled volume as defined by Figure 3-1. From the thermodynamic Conservation of Energy equation [67]:

$$\frac{dE_{cv}}{dt} = \dot{Q}_{cv} - \dot{W}_{cv} + \sum_i \dot{m}_i \left(h_i + \frac{V_i^2}{2} + g z_i \right) - \sum_e \dot{m}_e \left(h_e + \frac{V_e^2}{2} + g z_e \right) \quad \text{... 9}$$

where $\frac{dE_{cv}}{dt}$ is the change of energy of the controlled volume by time, $\dot{Q}_{cv}$, $\dot{W}_{cv}$ the addition of heat and performance of work, $\dot{m}_i$, $\dot{m}_e$ the masses of components *i* and *e* entering and leaving the controlled volume and h_x, V_x, z_x are the enthalpy, velocity and height of the components entering and leaving the controlled volume.

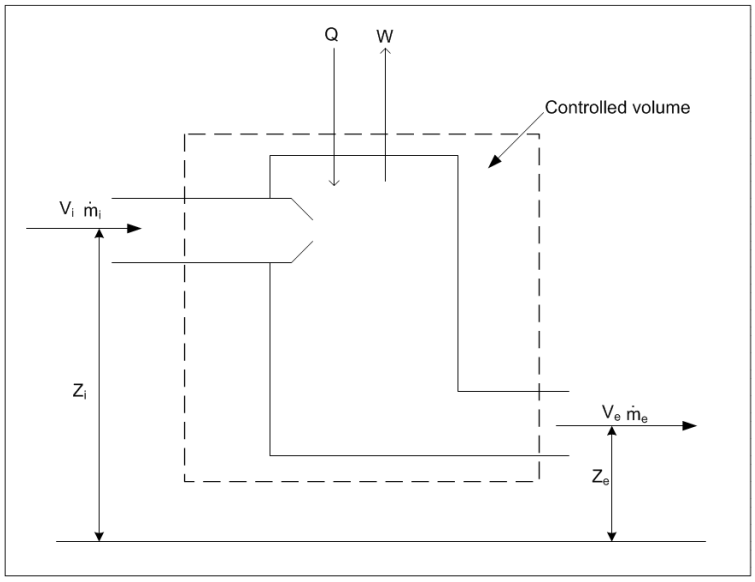

Figure 3-1 Expansion process controlled volume

For the nozzle expansion the following experimental conditions can be defined:

Energy in = Energy out, so $\frac{dE_{cv}}{dt} = 0$

Mass in = Mass out, so $\dot{m}_i = \dot{m}_e = \dot{m}$

Vessel is well insulated, so $\dot{Q}_{cv} = 0$

No work is done, so $\dot{W}_{cv} = 0$

One entry and exit point, so $i = e = 1$

In our experiments the velocities, V is very low and changes in height, z are small, so the kinetic energy and potential energy terms are very small compared to the enthalpy terms and can reasonably be ignored. Thus:

$$Kinetic\ energy\ terms, \quad \frac{V_i^2}{2}, \frac{V_e^2}{2} \approx 0$$
$$Potential\ energy\ terms, \quad gz_i, gz_e \approx 0$$

Substituting for the known values we get that

$$0 \quad = \quad 0 - \quad 0 + \dot{m}(h_i + 0 + 0) \quad - \quad \dot{m}(h_e + 0 + 0)$$

Simplifying to h_i=h_e, and thus the expansion of the gas through a nozzle can be considered to be a constant enthalpy process.

When lines of constant enthalpy are plotted onto a temperature-pressure diagram a curve results with both positive and negative slopes and a point where the slope is zero. The change in gas temperature caused by expansion is called the Joule Thomson affect and the slope of the constant enthalpy curve is called the Joule-Thomson coefficient. The Joule Thomson coefficient can be written as:

$$\mu_{jt} = \left(\frac{\partial T}{\partial P}\right)_h \qquad \text{... 10}$$

When the JT coefficient is positive a gas will cool when it is expanded adiabatically. Conversely when the slope is negative the gas will warm up on expansion.

When the points of zero slope are connected we obtain an inversion curve which reflects conditions where expansion of the gas causes no change in gas temperature.[68]

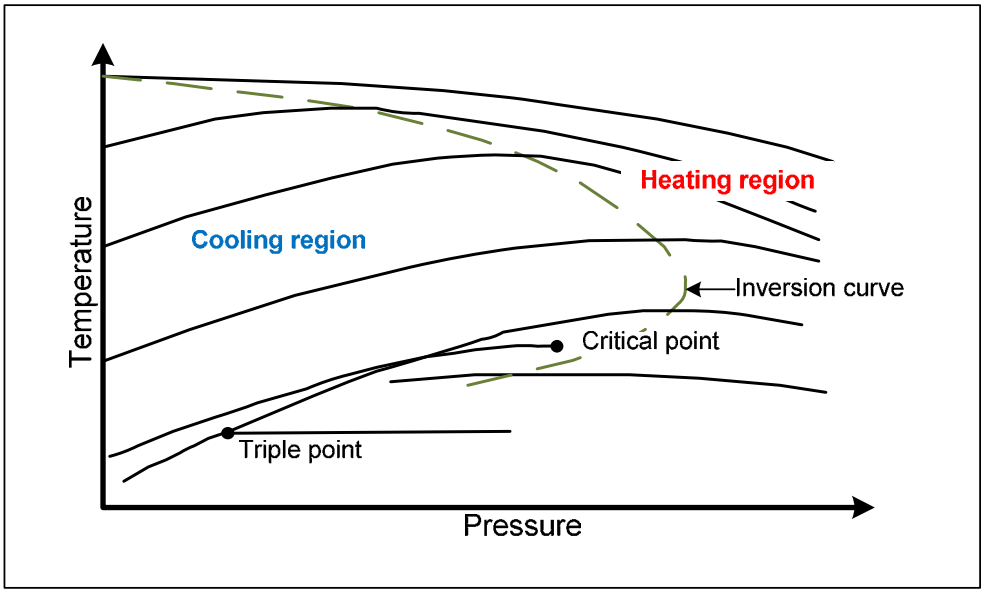

Figure 3-2 Joule Thomson inversion curve

At all temperature/pressure points inside the inversion curve a gas will cool on expansion.

For the dehydration process to operate successfully the Joule-Thomson coefficient of the gas stream at the pressure and temperature where the gas expansion occurs must be positive enough to ensure sufficient cooling of the gas stream occurs.

3.4.1.2 Nozzle flow

When we consider the Conservation of Energy equation from the perspective of the nozzle only it simplifies to:

$$h_i + \tfrac{1}{2}V_i^2 = h_e + \tfrac{1}{2}V_e^2 \qquad \text{... 11}$$

For an ideal gas the change in enthalpy is given by the equation:

$$h_e - h_i = C_p(T_e - T_i) \qquad \text{... 12}$$

Substituting this above and rearranging we can express the outlet velocity by the equation:

$$V_e = \left[V_i^2 + 2C_p(T_i - T_e)\right]^{1/2} \qquad \text{... 13}$$

The flow of an ideal gas through a smooth nozzle is an approximately reversible process so we can consider the process to be adiabatic. For an adiabatic process of an ideal gas the relationship between temperature *T* and pressure *P* can easily be shown to be:

$$\frac{T_2}{T_1} = \left(\frac{P_2}{P_1}\right)^{\frac{\gamma-1}{\gamma}} \quad \text{... 14}$$

where γ is the ratio of specific heats (C_p/C_v).

When we consider that the mass through the nozzle is constant we can write:

$$\frac{A_1 V_1}{v_1} = \frac{A_2 V_2}{v_2}, \text{ or rearranged: } \frac{A_1}{A_2} = \frac{v_1}{v_2}\frac{V_2}{V_1} \quad \text{... 15}$$

where the specific volume ratio (v_1/v_2) can simply be obtained by using the ideal gas law:

$$\frac{v_1}{v_2} = \frac{T_1 P_2}{T_2 P_1} \quad \text{... 16}$$

These equations allow us to calculate the nozzle flow based on the entry and exit conditions of the nozzle but do not place a sonic limit on the outlet speed. For converging nozzles the flow rate is limited by the maximum speed of the gas which cannot exceed the speed of sound. For our dehydration experiments it is desirable for the gas leaving the nozzle to be as cold as possible to maximise the water vapour super-saturation and increase the chance of droplet condensation. The nozzle should therefore be selected so that the outlet velocity is a maximum, i.e. near the sonic speed for the conditions. For experiments and production systems the nozzle can be sized to allow a certain mass flow at the choking condition (outlet velocity is Mach 1).

The mass flow rate equation is:

$$\dot{m} = \rho V A \quad \text{... 17}$$

where V is velocity, A is area and ρ is the density. The velocity can be expressed as:

$$V = M.a_s \quad \text{... 18}$$

where a_s is the speed of sound and M is the Mach number.

The speed of sound for an ideal gas can be expressed by the equation:

$$a_s = \sqrt{\gamma R^* T} \quad \text{... 19}$$

where γ is the specific heat ratio, R^* is the gas constant (Universal gas constant, 8.3415 J/mol.K divided by the Molecular weight in Kg/mol).

We can use the ideal gas equation of state to specify the density by the equation:

$$\rho = \frac{P}{R^* T} \quad \text{... 20}$$

Substituting the relationships we get:

$$\dot{m} = AMP\sqrt{\frac{\gamma}{R^* T}} \quad \text{... 21}$$

Using the isentropic flow equations:

$$\frac{T_2}{T_1} = \left(\frac{P_2}{P_1}\right)^{\frac{\gamma-1}{\gamma}} \quad \text{... 22}$$

and

$$\frac{T_2}{T_1} = \left(1 + \frac{\gamma-1}{2} M^2\right)^{-1} \quad \text{... 23}$$

we can obtain the following equation for the mass flow rate:

$$\dot{m} = \frac{AP_1}{\sqrt{T_1}}\sqrt{\frac{\gamma}{R^*}} M \left((1 + \frac{\gamma-1}{2} M^2\right)^{-\left(\frac{\gamma+1}{2(\gamma-1)}\right)} \quad \text{... 24}$$

Operating conditions	
Inlet temperature	27C (300.15K)
Inlet flow rate	560 std litres/min
Inlet pressure	10 MPa
Molecular weight of gas	18.08
Specific heat ratio	1.72
Calculated nozzle parameters	
Speed of sound	409 m/s
Orifice size	0.70 mm

Table 3-1 Estimated nozzle sizing for dehydration vessel

At the condition of choking flow (*M=1*) this simplifies to:

$$\dot{m} = \frac{AP_1}{\sqrt{T_1}}\sqrt{\frac{\gamma}{R^*}}\left(\frac{\gamma+1}{2}\right)^{-\left(\frac{\gamma+1}{2(\gamma-1)}\right)} \quad \text{... 25}$$

The nozzle sizing can then be calculated so that choking flow occurs at the maximum mass flow rate. Table 3-1 shows the operating conditions and calculated nozzle parameters for the nozzle required by the dehydration vessel for the dehydration experiments assuming the use of the maximum capacity of the compressor.

See Appendix B.1.1 for the detailed calculation.

3.4.1.3 Enthalpy calculation

Values for enthalpy of individual gas components have been measured experimentally for all natural gases of interest to this project. This data is available in tabular form from various sources such as the NIST-JANAF thermo chemical tables and online from NIST[59].

To allow for the automatic calculation of enthalpy a mathematical approach relating enthalpy to pressure and temperature is required. There are many works in literature which present equations of state that allow enthalpy to be calculated from the pressure and temperature.[68]

Enthalpy of ideal mixtures can be calculated by molar concentration:

$$h_{mixture} = \sum_i y_i . h_i \quad \text{... 26}$$

where $h_{mixture}$ is the calculated mixture enthalpy, h_i and y_i are the enthalpy and mole fraction of component *i.*

Enthalpy can be corrected for real gases by using a correlation based on three parameter corresponding states principles developed by Pitzer et al. [69, 70], who introduced the acentric factor (*ω*), and extended by Lee and Kesler [71] who introduced an improved method of calculating the acentric factor and defined a departure function for the enthalpy of mixtures.

The Lee and Kesler method for calculating the enthalpy correction (H - H*) for real gas mixtures such as natural gas uses the following departure equation:

$$\frac{H-H^*}{RT_c} = T_r\left\{Z - 1 - \frac{b_2 + 2b_3/T_r + 3b_4/T_r^2}{T_r V_r} - \frac{c_2 - 3c_3/T_r^2}{2T_r V_r^2} + \frac{d_2}{5T_r V_r^5} + 3E\right\} \quad \text{... 27}$$

where,

$$E = \frac{c_4}{2T_r^3\gamma}\left\{\beta + 1 - \left(\beta + 1 + \frac{\gamma}{V_r^2}\right)\exp\left(-\frac{\gamma}{V_r^2}\right)\right\} \quad \text{... 28}$$

T_c is the critical temperature and Z is the compressibility calculated using a modified BWR equation of state:

$$Z = \left(\frac{P_r V_r}{T_r} \right) = 1 + \frac{B}{V_r} + \frac{C}{V_r^2} + \frac{D}{V_r^5} + \frac{c_4}{T_r^3 V_r^2} \left(\beta + \frac{\gamma}{V_r^2} \right) \exp\left(- \frac{\gamma}{V_r^2} \right) \quad \text{... 29}$$

where,

$$B = b_1 - b_2 / T_r - b_3 / T_r^2 - b_4 / T_r^3, \quad C = c_1 - c_2 / T_r + c_3 / T_r^3 \ and \quad D = d_1 + d_2 / T_r$$

The departure equation above is evaluated twice, once for a simple fluid and once for a reference fluid, using the same values for the reduced temperature and volume properties T_r, V_r.

The enthalpy departure for the fluid of interest is then obtained using the equation:

$$\left[\frac{\left(H - H^* \right)}{RT_c} \right] = \left[\frac{\left(H - H^* \right)}{RT_c} \right]^{(0)} + \frac{\omega}{\omega^{(r)}} \left(\left[\frac{\left(H - H^* \right)}{RT_c} \right]^{(r)} - \left[\frac{\left(H - H^* \right)}{RT_c} \right]^{(0)} \right) \quad \text{... 30}$$

where the superscripts (*0*) and (*r*) refer to the results of the enthalpy departure equation evaluation for the simple and reference fluids, $\omega^{(r)}$ is the acentric factor of the reference fluid (0.3978) and ω is the acentric factor of the fluid of interest.

The acentric factor is calculated using a reduced vapour pressure equation using the normal boiling point temperature of the gas in question.

$$\omega = \frac{\ln P_{br}^s - 5.92714 + 6.09648 / T_{br} + 1.28862 \ln T_{br} - 0.169347 T_{br}^6}{15.2518 - 15.6875 / T_{br} - 13.4721 \ln T_{br} + 0.43577 T_{br}^6} \quad \text{... 31}$$

T_{br}, P_{br} are the reduced normal boiling point temperature and pressure

The constants used in the calculations are:

Constant	Simple Fluids	Reference Fluids	Constant	Simple Fluids	Reference Fluids
b_1	0.1181193	0.2026579	c_3	0.0	0.016901
b_2	0.265728	0.331511	c_4	0.042724	0.041577
b_3	0.154790	0.027655	$d_1 \times 10^4$	0.155488	0.48736
b_4	0.030323	0.203488	$d_2 \times 10^4$	0.65392	0.0740336
c_1	0.0236744	0.0313385	β	0.65392	1.226
c_2	0.0186984	0.0503618	γ	0.060167	0.03754

Table 3-2 Lee Kesler acentric factor equation constants

3.4.1.4 Inversion curve calculation using the Peng-Robinson equation of state

Inversion curves can also be defined by the equation:

$$T\left(\frac{\partial P}{\partial T}\right)_v + v\left(\frac{\partial P}{\partial v}\right)_T = 0 \quad \text{... 32}$$

When this inversion condition is applied to the Peng-Robinson equation we obtain the following equation[72]:

$$\begin{aligned} 0 &= T_r\left[\Omega_a m^2 (x-1)^2 (x^2+1) - \Omega_b (x^2+2x-1)^2\right] \\ &+ T_r^{0.5}\left[-\Omega_a m(1+m)(x-1)^2(3x^2+2x+1)\right] \\ &+ \left[2\Omega_a (1+m)^2 x(x+1)(x-1)^2\right] \quad where\ x = v/b \end{aligned} \quad \text{... 33}$$

As *m* can be calculated from the acentric factor of the gas using Peng-Robinson, the reduced inversion temperature at any dimensionless volume *x* can be calculated using the above equation.

The reduced Pressure is then calculated using the equation:

$$P_r = \left(\frac{T_r}{\Omega_b (x-1)}\right) - \left[\frac{\Omega_a \alpha(T_r,\omega)/\Omega_b^2}{x(x+1)+(x-1)}\right] \quad \text{... 34}$$

A reduced inversion curve can then be plotted against reduced pressure and reduced temperature. Dilay et al[73] plotted the reduced inversion curves for several equations of state including Peng-Robinson (PR) against experimental data as shown below (for nitrogen).

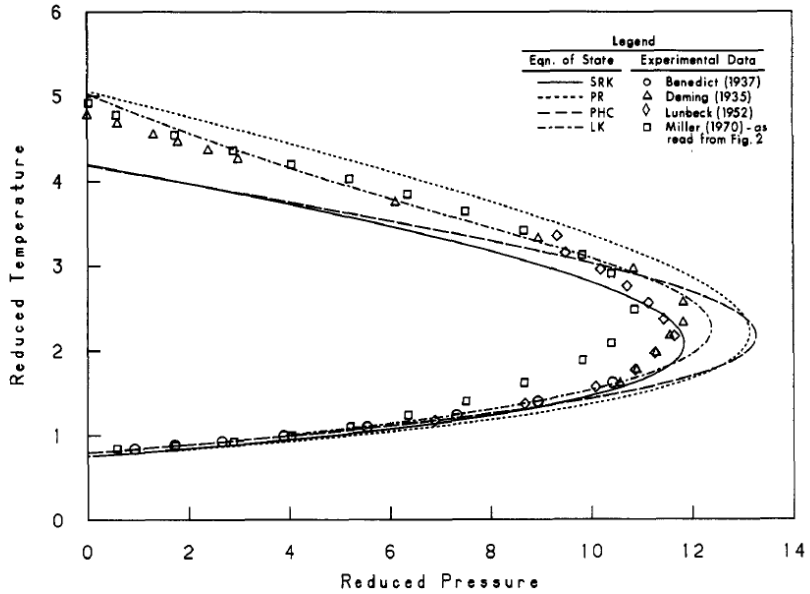

Figure 3-3 Reduced inversion curves for nitrogen using various equations of state

An excellent correlation between Peng Robinson EOS and experimental data is found at low reduced temperatures and pressures. Further work by Dilay that investigated the affect of different acentric factors also showed excellent correlation at low reduced temperatures and pressures but larger divergence at higher temperatures and pressures.

The region on the reduced temperature/pressure plot at which subsea natural gas dehydration operations will take place are at reduced temperatures between 1.2 and 1.5, and reduced pressures between 1.2 and 2.3. These points fall in the region where the Peng-Robinson EOS provides accurate predictions. All the points fall within the region of positive Joule-Thomson coefficients so using adiabatic expansion of the gases will for all gas conditions cause a drop in the temperature of the gas as required by the proposed dehydration process.

3.4.1.5 Joule-Thomson Coefficients

Using HYSYS[74] configured to utilise the Peng Robinson EOS the Joule-Thomson (JT) coefficient for the studied natural gas compositions can be determined for the pressures and temperatures to be encountered by the dehydration process.

The figure below shows the calculated JT coefficients for two West Australian gas fields, Macedon with a high methane content (99.5% of hydrocarbon content) and the richer Gorgon gas (methane 94.5% of hydrocarbon content). It is interesting to note that the richer gas has higher values for the JT coefficient so will require less expansion pressure drop to obtain the same temperature drop as the leaner gas.

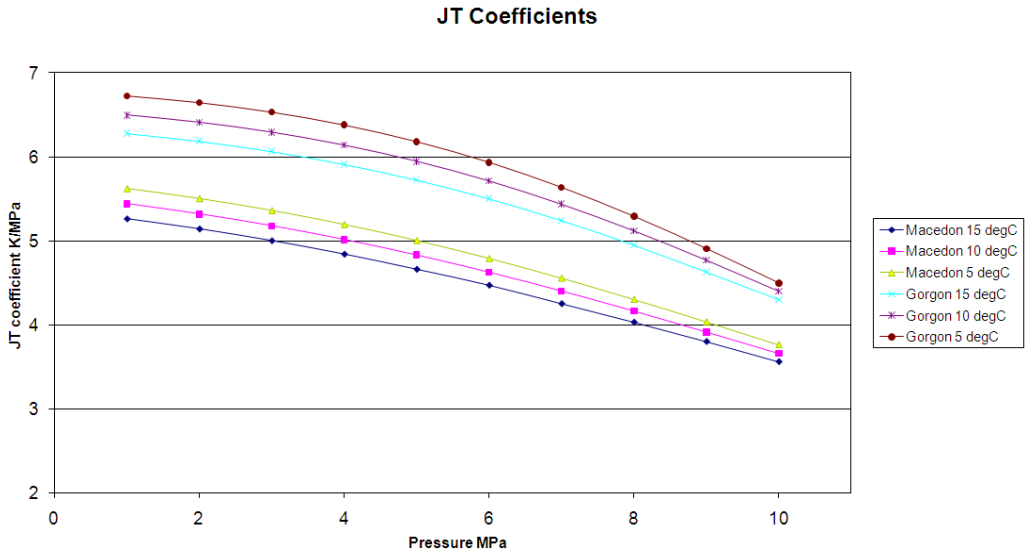

Figure 3-4 Joule-Thomson coefficients for Gorgon and Macedon gas streams

Over the region of interest we can expect a JT coefficient between 3.5 and 6 K/MPa pressure drop.

3.4.2 Gas hydrate depression of water content

This section provides an introduction to gas hydrates, the processes involved in their formation, the conditions under which they may form and the resultant water content of gases when in contact with hydrates.

3.4.2.1 What are gas hydrates?

Gas hydrates are crystalline solids composed of a number of water molecules that make up a cell that contains a guest molecule of gas. The water molecules utilise hydrogen bonding to form the cells and van der Waals forces to interact with the guest molecule. Two types of cages can be formed, small cages that are dodecahedron (12-sided) in shape and large cages that are tetrakaidecahedrons (14-sided). The larger cages can contain larger gas molecules than the small cages.

Two hydrate structures are most commonly encountered in the petroleum industry, structures I and II, type H is much less common. In a hydrate not all the cages are necessarily filled so the chemical composition is stochastic. Table 3-3 provides a comparison of type I and II hydrates.[75]

Property	Type I	Type II
Water molecules per unit cell	46	136
Cages per unit cell		
Small	2	16
Large	6	8
Cavity diameter (Å)		
Small	7.9	7.8
Large	8.6	9.5
Volume of Unit cell (m^3)	$1.728x10^{-27}$	$5.178x10^{-27}$
Typical formers	CH_4, C_2H_6, H_2S, CO_2	C_3H_8, i-C_4H_{10}, N_2

Table 3-3 Comparison of hydrate structures

Hydrates can form under pressure at much higher temperatures than ice as illustrated in Figure 3-5 that shows hydrate formation curves for various natural gas compositions.

3.4.2.2 Hydrate formation

When the temperature of a natural gas mixture falls below the hydrate formation temperature, hydrates can form from water and gas molecules. The hydrate formation temperature is dependent on the composition of the gas and the pressure and the availability of water in the liquid form.

Statistical thermodynamics can be used to predict the conditions at which hydrates can begin to form, i.e. the pressure and temperature condition at which ice or water is in equilibrium with hydrates.

The initial work to develop the thermodynamic equations was performed by van der Waal and Platteeuw who developed the following equations[76]:

$$\Delta\mu_w^H = -RT\sum_m v_m \ln\left(1-\sum_j \theta_{mj}\right) \quad \text{... 35}$$

where $\Delta\mu_w^H$ is the change of chemical potential as hydrate is formed, v_m is the number of cavities of type *m* per water molecule in the lattice and the fraction of type *m* cavities occupied by a guest gas molecule, *j* is given by:

$$\theta_{mj} = \frac{C_{ml} f_l}{1+\sum_j C_{mj} f_j} \quad \text{... 36}$$

where *f* is the fugacity and C_{ml} is the Langmuir constant given by the equation:

$$C(T) = \frac{4\pi}{kT}\int_0^\infty \exp\left[\frac{-w(r)}{kT}\right] r^2 dr \quad \text{... 37}$$

where *k* is Boltzmann's constant *T* is absolute temperature and the the Leonard Jones potential model was used to calculate $w(r)$. Parrish and Prausnitz[77] found that the Kihara potential with a line of spherical core gave better results than the Leonard Jones approach and subsequently redefined $w(r)$ as follows:

$$\mathrm{w(r)} = 2z_c\varepsilon\left[\frac{\sigma^{12}}{R_c^{11} r}\left(\delta^{10}+\frac{a}{R_c}\delta^{11}\right)-\frac{\sigma^6}{R_c^5 r}\left(\delta^4+\frac{a}{R_c}\delta^5\right)\right] \quad \text{... 38}$$

where $$\delta^N = \left[\left(1-\frac{r}{R_c}-\frac{a}{R_c}\right)^{-N}-\left(1+\frac{r}{R_c}-\frac{a}{R_c}\right)^{-N}\right]/N \quad \text{... 39}$$

z is the coordination number, ε is the characteristic energy, *a* is the core radius, $\sigma+2a$ is the collision radius and R_c is the cell cavity radius. Using experimental data Parrish and Prausnitz calculated Kihara parameters $(a, \sigma \text{ and } \varepsilon/k)$ for hydrate-gas interactions. They also extended the equation to predict hydrate formation for gas mixtures. This was found by Ng and Robinson[78] to be unreliable for gas mixtures with a tendency to predict a dissociation pressure that is too high, particularly when the concentration of the smaller hydrate forming molecule was high. Ng and Robinson proposed a modification to the

equations by the addition of a binary interaction parameter, α. The proposed equation for gas mixtures using this parameter is:

$$\Delta\mu_w^L = RT\left[\prod_j\left\{1+3(\alpha_j-1)y_j^2-2(\alpha_j-1)y_j^3\right\}\right].\left[\sum_m v_m \ln\left(1+\sum_j C_{mj} f_j\right)+\ln x_w\right] \quad \text{... 40}$$

where x_w is the mole fraction of water in the liquid phase and y_j is the mole fraction of j in the gas phase. Ng and Robinson published values for the binary interaction parameter for a number of gas pairs.

Later work, also by Ng and Robinson[79], recalculated Kihara parameters utilising the Peng Robinson EOS to calculate the fugacities rather than the Redlich Kwong EOS previously used by Parrish and Prausnitz.

For predicting the Hydrate formation curve of natural gas mixtures this project will utilise the equations developed by Ng and Robinson and using the Peng Robinson EOS.

3.4.2.3 Prediction of hydrate formation for Australian natural gas mixtures

Using the composition data for a range of Australian natural gas streams and HYSYS[80] configured to use the Ng and Robinson thermodynamic equations and Kihara potentials the predicted hydrate formation conditions have been calculated. The results are shown in Figure 3-5.

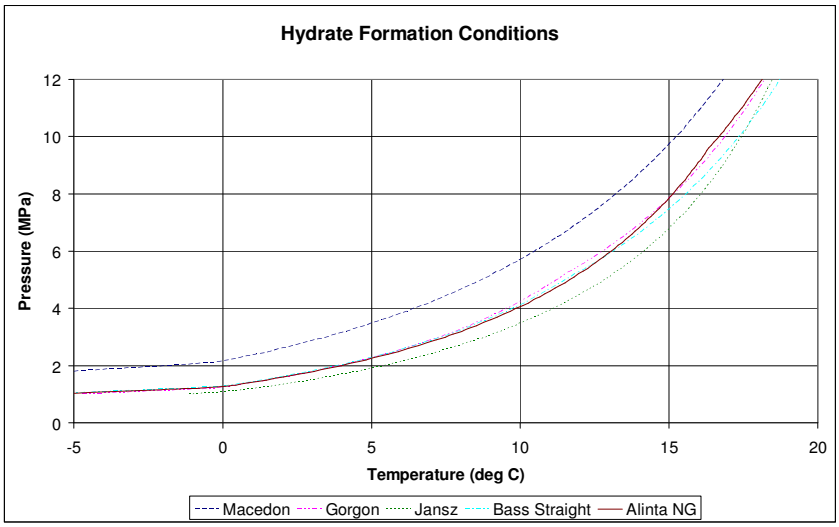

Figure 3-5 Hydrate formation curves for various Australian natural gas streams

For hydrates to form the pressure and temperature conditions must be to the left of the hydrate formation curve.

3.4.2.4 Hydrate kinetics

When Hydrates will form and at what rate is not predicted by the formation curve.

The rate of hydrate formation is affected by the combined effects of heat, transport and reactions.[81] Cooling is required to remove the heat of hydrate formation. Transport is required for natural gas to dissolve in available liquid water and to bring it into contact with growing hydrate crystals. Reactions concerned are the chemical kinetics of hydrate crystal growth.

Models that predict time dependant hydrate growth characteristics are typically an order of magnitude less accurate than the non-time dependant thermodynamic effects[82]. Two stages of hydrate growth are looked at separately; the nucleation time for hydrates to form a stable seed; and the growth phase on these stable seeds. The nucleation time depends on the system conditions including history and the predictions are somewhat unreliable. The nucleation time can vary from sub-minute to days. The growth rate prediction is more reliable depending largely on the more predictable rate at which guest gas molecules are delivered to the growing hydrate mass.

3.4.2.4.1 *Hydrate nucleation*

Studies of supercooled water suggest that water molecules cluster together due to hydrogen bonding as the temperature decreases around the freezing point.[82] This structuring could be the starting point for the hydrate nucleation process. When guest gas molecules of suitable size are present the structures can capture a single gas molecule and form a labile cluster. Theory suggests that these clusters will either grow or agglomerate into a small hydrate nucleus. The stability of this nucleus is dependent on its size and will only be stable once it reaches a critical radius. The definition of this radius depends on the type of nucleation, homogeneous nucleation in the absence of impurities or heterogeneous nucleation in the presence of a foreign body (e.g. dust) or a surface (e.g. fluid interface, vessel wall). The equations for the critical radius and Gibbs energy barrier that must be surmounted for hydrate seed stability are:

Homogeneous nucleation: $$r_c = \frac{-2\sigma}{\Delta g_v}, \quad \Delta G_{crit} = \frac{4}{3}\pi\sigma r_c^2 \qquad \text{... 41}$$

Heterogeneous nucleation: $\Delta G'_{crit} = \phi \Delta G_{crit}$, $where\ \phi = \left[(2+\cos\theta)(1-\cos\theta)^2\right]/4$ ... 42

where σ is the surface tension, Δg_v is the free energy change per unit volume and θ is the angle of contact between the hydrate crystal and the surface.

The published value for the critical radius of methane hydrate using these equations is around 32Å.

The Gibbs energy barrier for stable heterogeneous nucleation varies according to the wettability between 0 at complete wetting to ΔG_{crit} for complete non-wetting of hydrate to the surface. Thus heterogeneous nucleation occurs much easier than homogeneous nucleation.

The hydrate nucleation process is thought to be analogous to crystallisation processes such as the precipitation of salt from a concentrated solution. In crystallisation theory there are three regions:

- a region where the concentration of salt is below the maximum concentration (under-saturated) and crystals do not occur
- a region where the concentration is significantly above the maximum concentration (supersaturated) and crystallisation is spontaneous
- a metastable region between the under-saturated and supersaturated regions where spontaneous crystallisation is unlikely but if a seed crystal were inserted growth on the seed would occur.

With hydrate formation the analogous under-saturated zone is the region to the right of the hydrate formation curve. A metastable region is hypothesised to be present but current knowledge cannot predict where the metastable region ends and the supersaturated zone begins.

Nucleation of hydrate seeds are thought to occur readily in the supersaturated region due to high driving forces but much more slowly in the metastable region where the driving forces are lower.

Nucleation driving forces

A model based on the molar change of Gibbs energy of a system when hydrates are formed was developed by Christiansen and Sloan[83] that is applicable to gas mixtures:

$$\Delta G^{\exp} = n_w \left(v_w - v_h\right)\left(P^{eq} - P^{\exp}\right) + RT\sum\left(n_i\right)\ln\left[f_i^{eq} / f_i^{\exp}\right] \quad \text{... 43}$$

$$\Delta g = \Delta G^{\exp} / n_w \quad \text{... 44}$$

where n_w is the number of moles of water consumed, v_w, v_h the molar volume of water and hydrate and f_i^{eq}, $f_i^{\exp}$ are the fugacity of component *i* in the gas mixture at equilibrium and experimental conditions.

Using the Gibbs-Helmholtz relation in isobaric conditions this equation can be simplified to relate the Gibbs free energy to the temperature difference and entropy *s*:

$$\Delta g = \left(-s\right)\Delta T \quad \text{... 45}$$

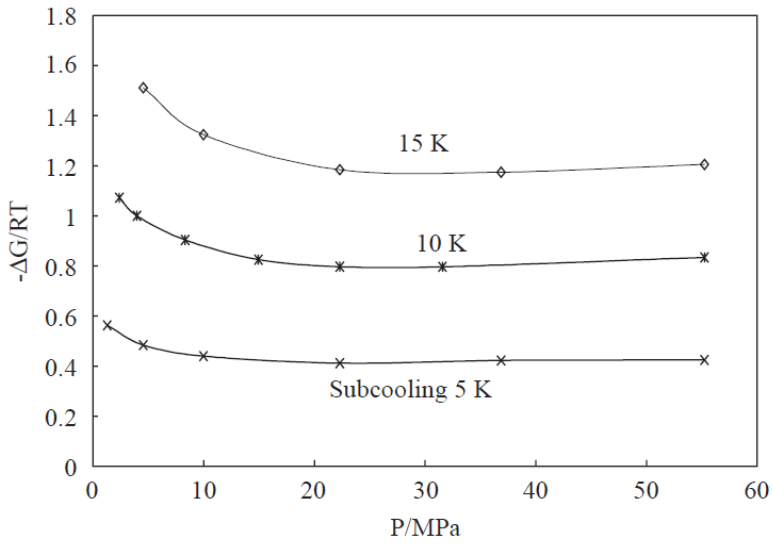

Figure 3-6 Driving force for hydrate formation in a natural gas – water system

Arjimandi et al[84] reviewed this equation and showed that whilst the driving force for a simple hydrate is to a reasonable approximation proportional to the temperature difference, the driving force for a double hydrate is only proportional to temperature at high pressures (above 20 MPa). At lower pressures it was found that in isothermal conditions the driving force is greater at lower pressures as illustrated by the diagrams taken from their paper.

In isobaric conditions the driving force is shown to be linear with the temperature difference. The change in driving force due to pressure change can be seen as a change in slope of the isobars.

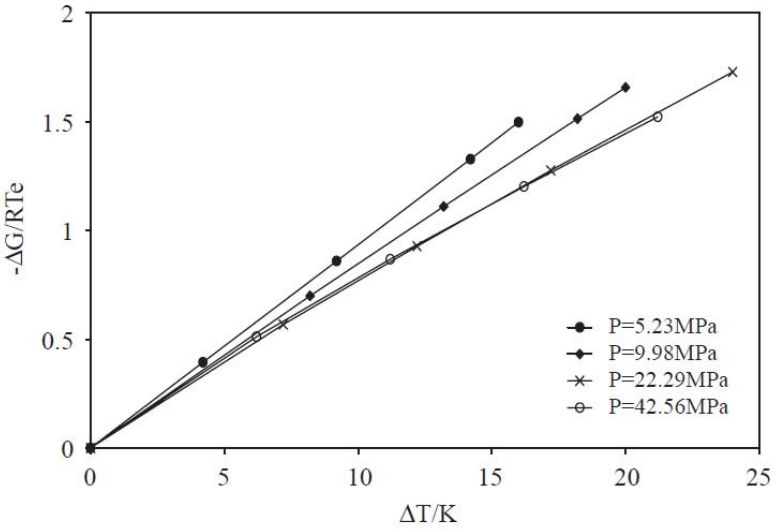

Figure 3-7 Driving force vs. sub-cooling at isobaric conditions for a natural gas mixture

3.4.2.4.2 *Temperature differential driving force for JT expansion of natural gas*

The design intent of the dehydration reactor is to take gas at just outside hydrate formation conditions, expand it through a Joule-Thomson choke reducing the pressure and thereby inducing cooling of the gas so that it enters the hydrate formation region.

Taking an example gas composition of a lean gas well (Macedon) the hydrate formation conditions, JT cooling and resultant temperature differential driving force can be plotted.

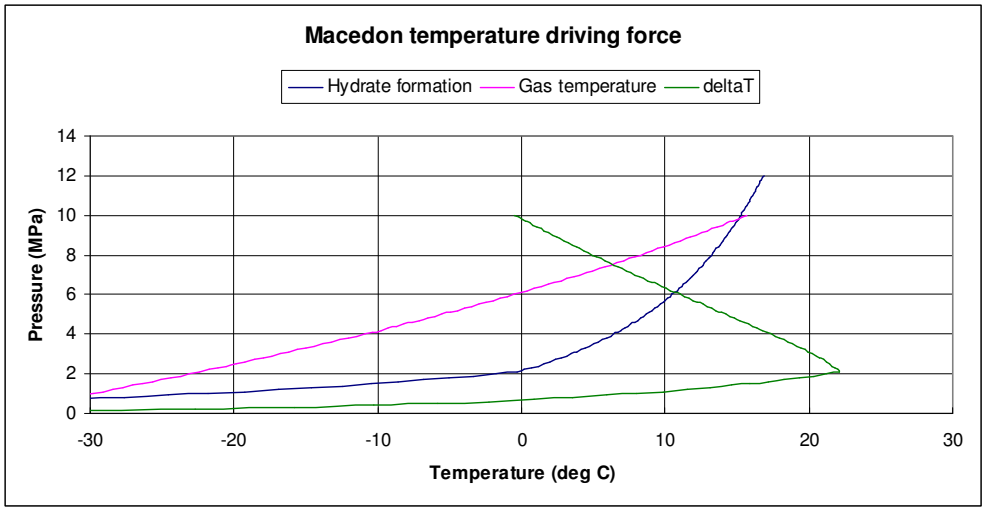

Figure 3-8 Temperature differential driving force for Macedon gas for 10MPa, 15.7C starting conditions

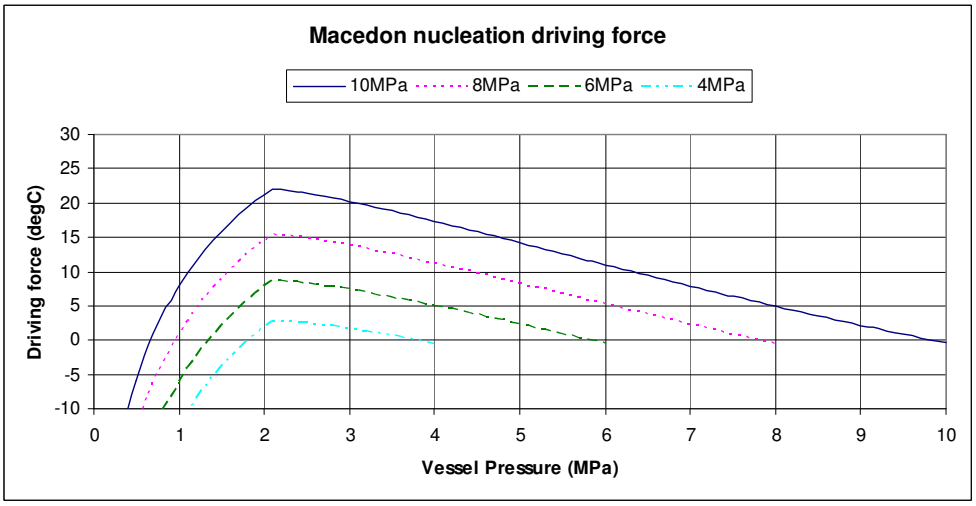

Figure 3-9 Macedon nucleation driving force at different gas input conditions

The hydrate formation line is calculated by HYSYS using the Macedon gas composition and the correlations of Ng and Robinson. The Gas temperature is the resultant temperature of the gas caused by the expansion through the JT choke. The 'delta T' line is the difference between the hydrate formation temperature and the gas temperature. When different starting

conditions of Pressure and temperature (0.5 C above hydrate formation temperature) are considered the following plot was obtained.

The shape of these curves vary with the gas composition, a richer gas such as Gorgon gives a curve set with higher temperature drive for the same operating conditions as a leaner gas.

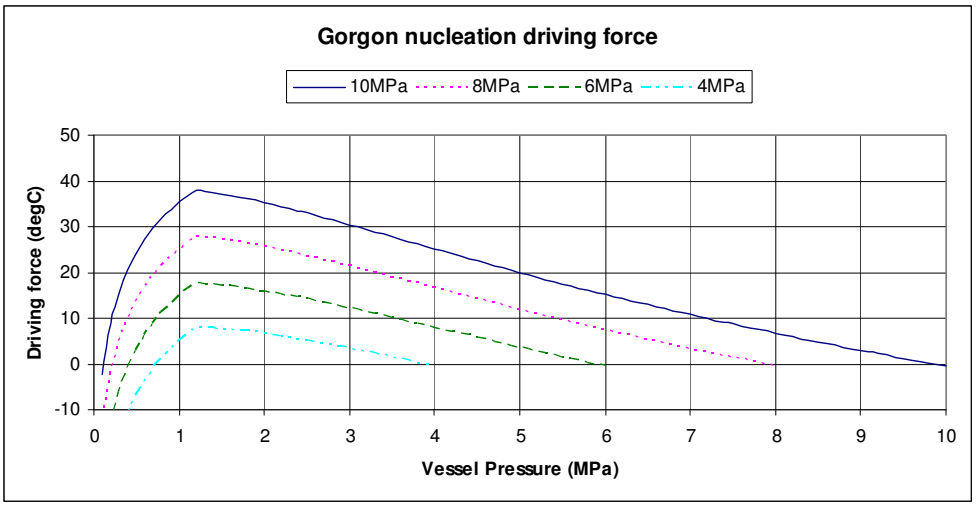

Figure 3-10 Gorgon nucleation driving force at different gas input conditions

3.4.2.4.3 *Nucleation correlations*

According to Sloan[85], there is substantial evidence that the hydrate nucleation process cannot be accurately predicted within the metastable region due to the lower driving forces of overpressure or sub-cooling.

The principle reasons that accurate correlations have failed to be developed are due to the nature of the nucleation process:

- nucleation is stochastic and consequently unpredictable
- measured nucleation times appears to be apparatus dependant
- nucleation time is affected by time dependant variables:
  - the history of the water, forming quicker in water from dissociated hydrates
  - presence of foreign particles
  - composition of the gas

3.4.2.4.4 *Nucleation considerations for an industrial subsea dehydration reactor*

When we consider the operating process and the industrial-type equipment utilised in this project there are a number of system factors that will affect the nucleation time of the hydrates utilised for dehydration.

Affect of impurities on induction time

An interesting study on the effect of impurities on nucleation of ethane hydrates was performed by Bylov and Rasmussen[86] that found that the induction time is extremely sensitive to the presence of impurities and that with the deliberate addition of impurities to experimental equipment the induction time is nearly instantaneous.

Particulate production is an inevitable consequence of fluid flow in wells including all gas wells.[87] Particulates may be inorganic including sand, clay and precipitated materials, such as carbonates and sulphates, or organic semi-soluble deformable particulates, such as asphaltenes, resins and paraffin waxes.

Most of the particles can be removed from the gas stream using separators upstream from the dehydration system. Cyclonic separators are used extensively for liquid and particle removal from gas streams. Due to their relatively small size and lack of moving parts cyclonic separators are ideal candidates for subsea operations and some trials are currently underway.[88] They provide particle removal efficiencies of up to around 96% capturing the larger particles but allowing some typically sub-micron particles to continue on in the gas stream.[89] These fine particles could act as seeding agents for hydrate formation in systems downstream from the separator.

This presence of seeding materials in the gas stream suggests that the long unpredictable induction time encountered in laboratory experiments may not be relevant to our industrial-type experimental setup and we could find that hydrates form as soon as conditions conducive to formation are encountered.

Memory effect on hydrate nucleation time

The nucleation time of hydrates is significantly affected by the history of the water. Experiments performed by Vysniauskas and Bishnoi[90] demonstrated that the nucleation time in a stirred reactor varied according to the source and history of the water with nucleation times of several minutes for distilled, hot or cold tap water, less than a minute for thawed ice and immediate for recently dissociated hydrate.

The dehydration reactor is designed to operate in a continuous mode, with the controlled management of hydrate growth and dissociation. The temperatures within the vessel will ensure that liquid water in the vessel as a result of hydrate dissociation will present the memory effect and show immediate nucleation once hydrate formation conditions are re-encountered.

Dehydration reactor operation

There are three operational modes that must be analysed in regards to the implications of hydrate nucleation times.

- Normal dehydration operations

- Warm start when system operations are recommenced after a shutdown
- Cold start of system after commissioning or major overhaul

During normal dehydration operations, hydrates will always be present within the reactor and zones of the reactor that have recently had the hydrate dissociated will be moist with water that will present the memory effect. In this operating mode the system is driven by hydrate growth rates and any nucleation time is not likely to have any significant impact.

During system shutdowns, the pressure and temperature conditions within the reactor may change to a point where dissociation of the hydrate in the vessel will occur. In subsea conditions it is unlikely that the temperature in the vessel will ever reach a level where the residual water in the vessel will lose its memory effect properties. During a warm start the memory effect will ensure a short nucleation time and the reactor should resume normal operations driven by the hydrate growth rate soon after start-up.

There are a number of approaches that can be taken to commission and commence first dehydration operations i.e. cold start. The approach taken will depend on system conditions such as seawater temperature, inlet gas stream pressure and temperature, gas composition and upstream heat exchanger configuration. The nucleation time for hydrate formation will be a consideration when designing the optimum start up procedure.

Industrial experience has demonstrated that hydrate nucleation is typically instantaneous in fluid flow environments when a sub cooling in the region of 5C is encountered.

3.4.2.4.5 *Hydrate growth*

Extensive research has been done on hydrate growth rates and models developed, with the majority of work relating to hydrate formation in stirred reactors[91-93] but with some work also relating to spray reactors[94].

The direct applicability of these models to the growth of hydrates in a system where water availability is driven by condensation due to cooling is considered unreasonable. However, a study of these models does give an insight into the factors that are likely to impact the rate at which hydrates will form.

The models of Englezos et al.[91], Skovborg-Rasmussen[92] and Herri et al.[95] relate to stirred reactors and concentrate on the rate at which gas molecules are transferred from the vapour phase to the liquid-hydrate interface. The model of Gnanendran-Amin[94], based on the work of Kashchiev-Firoozabadi[96], relates to a batch-spray reactor with the super saturation of gas molecules in the aqueous phase as the driving force. Ribeiro and Lage[97] reviewed the existing models and concluded that the rate at which hydrates grow once the nucleation has occurred is affected by a number of factors:

- Heat transfer processes due to the formation of hydrates being exothermic. As hydrates are formed the heat generated causes the temperature of the liquid-hydrate interface to increase. The rate at which this heat is removed impacts the rate at which hydrates will form.

- Mass transfer of gas molecules from vapour phase through vapour-liquid interface to liquid-hydrate interface. Due to low solubility of hydrocarbon gases in water this has a major impact on the hydrate growth rate.

- Driving force for nucleation at the operating temperature and pressure.

- Hydrate particle size distribution, including breakage and agglomeration.

- The history effect that impacts nucleation time has no impact on hydrate growth rates.[91]

Heat transfer

The formation of gas hydrate is an exothermic process that may be expressed by the equation:

$$Gas + n_h H_2O(ice\ or\ liquid) \Rightarrow Hydrate(s)$$
$$\downarrow$$
$$Heat$$

, where n_h is the hydration number

The process is heat-transfer limited where heat generated during formation changes the temperature and pressure at the formation location and will, if the generated heat is not removed, ultimately change the local conditions such that hydrates formation will cease.[98] For continuous growth of hydrates the system requires a suitable heat transfer design to remove the generated heat.

In the presence of an excess gas phase the enthalpy change due to hydrate formation can be calculated to a reasonable approximation using the Clausius-Clapeyron equation:

$$\frac{d\ln(p)}{d\left(1/T\right)} = \frac{\Delta h^f}{zR} \quad \text{... 46}$$

Figure 3-11 shows the enthalpy of formation for the Macedon field using the Clausius-Clapeyron equation with values of z calculated at each formation condition using the Peng Robinson EOS and hydrate formation curve using the correlation of Ng and Robinson.

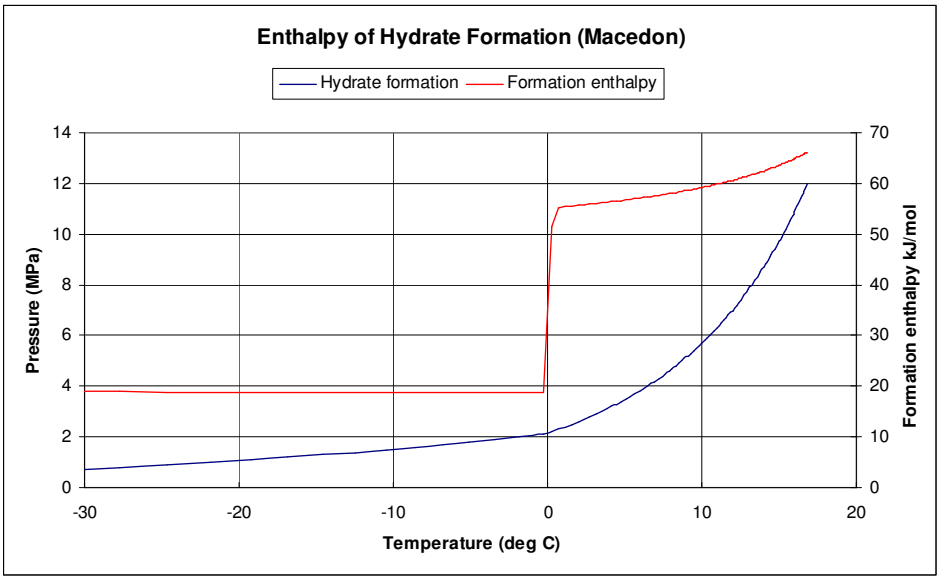

Figure 3-11 Enthalpy of formation for Macedon gas stream

The plot shows the discontinuity in the hydrate formation enthalpy at the ice-liquid water transition and predicts a gradual increase in formation enthalpy as the formation temperature increases.

The heat generated in the dehydration reactor through hydrate formation will need to be removed if continuous dehydration operations are to be possible. The heat will be removed in two principle ways, via conduction and convection with the gas phase passing through the reactor and via conduction through the hydrate layer and the vessel wall to the sea water where conduction, convection and radiation will dissipate the heat. See section 4.4.2.2 for a more in-depth discussion of the thermal design of the dehydration reactor.

Mass transfer

Mass transfer of the gas molecules from the vapour phase to the growing hydrate phase is a function of how much and how fast, that is the amount of gas in the liquid phase or solubility of natural gas in water, the diffusion rate from the vapour-liquid interface to the liquid-hydrate interface and the interfacial area.

The solubility of natural gas in water is affected by both the temperature and the pressure, increasing as the pressure increases and the temperature decreases.[99]

The diffusion rate is driven by the changes in concentration between the gas-liquid interface and the Hydrate-liquid interface.

The interfacial area of greatest interest in hydrate formation kinetics is the gas-liquid interface, where the super-saturation of gas in the liquid water is high enough for crystallisation processes to occur.[90] The greater the interfacial area, the higher the hydrate formation rate.

Driving force

The driving force for hydrate growth is the temperature differential between the dehydration reactor gas temperature and the hydrate formation temperature at the dehydration reactor pressure. For more details on driving force refer to section 3.4.2.4.2.

Particle size and distribution

Hydrate particle size distribution is primarily relevant when a bulk liquid phase is present and relates the growth rate to the distribution and size of particles.

3.4.2.5 Natural gas water vapour content in equilibrium with gas hydrates

A number of researchers, including Sloan[64], Song[65], Aoyagi[100] and Kobayashi[101] have measured the water content of natural gases when they are in equilibrium with hydrates and have found that the water content is considerably lower in the presence of hydrates than in the presence of metastable water. The methods used by these researchers were all batch based experiments where small test apparatus, typically less than 1 litre is used to establish equilibrium conditions between a gas phase and gas hydrates. Once equilibrium is reached the gas phase water content is measured by various techniques.

According to Sloan, the water content of natural gas in equilibrium with hydrates will vary depending on the type of hydrate structures that are formed. The formation of hydrate structures is a function of the content of the gas in question, hence a gas that contains significant quantities of gas that will form SII structure hydrate such as propane will have a different equilibrium water content to for instance pure methane that only forms SI structure hydrate. Refer to section 3.4.2.1 for details on these structures.

Mohammadi and Richon[102] have developed a semi-empirical method for determining the water content of methane-rich hydrocarbon gases in equilibrium with gas hydrates at temperatures in the region of 196 K to 270 K and pressures up to 10.34 MPa. The method estimates the water content of the gas using the vapour pressure of the empty hydrate lattice and the partial molar volume in the empty hydrate together with the system temperature and pressure. The predictions made using the developed method show excellent agreement with the independent experimental data taken from Sloan[64], Song[65], Aoyagi[100].

The gas hydrate equilibrium is calculated by equating the fugacity of the water in the two phases that are in equilibrium, i.e. the fugacity of water in the gas phase (f_w^g) and the fugacity of water in the hydrate phase (f_w^H):

$$f_w^g = f_w^H$$

The fugacity of water in the hydrate phase can be expressed as the chemical potential difference of water in the filled and empty hydrate in the following equation:

$$f_w^H = f_w^{MT} \exp\left(\frac{\mu_w^H - \mu_w^{MT}}{RT}\right) \quad \text{... 47}$$

where f_w^{MT} is the fugacity of the theoretical empty hydrate phase, and $\mu_w^H - \mu_w^{MT}$ is the chemical potential difference between the filled and the empty hydrate. Van der Waals-Platteeuw solid solution theory can be used to calculate $\mu_w^H - \mu_w^{MT} / RT$. For methane hydrates:

$$\left(\frac{\mu_w^H - \mu_w^{MT}}{RT}\right) = -\sum_i \overline{v}_i \ln(1 + C_i f_{CH_4}) \quad \text{... 48}$$

where $\overline{v}_i$ is the number of cavities of type *i* per water molecule in a unit hydrate cell, C_i is the Longmuir constant for methane's interaction with each type cavity and f_{CH_4} is the fugacity of methane in the gas phase which for simple gas hydrates including hydrates of methane can be set to pressure with good approximation at the pressures of interest. Hence we can easily get:

$$\exp\left(\frac{\mu_w^H - \mu_w^{MT}}{RT}\right) = \prod_i \left(1 + C_i P\right)^{-\overline{v}_i} \quad \text{... 49}$$

Equations for the Longmuir constants were determined to be a function of temperature with separate equations for small cavities and large cavities defined as follows:

$$C_{small} = \frac{3.7237x10^{-3}}{T} \exp\left(\frac{2.7088x10^3}{T}\right) \quad \text{... 50}$$

$$C_{large} = \frac{1.8373x10^{-2}}{T} \exp\left(\frac{2.7379x10^3}{T}\right) \quad \text{... 51}$$

According to Sloan[85] the fugacity of water in the empty lattice can be expressed by:

$$f_w^{MT} = P_w^{MT} \phi_w^{MT} \exp \int_{P_w^{MT}}^{P} \frac{v_w^{MT} dP}{RT} \quad \text{... 52}$$

If we take use the assumptions that the hydrate partial molar volume equals the molar volume and is independent of pressure and that P_w^{MT} is relatively small so that ϕ_w^{MT} is 1 then:

$$f_w^{MT} = P_w^{MT} \phi_w^{MT} \exp \frac{v_w^{MT} \left(P - P_w^{MT}\right)}{RT} \quad \text{... 53}$$

The fugacity of water in the gas phase is given by:

$$f_w^g = y_w \phi_w^g P \quad \text{... 54}$$

Using the above equations we can form the expression for calculating the water content of methane in the presence of gas hydrates:

$$y_w = \frac{P_w^{MT}}{\phi_w^g P} \exp\left[\frac{v_w^{MT}\left(P - P_w^{MT}\right)}{RT}\right] \quad x \quad \left[\left(1 + C_{small} P\right)^{-v_{small}} \left(1 + C_{l\arg e} P\right)^{-v_{l\arg e}}\right] \quad \text{... 55}$$

From Stackelberg and Müller[103]: $v_w^{MT} = 0.022655\ m^3 / kgmol$

From Sloan: $\bar{v}_{small} = \frac{1}{23} \quad and \quad \bar{v}_{l\arg e} = \frac{3}{23}$

From Dharmawardhana et al.[104] the vapour pressure of the empty hydrate structure can be expressed by:

$$P_w^{MT} = \exp\left(17.440 - \frac{6003.9}{T}\right) \quad \text{... 56}$$

The fugacity coefficient of water in the gas phase may be calculated by the equation[105]:

$$\phi_w^g = \exp\left(B'' P + C'' P^2 + D'' P^3\right) \quad \text{... 57}$$

where *B",C"* and *D"* are temperature dependent and can be satisfactorily represented by the following equations:

$$B'' = a + \frac{b}{T} \quad C'' = c + \frac{d}{T} \quad D'' = e + \frac{f}{T} \quad \text{... 58}$$

The constants *a, b, c, d, e* and *f* are calculated by regression and are published in their literature.

For high methane content hydrocarbon gases the water content can be calculated using a compensation equation as follows:

$$y_{w,\lambda} = y_{w,CH_4} \exp\left[-11.223(\lambda - 0.554) + 0.040(\lambda - 0.554)\left(\frac{P}{P_0}\right)\right] \quad \text{... 59}$$

where y_{w,CH_4} is the calculated water content of pure methane, λ is the gas gravity and P_0 is atmospheric pressure.

For temperatures in the region of 0 C to100 C a similar correlation was developed and published in the thesis of A. Chapoy from the Ecoles des Mines de Paris[66]. The correlation again uses the Poynting correction to solve the integral and defines the water content by:

$$y_w = \frac{(1-x_g)P_w^{sat}}{\phi_w P}\exp\left[\frac{v_w^L\left(P-P_w^{sat}\right)}{RT}\right] \quad \text{... 60}$$

where x_g is the gas solubility which can be assumed to be very much smaller than 1 and can be reasonably ignored. The fugacity coefficient of water (ϕ_w) can be expressed by:

$$\phi_w = \exp\left(BP_m + CP_m{}^2\right), \quad B = a + \frac{b}{T} \quad C = c + \frac{d}{T} \quad \text{... 61}$$

where P_m is the pressure in Mega Pascals, T is the temperature in Kelvin and the values for *a,b,c* and *d* for type SI and SII hydrates are given in Table 3-4.

Constant	SI hydrates	SII hydrates
a	-0.09148	0.042316
b	15.89613	-14.4573
c	-0.02518	-0.0023
d	7.3906	0.55955

Table 3-4 Coefficients for calculation of fugacity coefficient

The vapour pressure (P_w^{sat}) and molar volume of water (v_w^L) can be calculated using the relations reported by Daubert and Danner[106] and McCain[107]:

$$P_w^{sat} = 10^{-6}\exp\left(73.649 - \frac{7258.2}{T} - 7.3037\ln(T) + 4.1653x10^{-6}T^2\right) \quad \text{... 62}$$

where T is the temperature in Kelvin.

$$v_w^L = \frac{(1+\Delta V_{wP})(1+\Delta V_{wT})}{2.16122x10^{-4}} \quad m^3/mol \quad \text{... 63}$$

where, ΔV_{wP} and ΔV_{wT} are the volume changes due to pressure and temperature and can be expressed as:

$$\Delta V_{wP} = -\left(3.58922x10^{-7} + 1.95301x10^{-9}t_f\right)p - \left(2.25341x10^{-10} + 1.72834x10^{-13}t_f\right)p^2 \quad \text{... 64}$$

$$\Delta V_{wT} = 1.0001x10^{-2} + 1.33391x10^{-4}t_f + 5.50654x10^{-7}t_f{}^2 \quad \text{... 65}$$

where t_f is the temperature in Fahrenheit and p is the pressure in psia.

This correlation has been tested against experimental data from Aoyagi[100, 108] and Song[109] and shown to be accurate to a typical AD of 1% (10.2% maximum) The AAD% among all the experimental and calculated data was less than 5.1%.

We will use the above Chapoy correlation equations to predict the water content at various conditions of Temperature and Pressure of the dehydration vessel. A plot of the predicted water content in parts per million by volume for methane, a SI hydrate producer at various operating pressures is shown in Figure 3-12.

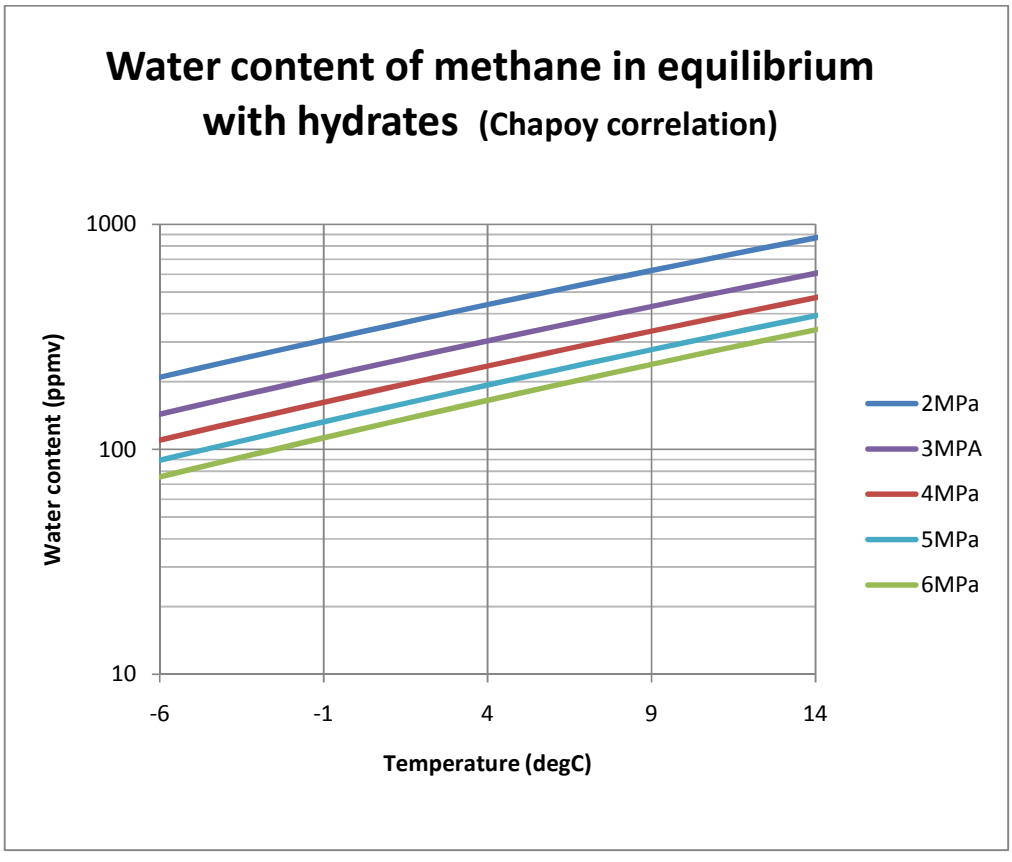

Figure 3-12 Predicted water content of methane vs. pressure and temperature

For methane rich gases a correction factor algorithm developed by Mohammadi et al. [105] using the gas gravity and temperature can be used to predict the water content.

$$F_{hh} = 1 + b_1(\gamma - 0.554) + b_2(\gamma - 0.554)\left(\frac{T}{T_0}\right) + b_3(\gamma - 0.554)^2\left(\frac{T}{T_0}\right)^2 \quad \text{... 66}$$

For the gas gravity $\gamma > 0.554$ and where T_0 is the reference temperature (273.15K).

3.4.3 Water droplet formation and flow

This section reviews water condensation processes, the formation of water droplets and means for their removal from the gas stream.

3.4.3.1 Gas supersaturating and condensation process

When the gas stream is cooled through the Joule Thomson effect the gas becomes supersaturated with water vapour. Liquid water will condense on cold surfaces or form droplets in the gas stream either homogeneously or heterogeneously around microscopic nuclei present in the gas. Clusters of water molecules can occur at any saturation level of a gas but it is only in conditions of super saturation that the probability of growth of the clusters is close to certainty. Super saturation, *S* is normally designated by the ratio of the vapour pressure to the saturation vapour pressure[110]:

$$S = \frac{p_v}{p_s(T)} \quad \text{... 67}$$

When we consider the expansion process of the gas stream through the inlet nozzle and apply Raoult's law the initial super saturation of the expanded gas can also be expressed as:

$$S_0 = \frac{(x_{H_2O})_{inlet}}{(x_{H_2O})_{vess_{eq}}} \quad \text{... 68}$$

where S_0 is the initial super saturation of the gas within the dehydration vessel, $(x_{H_2O})_{inlet}$ is the molar water content of the inlet gas stream and $(x_{H_2O})_{vess_{eq}}$ is the equilibrium molar water content of the gas at the dehydration vessel temperature and pressure conditions.

Using saturated gas of the experimental gas composition (see Appendix C.1 for composition data) and ignoring the effects of any hydrate formation a plot of the super saturation of the gas stream in the dehydration vessel can be plotted.

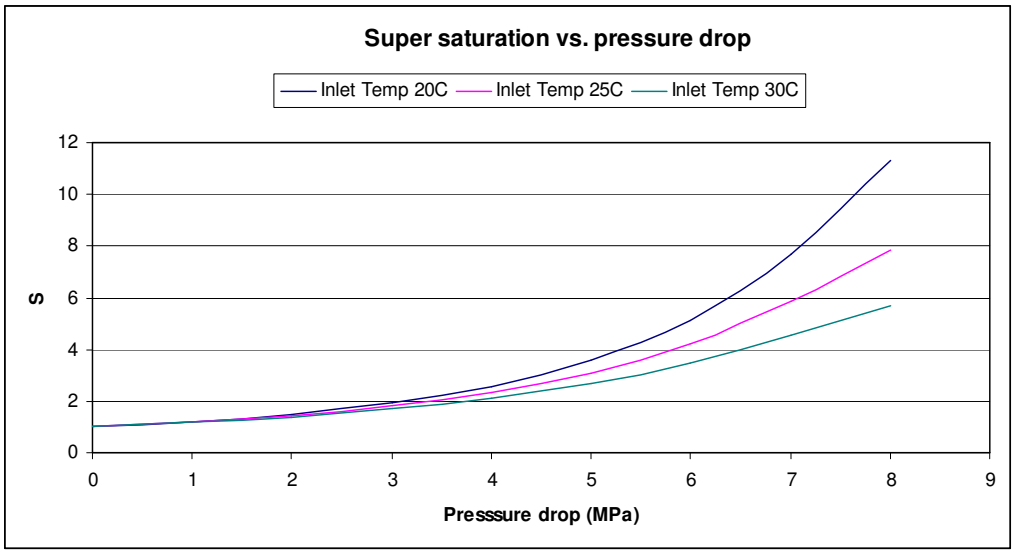

Figure 3-13 Initial super saturation of Alinta gas after expansion through nozzle

(Inlet pressure conditions: 10 MPa)

Examining the super saturation plot we can see that the initial super saturation of the gas after expansion increases with the pressure drop and decreases with increasing inlet temperature.

For clusters to grow to a stable droplet they must reach a critical size. The rate at which clusters reach this critical size per unit volume is called the nucleation rate. With homogeneous nucleation the cluster is built up completely from water molecules whilst with heterogeneous nucleation molecules build up around a nucleus. Consequently the energy barrier for homogeneous nucleation is larger than for heterogeneous nucleation and a greater super saturation is required for homogeneous nucleation to occur.

A gas stream from a well is likely to contain many small nuclei in the form of fines and hydrocarbon solids suitable to support heterogeneous nucleation of water droplets when it is suitably supersaturated. The expansion process of a gas stream in a nozzle is however primarily a homogeneous nucleation rather than heterogeneous. In a typical stream expansion $10^{15}/cm^3$ nuclei are spontaneously formed, a number that is several orders of magnitude larger than a credible number of suitable nuclei particles that may be present, consequently homogeneous nucleation will dominate.[111] The initial size of the condensed water droplets is very small, typically in the nanometre size range.

Once stable droplets have been formed a condensation growth phase commences where further vapour molecules are captured from the supersaturated gas. As the water molecules condense out of the gas stream the vapour content and the level of super saturation decrease. Also the water droplet warms up, due to the positive latent heat of condensation,

leading to an increase in the saturation vapour pressure and a further decrease in the super saturation.[110] Both nucleation and growth require time that varies with conditions so after the initial expansion there is a period of super saturation before equilibrium saturation conditions are established.

A study by Luijten[112], which included experiments using natural gas in a pulse expansion wave tube, measured the growth rate of droplet in natural gas. At pressures around 2 MPa and temperatures of around 240 K a typical droplet growth rate (radius^2) of around $2x10^{-11}$ m^2/s was measured. This corresponded closely with theoretical calculations based upon the diffusion controlled growth equation:

$$\frac{dr_d^2}{dt} = 2\frac{\rho_v}{\rho_l}\sum_{i=1}^{n} D_i (y_i - y_i^{eq}) \qquad \text{... 69}$$

where D_i denotes the diffusion coefficient, ρ_v and ρ_l the molar densities of the vapour and liquid phases, and y_i and y_i^{eq} are input and equilibrium fractions of component *i*. For the condensation of water alone *n = 1*.

Droplet radius growth through condensation processes is thus around 4.5 microns per second and the initial nanometre size droplets can grow quickly to several microns if the gas continues to be sufficiently supersaturated with water vapour.

Theoretical and practical studies on nucleation rates of water droplets in methane have been performed by Peeters[113]. His published results showing measured and theoretical nucleation rates are shown in Figure 3-14

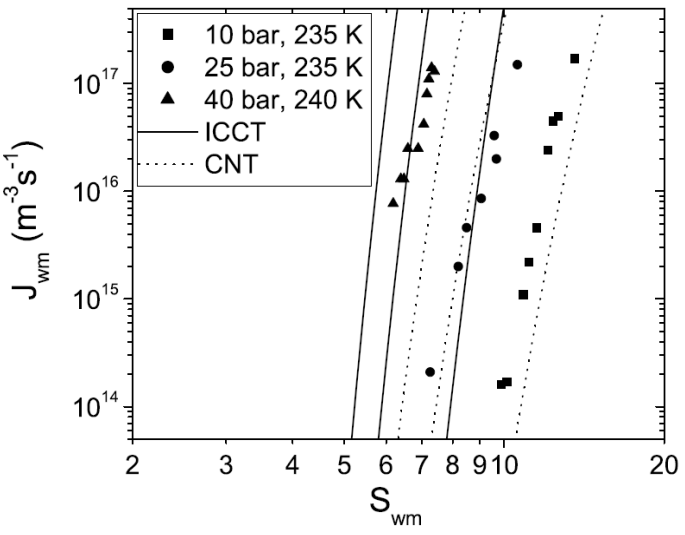

ICCT - internally consistent classical theory CNT - classical nucleation theory

Figure 3-14 Nucleation rates of water in methane vs. water super saturation[113]

Reviewing these results we can see that as the pressure is decreased the super saturation is required to increase to obtain the same nucleation rate.

Looking at conditions of 4 MPa and super saturation of 5 a nucleation rate of around $2x10^{13}$ clusters per cubic meter to be created every second can be expected. Considering the experimental parameters of the test dehydration system and the change in water content caused by the cooling process we can estimate the average size of the droplets. Assuming a constant number of droplets, i.e. no coalescence, the average diameter of a droplet when the gas stream reaches an equilibrium saturation level will be around 1.1 microns. Refer to Appendix B.1 for the calculations and additional assumptions.

3.4.3.2 Flow of condensed droplets

The movement of these condensed droplets is dependent on the gravity and drag forces applied to the droplets. The Souders Brown equation[114] was developed from studies of Fractionating columns to predict the maximum upward velocity of a gas stream in a vessel that could be established without carryover of droplets from the vessel. The Souders Brown equation equates the gravity forces with the drag forces to establish the maximum velocity and can be written as:

$$V = K\sqrt{\frac{\rho_l - \rho_v}{\rho_v}} \quad \text{... 70}$$

where ρ_l, ρ_v are the densities of the droplet and the vapour and K (the Souders Brown coefficient) is dependent on droplet size, d and drag coefficient, C_d and is expressed by the equation:

$$K = \sqrt{\frac{4gd}{3C_d}} \quad \text{... 71}$$

The Souders Brown equation is used extensively in industry when designing vessels such as gas scrubbers when particle sizes are at least of moderate sizes exceeding a few microns in diameter. The K-value is normally taken as a constant and is typically calculated empirically

When we consider the large proportion of very small particles created through condensation the Souders Brown equation is not applicable. When we consider their low Reynolds number and if we assume the droplets are spherical then Stokes law can be used to calculate terminal velocities for these smaller particles. Stokes Law defines the drag force exerted on a particle and is expressed by the equation:

$$F_d = 6\pi\mu Vd \quad \text{... 72}$$

By equating the gravity and drag force from Stokes Law the terminal velocity V_s of a spherical particle can be expressed by the equation:

$$V_s = \frac{2}{9}\frac{(\rho_p - \rho_f)}{\mu} g r^2 \quad \text{... 73}$$

where ρ_p, ρ_f are the densities of the particle and the fluid (kg/m^3), μ is the dynamic viscosity (Pa.s), g is gravity (m/s^2) and r the radius of the particle (m).

If we consider a typical lean natural gas mixture and likely vessel operating conditions we can estimate the terminal velocity of condensed water droplets within the vessel. The graph below shows typical terminal velocities for various droplet sizes with a Reynolds number, *Re < 1*.

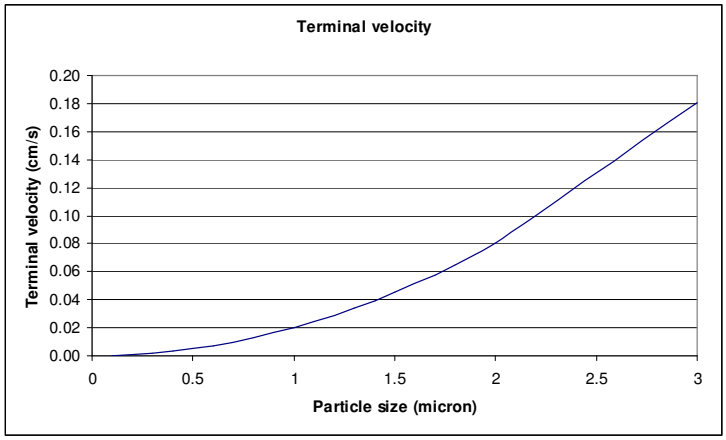

Figure 3-15 Water droplet terminal velocity

With the large population of sub-micron droplets encountered with condensation processes we can see that even very low vertical flow rates in a pressure vessel will exceed the terminal velocity and droplets will be entrained within the gas stream.

3.4.3.3 Removal of water droplets from the gas stream

To prevent entrainment of water droplets in the exiting gas stream preventative measures must be taken to either enlarge the droplets so that the terminal velocity increases and gravity separation occurs or by other physical capturing means.

Enlargement of droplets can occur by two methods, condensation of further water on an existing droplet or by coalescence when water droplets collide.

As has been discussed earlier, in the dehydration system the condensation process can produce droplets of around 1 micron fairly quickly leaving the gas saturated at the vessel

conditions. No further condensation growth can occur unless additional water vapour is added to the system and it again becomes supersaturated.

Droplet enlargement through the collision-coalescence process may increase the size of droplets. When droplets collide they may bounce, coalesce, disrupt or fragment depending on the collision kinetic energy.[115]

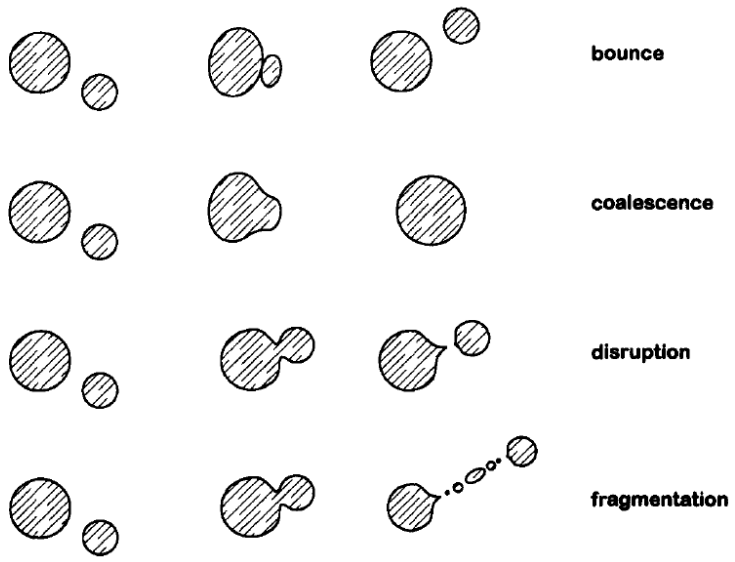

Figure 3-16 Droplet collisions and effects

When drops collide there is a film of gas between the drops which is squeezed out by the energy of the collision. If the energy is insufficient to squeeze out enough of the gas the droplets will bounce. Once enough energy is present the drops will coalesce either temporarily or permanently again depending on the collision kinetic energy. Temporary coalescence occurs when the collision kinetic energy is higher than the level for stable coalescence and disruption or fragmentation of the drops will occur.

The collision kinetic energy was defined by Low and List[116] as the following equation:

$$CKE = \frac{\rho\pi}{12}\left(\frac{D_L^3}{R_s^{\,3}+1}\right)(V_L - V_S)^2 \qquad \text{... 74}$$

where ρ is the droplet density, D is the droplet diameter, V the droplet velocity, R_s the droplet size ratio and the suffixes L and S reference the large and small droplet respectively. It can be seen from this equation that the energy decreases as the droplet ratio increases and increases as the velocity difference between the large and small droplets increases. Consequently droplets of similar diameter and moving at large differential speeds will have higher collision kinetic energy and are more likely to coalesce. Studies of droplet size distribution formed by condensation flow show a fairly narrow band of droplet sizes.[110]

This observation combined with the turbulent environment of the near sonic gas stream suggest that collision kinetic energies are likely to be high enough for some coalescence of droplets to occur within the process vessel.

To remove the entrained water droplets from the gas stream will require other interventional methods. Methods that are investigated in this research are the fitting of a physical mechanism known as a mist eliminator and a method to enhance coalescence through increasing the vessel population of droplets through spraying of condensate into the vessel.

3.4.3.4 Mist eliminator

The construction of filter type mist eliminators varies with the size of particle to be removed due to the physical capture mechanisms and the behaviour of particles of different size. There are three mechanisms to consider; direct impact, interception and diffusion.[117]

In the “direct impact” mechanism, particles 2 microns and larger in diameter have sufficient mass and momentum to leave the gas flow stream line and impact on the mesh of the filter.

With the “interception” mechanism, particles of between 0.2 and 2 microns that are too small to leave the stream line are captured by having a filter material with sufficiently small pore size.

The “diffusion” mechanism relies on the rapid random Brownian motion that is a characteristic of very small particles and can remove particles down to 0.001 microns.

A typical coalescing filter suitable for removing the sub-micron water droplets created through condensation in a dehydration vessel will make use of all three mechanisms to capture the water droplets, encourage them to coalesce into larger droplets and remove them through gravity separation from the gas stream.

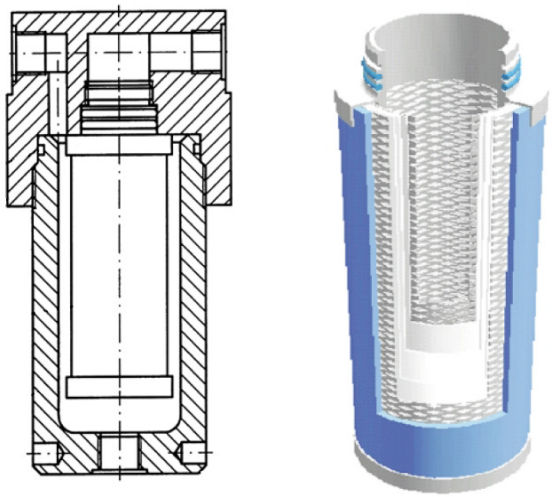

Figure 3-17 Coalescing filter and filter element [118]

The coalescing mechanism of a filter is illustrated in Figure 3-18.

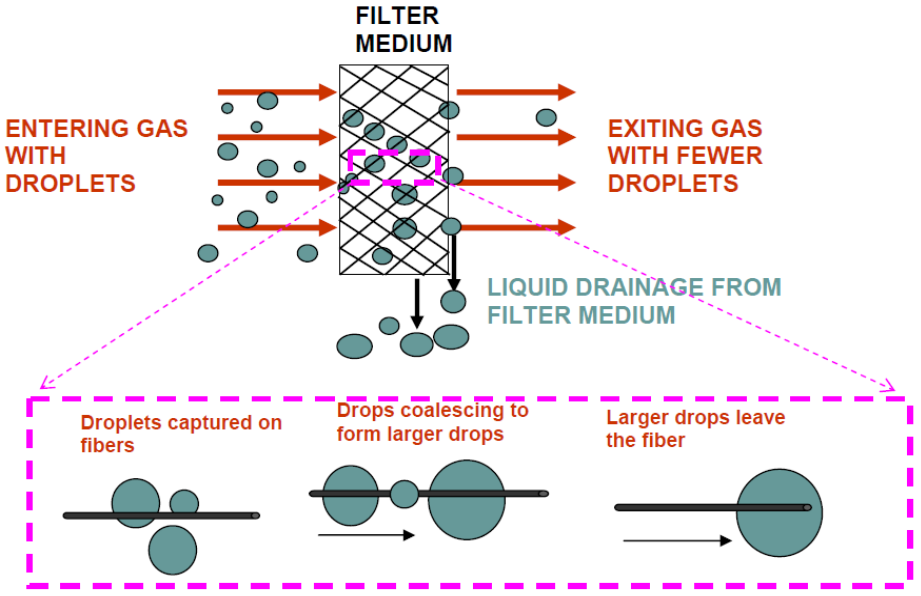

Figure 3-18 Coalescing process in a filter medium[119]

Experimental work performed by Dawar[119] demonstrated that droplets will build up on fibres in a coalescing filter until they reach a size where the drag force of the passing gas stream is sufficient to pull the droplet from the fibre. Correlations developed from the experimental work concluded that the drag coefficient for transverse motion of droplets through an array of fibres is dependent on the Reynolds and capillary numbers and the fibre and droplet sizes.

Other considerations in defining a suitable coalescing filter include the orientation and wettability of the fibres and the velocity of the gas stream.

The design construction of fibre-mat coalescence filters encourages the coalescence of the droplets and the controlled release of the large droplets to prevent re-entrainment in the gas stream. This is achieved through the layering of fibres mats with different pore sizes, selection of suitable fibre sizes and orientation and suitable physical constraints.

3.4.3.5 Other methods

Alternative methods used to remove particles from a gas stream include cyclonic separators and electrostatic precipitators. Cyclonic separators are efficient at removing particles down to 2 microns but fail to remove smaller particles so are not suitable for this application. Electrostatic precipitators can remove sub-micron particles but are typically bulky fairly complex pieces of equipment and are unlikely to be suitable for sub-sea operations.

3.5 Dehydration process enhancement

When we reviewed the thermodynamics of the dehydration process in section 3.4.1.1 we considered the closed volume to encompass the entire dehydration vessel and concluded that we had a constant enthalpy process. If we look at the situation within the vessel, due to the choked flow, the gas velocity will be close to the speed of sound as it exits the nozzle, that is much faster than the velocity it entered or left the dehydration vessel. As a result of this much higher gas velocity the enthalpy of the gas leaving the nozzle will be lower than that of the gas entering or leaving the dehydration vessel. The pressure of the gas leaving the nozzle will be the same as that leaving the dehydration vessel so this change in enthalpy must result in a change of temperature of the gas stream. The higher velocity gas will therefore be cooler than the gas leaving the dehydration vessel.

As the water content of gas is a function of the temperature and lower temperature gas will hold less water vapour, a consequence of this colder gas in the vicinity of the nozzle will be a higher super-saturation of water vapour in the gas stream. If we can encourage the water vapour to condense out while the super-saturation is at its highest level it may be possible to remove more water as liquid and improve the dehydration performance of the system.

Condensation of water from a super saturated gas stream occurs best if the process is heterogeneous, a process that can be encouraged by the introduction of particles in the gas stream that can act as seeds for the formation of water droplets.

Any seeding material that is to be added to the process must be readily available in the subsea environment and must not interfere with or causes blockage of the dehydration system. The lack of local availability and the likely blockage problems that would occur with solid particles discounts them as a potential seeding material. Looking at possible liquids available in the gas stream, there is the extracted water and in many wells some liquid hydrocarbons.

Seeds can be created in the dehydration vessel by introducing the liquid at pressure via a misting nozzle. The liquid passing through the nozzle will be transformed from a liquid stream to a fine mist of particles that can than act as seeds for further condensation of water from the expanded gas stream.

3.5.1 Properties of misting nozzles

The droplet size and size variability are dependent on a number of factors[120] that include:

- Spray nozzle design, full cone nozzles have the largest drop size followed by flat spray and hollow cone nozzles. Gas assisted nozzles produce very fine droplets.

- Flow rate, the droplet size increases with an increase in the flow rate through the nozzle
- Pressure, the droplet size decreases as the pressure drop across the nozzle increases
- Spray angle, the droplet size decreases as the spray angle increases
- Liquid properties of viscosity and surface tension increases the amount of energy required to atomise the spray so as a consequence an increase in these properties typically leads to an increase in the droplet size.
- Specific gravity of the liquid affects the flow rate with larger flow rates with lower specific gravity liquids.

What is the affect of nozzle diameter? When we consider a constant flow of incompressible fluid through two nozzles of different diameters, it is trivial to show that the liquid velocity in the smaller diameter nozzle will be larger than with the larger diameter nozzle. Looking at Bernoulli's equation for incompressible flow down a stream line:

$$\gamma z + p + \frac{1}{2}\rho v^2 = const. \quad \text{... 75}$$

if the inlet conditions of height *(z*), pressure (*p*) and velocity (*v*) for the two nozzles are the same then the constant will be the same for the stream of each nozzle and the outlet equation will take the form:

$$\gamma z_1 + p_1 + \frac{1}{2}\rho v_1^2 = \gamma z_2 + p_2 + \frac{1}{2}\rho v_2^2 \quad \text{... 76}$$

As *z* is the same for both nozzles and the velocity for the small nozzle is greater than for the large nozzle it is clear that the large diameter nozzle will require a smaller pressure drop across the nozzle for a similar flow rate. This smaller pressure drop across a nozzle leads to larger droplets.

At a constant flow rate a decrease in the nozzle diameter will lead to a decrease in the droplet size.

The droplet size distribution from a nozzle can vary by a significant amount typically over a range from sub micron droplets to droplets around 0.5 mm in diameter with a distribution profile that may be normal or weighted on the larger droplet size depending on the nozzle type.[121] Data on mean droplet size and distribution is typically published by the nozzle manufacturers.

4 Experimental set up

The principle purpose of the experiment program is to determine whether a simple JT cooling method can be effective in reducing the water content of a saturated gas stream to a level low enough for transport in subsea pipelines and to determine the bounds of operation for this approach.

This section describes the experimental equipment setup; the suite of experiments that were performed and provides details of the results.

The final equipment setup as described evolved over the integration period as over 60 integration tests were performed and system shortcomings identified. System enhancements were also made as issues were identified during the experimental runs. Particular issues that were identified and rectified in the system development phase included:

- Inlet gas nozzle blockages at start-up and during operations required the addition of nozzle heating capability and careful control of the inlet gas temperature
- When water temperatures were higher than the operating temperature of the dehydration vessel the JT cooling effect was less effective. To alleviate this and ensure a maximum JT effectiveness the vessel had to be thoroughly insulated.
- High dewpoint readings at the dewpoint meter and identification of water entrainment in the outlet gas stream required the addition of a coalescing filter to the outlet and repositioning of the nozzle further from the outlet port.
- The dewpoint meter was found to be very sensitive to its operating conditions. To ensure consistent repeatable results a number of dewpoint meter subsystem enhancements were introduced
    - a water bath was added upstream of the control valves to warm the gas sample and ensure that no hydrate blockages occurred in the control valves while expanding the sample gas from experimental to atmospheric pressure.
    - a flow meter was fitted to the sample gas stream after the expansion to atmospheric pressure to ensure that a constant sample flow rate could be utilised for all measurements.
    - The sample test point was fitted close to the outlet of the dehydration vessel taking gas vertically upwards from the outlet tubing to protect the dewpoint meter from liquid water that was sometimes present when back flowing gas through the system.

The scope of work for this research project included the design and build of the system, a process that took around 8 months from first design to connection of the natural gas supply and commencement of the system integration tests. System integration and dehydration experiments were performed in phases over a period of 15 months.

4.1 Dehydration pilot plant overview

The experimental dehydration system comprised of the following main subsystems:

- the high pressure gas delivery subsystem to provide a constant supply of natural gas at adjustable pressures up to 10 MPa and flow rates up to 560 standard litres per minute;
- the gas conditioning subsystem to fully water saturate the gas stream;
- the gas dehydration subsystem to precondition the gas stream and implement the JT cooling process; and
- the fluid injection subsystems designed to allow top injection of liquids in stream with the gas flow or bottom injection of condensate with recirculation
- the system sensors and instrumentation subsystem to measure and record all the dehydration system operations.

The system was designed to allow monitored operation for up to 12 hours. For continuous autonomous operations additional subsystems would be required to monitor and control the system operations, including hydrate management within the dehydration vessel.

Photographs of the experimental equipment are provided in Appendix D.6.

4.2 Gas delivery subsystem

The gas delivery system used a high pressure natural gas compressor, gas storage vessels and control regulators to implement a closed gas loop that could deliver natural gas at pressures up to 10 MPa to an experiment and recirculated exhaust gas from the experiment. This design approach allowed long experimental run times while minimising both the amount of natural gas extracted from the gas main and the amount vented to the atmosphere.

Some provisions were made within the gas delivery system for future experiments not related to this research.

The Gas delivery subsystem is illustrated in Figure 4-1.

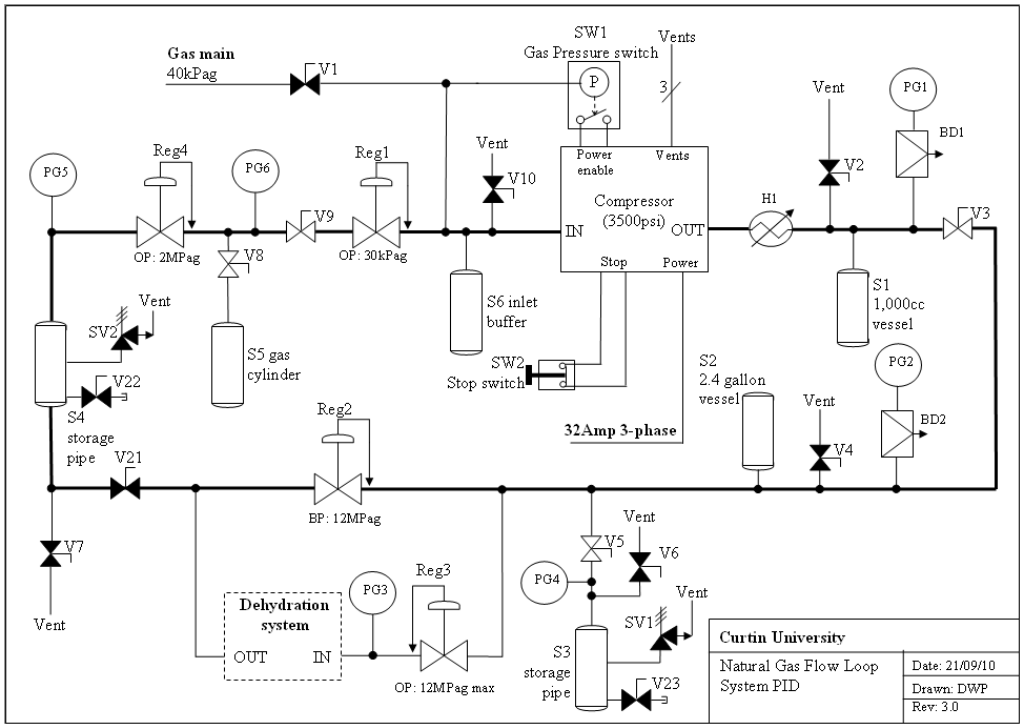

Figure 4-1 Gas delivery subsystem

4.2.1 Compressor

The compressor used was a 4-stage piston compressor manufactured by Hoerbiger and capable of providing 560 standard litres per minute at pressures up to 35 MPa. The compressor was powered with 3-phase mains power and had a low pressure interlock to ensure sufficient gas supply pressure was present at the compressor (Figure 4-1 SW1) and an emergency stop (Figure 4-1 SW2). The maximum output pressure of the compressor was set on the compressor's overpressure cut-out switch to 14 MPa. An inlet storage buffer (Figure 4-1 S6) was attached to the compressor inlet to ensure that peak gas supply requirement of the compressor was available at all points of the compressor cycle.

The gas supply to the compressor was selectable by valve operation (Figure 4-1 V1 and V9) from either the gas main at 40 kPag or from the gas loop storage at 50 kPag.

Vents were connected from the compressor to a safe external location for compressor venting during normal operations and for the compressor's overpressure safety release valves.

Figure 4-2 Gas compressor

Figure 4-2 shows a picture of the compressor. On the right hand side of the compressor can be seen the inlet gas buffer (Figure 4-1 S6) and the orange coloured inlet regulator (Figure 4-1 Reg 1). The valves to allow for switch over of gas from gas main to gas loop are on the wall below the power point and just upstream of the inlet regulator. They were positioned so that a changeover could be accomplished safely without having to stop the compressor.

4.2.1.1 Gas loop controls

Correct operation of the gas loop was controlled by three pressure regulators and a heat exchanger.

Gas exiting the compressor was warmed by a heat exchanger (Figure 4-1 H1) to ensure that temperatures in the immediately downstream pressure regulators (Figure 4-1 Reg2 and Reg3) were kept above hydrate formation temperatures and regulator flow/pressure operations were reliable. The heat exchanger used the flow of heated water from a thermo-regulator set to 50 C and a jacketed 5 m coil of ½" tubing to warm the gas stream.

A back pressure regulator (Figure 4-1 Reg2) was used to set the pressure of the high pressure storage vessel (Figure 4-1 S3). The maximum storage pressure of 12 MPa was

enforced by the fitting of a calibrated safety release valve (Figure 4-1 SV1) to the high pressure storage vessel.

Figure 4-3 Gas loop control panel

The pressure of the gas used in experiments was set with a forward pressure regulator (Figure 4-1 Reg3).

Gas returning from the experiment was stored in the low pressure storage vessel (Figure 4-1 S4) and was passed to the gas compressor via a high flow high pressure regulator (Figure 4-1 Reg 4) and a low output pressure regulator (Figure 4-1 Reg1). The maximum pressure of the low pressure storage vessel was 12 MPa and was protected by a safety release valve (Figure 4-1 SV2)

Figure 4-3 is a picture of the Gas loop control panel that was built for this project and mounts the control regulators, isolation and vent valves and pressure gauges for the gas loop. The red switch above the panel is the Emergency stop switch (Figure 4-1 SW2)

4.2.2 Gas storage

The high pressure storage vessel (Figure 4-1 S3) is provided by a 10 m length of ANSI Class 900 3 inch pipe that provides approximately 65 litres of gas storage at pressures up to 12 MPa.

The low pressure storage vessel (Figure 4-1 S4) is provided by a 15 m length of ANSI Class 900 3 inch pipe that provides approximately 100 litres of gas storage at pressures up to 12 MPa.

A 2.4 gallon storage vessel (Figure 4-1 S2) is provided adjacent to the experiment pressure setting regulator (Figure 4-1 Reg3) to smooth the gas flow during periodic compressor venting.

A small 1 litre pressure vessel (Figure 4-1 S1) is provided for future high pressure experiments.

Safety valves and burst discs are fitted to protect all of the pressure vessels.

All gas loop connections were made with ½ inch stainless steel tubing except for the high pressure storage vessel which was connected with 3/8" stainless steel tubing.

4.3 Gas conditioning subsystem

The Gas conditioning system consisted of a 24 litre pressure vessel filled with 20 litres of tap water and fitted with a custom made gas sparger at the bottom of the vessel.

The pressure vessel was certified for operation up to 12 MPa. The Gas conditioning system is illustrated in Figure 4-4.

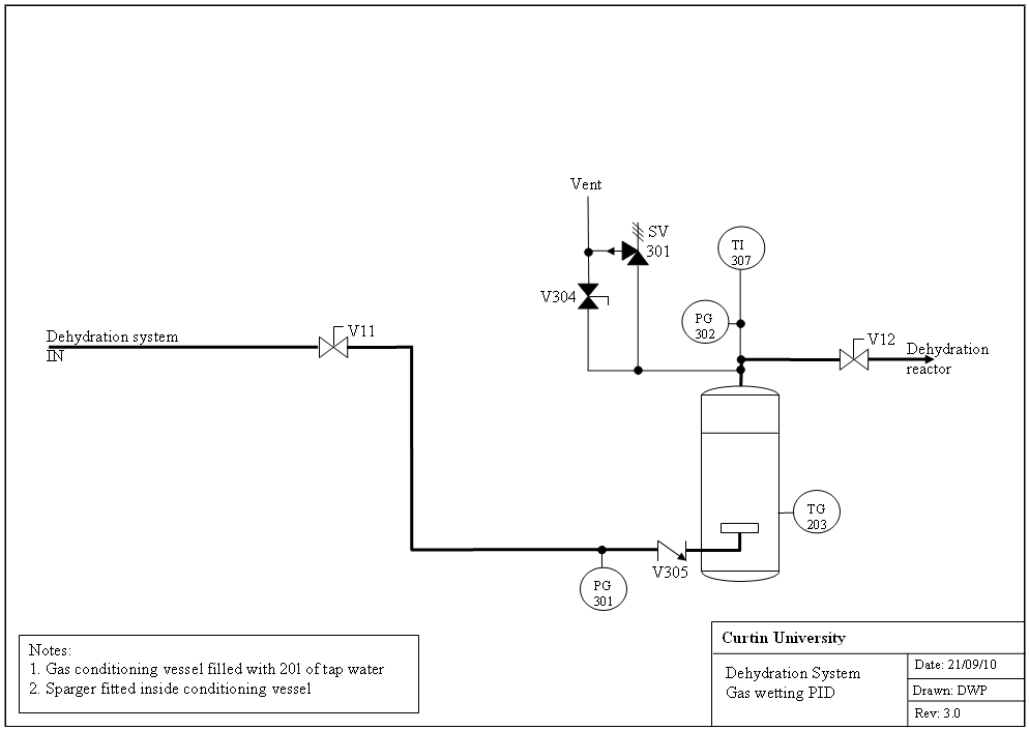

Figure 4-4 Gas conditioning subsystem

Gas from the gas delivery subsystem is passed to the Gas conditioning system at the experimental pressure and is bubbled through the water in the pressure vessel.

The gas leaves from the top of the pressure vessel saturated with water vapour at the temperature and pressure conditions of the pressure vessel.

The temperature of the gas leaving the pressure vessel is measured by a temperature sensor (Figure 4-4 TI307) and was manually recorded during experimental runs.

A safety pressure release valve (Figure 4-4 SV301) is fitted to the pressure vessel to protect against over pressure.

4.4 Gas dehydration subsystem

The gas dehydration subsystem is the principle piece of equipment developed and used by this research project to control the operational environment and the experimental bounds and measure the resultant effectiveness of the dehydration process.

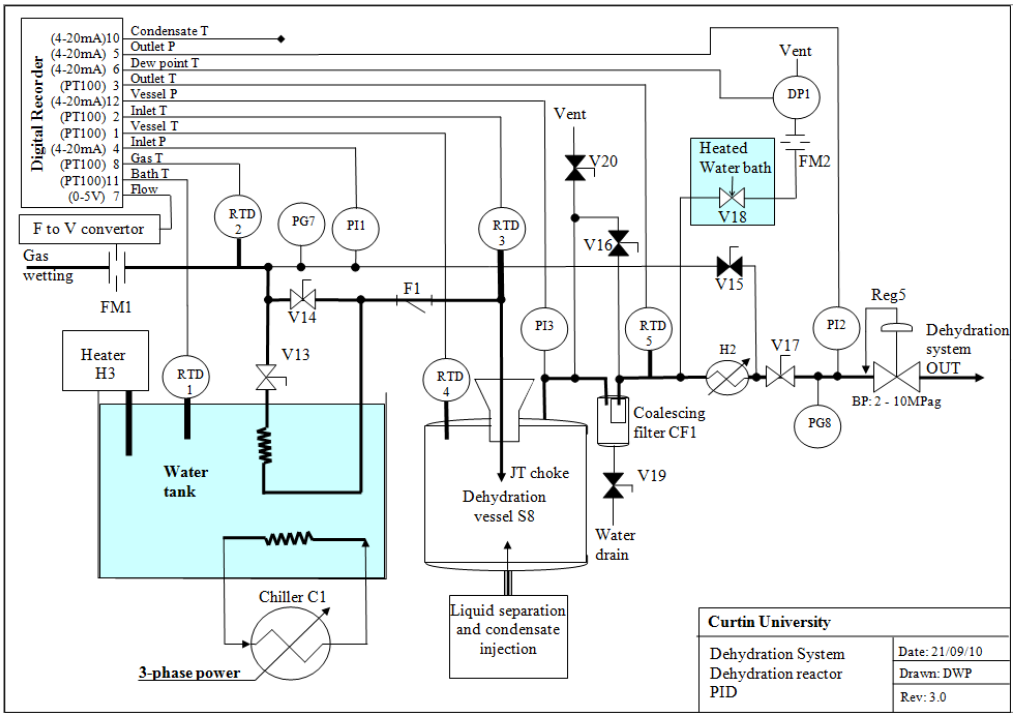

Figure 4-5 Gas dehydration subsystem

The dehydration subsystem comprises an insulated pressure vessel with a choking nozzle input installed in a water tank. The tank could be filled with water to submerge the dehydration vessel and the water temperature in the tank controlled. Controls were present on the input and outlet gas flows and an array of sensors fitted to measure system conditions. The gas dehydration subsystem is shown in Figure 4-5.

4.4.1 Gas inlet system

The gas inlet system comprised of the following elements through which the inlet gas passed in sequence:

- Gas flow meter
- Inlet gas heat exchanger
- Particulate filter
- Nozzle adaptor

The flow meter (Figure 4-5 FM1) was a FT series calibrated turbine flow meter from Flow Technology that accurately measured the gas flow rate to within 0.3% of reading.

The inlet gas heat exchanger was a custom built device and is illustrated in Figure 4-6.

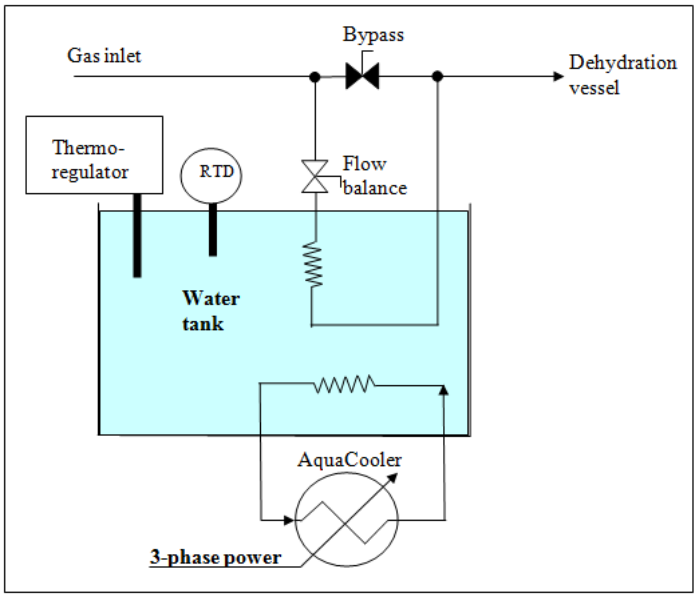

Figure 4-6 Inlet gas stream heat exchanger

The heat exchanger provided 2 gas paths, one through a 5 m coil of stainless steel tubing submerged in a temperature controlled water bath and the other via a short bypass. The water bath temperature could be controlled by two methods, for below ambient water temperatures a copper coil connected to the water cooler (AquaCooler) was used and for above ambient a 2 kW thermo-regulator was used.

When operating at a sub-ambient temperature water bath the temperature of the inlet gas stream could be controlled to within 1 C by adjusting the two valves. A better accuracy of 0.5 C was possible when using the thermo-regulator to control the temperature of the water and the bypass valve was closed.

A particulate filter (Figure 4-5 F1), a Swagelok TF series Tee-type filter fitted with a 140 micron strainer type element was fitted before the nozzle adaptor to capture any particulate matter in the gas stream that could have blocked the nozzle.

The key functions of the nozzle adaptor were to:

- allow the connection of gas tubing to dehydration vessel
- provide a mounting for the inlet nozzle
- provide a heating option for removal/prevention of hydrate build up in the nozzle.

The first nozzle adaptor used is shown in Figure 4-7. It was a simple mechanical adaptor manufactured from stainless steel that screwed into the 1" BSP female thread on the side of the dehydration vessel. It provided a ½" NPT female thread for connection of the inlet gas tubing via a standard Swagelok adaptor on the outside and a 3/8" NPT female thread on the inside for connection of the nozzle via a suitable adaptor.

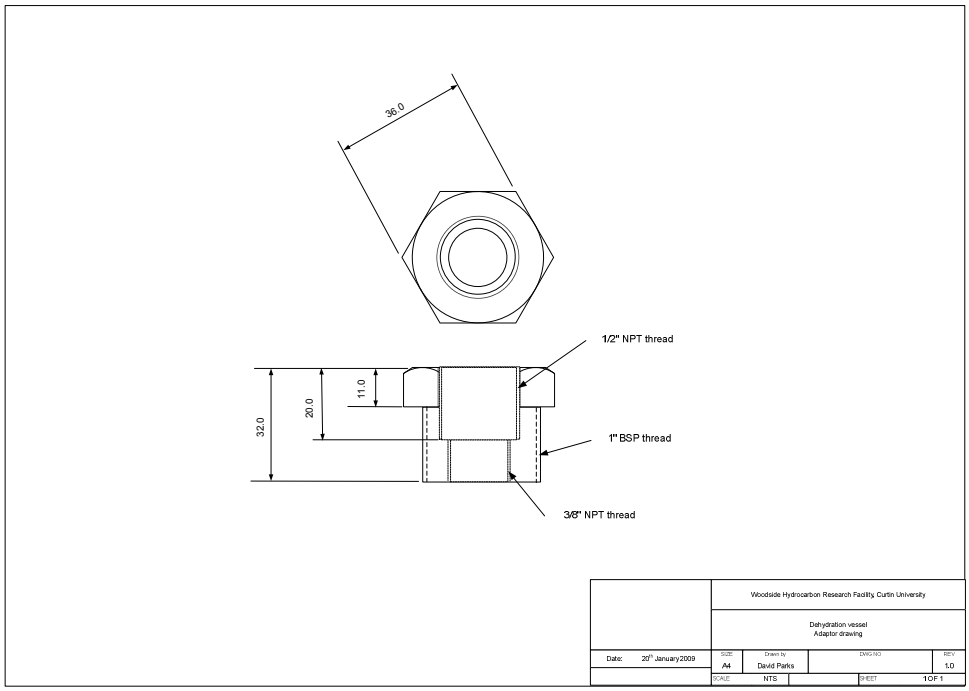

Figure 4-7 Simple nozzle adaptor

In the first integration tests using bottled natural gas the nozzle blocked within minutes of commencing a test run and took several hours to clear.

Reviewing the operating conditions it was apparent that the temperature and pressure of the gas stream at the exit of the nozzle was in the region where hydrates could form and that hydrates were the likely to be forming at the nozzle exit and blocking the gas flow.

4.4.1.1 Prevention of hydrate blockage of the nozzle

During the integration tests of the dehydration system two approaches to preventing hydrate formation were trialled. The first method was to implement a heating technique whereby the nozzle could be heated with just enough power to prevent hydrate formation. The benefit of this was that blockages could also be cleared relatively easily if they occurred. Detail on the development of the heated nozzle adaptors is provided in section 4.4.1.2.

The alternative method to the heated nozzle was to control the temperature of the inlet gas stream so that at the nozzle exit conditions hydrates did not form and cause blockage. The inlet heat exchanger described shown in Figure 4-6 was used to control the inlet gas stream temperature and provided the ability to set the temperature within 0.5 C during an experimental run.

4.4.1.2 Heated nozzle implementation

A number of techniques for heating nozzles were investigated including electrical heaters and recirculating warmed water through a jacket surrounding the nozzle which was used successfully in Aly's research [55].

The space and mounting constraints of the dehydration vessel made the water circulation approach impractical so an electrical approach using commercially available heating cartridges was chosen.

A diagram of the heated nozzle electrical assembly is shown in Figure 4-8 and a picture in Figure 4-9.

The heater cartridges were powered by a standard lighting dimmer circuit fitted in a weatherproof enclosure and connected up via a sealed junction box. For electrical safety the mains dimming circuit was connected to the mains via a residual current device (RCD) so that any electrical leakage of the heating cartridges or cabling would cause the power to be immediately isolated from the system.

The heater cartridges were found to be hygroscopic and prone to internally shorting out if they got internally damp, so sealing against water ingress was required for operation outdoors and under water.

Effective sealing of the cartridges proved problematic and a number of techniques were attempted including high temperature silicon and epoxies, glue filled heat shrink and self amalgamating PIB tape. The main problem sealing the unit was due to the very limited clearance available around the cartridge due to the dimensional limitations imposed by the mounting for the nozzle adaptor.

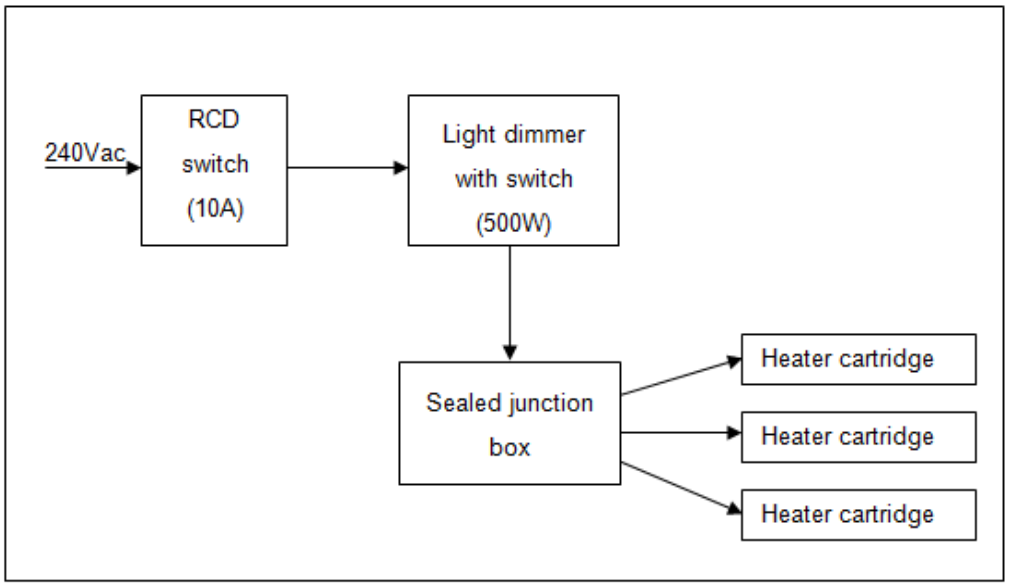

Figure 4-8 Heater nozzle electrical assembly

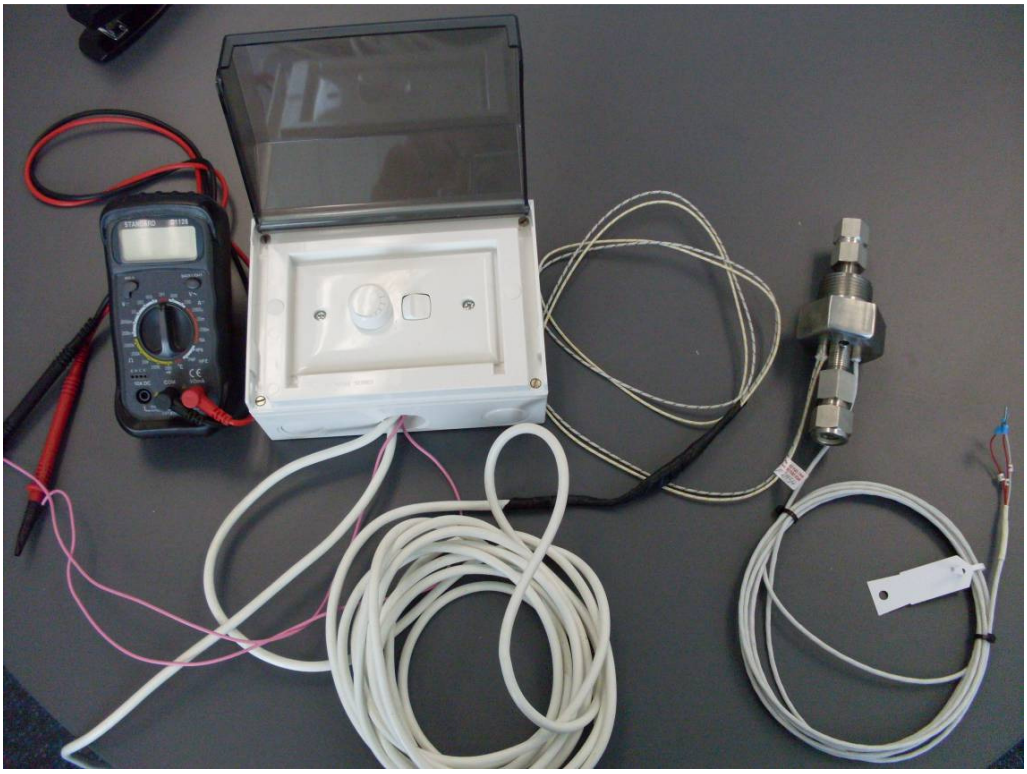

Figure 4-9 Heated nozzle adaptor system picture

Figure 4-10 illustrates the techniques that were attempted; the first two attempts sealed the cartridge as an assembly while the third and fourth methods glued the sealed cartridge assembly to the nozzle adaptor.

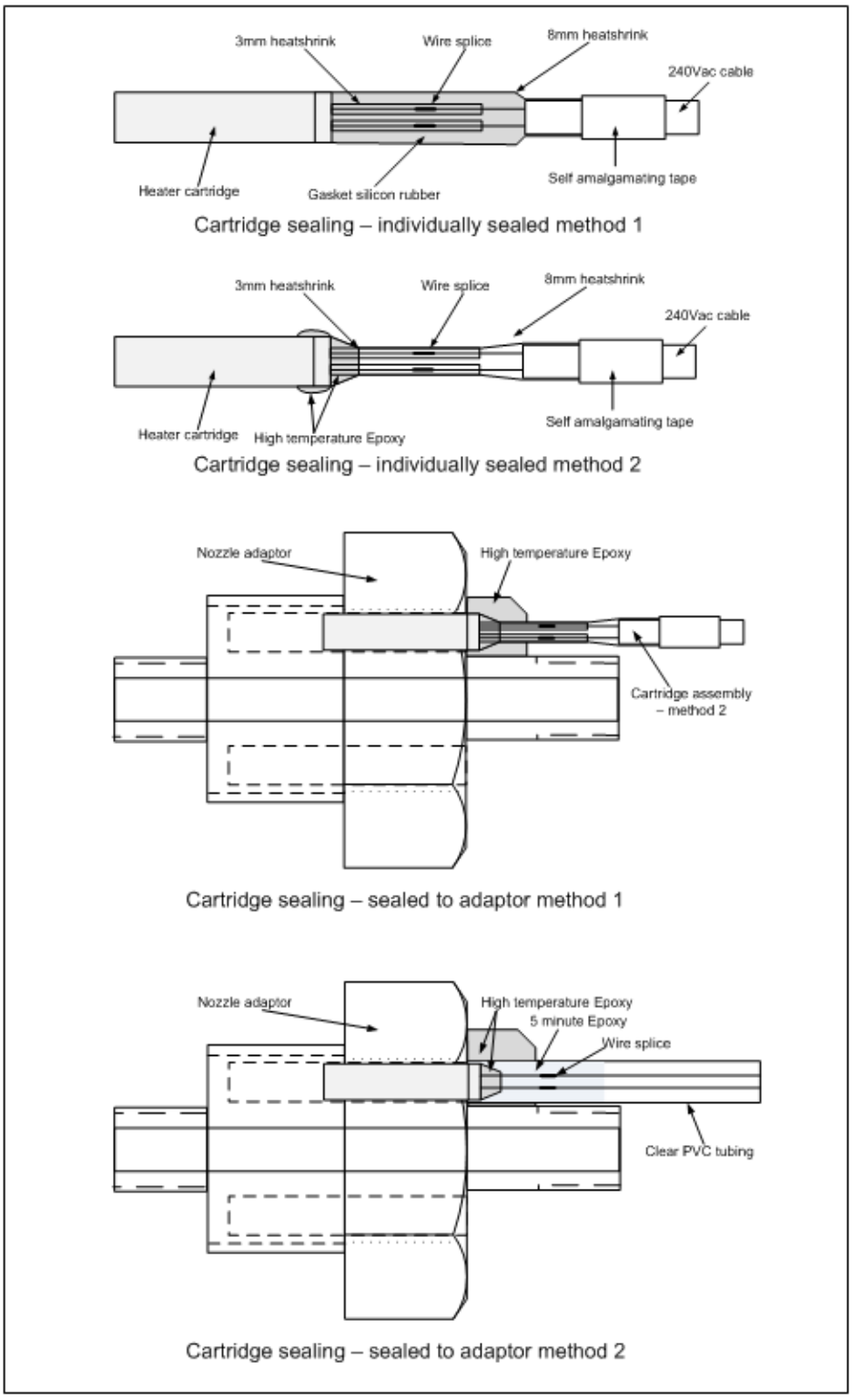

Figure 4-10 Heater cartridge sealing methods

The fourth method using clear PVC Tubing from the heater cartridge all the way to an electrical junction box combined with sealing using epoxies at the nozzle adaptor end proved ultimately to provide the best solution. Even then the assemblies proved to be brittle when handled and we only managed to get at best a few weeks operation before repairs were required.

A picture of the first version of a heated nozzle adaptor that could use standard ¼" heating cartridge elements is shown in Figure 4-11. A detailed drawing is provided in Appendix D.2.1. The nozzle adaptor again mounted to the dehydration vessel via a 1" BSP female thread. The nozzle was fitted to the ¼" NPT thread on the bottom of the nozzle adaptor. A 240 Vac, 175 W heater cartridge and a PT100 temperature sensor were fitted into opposite holes in the top of the adaptor. The nozzle utilised was a standard Swagelok ¼" NPT cap with a 0.95mm hole drilled into the centre.

Some integration tests were performed using this nozzle assembly at an input pressure of 9.5 MPa, outlet pressure at 6.5 MPa and gas inlet temperature at ambient temperature of around 19 C. With the nozzle heater set to full power, i.e. 175 Watts, it was found that after a period of cooling of the dehydration vessel that the flow became erratic and eventually dropped to zero due a complete blockage of the nozzle.

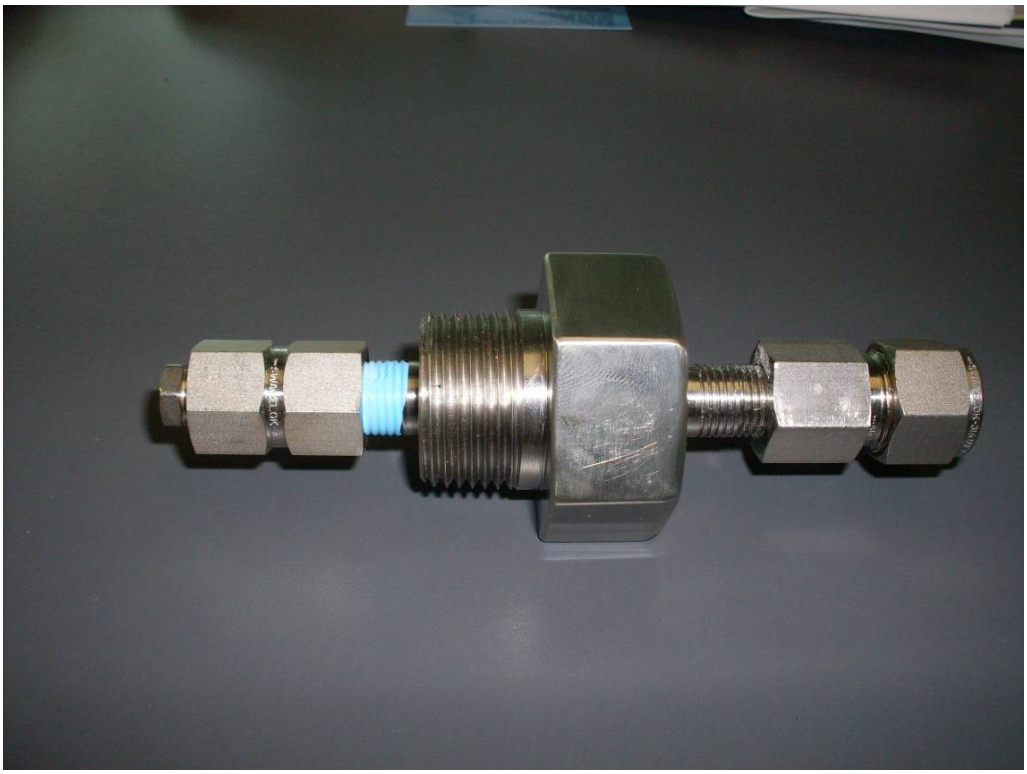

Figure 4-11 Heated nozzle adaptor version 1

A review of the results and the adaptor design was performed and it was concluded that the thermal pathway between the heater cartridge and the nozzle was not optimal and to prevent nozzle blockages during experiments a better thermal solution was required.

To improve the thermal connectivity of the nozzle to the heaters it was necessary to shorten the thermal path and ensure optimum thermal conductivity of the heater cartridge and nozzle with the nozzle adaptor.

The dehydration vessel was examined and it was found possible to install a new nozzle adaptor with an extension into the vessel by marginally enlarging the clearance hole behind the 1" BSP mounting hole of the dehydration vessel. This extension of the adaptor allowed the heater cartridges to be fitted deeper into the nozzle adaptor providing significantly improved thermal connectivity of the heater cartridge.

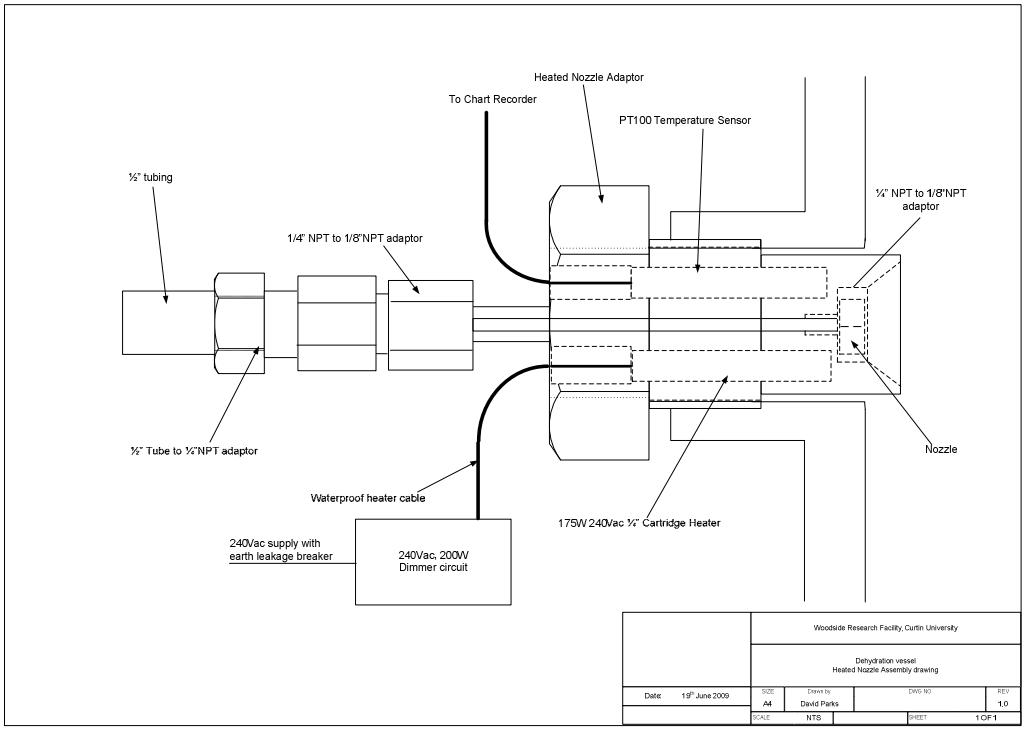

Figure 4-12 Heated nozzle assembly version 2

To improve the thermal connectivity of the nozzle a new smaller nozzle was sourced that could be screwed directly into the nozzle adaptor and that provided a flat surface to surface connectivity to improve the thermal contact.

A drawing of the new nozzle assembly is shown in Figure 4-12. A detail drawing of the adaptor is provided in Appendix D.2.2.

4.4.1.3 Nozzles

The nozzles used in experiments illustrated in Figure 4-13 were commercial misting nozzles sourced from Cool Mist Systems with orifice diameters of between 0.6 and 1.0 mm.

Figure 4-13 Nozzle with 0.6mm orifice

4.4.2 Dehydration vessel

The dehydration vessel was a custom made pressure vessel consisting of a vessel body and a blind flange. The body was of welded construction consisting of a NPS6 Schedule 80 steel pipe body with an ANSI pressure class 900 flange on the top and a hemispherical head at the bottom. On the right hand side of the vessel body the simple nozzle adaptor can be seen.

Figure 4-14 Dehydration vessel

Figure 4-14 shows the dehydration vessel with no insulation fitted. A detail drawing of the dehydration vessel is provided in Appendix D.1.

There were 3 ports on the top blind flange used for the gas input nozzle assembly (middle connection, 1" BSP female), the gas outlet (left connection, ½" NPT female) and the vessel temperature sensor (right connection, ½" NPT female). A connection on the bottom of the vessel (1/2" NPT female) was connected to a vent used for collecting liquids captured in the vessel and in later experiments to a water/condensate separator. A connection on the middle of the pipe section (1" BSP female) was used fitting the side nozzle adaptor for side gas flow injection experiments.

The dehydration vessel had an internal volume of 11.8 litres and was pressure tested to 12 MPa.

4.4.2.1 Dehydration vessel installation

The dehydration vessel was installed within a galvanised steel water tank 1.2 m diameter by 1.56 m tall. To minimise heat transfer between ambient and the cooled water in the tank the tank was insulated on the outside and bottom with 2 layers of aluminium foil covered 8mm polyethylene foam and a lid made of the same polyethylene foam was installed on top of the water which was filled to within 200 mm of the top of the tank.

The water in the tank was chilled using a three phase powered industrial water cooler, an AquaCooler R1330 A3-P4. The cooler was designed for cooling system with a closed flow loop which was impractical to implement with the open tank in which the test equipment was installed. An open circuit flow loop solution was established by using a submersible pump fitted at the bottom of the water tank to pump the water from the tank to the cooler. To balance the flow pumped out by the cooler with that returned by the submersible pump a bypass connecting the cooler output back to its input via a float valve fitted to the cooler's water tank was installed. This implementation provided a reliable solution capable of unattended operation for many hours.

The minimum set point of the AquaCooler was set to 3 C and the Hysteresis to 1 C. The cooler was tested and was able to sustain a tank water temperature down to 4 C. Overnight increases of tank water temperature from low set points were typically less than 2 C, even in summer. The cooler was able to return this temperature of the tank water to its set point in less than 100 minutes.

4.4.2.2 Dehydration vessel insulation

To determine the optimum design configuration of the dehydration vessel a number of dehydration vessel configurations were tested. The main criteria for selection of the configuration to be used for dehydration tests were:

"the maximum temperature depression that could be attained through the Joule Thomson cooling process for external water temperature conditions of 4 degrees Celsius".

The following dehydration vessel configurations were tested:

- Uninsulated vessel fully submerged in water
- Moderately insulated vessel fully submerged in water
- Thoroughly insulated dehydration vessel

Initial insulation tests were performed while waiting for the connection of the gas compressor to the mains gas supply so the tests were performed with air.

Figure 4-15 shows the Joule-Thomson coefficients for air from which we can determine that the Joule Thomson coefficient for air at the experimental conditions is between 2 and 3 MPa. With experimental pressure drops of around 6 MPa a temperature drop of around 15 C could be expected.

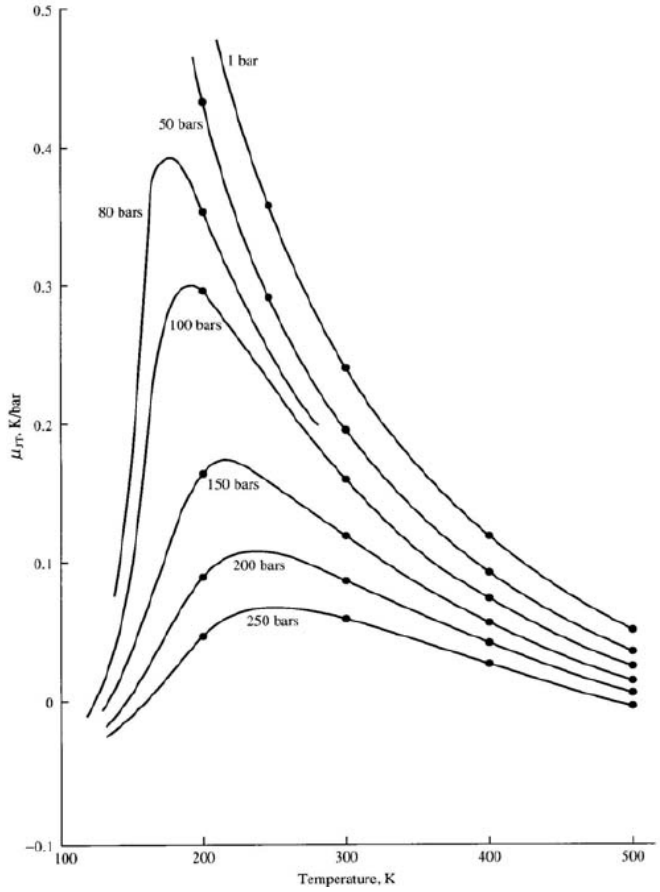

Figure 4-15 Joule-Thomson coefficients for air[122]

Two test runs with compressed air were performed with different inlet air temperatures. Air temperature was set by passing the air to the inlet side mounted nozzle adaptor either

directly or via a 5 m coil of tubing immersed in the water bath. For both runs the maximum gas flow rate of the compressor was used (560 sl/min) and the water bath temperature was 4.5 +/- 0.5 C. Table 4-1 presents the operating parameters for the two experimental runs and the calculated JT coefficient from the measured temperature drop and applied pressure drop.

Inlet flow path	Inlet temp. (Celsius)	Inlet pressure (MPa)	Outlet pressure (MPa)	Outlet temp. (Celsius)	Calc. JT coefficient (K/MPa)
Direct	16	8.2	2.2	4.3	1.95
Via heat exchanger	4.9	8.7	2.2	0.8	0.6

Table 4-1 Calculated JT coefficients for uninsulated vessel using compressed air

The run with the cold inlet gas had a temperature drop of 8.5 C less than that predicted. This was attributed to thermal losses between the vessel and the warmer water bath. In the dehydration experiments to be performed it is anticipated that the vessel temperature will normally be lower than 4 C so to ensure that thermal losses did not restrict the effectiveness of the JT cooling operations, it was decided to add some insulation to the vessel surface.

The body of the dehydration vessel was wrapped in 2 layers of 8 mm thick aluminium foil covered polyethylene foam and the top flange covered with the same material to a thickness level with the top of above the bolts.

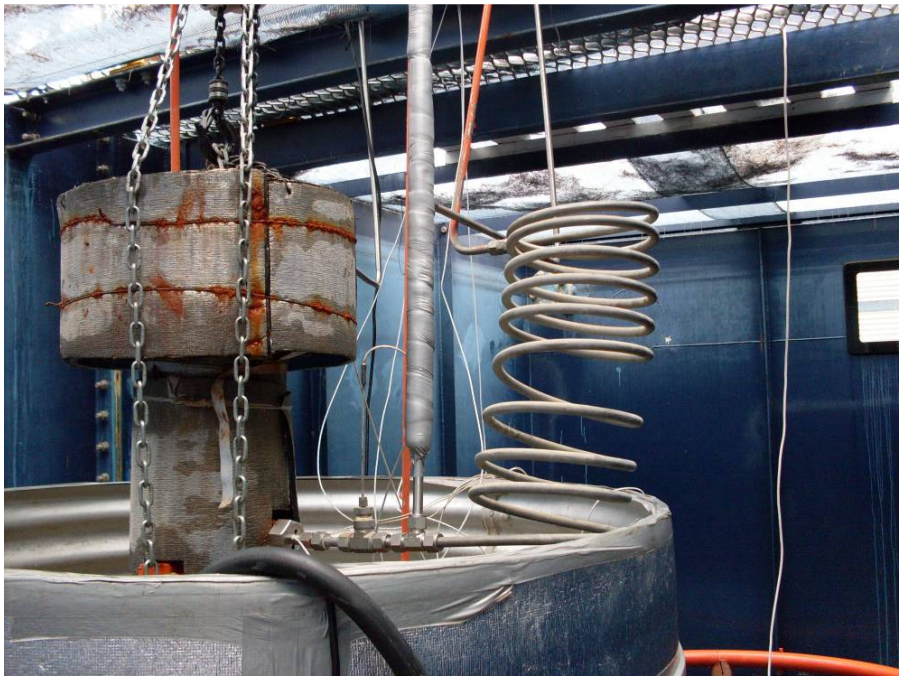

Figure 4-16 Dehydration vessel with foam insulation and inlet heat exchanger

A test run with gas passed via the heat exchanger was performed and an improved temperature drop of an additional 1.5 C was measured, giving an experimental JT coefficient of 0.9 K/MPa. This was considered to be a step in the right direction but did still not provide a JT coefficient close to the predicted value and a better insulation technique was required.

To provide a more thorough insulation the dehydration vessel was insulated with a minimum thickness of 150 mm of polyurethane foam around the bottom and body and 100 mm thickness of expanded polystyrene around and on top of the flange. The body insulation was achieved by placing the dehydration vessel in a closed tube made from the foil coated polyethylene foam and filling it to just below the flange with two pack expanding polyurethane foam (12 kg of GP2 foam from Kirkside Products, Osborne Park, WA). This solution provided to be completely waterproof. A picture of the fully insulated dehydration vessel is shown in Figure 4-17.

All tests of the fully insulated dehydration vessel were performed with natural gas. Tests were performed with the vessel in chilled water and in ambient air conditions. It was found that submerging the vessel in water was no longer necessary due to the effectiveness of the insulation.

Figure 4-17 Insulated dehydration vessel

The effectiveness of this new insulation technique was also evident by the measured JT coefficients. The results from a number of typical natural gas experiments are shown in Table 4-2.

Inlet temp. (Celsius)	Inlet pressure (MPa)	Outlet pressure (MPa)	Outlet temperature (C)	Measured JT coefficient (K/MPa)	Calculated JT coefficient (K/MPa)
25.1	10.1	6.3	8.3	4.4	4.6
27.6	9.8	4.7	5.0	4.3	4.8
25.1	9.3	3.8	1.0	4.4	5.2
26.7	9.7	2.5	-5.0	4.4	5.5

Table 4-2 JT coefficient measured for a typical natural gas experiment
(Calculated JT coefficients were obtained from HYSYS using the Alinta gas composition)

From these results it can be seen that the measured JT coefficients are much closer to the ideal calculated values for an adiabatic constant enthalpy process. We can conclude that a significant improvement in the cooling has been achieved through this thorough insulation of the vessel. The difference in the measured and calculated JT coefficients does show that there is still potential to improve the JT cooling performance.

It is also apparent that as the vessel temperature decreases the measured JT coefficient diverges more from the calculated value. This can be explained by looking at the thermal performance of the system.

4.4.2.2.1 *Thermal analysis of the fully insulated dehydration vessel*

A diagram of the insulated dehydration vessel is shown in Figure 4-18. If we consider the vessel to be comprised of two cylinders and two circular flat plates we can use standard heat transfer equations to estimate the heat flux of the dehydration vessel in free air and submerged in cold water to a fair level of accuracy. The simplified heat transfer surfaces to be considered are:

1. Main dehydration vessel body (Tall cylinder)
   (Length 0.7 m, internal radius 73 mm, wall thickness 12 mm)

2. Dehydration body flange- length (Short cylinder)
   (Length 6 cm, internal radius 73 mm, wall thickness 192 mm)

3. Top plate
   (Radius 73 mm, thickness 58 mm)

4. Bottom plate
   (Radius 73 mm, thickness 12 mm)

For cylindrical bodies the heat flux q_r transferred due to a temperature differential can be expressed by the equation[123]:

$$q_r = \frac{T_{\infty,1} - T_{\infty,n}}{\frac{1}{2\pi r_1 L h_1} + \frac{\ln(r_2/r_1)}{2\pi k_A L} + \ldots + \frac{\ln(r_n/r_{n-1})}{2\pi k_N L} + \frac{1}{2\pi r_n L h_n}} \quad \ldots 77$$

where suffixes *1* to *n* refer to the surface interfaces, *L* is the length of the cylinder, r_i the radius of surface *i*, T_∞ the temperatures of the fluids, k_A to k_N the thermal conductivity coefficients and h_1, h_n the convection coefficients

Similarly for flat plates the heat flux q_x can be expressed by the equation:

$$q_x = \frac{T_{\infty,1} - T_{\infty,n}}{\frac{1}{h_1 A} + \frac{L_A}{k_A A} + \ldots + \frac{L_N}{k_N A} + \frac{1}{h_n A}} \quad \ldots 78$$

where *A* is the surface area and L_A to L_N are the thicknesses of each material layer.

Using these equations the heat transfer was calculated for each surface for the vessel submerged in a water bath of 4 C and for the vessel in air at 22 C. The results are tabulated in Table 4-3 for an internal natural gas temperature of -4 C and assuming equilibrium conditions have been met.

Surface	**In water bath at 4 C**	**In air at 22 C**
Large cylinder	0.56 Watts	1.79 Watts
Small cylinder	0.24 Watts	0.77 Watts
Top plate	0.05 Watts	0.15 Watts
Bottom plate	0.08 Watts	0.08 Watts
Total heat flux	**0.93 Watts**	**2.80 Watts**

Table 4-3 Calculated heat flux for insulated dehydration vessel

The calculation details are given in Appendix B.2.

Using the simulator HYSYS we can calculate the effect of this heat flux on the gas stream in the dehydration vessel. Using a gas stream of Alinta gas composition at a temperature of -4 C and pressure of 2.5 MPa, the addition of 2.8 Watts onto the experimental gas flow of 560 sl/min results in a gas stream temperature increase of less than 0.2 C. This result confirms the suitability of the extensive insulation that was fitted to the dehydration vessel.

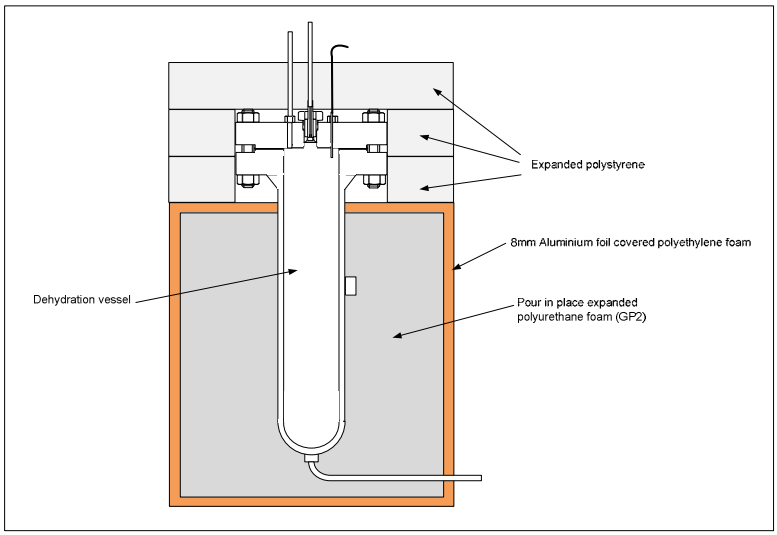

Figure 4-18 Diagram of dehydration vessel insulation

The small difference between the two conditions and the small impact of gas temperature in the dehydration vessel also validates the decision to operate the system in air. This decision removed the costly and time consuming maintenance of the large cold water bath for the experiments.

4.4.2.2.2 *Nozzle positioning in dehydration vessel*

A number of different nozzle assemblies and injection positions were trialled during the integration and experimental phases. The following nozzle configurations were trialled:

- Side fitted simple nozzle adaptor
- Side fitted heated nozzle adaptor
- Side fitted heated nozzle adaptor with extension
- Central top fitted heated nozzle adaptor with extension
- Central top fitted nozzle adaptor with cowling
- Central top fitted nozzle adaptor with nozzle on tubing extension

4.4.3 Liquid injection systems

The liquid injection systems provided the ability to inject cold liquids into dehydration vessel. Two injection systems were utilised during experiments, one that injected liquids from the top premixed with the gas stream prior to expansion through the choke and the other that injected liquids as a spray from the bottom of the vessel. The top injection system is illustrated in Figure 4-19 and the bottom injection system in Figure 4-20

The top injection system comprised the following components:

- Liquid storage vessel
- Compressed air pressure control regulator
- Compressed air powered high pressure fluid pump
- Fluid flow control valve
- Heat exchanger
- Injection liquid temperature sensor (PT100)
- Liquid injection point

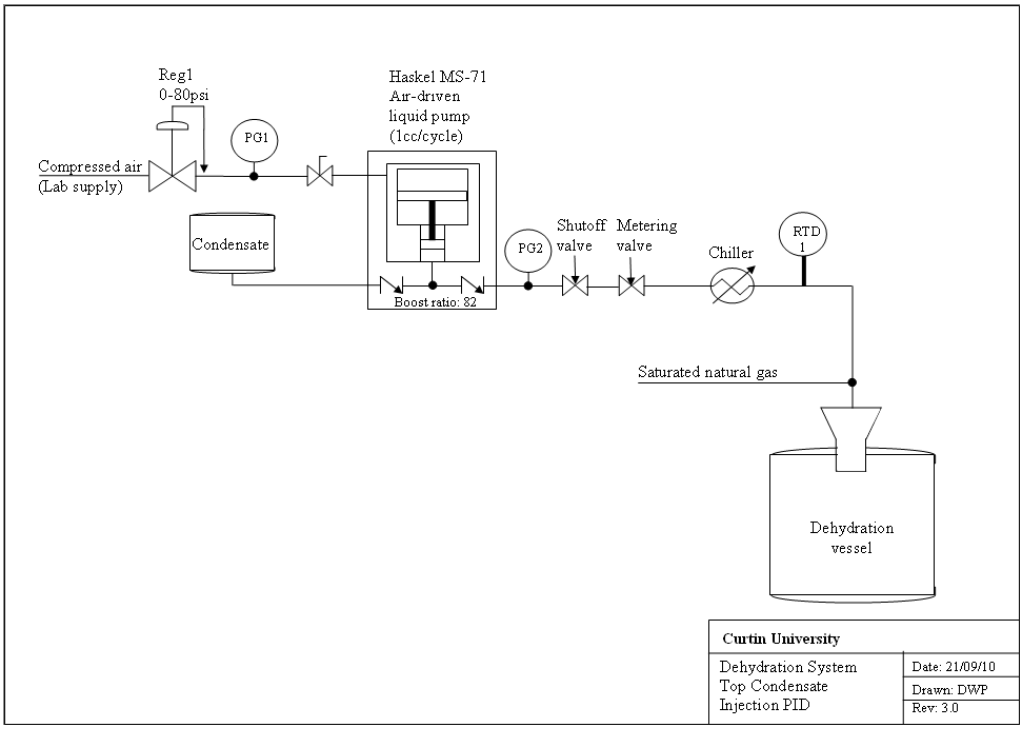

Figure 4-19 Top liquid injection system

The liquid storage vessel was an eight litre polycarbonate vessel with a bottom outlet that provided a constant supply of injection liquid to the liquid pump.

The liquid pump was a Haskell MS-71 air-driven liquid pump providing an 82:1 pressure boosting ratio and a 1 cc/cycle injection rate. A pressure regulator and valve were used on the compressed air supply line to switch on and control the outlet pressure of the pump.

Shutoff and metering valves in the high pressure liquid injection line were used together with the set pump pressure to control the liquid flow rate.

The liquid injection point was a standard Swagelok T union that was fitted vertically above the filter and nozzle assembly. This allowed chilled liquid to be injected directly into the gas stream.

The high pressure liquid was passed through a tubing coil submerged in a methanol bath prior to injection into the gas stream. The methanol bath was cooled with dry ice to obtain the required temperature.

The high pressure condensate flow lines were made with ¼" stainless steel tubing and fittings.

The bottom injection system was very similar in construction to the top injection system with the addition of a separator to allow recirculation of the injected fluids. The addition of recirculation allowed much longer injection times during experiments.

As the injection was directly into the dehydration vessel that was operating in hydrate formation conditions and addition of heaters to the nozzle was not possible, the injection of water with the bottom injection system was not plausible. The injection fluid used for bottom injection tests was heptane.

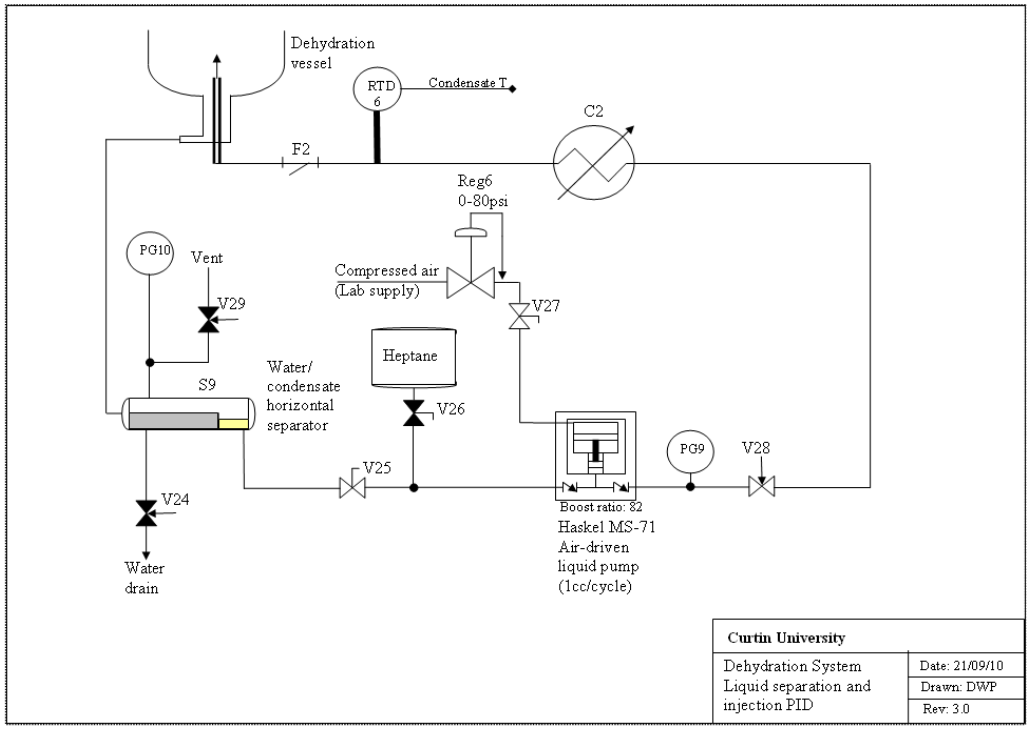

Figure 4-20 Bottom liquid injection system

The bottom injection system comprised the following components:

- Heptane/water separator
- Compressed air pressure control regulator

- Compressed air powered high pressure fluid pump
- Heat exchanger
- Injection nozzle and fluid return

Heptane was supplied to the system from either the two phase separator or a top up condensate storage vessel.

The liquid pump was a Haskell MS-71 air-driven liquid pump providing a 82:1 pressure boosting ratio and a 1 cc/cycle injection rate. A pressure regulator and valve were used on the compressed air supply line to switch on and control the injection fluid flow rate

The injection fluid was passed through a tubing coil submerged in a methanol bath prior to injection into the bottom of the dehydration vessel. The methanol bath was cooled as required with dry ice to obtain the required injection fluid temperature.

The nozzle used was a hollow cone type with a 0.7 mm orifice.

The port at the bottom of the dehydration vessel allowed injected fluids and other fluids accumulated in the dehydration vessel to be transported to the inlet of the separator.

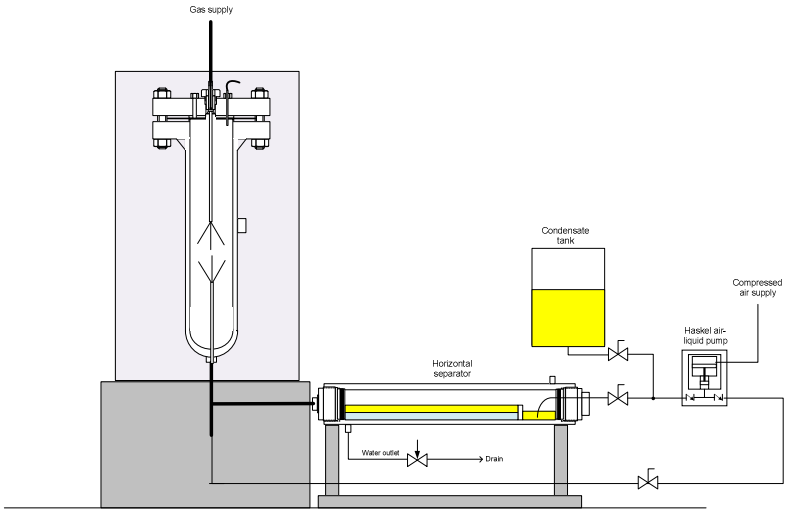

Figure 4-21 Physical implementation of bottom injection solution

The separator was built from a pressure vessel with a custom made weir fitted near the centre of the pressure vessel. An assembly drawing of the separator system is shown in Figure 4-21 .

Assembly and detail drawings of the parts manufactured to convert the pressure vessel to a separator are presented in Appendix D.3.

4.4.3.1 Gas outlet system

The Gas outlet system comprised of the following components:

- Coalescing filter
- Dewpoint meter test point
- Gas outlet heat exchanger
- Back pressure regulator

The outlet from the gas dehydration vessel is passed to a coalescing filter to remove any liquid droplets entrained in the gas stream and is then passed through a heat exchanger that warms the gas before it passes through to the back pressure regulator. A bypass valve was installed to allow the flow to bypass the coalescing filter. A pressure sensor was also fitted between the dehydration vessel and the filter so, together with the outlet pressure sensor, the pressure across the filter could be monitored.

The coalescing filter fitted was a Donaldson HD filter housing with an Ultradepth sub-micron filter designed to remove particles down to 0.01 microns from a gas stream with minimal pressure drop. The coalescing filter was insulated to minimise any increase in the gas temperature prior to the dewpoint meter test point.

The dewpoint meter test point comprised of a Swagelok 'T' junction mounted so that test outlet flow was vertically upwards from the horizontal gas flow at the test point position. This ensured that any liquid water that may accumulate in the tubing when there was no gas flowing did not pass to the dewpoint meter and potentially cause damage to the sensor.

During experiments the gas flow rate at the test point was in the region of 2 to 5 metres per second. According to Tatel and Dukler[124], if there was any liquid water present, the flow regime under these conditions would have been annular dispersed so some water could be present at the test point. However, the flow rate of gas going to the dewpoint sensor was only 0.3 sm^3/hr +/- 20%. At a outlet line pressure of 2.5 MPa this is equivalent to a gas flow rate through the ¼" tubing of less than 3 centimetres per second which is low enough to ensure that no liquid water would take the path to the dewpoint meter.

Control of the dehydration vessel pressure was performed by a back pressure regulator (Reg5) whose output was connected to the low pressure storage vessel. With the cold gas coming from the dehydration vessel and a significant pressure drop across the regulator in early integration runs the performance of the regulator was poor. This was presumed to be due to the formation of hydrates in the regulator.

To prevent this occurrence recurring a gas outlet heat exchanger was fitted to warm the cold gas coming from the dehydration vessel before it passed to the back pressure regulator. The heat exchanger consisted of a 5 m coil of ½" stainless steel tubing jacketed with a plastic

pipe through which water at 50 C from a thermo-regulator was circulated. When the heat exchanger was operating correctly no further dehydration vessel pressure regulation problems occurred.

4.4.4 System instrumentation

The system instrumentation comprised of an electronic data recorder, multiple measuring sensors, connection cabling and conditioning circuits. The following measuring sensors were attached to the experimental system:

- Temperature sensors (PT100)
  - Conditioning vessel temperature
  - Gas inlet temperature of inlet heat exchanger
  - Gas inlet temperature of dehydration vessel
  - Nozzle assembly temperature
  - Dehydration vessel temperature
  - Gas outlet temperature
  - Injected liquid temperature
  - Water tank temperature
  - Inlet heat exchanger water bath temperature
- Pressure gauges
  - Dehydration vessel inlet gas pressure
  - Dehydration vessel outlet gas pressure
  - Liquid injection pump compressed air inlet pressure
  - Liquid injection pump outlet liquid pressure
  - Low pressure storage loop pressure
  - High pressure storage loop pressure
  - Compressor regulator inlet pressure
  - Heptane/water separator pressure
- Pressure transducers (4-20 milliamp current loop output)
  - Inlet pressure
  - Vessel outlet pressure
  - Filter outlet pressure

- Flow rate
  - Gas inlet flow rate (electrical pulse output)
  - Dewpoint meter gas flow rate (no output - variable area flow meter)
- Moisture measurement
  - Outlet gas moisture content (4-20 milliamp current loop output)

4.4.4.1 Sensor device calibration

Temperature sensors were all new devices and were tested for correct operation using an iced water test before installation.

The pressure transducers were tested against a calibrated pressure device and the calibration data programmed into the data recorder.

The dewpoint meter was a new device calibrated at the factory before delivery.

4.4.4.2 Dewpoint meter

The selection and correct installation of the dewpoint meter was critical to the success of the research. The key selection requirements of the sensor were:

- The sensor must be suitable for installation in an outdoor environment
- The sensor must be able to provide a continuous reading of the dewpoint without excessive delay
- The sensor had to have an output suitable for connection to the data capturing recorder
- The sensor had to provide dewpoint readings between 20 C and -50 C and be as accurate as possible within budgetary limits.

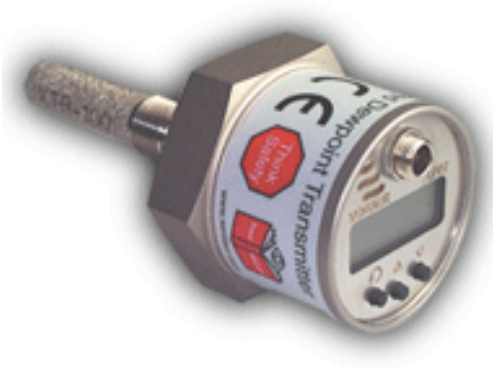

Figure 4-22 Xentaur LPDT Dewpoint transmitter

An extensive search and analysis of available dewpoint meters was performed and seven potential devices made the shortlist. The Xentaur LPDT Dewpoint transmitter was selected in preference to the other devices due to its faster response time, the ease of recalibration, the provision of a display and user controls and its acceptable cost. It provided an accuracy of +/-3C and repeatability of +/-0.5C.The device allowed calibration through a simple end point saturated calibration.

The dehydration tests that make up the reported results were completed within 2 months of receiving a newly calibrated sensor from the supplier and no recalibration was deemed necessary during that period.

Details of the transmitter are provided in Appendix F.

The set up of the dewpoint transmitter in the system was critical to obtain consistent and reliable dewpoint readings. To obtain reliable measurements the following system precautions were taken:

1. The measurement point was taken close to the outlet using a T connection with the test tubing connected vertically above the gas flow.

2. All measurements were taken with the gas at atmospheric pressure so variations in system pressure did not affect the readings

3. The gas and control valve were warmed using a tubing coil submerged in a thermostatically controlled water bath set to 32 C. This ensured that no hydrate formation could occur whilst the gas was expanded from the experimental pressure to atmospheric pressure.

4. The flow of gas through the dewpoint transmitter test cell was set using the control needle valve and measured using a variable area type flow meter fitted upstream of the test cell. A constant flow rate of 0.3 sm^3/hr +/-20% was used for all experiments. Gas downstream of the test cell was vented to the atmosphere.

5. Dewpoint measurements were only taken after sufficient time was given for readings to stabilise.

4.4.4.3 Cabling and signal conditioning

Sensor cabling junction boxes were installed adjacent to the sensors and connected back to the test instrumentation in the laboratory using 4 cables each with 8 wires configured as 4 twisted pairs.

Current loop signals were converted to the voltage signals required by the data recorder using precision, low temperature coefficient, 0.1% 10 ohm resistors.

The pulse signals from the flow meter were converted to a voltage signal using a custom designed and built frequency to voltage convertor. See Appendix E for details on the convertor.

A 24 volt output mains powered power supply was used to supply power to the pressure sensors, dewpoint meter and flow meter electronics.

A detailed wiring diagram for the system instrumentation is provided in Appendix D.5.

4.4.4.4 Data capture

The data collected from sensors was captured by a 16 channel Yokogawa XL100 Portable Data Station and stored on a 1 gigabyte compact flash card to provide a simple means for data transfer to a personal computer for data analysis.

Data was recorded at 1 second intervals by the recorder.

To allow remote monitoring of the data recording a wireless LAN access point was connected to the data recorder.

Twelve of the available 16 data channels were used and are listed in the table below:

Channel	Sensor	Signal type	Range
Channel 1	Vessel temperature	PT100	-10 to +30 C
Channel 2	Vessel inlet temperature	PT100	-10 to +30 C
Channel 3	Filter outlet temperature	PT100	-10 to +30 C
Channel 4	Gas inlet pressure	4-20mA loop	0 to 12 MPa
Channel 5	Dehydration vessel pressure	4-20mA loop	0 to 12 MPa
Channel 6	Dewpoint sensor	4-20mA loop	-70 to +20 C
Channel 7	Inlet flow rate	Voltage	0 to 20 l/min
Channel 8	Heat exchanger inlet temp.	PT100	0 to 30 C
Channel 9	Nozzle temperature	PT100	0 to 40 C
Channel 10	Condensate temperature	PT100	-40 to 40 C
Channel 11	Water tank/bath temperature	PT100	0 to 20 C
Channel 12	Vessel outlet pressure	4-20mA loop	0 to 12 MPa

Table 4-4 Data capture channel assignment

5 Dehydration system tests

The research project testing comprised a number of distinct phases:

- Integration testing of the gas delivery system
- Dehydration system development and optimisation
- Dehydration system performance testing
- Dehydration system enhancement testing

The total test program took place over a period of 20 months from January 2009 when pressure testing of the system commenced to September 2010 when the final system enhancement testing was completed. During this period over 110 test runs were performed and the data recorded. A summary of the test runs is provided in Appendix H.

A typical dehydration test run took a period of around 6 hours, comprising an initial 3 hour stabilisation period followed by the taking of experimental readings. The long stabilisation time was required for the dehydration vessel to reach equilibrium at the test conditions and for the dewpoint meter to provide accurate readings. During an experiment, test point readings could be taken every 40-50 minutes depending on the change of system conditions between readings.

Some program delays were experienced whilst system modifications were implemented and due to some equipment failures, in particular the dewpoint sensor which failed twice and had to be returned to the manufacturer for repair.

In the following sections the results of the runs are provided in a logical rather than strictly sequential manner. For instance, data presented against flow tests was obtained from runs during all the phases but for ease of presentation is presented in the system development and optimisation section.

5.1 Integration testing of the gas delivery system

The scope of this research project included the design, build and testing of the gas delivery system. The work undertaken included:

- Component identification and procurement
- Building of control panels including mechanical construction and installation of control components
- Installation and commissioning of the gas compressor

- Installation of tubing to connect all the system components
- Formal HAZOP review and creation of operating and safety instructions
- Pressure testing of gas loop components
- Operational testing of the gas loop to confirm it met the design requirements

System commissioning was completed in mid June 2009.

5.1.1 Natural gas composition

The gas used for all experiments was supplied by Alinta gas through a 40 kPa gas main connection. The gas content from the mains supply varied to a small degree on a daily basis due to variation in the volumes of gas supplied by the multiple gas producers supplying gas to the mains. Due to the method used to measure the dewpoint where a small flow of gas was continuously vented to the atmosphere periodic topping up of the gas loop from mains gas was required, typically once per hour during experimental runs.

Data on the composition of the gas was obtained from Alinta for two different days. An average of the compositions was utilised for all calculations. Table 5-1 details the measured compositions and provides the averaged data.

Component	Day 1	Day 2	Average
Methane	86.82	87.06	86.9
Ethane	6.57	6.42	6.5
Propane	1.45	1.02	1.3
i-Butane	0.08	0.05	0.07
n-Butane	0.10	0.05	0.07
i-Pentane	0.01	0.00	0.005
n-Pentane	0.01	0.00	0.003
Hexane	0.00	0.00	0.002
Nitrogen	1.56	1.62	1.55
Carbon Dioxide	3.41	3.77	3.6

Table 5-1 Alinta natural gas composition (%)

The percentage of methane of the hydrocarbon gases is 91.6%.

5.1.2 Nozzle sizing

The system design placed the following constraints on the nozzle fitted within the dehydration vessel:

- It had to be small in size so it could fit through the mounting ports in the dehydration vessel (1" BSP threaded holes)

- Replacement of the nozzle required depressurisation of the dehydration vessel so this was not possible during runs and was to be avoided if possible between experiments

These constraints meant that use of an adjustable nozzle was not possible and it would be desirable to have a nozzle size that would support multiple experimental flow conditions. It was decided to use a nozzle that would support the maximum output of the compressor at the highest pressure drop across the nozzle. For choked flow the nozzle diameter for a flow of 560 standard litres per minute from the compressor at 10 MPa inlet pressure was calculated to be 0.7 mm (refer to section 3.4.1.2).

Nozzle flow experiments were performed to confirm this sizing estimate. The initial nozzle sizing experiments were performed using air due to the delay in connection of the natural gas supply to the compressor. To check the validity of using air we revisited the nozzle calculation using the properties of air. Air has a specific heat ratio of 1.40 at the experimental conditions and its molecular weight is 28.97. When using these values in the nozzle sizing calculation the nozzle size for choking flow was calculated to be 0.81 mm. This is 16% greater than that calculated for natural gas. The use of air to test nozzles is experimentally useful to validate the calculation but final sizing experiments using natural gas were required.

The nozzle test with air was performed with the nozzle fitted into the dehydration vessel. The compressor outlet was connected directly to the nozzle input and the dehydration vessel output connected via a vent to the atmosphere. The compressor was run and the pressure output of the compressor was monitored. The compressor outlet pressure stabilised when the flow through the nozzle matched the output flow of the compressor (fixed at 560sl/min). A number of different nozzle sizes were trialled:

- 1mm diameter nozzle- compressor pressure maximum only 1.2 MPa

- 0.61 mm diameter nozzle – compressor cut out at 14 MPa (limit)

- 0.84 mm diameter nozzle – pressure stabilised at 10 MPa

The experimental nozzle size of 0.84 mm is within 4% of the calculated nozzle size for choked flow, so our calculation method appears valid.

In later experiments with natural gas nozzle sizes of 0.6 mm, 0.8 mm and 0.85 mm were used successfully with 0.85 mm being the maximum size that would allow the compressor to establish a 10 MPa inlet pressure.

Figure 5-1 shows the flow through a 0.8 mm nozzle for a typical flow experiment. During the experiment the inlet pressure was kept constant at a nominal 10 MPa and the outlet pressure was gradually reduced in 8 steps to a minimum outlet pressure of 2.4 MPa. The points plotted are taken directly from the data recorder with no post processing. The concentration of dots is due to the large number of readings taken at each stabilisation step. The larger dispersion at the higher pressure drops are due to some irregularity in the flow experienced due to lower temperatures experienced at the nozzle due to the larger pressure drop, higher JT cooling. This is evidence of some hydrate formation at the nozzle causing a restriction in the nozzle diameter and a drop in the flow rate.

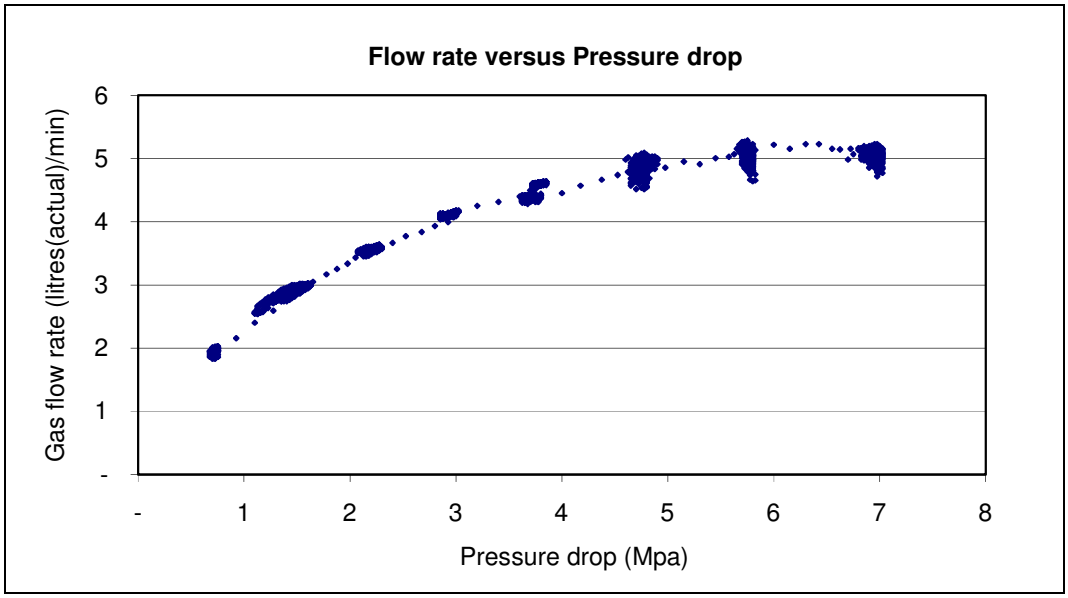

Figure 5-1 Flow rate versus pressure drop at nominal 10 MPa inlet pressure

(Nozzle size 0.8 mm, flowing natural gas, nozzle heater on)

The flow rate increases with increased pressure drop across the nozzle until around 5.5 MPa where it levels off suggesting choked flow from this point on.

5.2 Dehydration system development and optimisation

The development and optimisation phase of the research was the phase during which system operation was tested, analysed, system enhancements identified and modifications implemented. This was a cyclical process that gradually identified system constraints and implemented the solutions.

System enhancements that were identified and implemented during this phase included:

- Dewpoint meter sampling solution (refer to section 4.4.4.2)
- Insulation of dehydration vessel (refer to section 4.4.2.2)

- Nozzle hydrate blockage prevention controls (refer to section 4.4.1.1)
- Location of nozzle within dehydration vessel
- Water carry-over prevention

5.2.1 Development of Inlet gas flow system

A critical design element of the system is the inlet gas flow system due to the ease at which the inlet nozzle could be blocked with hydrates deposited around the nozzle during the gas expansion and cooling process occurring at the nozzle.

- Implementation of heated nozzle assemblies
- Control of inlet gas temperature
- Nozzle design
  - Type – tubular, de Laval
  - Orifice size
- Positioning of the nozzle in the dehydration vessel
  - Side mounted or top mounted
  - Porting design

5.2.1.1 Prevention of hydrate blockage of inlet nozzle

The blockage of the inlet nozzle was experienced during the first experimental run using natural gas. On reviewing the conditions within the vessel at the nozzle it was clear that the temperature and pressure conditions were conducive to the formation of hydrates and that it was likely that it was hydrates causing the blockage. On leaving the system to warm up the blockages cleared with no other intervention so a blockage with dirt could be ruled out and the case for hydrate causing the blockage supported.

Two approaches to prevent hydrate blockage were used during experiments, implementation of a heated nozzle assembly and the pre-heating of the gas before it was passed to the dehydration vessel. The appearance of hydrates on the nozzle was easily detected during experiments by monitoring the flow rate on the data recorder.

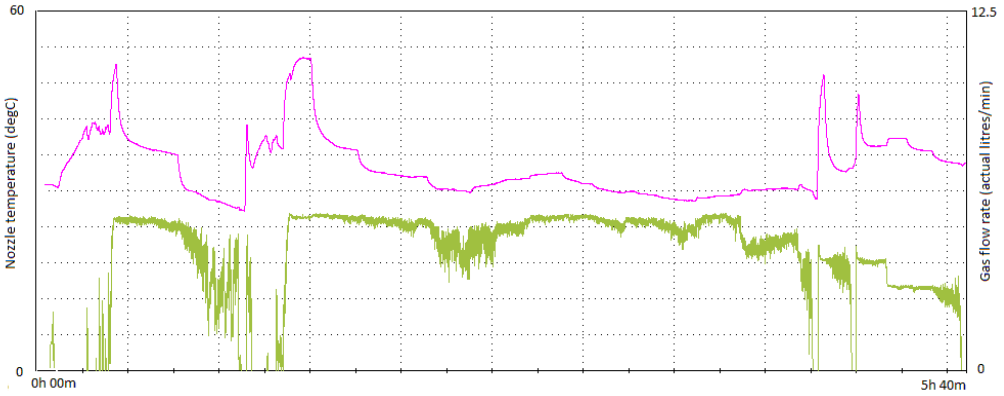

Figure 5-2 Experimental plot with blocked flow

(Purple: Nozzle adaptor temp, Green: Gas flow rate)

In the experimental plot shown in Figure 5-2, the flow trace in green shows smooth zones where the flow is constant, irregular zones where hydrate build-up is starting to block the nozzle and also complete blockage where the flow drops to zero. The nozzle adaptor temperature trace illustrates how a blockage could be removed by adding power to the heaters and increasing the temperature of the adaptor. After a few minutes the hydrate melted and flow recommenced.

Tests of the dehydration system using different nozzle heater settings were performed where the inlet and outlet pressure were kept constant. The initial power setting of the nozzle was high and the system was run until it stabilised. The nozzle power was then backed off in steps with the vessel allowed to stabilise at each step

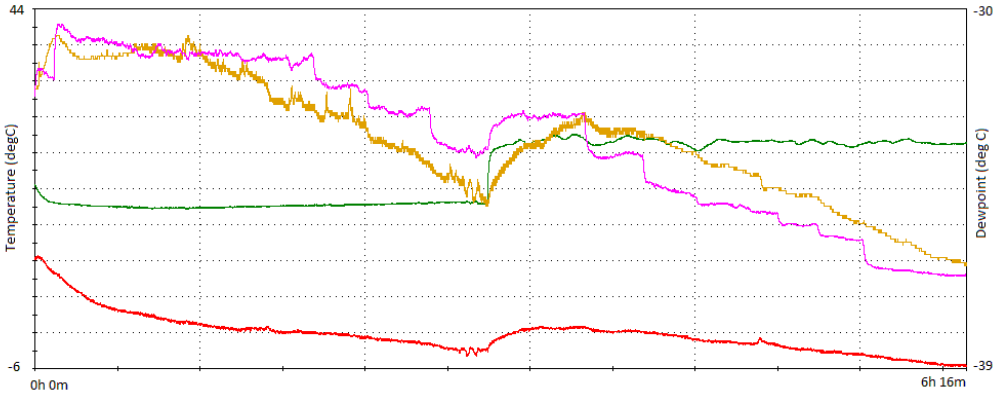

Figure 5-3 Experimental plot for constant pressure, variable nozzle power run

(Red: Vessel T, Green: Inlet T, Purple: Nozzle T, Orange: Dewpoint)

An example of such an experimental run is shown in Figure 5-3 where two different inlet gas temperatures were trialled during the same experimental run. The initial inlet gas was passed though a coil submerged in a cold water bath and measurements taken at a number

of nozzle power settings. When the flow became erratic, i.e. hydrates starting to block the nozzle the inlet gas temperature was increased by opening a bypass in the inlet gas pathway so that the gas was not cooled by the water bath. Nozzle power was then stepped down until the power to the heater nozzles was zero.

The lowest dewpoint was measured under the conditions of a higher inlet gas temperature but with the nozzle heaters switched off. In the experiment illustrated the results are tabulated in Table 5-2.

Condition	Run 1	Run 2
Inlet temperature	17 C	25.4 C
Inlet Pressure	9.8 MPa	9.8 MPa
Outlet pressure	2.5 MPa	2.5 MPa
Nozzle temperature	23.7 C	Power OFF
Vessel temperature	-3.5 C	-5.5 C
Hydrate formation temperature	7.0C	7.0C
Lowest dewpoint	-34.5 C	-36.5 C

Table 5-2 Results of dehydration experiment with varying nozzle power

The results of this test suggested that the best approach to obtaining optimum dehydration was to control the inlet gas temperature rather than by heating the actual nozzle. This test was repeated at the same pressure conditions and also at higher outlet pressure. The results of all these tests were consistent with this example.

There is no obvious explanation why using a warm inlet gas operates better than a cold gas with a heater at the nozzle when one considers the nozzle adaptor in isolation. When we consider the gas flow between the conditioning vessel and the inlet to the nozzle adaptor a potential explanation is apparent. The warm gas fed to the nozzle adaptor is within 4 C of the outlet temperature of the gas conditioning vessel whilst that coming after the transit through the cold water bath is nearly 13 C cooler. As the gas stream from the conditioning vessel is close to saturated with water vapour as it is cooled by this larger temperature drop condensation of water from the gas stream will occur. The water content of natural gas at 17 C is nearly half that of gas at 30 C. The Reynolds number for the flow through the coiled tubing is around 65,000 which place the flow regime for drawn tubing in the turbulent region . In this flow regime droplets are likely to be carried by the gas stream to the nozzle adaptor. It is thought that these droplets are likely to wet the nozzle surfaces and make it more prone to hydrate formation and consequent blockage.

As a consequence of these results, the use of heated nozzles was discontinued in future tests. This approach also allowed for greater options in the mounting position of the nozzles, e.g. suspended on tube extensions in the centre of the dehydration vessel.

5.2.1.2 Positioning of the nozzle

A number of different nozzle mounting configurations were trialled during the development and optimisation phase:

- Radial side entry at middle of the dehydration vessel
- Top entry
- Top entry with cowling extending half way down the dehydration vessel
- Top entry with no cowling but tubing extension into the dehydration vessel.

Swirling of the gas flow to implement some centrifugal forces to assist with condensed droplet removal was considered but deemed to be unachievable due to the low flow rates achievable with the compressor. A review of hydro-cyclones characteristics also suggested that removal of very small droplets with this technique is unlikely to be successful.

The measured dewpoint for two radial side entry experiments with different nozzle sizes are shown in Table 5-3 together with the dewpoint calculated at the vessel pressure and temperature conditions. The calculation were made using the Goff-Gratch equation (see section 3.3.1.1) to convert parts per million (by volume) values obtained from HYSYS to dewpoint.

Date	Inlet pressure	Outlet pressure	Nozzle	Vessel temperature	Measured dewpoint	Calculated dewpoint
23 Sept 09	10 MPa	4.4 MPa	0.8 mm	0.6 C	-25.6 C	-36.7 C
28 Sept 09	10 MPa	4.2 MPa	0.6 mm	-0.1 C	-25.2 C	-36.8 C

Table 5-3 Radial side entry experiments

The results of the experiments for the two different nozzle sizes were very similar and both measured dewpoints were much higher than the calculated dewpoint at the vessel conditions.

The flow rates for these experiments were 5.4 litres per minute for the 0.8 mm nozzle and 2.8 litres per minute for the 0.6 mm nozzle. The gas residence time for the 0.6 mm nozzle was therefore nearly double that for the 0.8 mm nozzle. As the measured dewpoint results were very similar it was concluded that gas residence time was not a controlling factor in the dehydration performance.

Reviewing the measured dewpoint against the calculated dewpoint at the vessel conditions it was felt likely that some carryover of condensed water droplets to the outlet stream was occurring and impacting the measured dewpoint. A review of expected condensation behaviour (refer to section 3.4.3 Water droplet formation and flow) suggested that sub micron sized droplets were likely to be present in the vessel and that with the gas velocities present in the vessel that transport of these droplets out of the vessel outlet against gravity forces was probable. To see if carry over was occurring a 'T' section was added upstream of the dewpoint test point with a sealed tube connected vertically downwards. After a run the tube was removed and water was found confirming some carryover of fluid.

To try to prevent water carryover it was decided to trial a new nozzle location with the gas stream flowing into the vessel in a contra-flow to that exiting the vessel. The nozzle adaptor was thus moved to the centre of the vessel's top flange so that the gas flowed downwards into the vessel away from the upward direction of the gas leaving the vessel. All further experiments were performed with this gas contra-flow with various nozzle positions and configurations. Improved vessel insulation was also installed at this time.

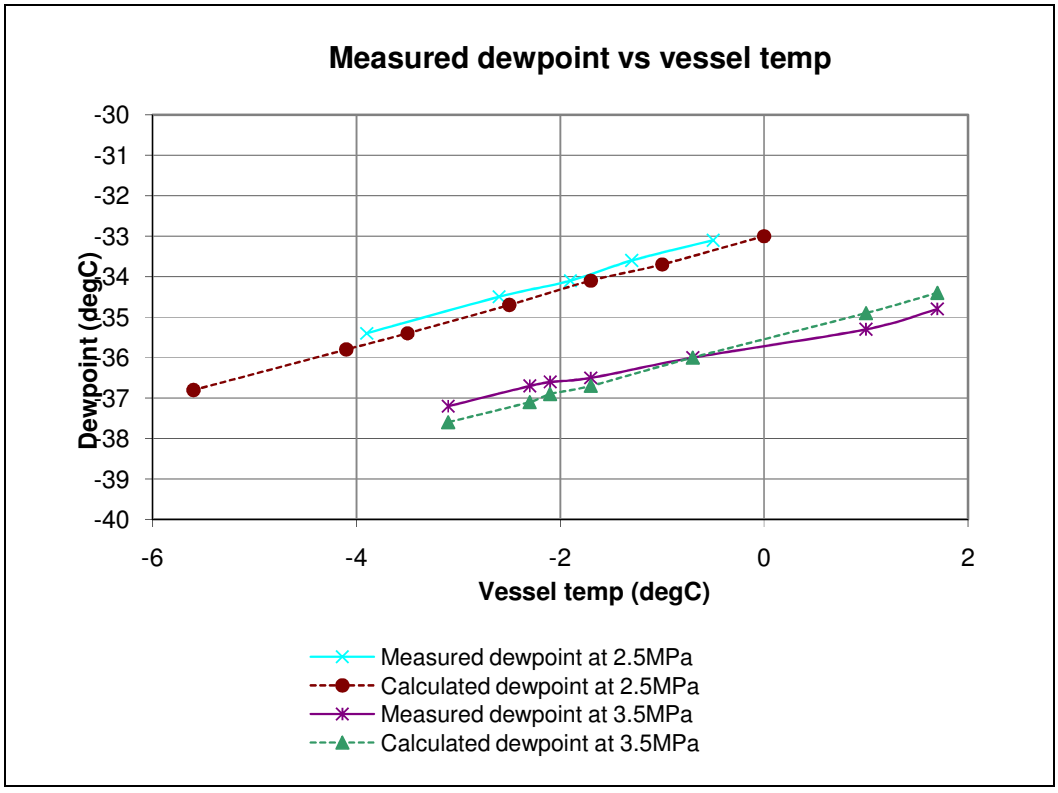

Figure 5-4 Dewpoints for top gas flow at 2.5 MPa and 3.5 MPa

A number of runs were performed with constant inlet pressure and variable outlet pressure, with the nozzle heater power adjusted to the minimum sustainable level at each pressure. The results were inconsistent and it was decided to limit the number of variable during the runs so that repeatability was easier to achieve. Fixed inlet and outlet pressures were used

and only the inlet gas temperature changed during the run using nozzle power and the inlet heat exchanger.

The plots in Figure 5-4 show the results for the measured dewpoint for experimental runs under constant inlet and outlet pressures while adjusting the inlet gas temperature. The dewpoints for an outlet pressure of 2.5 MPa and 3.5 MPa are plotted against the vessel temperature together with the dewpoints calculated by HYSYS/Goff-Gratch (see section 3.3.1.1). The difference between measured and calculated is small, well within the error bounds of the dewpoint sensor.

HYSYS when calculating the water content assumes no presence of hydrates. Figure 5-5 shows the hydrate curve for the Alinta gas composition with the experimental test points overlaid. From this plot it is clear that the environmental conditions within the vessel are conducive to the formation of hydrates. The experimental results suggest either that no water content suppression by hydrate presence has occurred or an over-reading of the dewpoint meter caused by water carry over as previously experienced.

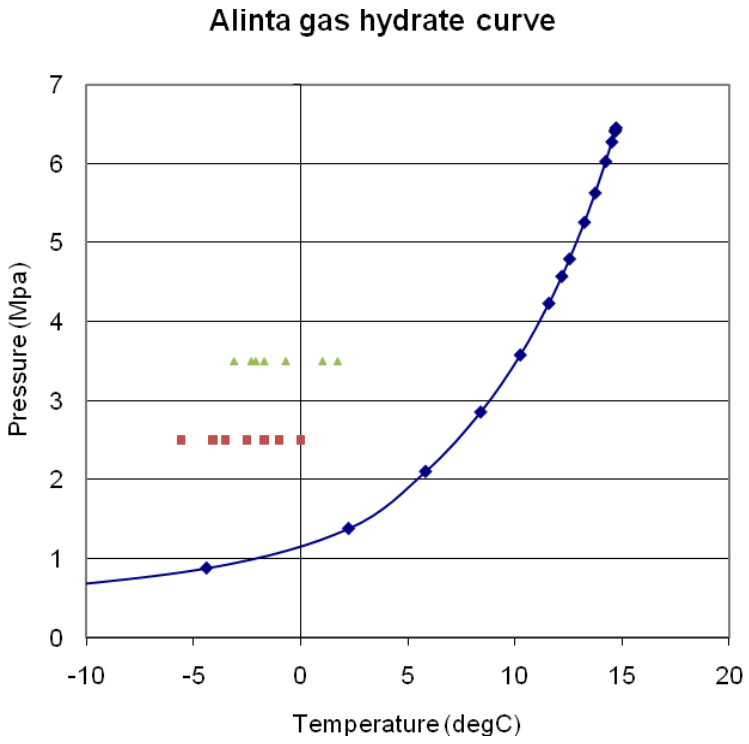

Figure 5-5 Hydrate curve for Alinta gas with experimental test points

To attempt to reduce any carryover of water droplets to the outlet stream a PVC tube cowling was fitted within the dehydration vessel to separate the inlet and outlet points and ensure the gas flowed at least halfway down the vessel as illustrated by Figure 5-6.

Two experimental runs were performed with the new cowling using 10 MPa input pressure and output pressures of 2.5 MPa and 4.9 MPa. The resulting measured dewpoints were -34.2 C and -35.0 C respectively and calculated dewpoints were -35.5 C and -36.9 C. There was no apparent benefit in the fitting of the cowling to the dehydration vessel.

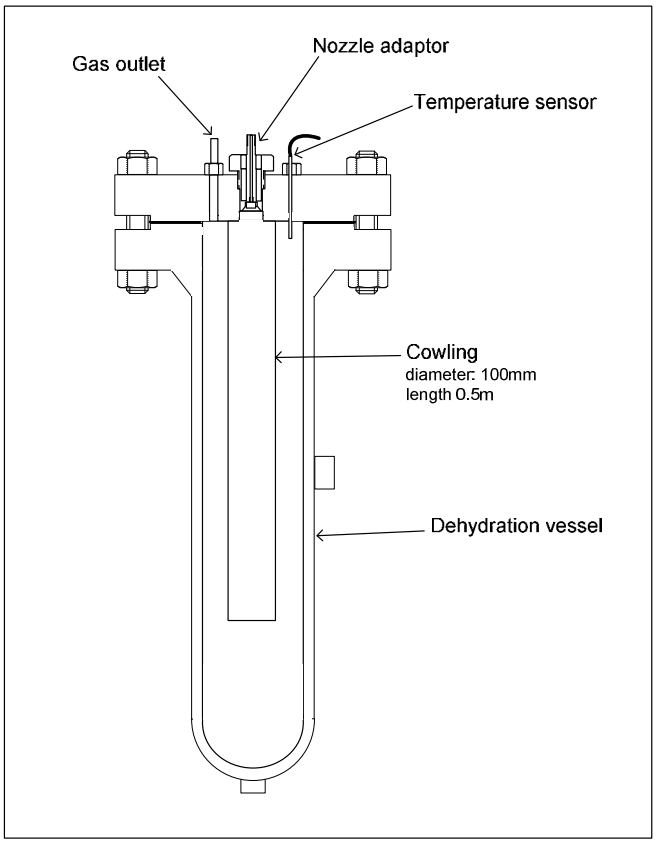

Figure 5-6 Dehydration vessel with internal cowling

A coalescing filter capable of capturing down to sub-micron particles was procured and fitted to the outlet of the dehydration vessel, upstream from the dewpoint measurement sample point. The coalescing filter was insulated by encapsulating the unit within 200 mm thick sheet of expanded polystyrene.

In the runs with the cowling configuration and the coalescing filter in circuit small amounts of water were collected from the coalescing filter, typically in the order of 2 to 4 ml per run. When we consider the vessel inlet and outlet conditions an estimate of the amount of water that should be collected by the process can be made.

For run of 20 January 2010:

At 10 MPa, 25 C inlet conditions the calculated water content is:	504 ppmv
At 2 MPa, -10 C vessel conditions the calculated water content is: (excluding any hydrate depression of water content)	156 ppmv
Rate of water removal by process:	348 ppmv
Gas flow rate (560 sl/min):	1,500 mol/hr
Predicted water capture rate:	0.52 mols/hr
or	**9.4 ml/hr**

It took an hour from the start of the run to reach the vessel operating temperature and the total run duration was 5 hours. Using the predicted water capture rate and assuming half the capture rate for the cool down period we would expect to capture 42.3 ml of water.

At the end of the run the coalescing filter was depressurised and allowed to reach ambient temperature to ensure no water was in ice or hydrate form in the filter. The water captured by the filter during this run was 5 ml, or nearly 12% of the predicted water capture.

Water capture within the vessel was also measured by opening the vent connected to the bottom of the vessel and capturing as much fluid as was possible. Venting was performed immediately after the run and the liquid collected. The vessel was then depressurised and left overnight after which the vessel was pressurised to a pressure sufficient to drain the bottom vent and collect the liquid. Immediately after each run only a small amount of water was collected, typically 5 to 10 ml. The amount of water collected after the vessel had been left to allow ice and hydrates to melt was around 110 ml. This large collection of water after depressurisation confirms that water is being stored in the dehydration vessel in the form of hydrates on the walls of the vessel.

An issue that requires explanation is that the total water captured was greater than that was predicted, There are two explanations for this over capture, firstly if we examine the conditions of the conditioning vessel we note that the conditioning vessel temperature was around 35 C. Consequently the water content of the gas leaving the conditioning vessel at 10 MPa is greater than that at the entry conditions to the dehydration vessel, 861 ppmv versus 504 ppmv. Within the path between the conditioning vessel and the dehydration vessel there was no location for this water to be removed so it is likely that this water was carried by the gas stream and entered the dehydration vessel where it added to the amount of water collected. If we consider the input water saturation to be 861 ppmv the predicted water capture rate changes to 19 ml/hr, or 114 ml for an experimental run period of 6 hours.

The second explanation on the excess of water captured is the depression of water content due to the presence of hydrates. As noted above, the presence of hydrates in the vessel has

been confirmed so some depression in the water content due to these hydrates would be expected and a resultant increase in water captured.

A new phenomenon that occurred during the experimental runs with the coalescing filter in the output stream was the reversal of the vessel temperature and outlet temperature. During all previous experiments the outlet sensor, fitted on the outlet tubing from the dehydration vessel, was always higher than the temperature within the dehydration vessel. With the coalescing filter in place after a few hours of operation the measured temperature of the gas leaving the coalescing filter became colder than that of measured temperature of the dehydration vessel gas. This phenomenon is illustrated in Figure 5-7 for the experimental run of 19 Jan 2010.

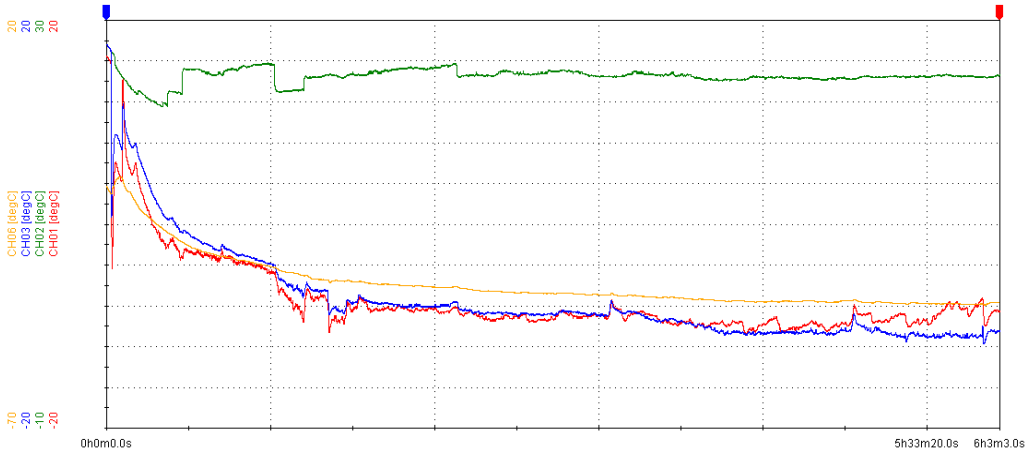

Figure 5-7 Temperature reversal phenomena with coalescing filter

(CH1: Vessel temp., CH2: Inlet temp., CH3: Outlet temp., CH6: Dewpoint temp.)

In the early stages of the run the vessel temperature (red trace) is below the outlet temperature (blue trace). Half way through the run they become equal and later in the run the outlet temperature is lower than the vessel temperature with the difference become marked at the end of the run. There are two possible explanations for this behaviour.

We know that water is being captured by the coalescing filter and that the pressure and temperature conditions within the coalescing filter are conducive to the formation of hydrates. It is probable that some hydrate formation is occurring within the filter cartridge within the coalescing filter. If this hydrate build up becomes sufficient to cause some choking of the gas flow we would get a pressure drop established across the coalescing filter. Some JT cooling would then occur and a temperature drop from vessel to filter output would result. As the total pressure drop between dehydration vessel input and coalescing filter output is fixed, if a pressure drop establishes across the filter then the pressure drop across the dehydration vessel choke must decrease. A decrease in pressure drop across the dehydration vessel

choke would result in a reduction of the JT cooling effect and an increase in the temperature within the dehydration vessel, a feature present in the above experimental plot.

An alternative explanation is that a build up of hydrates takes place on the temperature sensor measuring the temperature of the dehydration vessel gas. Hydrate formation is exothermic so if it formed on the surface of the temperature sensor the sensor would be expected to show a temperature increase while the process continued and be fairly constant in its effect.

The irregular nature of the dehydration vessel temperature trace in particular the sharp drops is more consistent with sudden changes in pressure within the vessel than likely changes due to hydrate formation of the temperature sensor. To investigate this phenomena further a bypass valve across the filter and a pressure sensor on the inlet to the filter were added to the system to allow the filter to be taken out of circuit and for the pressure drop across the filter to be monitored.

At the same time as the bypass and sensor were fitted the internal configuration of the dehydration vessel was also changed, the cowling was removed and the nozzle was placed further into the dehydration vessel. A consequence of these internal changes was that no further fluid was captured by the coalescing filter and the temperature cross over phenomena was never seen again. During subsequent runs no pressure drop was ever measured across the coalescing filter.

5.3 Dehydration system performance testing

5.3.1 Joule Thomson cooling efficiency tests

During the experimental runs of the well insulated dehydration vessel the JT coefficient was calculated when no nozzle power was used and the results are shown in Figure 5-8.

The average JT coefficient over all the experiments was 4.37. The results show a downward trend on the JT coefficient as the inlet pressure increased, though with the small range of inlet pressures utilised this is hardly definitive.

Using HYSYS and the Alinta gas composition the JT coefficient for each of these experimental runs was calculated and the calculated average JT coefficient was 4.79. A plot of the calculated JT coefficients is also shown in Figure 5-8. A detailed table of all the results providing the experimental data and the calculated JT coefficients is provided in Appendix H.1.

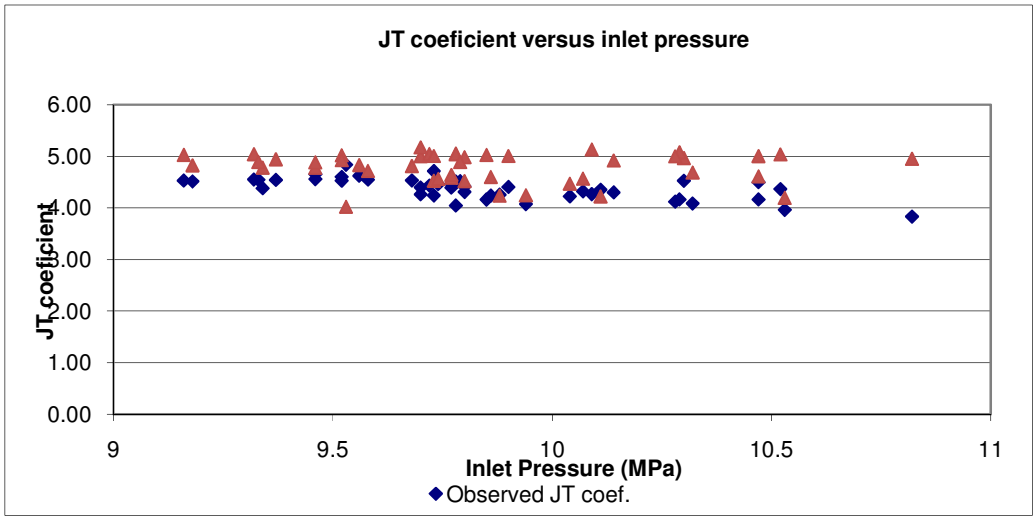

Figure 5-8 Observed and calculated JT coefficients for experimental runs vs. input pressure

Comparing the experimental results with the calculated values for the JT coefficients we can conclude that the JT cooling for the experiments operated as expected and achieved fairly good results.

5.3.2 Dehydration experiments

After many months performing integration tests and enhancing the system to obtain the best possible dehydration results we finally arrived at a design of dehydration vessel that gave good JT cooling and minimal water carry over in the outlet gas stream. Figure 5-9 shows the resultant dehydration vessel configuration with the nozzle fitted on a tubing extension. The nozzle was positioned 53 cm into the dehydration vessel with the gas flowing downwards.

5.3.2.1 Test method

The dehydration experiments were performed as a series of runs at different fixed vessel pressure keeping the inlet pressure nominally fixed to the maximum output pressure of the gas storage loop and varying the temperature of the inlet gas stream.

The nature of the dew point measuring sensor used is that it is relatively slow to measure a drying gas stream but fairly quick to measure a stream with increasing moisture content. Consequently the experimental runs were designed to start at the driest conditions allowing sufficient time for the sensor to stabilize and then gradually increasing the moisture content.

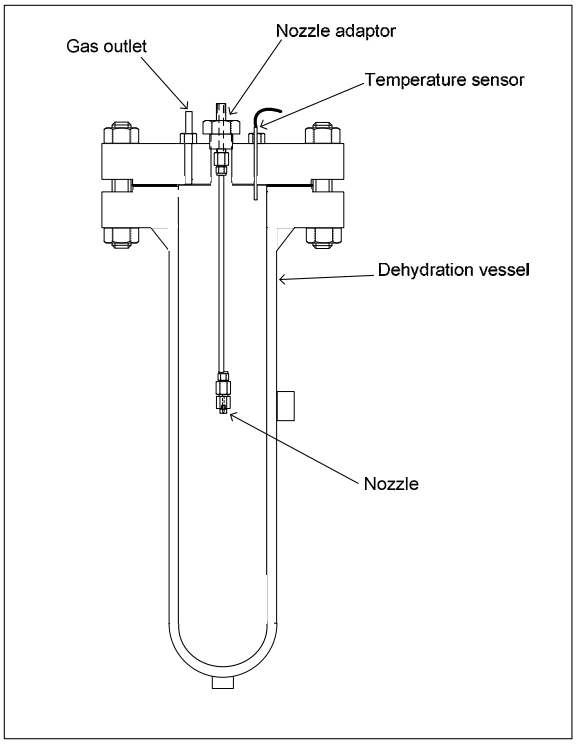

Figure 5-9 Dehydration vessel configuration for final dehydration runs

At the start of each run the inlet gas temperature was set using the Jelabo digital temperature controller that was fitted to the gas inlet water bath. The water bath temperature was set to a temperature that would just allow a steady gas flow through the nozzle without hydrate blockages occurring at the nozzle. Once the water bath temperature was stable the experimental run commenced.

The gas compressor was switched on and the high pressure storage loop pressurized to around 10.5 MPa with domestic Alinta gas.

The experimental inlet pressure was set using the forward pressure regulator and the dehydration vessel pressure was set using the back pressure regulator. Natural gas at the experimental pressure was passed through the conditioning vessel where it was bubbled through a 0.6 m water column, within the pressure vessel, to saturate the gas stream with water vapour. The saturated natural gas was then passed through a heat exchanger to set the inlet gas temperature to the required value and then to the nozzle fitted within the dehydration vessel. The nozzle used had a 0.85 mm round orifice, a length of 0.5 mm and a maximum flow rate of 6.1 litres/minute at a pressure of 10 MPa. The natural gas passed through the nozzle into the dehydration vessel and then out via the back pressure regulator to the low pressure storage loop. From the low pressure storage loop the gas was recycled to the compressor.

After the experimental pressures and flow had stabilised the dew point sensor was switched on. The dew point sensor measured the outlet gas dew point at atmospheric pressure and at a constant flow rate of 0.3 sm^3/hr (+/- 20%)

The system was run for around 2½ hours to allow the dehydration vessel operating conditions to reach equilibrium and for the dew point sensor reading to stabilize. After system equilibrium was reached and at subsequent intervals of around 40 minute the temperature of the inlet gas was increased in steps of 2 C. The dew point of the gas stream was constantly measured and captured electronically by a Yokogawa XL100 data station. Figure 5-10 shows the data capture results for a typical experimental run at 3.8 MPa.

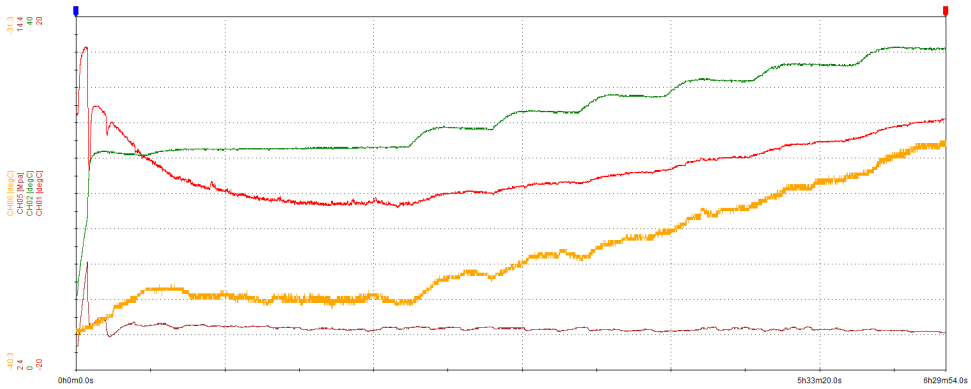

Figure 5-10 Data capture for test run at dehydration vessel pressure of 3.8 MPa
(CH1 – Vessel temp., CH2 – Inlet gas temp., CH5 – Vessel Pressure, CH06 – Dew point)

Additional data capture pots are provided in Appendix D.7

5.3.2.2 Validation of the test method

To validate the experimental approach to the measurement of the dew point at varying inlet conditions a number of fixed condition equilibrium tests were performed and the results compared with those obtained from the runs described above. The equilibrium tests gave results for measured dew points within 0.6 C of the dew point measured by the varying gas stream temperature runs. This is well within the error bounds of the sensor and successfully confirmed the validity of the measurement approach.

5.3.3 Experimental results

The experimental data captured by the data recorder was processed to extract the results at each set point and was plotted as dew point measured versus the dehydration vessel temperature at the various run pressures.

Figure 5-11 shows the final experimental results for dehydration vessel pressures between 2.4 MPa and 4.8 MPa.

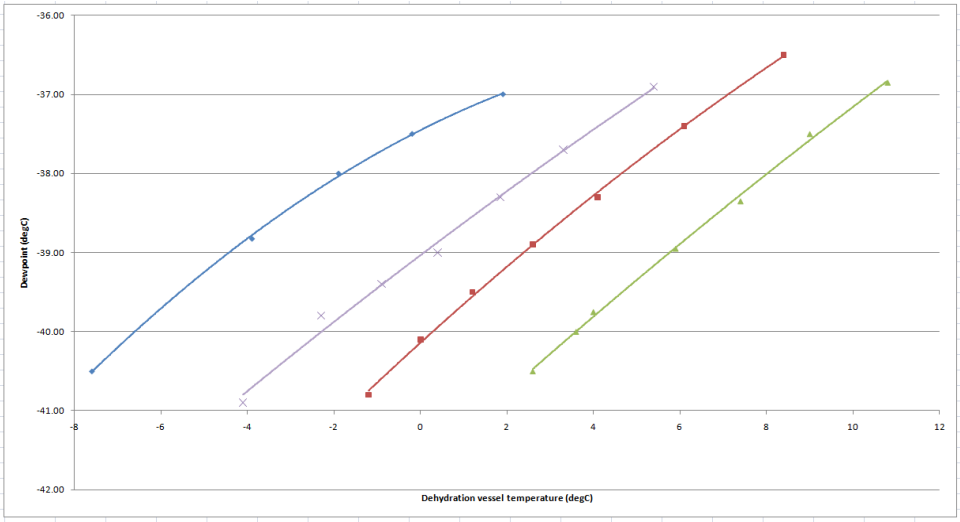

Figure 5-11 Dew point vs. Dehydration vessel temperature at various pressures

A summary of the lowest dewpoints achieved for each run is provided in Table 5-4.

A quick review of the data shows a noticeable trend of lower dewpoints being measured in later experimental runs that needs to be investigated. As the dewpoint is a function of temperature and pressure and values of these varied from run to run it is necessary to make some corrections to the results so that results can be looked at chronologically to see if a reducing trend existed.

To correct for differences in dehydration vessel temperature at constant pressure the results of our dehydration experimental runs shown in Figure 5-11 can be used. When linear trend lines are fitted to these data plots a dewpoint slope that is approximately 0.4 is obtained.

To minimise the correction for pressure, the results can be grouped into pressure ranges and then a small correction made within the selected ranges. To obtain a correction for pressure at constant temperature HYSYS was used to calculate the change in water content and Goff-Gratch (see section 3.3.1.1) to convert this to a change in the dewpoint.

Run Date	Inlet Pressure (MPa)	Outlet Pressure (MPa)	Vessel Temperature (C)	Dewpoint temperature (C)
30-Jul-10	9.36	2.08	-7	-38.3
2-Aug-10	9.18	3.73	0.4	-37.7
3-Aug-10	9.73	5.18	4.5	-37.8

Run Date	Inlet Pressure (MPa)	Outlet Pressure (MPa)	Vessel Temperature (C)	Dewpoint temperature (C)
6-Aug-10	9.94	6.43	9.7	-36.8
9-Aug-10	9.71	2.49	-5	-39.4
10-Aug-10	10.11	6.25	8.3	-37.6
11-Aug-10	9.34	3.84	1	-39.4
13-Aug-10	10.04	5.14	4.2	-39.3
16-Aug-10	9.52	2.41	-5.4	-40.6
17-Aug-10	10.33	6.24	8.1	-38.4
18-Aug-10	9.77	3.99	3.6	-38.5
18-Aug-10	9.37	2.39	-2.7	-39.6
19-Aug-10	9.43	6.15	17.7	-36.7
19-Aug-10	9.88	4.96	12.5	-35.2
20-Aug-10	9.78	2.36	-6.3	-40.9
23-Aug-10	9.46	3.81	-1.1	-40.7
24-Aug-10	9.74	4.81	2.7	-40.5
25-Aug-10	9.79	3.06	-4	-40.9

Table 5-4 Measured dewpoints for dehydration experimental runs

The calculated adjustments to the measured dewpoints to bring the results to a constant vessel pressure and temperature are shown in Table 5-5 and the results are plotted versus time in Figure 5-12.

Run date	Inlet pressure (MPa)	Outlet pressure (MPa)	Vessel temp. (C)	Measured dewpoint (C)	Temp. adjust (C)	Pressure adjust (C)	Adjusted dewpoint (C)
Dehydration vessel: Pressure 2.36 MPa Temperature -6.3 C							
9-Aug	9.71	2.49	-5	-39.4	-0.52	0.4	-39.7
16-Aug	9.52	2.44	-5.8	-40.6	-0.2	0.2	-40.7
20-Aug	9.78	2.36	-6.3	-40.9	0	0	-40.9

Run date	Inlet pressure (MPa)	Outlet pressure (MPa)	Vessel temp. (C)	Measured dewpoint (C)	Temp. adjust (C)	Pressure adjust (C)	Adjusted dewpoint (C)
Dehydration vessel: Pressure 3.81 MPa Temperature -1.1 C							
2-Aug	9.18	3.73	0.4	-37.7	-0.6	-0.2	-38.6
11-Aug	9.34	3.84	1	-39.4	-0.84	0	-40.4
23-Aug	9.46	3.81	-1.1	-40.7	0	0	-40.7
Dehydration vessel: Pressure 4.81 MPa Temperature 2.7 C							
3-Aug	9.73	5.18	4.5	-37.8	-0.72	0.5	-37.9
13-Aug	10.04	5.14	4.2	-39.3	-0.6	0.4	-39.4
24-Aug	9.74	4.81	2.7	-40.5	0	0	-40.5
Dehydration vessel: Pressure 6.24 MPa Temperature 8.1 C							
6-Aug	9.94	6.43	9.7	-36.8	-0.64	0.1	-37.3
10-Aug	10.11	6.25	8.3	-37.6	-0.08	0	-37.7
17-Aug	10.33	6.24	8.1	-38.4	0	0	-38.4

Table 5-5 Grouped and adjusted dehydration data

Reviewing the dewpoints versus date confirms that the measured dewpoints did in fact drop as further runs were performed. It is hypothesised that this improvement in dehydration performance over time was due to the build up of hydrates within the dehydration vessel. This hypothesis can be justified for the following reasons:

- During the period that the dehydration runs were performed the dehydration vessel was kept pressurised. Between runs the dehydration vessel pressure was the average system pressure of around 5 MPa.

- The runs were performed over winter months and with the good insulation installed around the dehydration vessel. At no time was the temperature in the dehydration vessel seen to exceed the dissociation temperature for hydrates at the dehydration vessel pressure.

- An increase in the presence of hydrates in the vessel should lead to better gas/hydrate contact thereby reducing the water content of the gas and reducing the dewpoint.

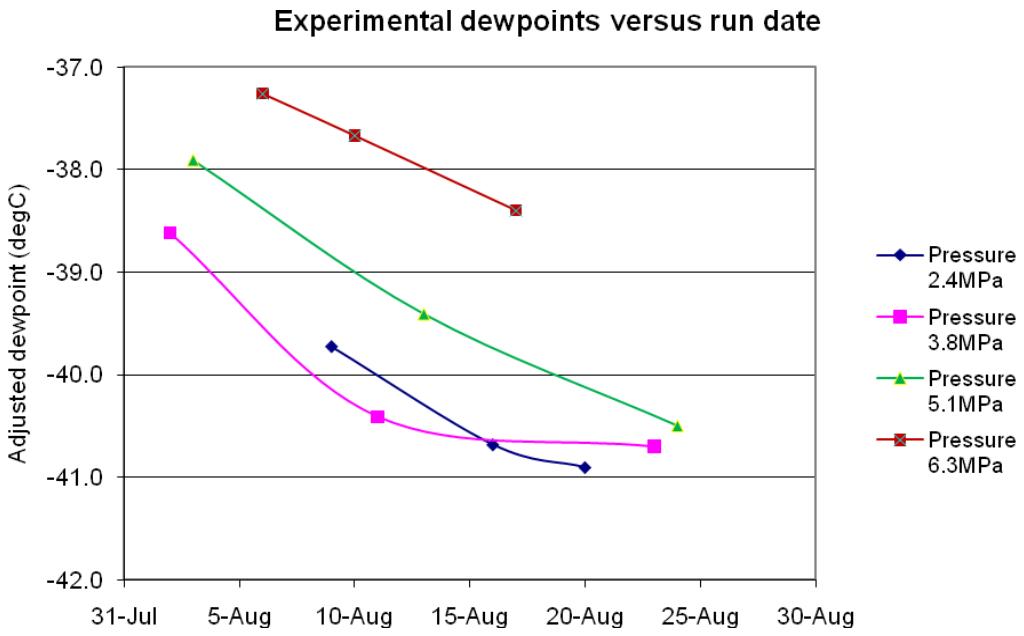

Figure 5-12 Adjusted experimental dewpoints versus run date

5.3.4 Analysis of measured dewpoints versus batch experiments

As reviewed in section 3.4.2.5, the equilibrium water content of natural gases is lowered by the presence of hydrates and a correlation was developed by Chapoy[107] from batch experimental data to allow the equilibrium water content to be predicted. It is useful to compare the results we obtained from constant flow experiments with the results of batch experiments.

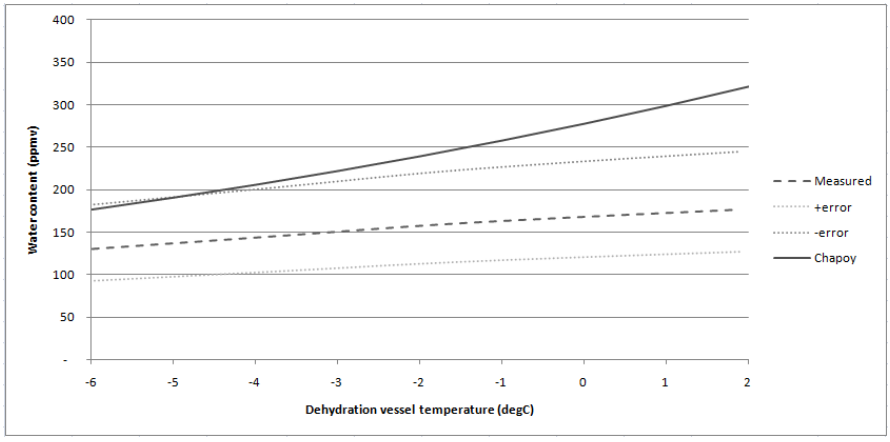

Figure 5-13 Comparison of predicted and measured water content at dehydration vessel pressure of 2.4 MPa

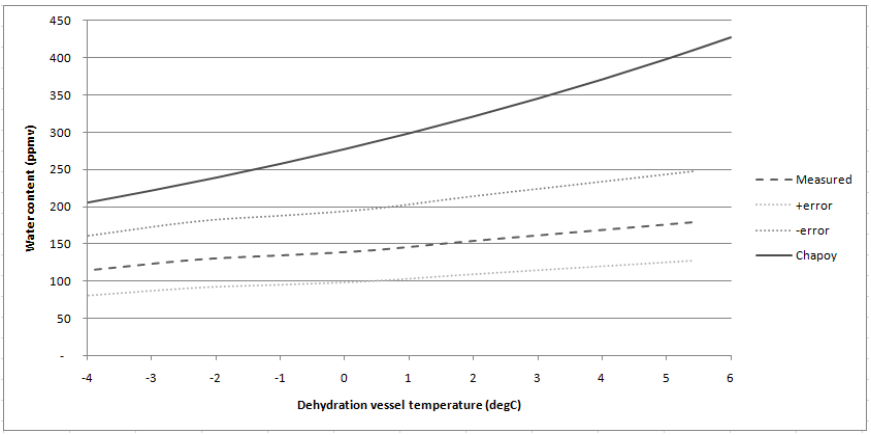

Figure 5-14 Comparison of predicted and measured water content at dehydration vessel pressure of 3.1 MPa

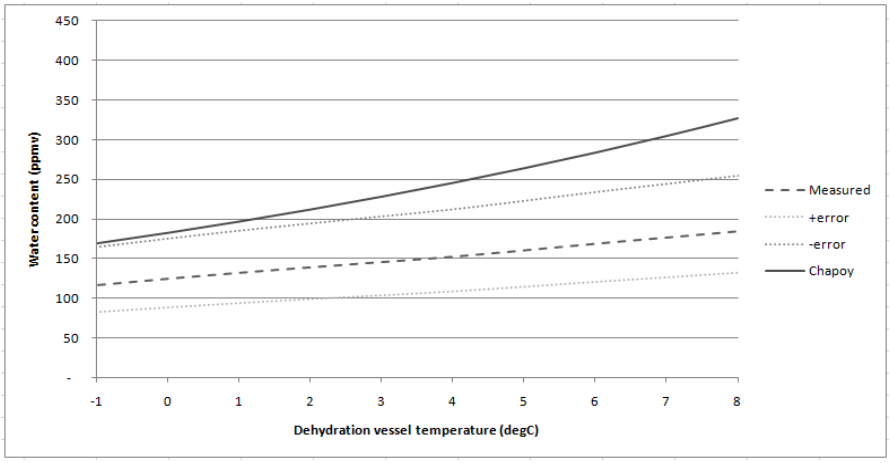

Figure 5-15 Comparison of predicted and measured water content at dehydration vessel pressure of 3.8 MPa

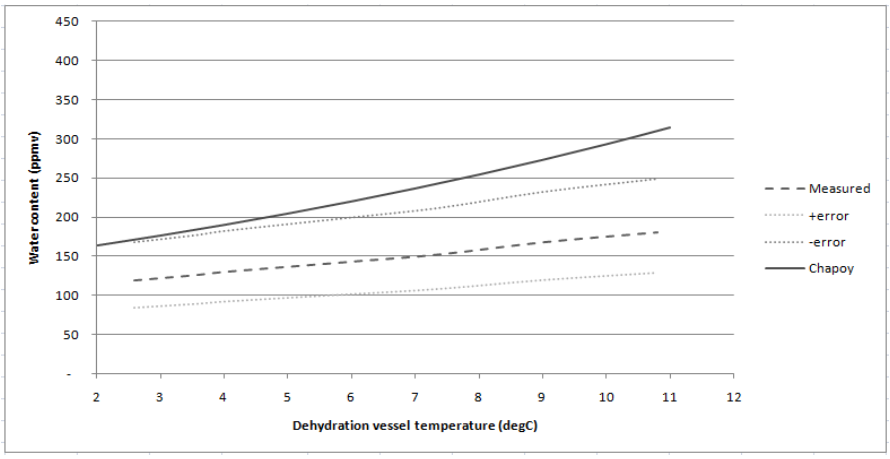

Figure 5-16 Comparison of predicted and measured water content at dehydration vessel pressure of 5.1 MPa

Using the Goff-Gratch equation (see section 3.3.1.1) the measured dew points are converted to the equivalent water content in parts per million (by volume) and then compared to the water content predicted by the Chapoy correlation. The results for each dehydration vessel pressure are given in Figure 5-13 through Figure 5-16 together with the accuracy bounds (+/- 3 C) of the dew point sensor.

The insulation and gas flow regime ensure that no significant temperature gradients exist in the vessel so the temperatures measured at the top of the vessel are representative of the temperature throughout the vessel.

From the plotted results it can be clearly seen that under all dehydration vessel pressure and temperature conditions, the measured water content in the constant flow operating environment is lower than that predicted by the batch experiment based Chapoy correlation.

It is also apparent that the improvement in the dehydration versus batch results is also better at higher temperatures at all experimental pressures. The conditions of the gas stream prior to being heated in the inlet heat exchanger were typically 19 C and 10 MPa. The calculated dewpoint of a saturated gas stream at these conditions is around -35.2 C. As the water content of the inlet gas stream is limited by the input condition of the gas to the heat exchanger the resulting water content of the gas as it passes through the system approaches the inlet water content. This could explain the increased divergence from the conditions predicted by the Chapoy correlation.

Figure 5-17 shows a plot of the experimentally achieved dewpoints versus the required pipeline dewpoints for different seawater temperatures.

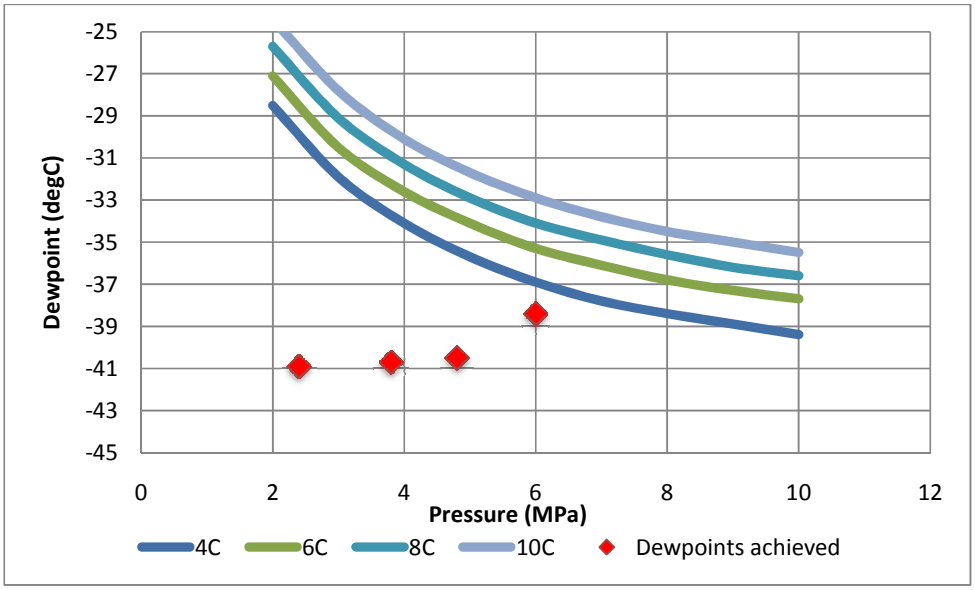

Figure 5-17 Dewpoints achieved versus pipeline requirements

The pipeline condition curves were determined by using HYSYS to calculate the water content of the Alinta gas composition at pipeline pressures and seawater temperatures and then converting to Dewpoint at atmospheric pressure using Goff-Gratch.

The plot shows that the experimentally achieved dewpoints are low enough to ensure that no condensation of water will occur to gas flowing through the pipelines at low seawater temperatures of 4 C.

5.4 Dehydration system enhancements

5.4.1 Injection tests

To enhance the dehydration process a method to improve the condensation of water from the super saturated gas stream exiting the nozzle was trialled as part of this research project (refer to section 3.5 for background).

As the formation of condensed droplets from supersaturated water vapour can be encouraged by providing seeds for the water vapour to condense around the basis for the experiments was to introduce suitable seeds. To trial this approach we performed a series of experiments where we injected liquid hydrocarbons into the vessel via a misting nozzle.

Three system configurations were trialled:

- Top injection where the liquid hydrocarbons were injected into the gas feed to the dehydration vessel upstream from the nozzle in the dehydration vessel
- Bottom injection with cowling fitted. A separate misting nozzle placed close to the gas nozzle was used
- Bottom injection with cowling removed and both gas and injection nozzle moved towards the bottom of the dehydration vessel.

The injection system implementations are described in section 4.4.3

5.4.1.1 Top injection

Experimental runs were performed at a constant inlet pressure of 10 MPa and different vessel pressures. The system was run for several hours and then injection of condensate commenced, The condensate temperature was either at ambient or cooled by passing through a dry-ice chilled methanol bath. Injection rates between 5 and 40 ml per minute were trialled. Table 5-6 shows the achieved dewpoints for each of the top injection runs.

Vessel pressure	Vessel temperature	Flow rates	Condensate temperature	Achieved dewpoint
2.8 MPa	-7.4 C	5 to 44 ml/min	12.4 C	-38.5 C
4.0 MPa	1.8 C	8 to 28 ml/min	15.6 C	-35.4 C
2.6 MPa	-8.0 C	24 ml/min	-8.4 C	-36.5 C
2.9 MPa	-9.8 C	42 ml/min	-36.8 C	-38.4 C

Table 5-6 Results of top injection experiments

During the last two runs after the injection period the system run was continued for an additional period and the dewpoints noted. The final measured dewpoints are shown in Table 5-7.

Vessel pressure	Vessel temperature	Flow time post injection	Final dewpoint
2.6 MPa	-8.1 C	22 mins	-37.3 C
2.9 MPa	-8.9 C	12 mins	-39.1 C

Table 5-7 Measured dewpoints after condensate injection ceased

Looking at the achieved dewpoints during the condensate injection and the dewpoints measured after the injection was stopped there was no apparent improvement in the dehydration performance caused by the top injection process.

Looking at the properties of misting nozzles, (see section 3.5.1) with two phase flow it is found that the droplets formed are much smaller than when a single liquid phase is sprayed through a nozzle. With our previous experience of carryover of water droplets from the vessel it is thought that the very fine mist occurring due to the two phases may be also carrying over into the outlet stream. This proposition was supported by an accounting of injected fluid with the fluid collected at the end of each run when only 50% of the injected condensate was recovered from the dehydration vessel.

To allow for a separate injection nozzle for the hydrocarbon fluid and to support both longer injection times and greater injection rates it was decided to implement bottom injection.

5.4.1.2 Bottom injection

To allow for longer durations it was necessary to remove the injected liquids from the dehydration vessel to prevent the vessel from filling with the injected liquids. A bottom assembly was fitted to the dehydration vessel that included a path for spraying of fluids into the gas stream and a return path for the injected liquids to exit the vessel. Also a

hydrocarbon liquid – water separator and recirculating injection pump were added to the system (refer to section 4.4.3 for more information)

As recirculation of fluids was to be used during bottom injection experiments it was decided to use laboratory grade Heptane instead of condensate as the hydrocarbon fluid to be injected.

Two suites of bottom injection experiments were performed with different internal configurations within the dehydration vessel as illustrated in Figure 5-18.

With the removal and recirculation of the injected Heptane injection rates up to 150 ml per minute were trialled with injection durations up to 5 hours.

The results of the completed experimental runs with the cowling fitted into the dehydration vessel are shown in Table 5-8.

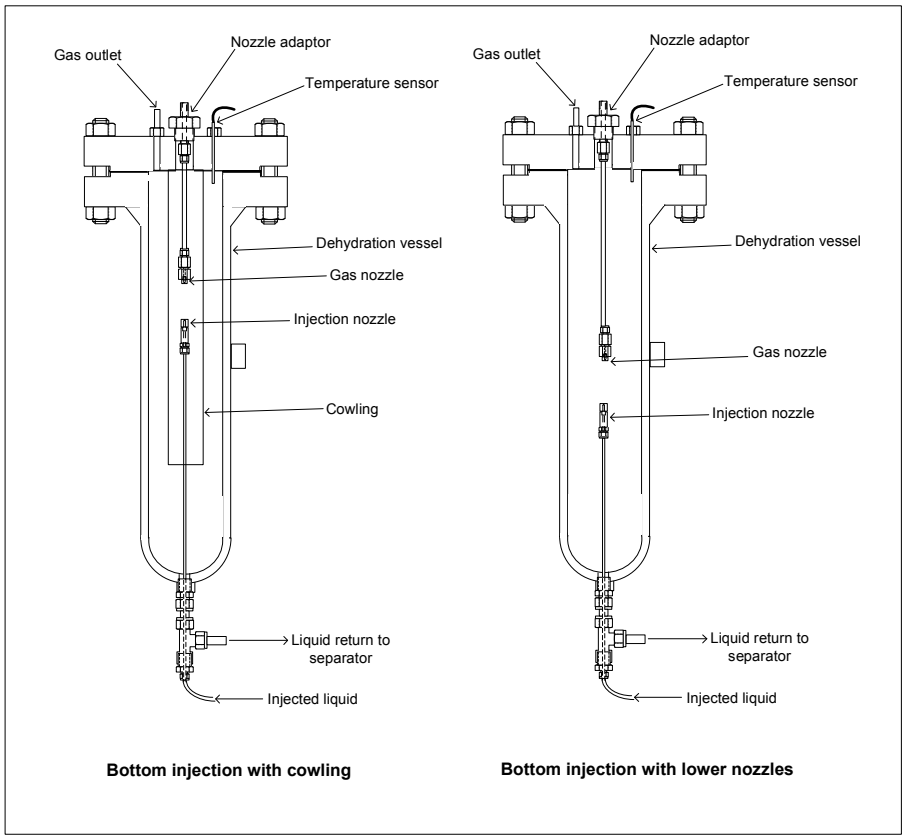

Figure 5-18 Bottom injection configurations of dehydration vessel

In both runs the dewpoint measured after the injection of cold heptane was stopped were lower than during the injection period. The changes in vessel conditions were not sufficient to explain the dewpoint change so it could be concluded that there was no apparent benefit in the injection of heptane on the dehydration process.

Vessel pressure	Vessel temp.	Flow rates/time since injection stopped	Heptane temp.	Achieved dewpoint	Dewpoint after injection end
2.0 MPa	-8.5 C	80-130 ml/min	-33 C	-40.0 C	
2.0 MPa	-9.8 C	57 minutes	-		-41.3 C
2.1 MPa	-9.1 C	40-80 ml/min	-39 C	-39.1 C	
2.1 MPa	-9.3 C	63 minutes	-		-39.8 C

Table 5-8 Results of bottom injection experiments with cowling

Vessel pressure	Vessel temp.	Flow rates/time since injection stopped	Heptane temp.	Achieved dewpoint	Dewpoint after injection end
Injection run 1 (10 Sept 2010)					
4.0 MPa	2.3 C	40 ml/min, 1hr	15 C	-35.5 C	
4.0 MPa	1.5 C	35 mins	-		-36.4 C
3.9 MPa	1.9 C	100 ml/min, 35mins	15.5 C	-35.5 C	
3.9 MPa	1.6 C	40 mins	-		-36.6 C
Injection run 2 (14 Sept 2010)					
2.9 MPa	-1.8 C	80 ml/min, 2 hrs	-18 C	-38.2 C	
2.9 MPa	-1.9 C	40 mins			-38.5 C
2.9 MPa	-1.6 C	70 ml/min, 30 mins	-18 C	-38.7 C	
3.1 MPa	-1.3 C	20 mins			-39.3 C
Injection run 3 (16 Sept 2010)					
4.7 MPa	5.2 C	140 ml/min, 1 hr	-20 C	-36 C	
4.6 MPa	5.6 C	30 mins			-35.7 C
4.7 MPa	5.6 C	105 ml/min,30 mins	-35 C	-36 C	
4.6 MPa	7.0 C	30 mins			-35.6 C

Table 5-9 Results of bottom injection experiments with lower nozzles

With the cowling removed and the nozzles lowered into the dehydration vessel experimental runs with injection of Heptane were performed. In these experiments the system was run for a few hours to reach stable conditions in the dehydration vessel and then a series of alternate injection then no injection periods were trialled and changes in dewpoint assessed.

A summary of the results for these runs is provided in Table 5-9.

From these results we can see that there were small changes in the dewpoint each time the injection was stopped and also small changes in the dehydration vessel temperature. The dewpoint changes can be explained by the changes in dehydration vessel conditions.

The injection of heptanes into the dehydration vessel may cause the gas gravity to increase a small amount. Increases in gas gravity at the low temperature of the dehydration vessel will cause a very small decrease in the saturated water content of the gas. Identification of this trend was not apparent in the measured results.

Again there is no evidence provided by these experiments that the spraying of a hydrocarbon mist into the dehydration vessel assists in improving the dehydration process.

5.4.2 Scope for system improvements

The size of the experimental system is thought to have imposed a number of limitations on the performance of the system that may not be as severe in a larger scale implementation.

With the maximum available flow rate we had to use relatively small nozzles, all less than 1mm in diameter. These small orifice nozzles were prone to blocking quickly if the inlet gas stream was not warm enough. With a larger flow rate and larger orifice nozzles it is anticipated that the inlet gas stream could be run at a lower temperature before blocking became an issue. Any decrease in the inlet gas stream temperature will results in either a lower vessel temperature or a lower pressure drop to obtain the same vessel temperature. Both of these will result in a lower water content of the gas.

In our experiments we obtained JT coefficients of typically 0.4 K/MPa less than was theoretically predicted. It is considered likely that part of this inefficient cooling was due to a sub-optimum gas path within the nozzle. With larger nozzles it will be possible to provide a smoother gas flow upstream from the nozzle orifice and most likely a higher JT coefficient. A. higher JT coefficient will improve the dehydration performance.

The experiments performed with injection of hydrocarbon fluids failed to provide any measurable benefits in dehydration. It is possible that some benefits may be obtainable with this approach particularly if the fluid droplets can make contact with the gas stream immediately after it leaves the nozzle. With a larger system implementation separate top injection points adjacent to the nozzle orifice could be implemented allowing immediate contact with the gas and the potential increase in water condensation while it is in its highest super-saturation state.

6 Subsea system implementation

This section utilises the results obtained through the experimentation and proposes a method whereby the dehydration performance demonstrated can be applied to a subsea implementation.

6.1 Subsea wellhead conditions

The typical temperature profile for a well fluid as it passes up the well is illustrated in Figure 6-1. The profile shown is impacted by the production flow rate, with higher flow rates the fluid stream has less time to reach thermal equilibrium with the surrounding formations and will be warmer at the wellhead. As an example, the temperature at the wellhead for the Ormen Lange gas field in the North Sea at production flow rates is around 80 C[126].

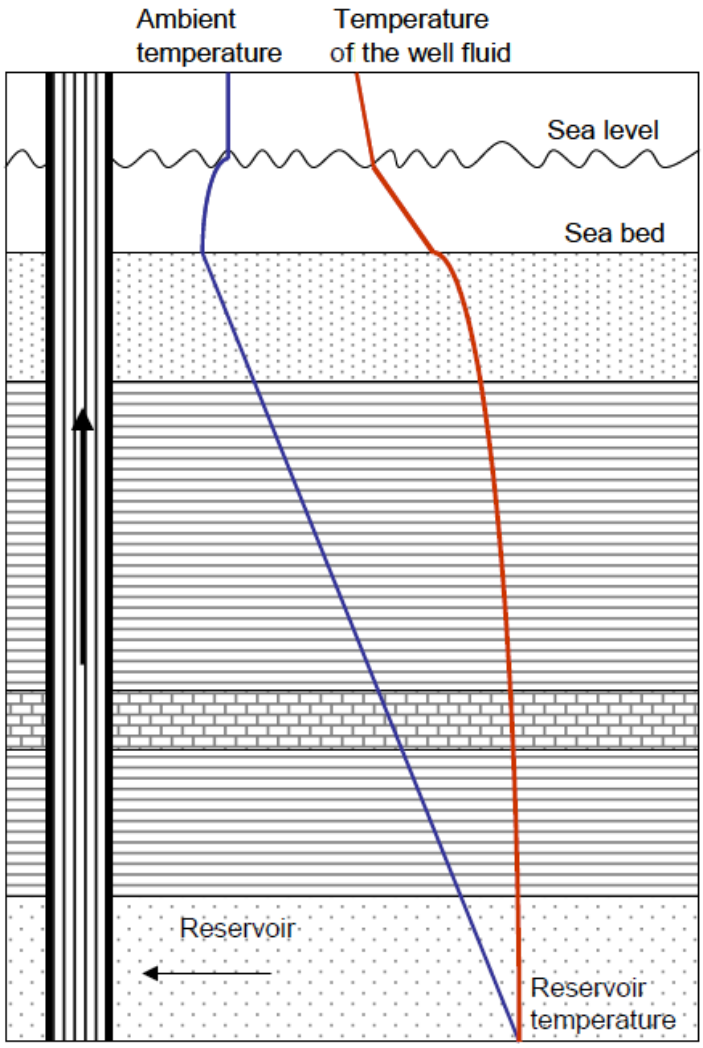

Figure 6-1 Well fluid temperature profile [125]

Wellhead pressures can vary enormously depending on the depth of the producing formation and whether overpressure conditions are present. Many land based gas wells have a typical gas wellhead pressure of between 10 to 12 MPa.[126] Some deep subsea wells have much higher pressures with gas condensate wells with a shut-in pressure of 90 MPa[127].

6.2 Subsea dehydration system

The implementation of a subsea dehydration system will require the implementation of the following subsystems:

- Wellhead separator
- Inlet gas heat exchanger
- Inlet separator
- Dehydration vessel with management systems
- Liquids disposal system
- Monitoring and control system

A simple HYSYS model of the subsea system is shown in Figure 6-2.

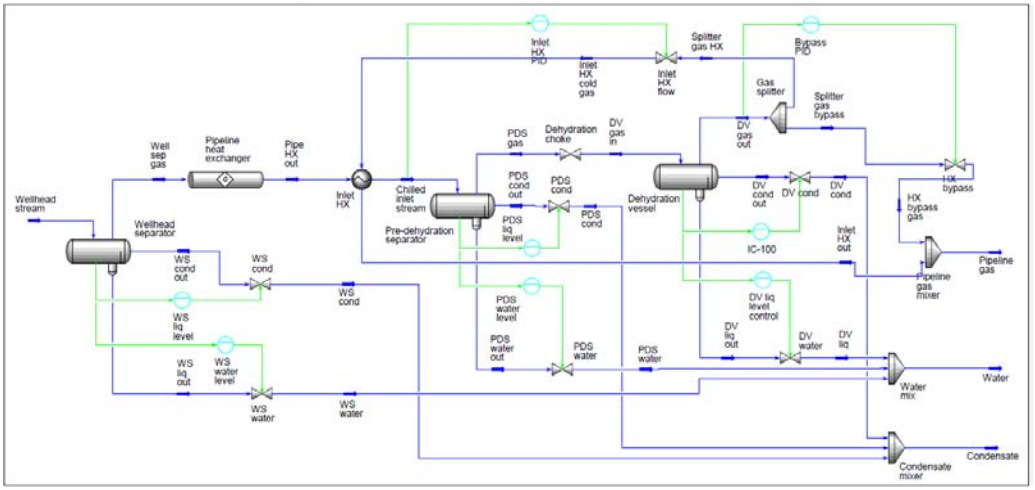

Figure 6-2 HYSYS model of subsea gas dehydration system

The next sections discuss each of the subsystems and provide some sizing calculations for a solution scenario for a gas/condensate production well that is detailed in Table 6-1. The wellhead stream composition used is given in Table 6-2.

Property	Value
Wellhead pressure	15 MPa
Wellhead temperature	80 C
Gas production rate	105,000 sm^3/hr (89 MMSCFD)
Condensate production rate	55 m^3/hr (8,300 bpd)
Wellhead gas stream water content (vapour and liquid phase)	1%
Pipeline pressure	6 MPa
Seawater temperature	4 C

Table 6-1 Assumed wellhead conditions

Component	Total mole fraction	Vapour phase	Liquid phase	Aqueous phase
Methane	65.35%	67.99%	45.02%	0.0007%
Ethane	13.86%	13.92%	14.07%	0.00%
Propane	8.91%	8.64%	11.86%	0.00%
i-Butane	0.95%	0.89%	1.52%	0.00%
n-Butane	3.34%	3.09%	5.76%	0.00%
i-Pentane	0.50%	0.45%	1.04%	0.00%
n-Pentane	0.99%	0.87%	2.14%	0.00%
n-Hexane	0.99%	0.81%	2.64%	0.00%
n-Heptane	0.99%	0.75%	3.16%	0.00%
n-Octane	0.99%	0.69%	3.73%	0.00%
n-Nonane	0.99%	0.63%	4.31%	0.00%
n-Decane	0.83%	0.47%	4.11%	0.00%
Carbon dioxide	0.18%	0.18%	0.15%	0.0033%
Nitrogen	0.13%	0.14%	0.07%	0.0002%
Water	0.99%	0.48%	0.43%	99.996%

Table 6-2 Wellhead stream composition

6.2.1 Wellhead separator

The wellhead separator will be provided to remove entrained liquids and solids from the gas stream leaving the wellhead.

There are a number of subsea wellhead separators in operation today at various locations around the world. Refer to section 1.1.2 for more information on current subsea separator implementations.

For the modelled scenario the outputs from the wellhead separator are shown in Table 6-2.

Component	Gas stream	Condensate stream	Aqueous stream
Methane	67.99%	45.02%	0.001%
Ethane	13.92%	14.07%	0.00%
Propane	8.64%	11.86%	0.00%
i-Butane	0.89%	1.52%	0.00%
n-Butane	3.09%	5.76%	0.00%
i-Pentane	0.45%	1.04%	0.00%
n-Pentane	0.87%	2.14%	0.00%
n-Hexane	0.81%	2.64%	0.00%
n-Heptane	0.75%	3.16%	0.00%
n-Octane	0.69%	3.73%	0.00%
n-Nonane	0.63%	4.31%	0.00%
n-Decane	0.47%	4.11%	0.00%
Carbon dioxide	0.18%	0.15%	0.003%
Nitrogen	0.14%	0.07%	0.000%
Water	0.48%	0.43%	99.996%
Properties			
Molar flow (Kgmol/hr)	4,706	523.6	27.1
Molecular weight	26.1	44.4	18.0
Mass flow (Kg/hr)	122,787	23,274	489

Table 6-3 Composition and flow rates for streams leaving wellhead separator

6.2.2 Inlet Heat exchanger

The inlet heat exchanger must be able to take the inlet gas stream at the wellhead temperature and cool it to the required inlet temperature of the dehydration vessel.

Using the HYSYS model and the scenario conditions of Table 6-1 the heat to be removed by the heat exchanger can be calculated. To obtain an inlet gas stream temperature of 25 C the heat exchanger must remove heat at a rate of around 6.7 MW to cool the inlet stream from the well head temperature of 80 C.

It is envisaged that a two stage heat exchanger will be the most appropriate design approach. The first stage would comprise of a section of pipeline surrounded by low ambient temperature sea water. The connection point to the pipeline may be switchable using valves to allow some coarse adjustment in the performance of the first stage heat exchanger. The second heat exchanger stage would comprise of a tube-shell heat exchanger with the gas to be cooled passing through the tubes and the shell fed with a controlled proportion of the cold gas from the dehydration vessel outlet. The second stage will then have the ability to finely adjust the gas temperature of the dehydration vessel feed. The bulk of the cooling would be performed by the pipeline exchanger and the fine temperature adjustment performed by the tube-shell heat exchanger.

Using this approach allows for some variation in seawater temperatures, speed of seawater currents and gas stream flow rates whilst still being able to maintain an accurate setting of the inlet gas temperature to the dehydration vessel.

For the purpose of the sizing estimate it is assumed that the pipeline heat exchanger will reduce the gas from the wellhead temperature of 80 C to 28 C and the tube shell heat exchanger will further reduce the temperature to the required 25 C as the feed temperature to the dehydration vessel.

6.2.2.1 Pipeline heat exchanger

To calculate the dimensional parameters of the pipeline heat exchanger the HYSYS simulator was used. The HYSYS simulator requires the overall heat transfer coefficient for the piping to be used in the heat exchanger. Figure 6-3 illustrated the tubing and the relevant parameters.

The overall heat transfer coefficient of the tubing section to the seawater can be expressed by the equation[123]:

$$U = \frac{1}{\frac{1}{h_1} + \frac{r}{k}\ln\frac{r+t}{r} + \frac{r+t}{r}\frac{1}{h_2}} \quad \text{... 79}$$

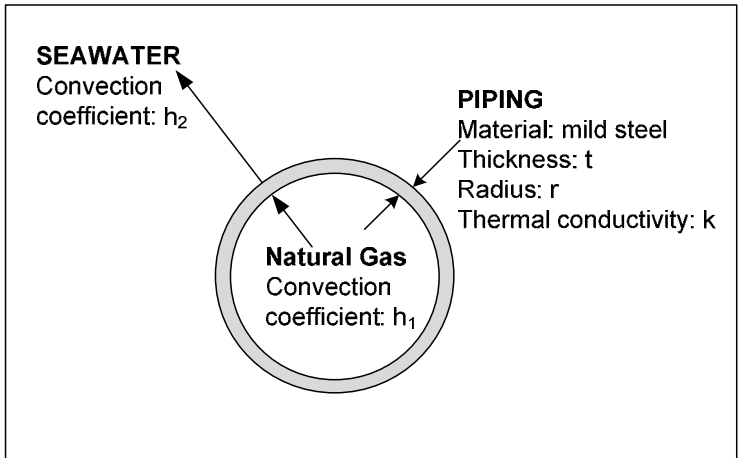

Figure 6-3 Heat exchanger section and parameters

For turbulent flow in the piping, the Dittus-Boelter correlation can be used to calculate the forced convection coefficient h_1 for the natural gas to tubing:

$$h_1 = \frac{k_f}{D_H} Nu \quad \text{... 80}$$

where k_f is the thermal conductivity of the fluid, D_H is the hydraulic diameter and Nu is Nusselt number which for cooling can be expressed by the equation:

$$Nu = 0.023 \,\mathrm{Re}^{0.8} \,\mathrm{Pr}^{0.33} \quad \text{... 81}$$

where *Re* is the Reynolds number: $\mathrm{Re} = \frac{QD_H}{\nu A}$ ... 82

and *Pr* is the Prandtl number $\mathrm{Pr} = \frac{c_p \mu}{k}$ ... 83

Using the defined well parameters we can use the above equations to calculate the convection coefficient for the natural gas. Assuming the heat exchanger consists of a single length of pipe the calculated value for the coefficient h_1 is over 500 W/m^{2}K (see appendix B.3 for the calculation). This is over an order of magnitude greater than the conduction coefficient for the steel tubing (For carbon steel *k* is taken to be 43 W/m.K) and the likely convection coefficient for the seawater so can largely be ignored when calculating the overall heat transfer coefficient of the heat exchanger tubing.

The convection coefficient for the seawater surrounding the heat exchanger is a function of a number of factors some of which are unknown including the heat exchanger orientation and

the subsea flow environment i.e. local current. In literature, typical coefficients for free convection of water between 20 and 100 W/m^2.K are stated. For the purpose of this sizing estimate a convection coefficient, h_2 of 50 W/m^2.K has been assumed.

The total heat transfer coefficient for the heat exchanger tubing, U can then be calculated as 45.7 W/m^{2}K.

Using Schedule 160, 24 inch mild steel piping (rated to 25.3MPa at 205C [128]) and the defined well parameters a heat exchanger made of one pipe of 293 metres in length would reduce the inlet temperature from 80 C to 28 C in seawater of 4 C. With the addition of heat sinks to the external surface of the pipe the thermal conductivity between the pipe and the seawater could be improved and a shorter length of piping would suffice. The ability to add or remove heat sinks could be beneficial when installing the pipe heat exchanger and tuning its performance.

Depending on the properties of the production fluid, deposition of contaminants within the heat exchanger may occur. The predicted operating temperatures of the bulk heat exchanger are high enough to ensure that wax deposition is unlikely to be a problem. Other mineral deposits from liquid carry over from the wellhead separator may occur as well as other components, e.g. sulphur compounds, which drop out of the gas phase due to the temperature and pressure drops within the heat exchanger. Systems may have to be incorporated within the system to provide the means of removing these deposits, e.g. pigging or flushing techniques.

6.2.2.2 Tube-shell heat exchanger

The Tube-shell heat exchanger will perform the fine adjustment of the inlet gas stream temperature before it is fed to the choke input of the dehydration vessel.

The gas stream to be cooled will be passed through the tubes of the heat exchanger whilst a proportion of the cooled outlet gas from the dehydration vessel is passed through the shell section of the heat exchanger.

The developed HYSYS model was used to estimate the size of the required tube-shell heat exchanger using a simple ‘Steady State’ model. To size the heat exchanger it is necessary to calculate the overall heat transfer coefficient for the heat exchanger from the flow conditions in the tubes and the shell of the heat exchanger. The calculation is summarised below:

TUBE SECTION		
Physical parameters		
Internal pipe radius	18	mm
Pipe area	0.001	m^2
Number of tubes	16	

Calculated parameters (HYSYS)			
Molecular weight	26.09		
Gas flow rate to heat exchanger	426.3	m^3/hr	
Gas flow per tube	0.0074	m^3/s	
Gas velocity in tubes	7.3	m/s	
Kinematic viscosity	0.1181	cSt	
Dynamic viscosity	0.0321	cP	
Specific heat	3,646	J/kg.K	
Thermal conductivity	0.0704	W/m.K	
Reynolds number	2,216,412		
Prandtl number	1.66		
Nusselt number	3,244		
Heat transfer coefficient - gas in tube	6,346	$W/m^2.K$	
SHELL SECTION			
Physical parameters			
Internal pipe radius	150	mm	
Shell area	0.071	m^2	
Calculated parameters (HYSYS)			
Molecular weight	19.94		
Gas flow rate to heat exchanger	600.6	m^3/hr	
Gas velocity in shell	2.4	m/s	
Kinematic viscosity	0.1805	cSt	
Dynamic viscosity	0.0128	cP	
Specific heat	4,525	J/kg.K	
Thermal conductivity	0.0353	W/m.K	
Reynolds number	3,922,785		
Prandtl number	1.63		
Nusselt number	5,272		
Heat transfer coefficient - gas in shell	620	$W/m^2.K$	
Conduction coefficient - carbon steel	43	w/m.K	
Tube thickness	2	mm	
Calculated overall coefficient U	**551**	**$W/m^2.K$**	**2 $MJ/h.m^2.K$**

To reduce the inlet gas stream from 28 C to 25 C the total heat to be removed from the stream calculated by HYSYS is 77.8 MJ/h.K. The resultant design parameters for a heat exchanger suitable to meet the design requirements are summarised in Table 6-4.

The smaller pressure and temperature drops experienced in the tube-shell heat exchanger will ensure that deposition problems will be less significant than in the case of the pipe heat exchanger. The deposit removing subsystem implemented for the pipe heat exchanger may also be able to support the removal of deposits in the tube section of the tube-shell heat exchanger.

Tube-shell heat exchanger configuration	
Number of shell passes/ shells in series	2/2
Tube passes per shell	2
Baffle type	Single, 20% baffle cut
Number of tubes per shell	16, 60 mm pitch, triangular layout
Tube sizing	Outside diameter: 40 mm Wall thickness: 2 mm
Thermal parameters	Tube conductivity: 43 W/m.K Counter flow (first pass)
Operating assumptions	
Tube section	Inlet temperature: 28 C Outlet temperature: 25 C
Shell section	Inlet temperature: 2.6 C Outlet temperature: 14.0 C
Split of cold gas passed to shell stage	70% (2,127 Kgmol/hr)
No thermal losses to seawater, no tube fouling, vertical orientation	
Calculated heat exchanger sizing and performance	
Heat exchanger volumes per shell	Tubes: 0.16 m^3 Shell: 0.47 m^3
Heat exchanger dimensions	Tube length: 9.7 m Shell diameter: 0.30 m
Overall UA	77.8 MJ/h.K (area A: 39 m^2) U = 2.0 MJ/h.m^2.K

Table 6-4 Design parameters for tube-shell heat exchanger

6.2.3 Inlet separator

The gas stream leaving the heat exchanger is significantly cooler than that at which it entered saturated with water vapour. As a consequence some liquids will have condensed from the gas stream and will need to be removed before the gas stream is passed to the dehydration vessel. Table 6-5 lists the properties of the stream leaving the heat exchanger.

	Total	Vapour Phase	Liquid Phase	Aqueous Phase
Fraction	100%	83.3%	16.3%	0.4%
Temperature (C)	25	25	25	25
Pressure (MPa)	15	15	15	15
Mass flow (Kg/hr)	122,787	99,698	22,717	372
Molecular weight	26.1	25.4	29.7	18.0
Mass density (Kg/m3)	296	284	360	1,012
Composition				
Methane	68.0%	69.5%	62.3%	0.00004%
Ethane	13.9%	13.8%	14.7%	0.00%
Propane	8.6%	8.4%	10.1%	0.00%
i-Butane	0.9%	0.9%	1.1%	0.00%
n-Butane	3.1%	2.9%	4.0%	0.00%
i-Pentane	0.4%	0.4%	0.6%	0.00%
n-Pentane	0.9%	0.8%	1.2%	0.00%
n-Hexane	0.8%	0.7%	1.2%	0.00%
n-Heptane	0.8%	0.7%	1.2%	0.00%
n-Octane	0.7%	0.6%	1.2%	0.00%
n-Nonane	0.6%	0.5%	1.2%	0.00%
n-Decane	0.5%	0.4%	0.9%	0.00%
Carbon dioxide	0.2%	0.2%	0.2%	0.0057%
Nitrogen	0.1%	0.1%	0.1%	0.00038%
Water	0.5%	0.0%	0.0%	99.99%

Table 6-5 Properties of stream leaving heat exchanger

The Inlet separator is provided in the proposed system solution to capture the condensate and water and from the heat exchanger outlet stream. The Inlet separator may be a 2 or 3 phase separator depending on the gas composition, the inlet temperature and whether condensate removed from the gas stream is being recovered or disposed of with the water. For the worked scenario, enough hydrocarbon liquids are present so a 3-phase separator would be appropriate.

6.2.4 Dehydration vessel

A possible design configuration of a production dehydration vessel is shown in Figure 6-4. The major subsystems incorporated in this design are:

- Insulated pressure vessel
- Heated inlet nozzle
- Hydrate management system
- Hydrate dissociation system

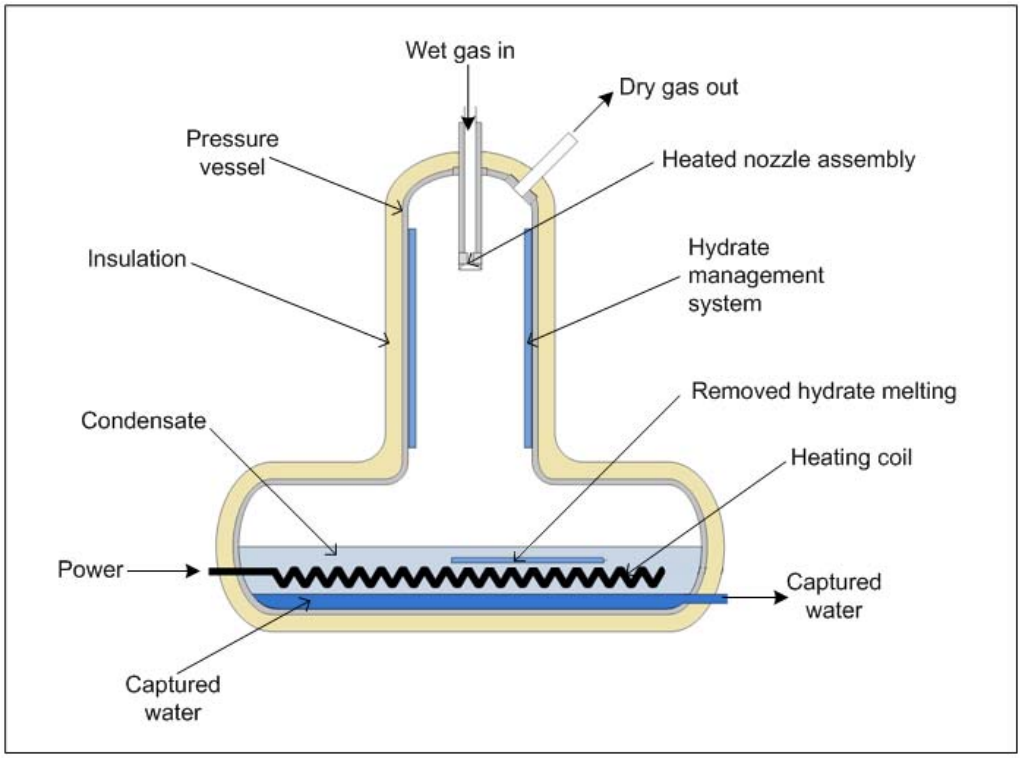

Figure 6-4 Production dehydration vessel configuration

6.2.4.1 Sizing of the dehydration vessel

The performance of the dehydration vessel is dependent on the physical characteristics of the dehydration vessel:

- the residence time of the gas in the vessel
- the flow patterns of the gas in the vessel, turbulent flow being preferred to increase mixing, and
- the gas contact with hydrate formed on the vessel walls.

Residence time is a simple function of flow rate and volume whilst gas hydrate contact is more a function of the vessel dimensions, a tall thin vessel should perform better than a short fat vessel. Internal structures where hydrates can be deposited and increase gas/hydrate contact may be beneficial, though this approach is likely to complicate the hydrate management solution. Positioning of the nozzle assembly will also affect the performance.

During the experimental phase all experiments were performed on a fixed dehydration vessel volume and utilising as much flow from the compressor as was possible whilst maintaining reasonably stable flow conditions. Some runs were performed with a smaller nozzle to increase the gas residence time within the vessel. These runs did not appear to improve the dehydration performance suggesting that the residence time at maximum flow rate was sufficient for the dehydration process to occur. No experiments were performed with a shorter residence time so it is impossible to say whether the residence time during the experiments was optimum and a shorter residence time may be viable.

More studies and experiments will be required before any more than a guess can be made as to vessel sizing and topology. If the residence time of the experimental system is to be replicated in the production system with the flow rate for the production scenario being 3,874 Kgmol/hr or 2,600 times greater than the experimental system the experimental system volume must increase by this factor. To achieve this residence time the overall vessel with a dimensionally scaled production system each dimension would increase by a factor of 13.7. The hydrate formation portion of the dehydration vessel would then be approximately 2.4 m in diameter and 10.5 m tall. If we assume the bottom separator section is the same diameter and half the length, a pressure vessel rated to 15 MPa using 6 inch steel plate would weigh around 160 tons. After the addition of a skid and supporting infrastructure the total weight should be comfortably within the normal weight limits for subsea installation.

To keep the weight of this component down to levels that will be deployable in subsea environments the geometry of this vessel will need careful consideration. A tall thin vessel will weigh much less than a short fat vessel at the same pressure rating.

Further studies are required to determine the optimum design configuration of the dehydration vessel and whether the performance of the trial system can be achieved in a scaled up production sized solution.

6.2.4.2 Dehydration performance of the dehydration vessel

The experimental results of our dehydration experiments concluded that it was possible to obtain dehydration performance with the constant flow process though the dehydration vessel comparable with that achieved in batch experiments.

Looking at the inlet temperature and pressure and the pressure drop across the inlet nozzle, the gas temperature and pressure within the dehydration vessel can be calculated. Using the Chapoy correlation[100] the likely water content of the gas stream leaving the dehydration vessel can then predicted.

The operating conditions, parameters and predicted results are summarised in Table 6-6.

Inlet conditions and operating parameters	
Inlet temperature	25 C
Inlet pressure	14.9 MPa
Nozzle pressure drop	8.9 MPa
Calculated conditions	
Outlet pressure	6 MPa
Outlet temperature	2.6 C
Outlet water content	149 ppmv, Gas dewpoint -38.6 C

Table 6-6 Predicted dehydration performance of defined scenario

The measured JT coefficient during experiments was 4.4 K/MPa compared to the HYSYS prediction of 4.8 K/MPa. Assuming it is possible to achieve similar performance in a production system with a pressure drop of 8.9 MPa the vessel temperature is estimated to be 2.6 C. (HYSYS calculated temperature -1C + JT cooling inefficiency (8.9*0.4))

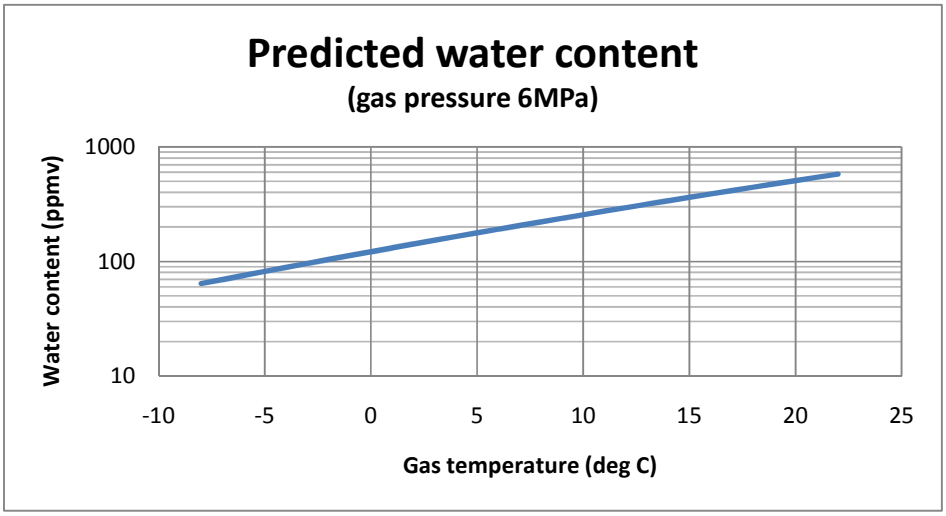

Figure 6-5 Predicted water content of gas stream leaving dehydration vessel at 6MPa vessel pressure

Using the correlation developed by Chapoy[100] (as discussed in section 3.4.2.5) and the vessel pressure of 6 MPa a plot of the predicted water content versus the vessel temperature was generated as shown in Figure 6-5.

At the predicted vessel gas temperature of 9.6 C the predicted water content of the gas leaving the dehydration vessel will be 149 ppmv equivalent to a dewpoint of -38.6 C

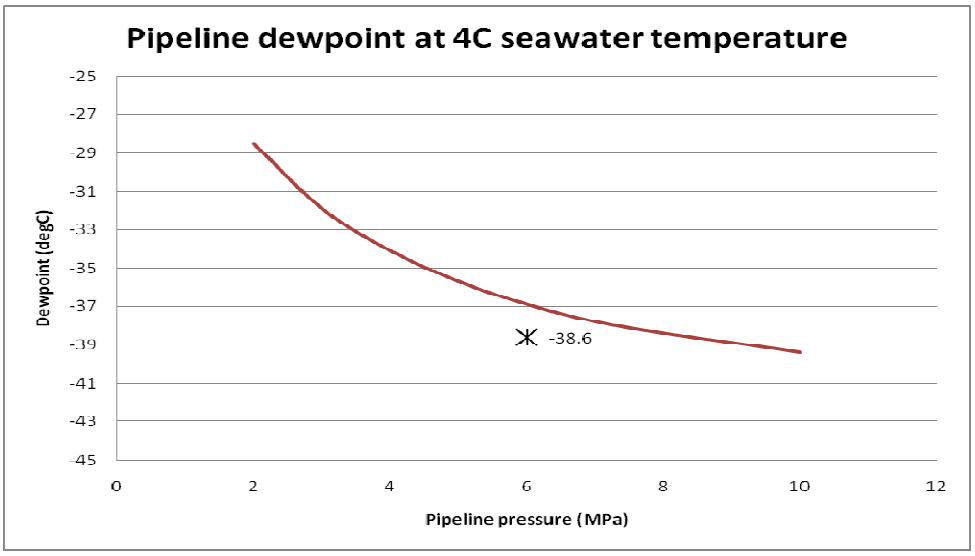

Figure 6-6 Predicted dewpoint versus dewpoint line for pipeline gas

Figure 6-6 shows a plot of the predicted dewpoint on the curve of maximum gas stream dewpoint for variable pipeline pressures at the ambient seawater temperature of 4 C. The predicted dewpoint is below the maximum gas stream dewpoint for a pipeline running at 6 MPa and seawater of 4 C, so water will not condense out of the gas as it passes through the pipeline. Experimentally we managed better water reduction than predicted by the Chapoy correlation so we could expect an even better margin than shown here.

Property	Condensate	Dry Gas	Water
Temperature (C)	2.6	2.6	2.6
Pressure (MPa)	6.0	6.0	6.0
Molar flow (kgmol/hr)	880	3,039	1.07
Mass flow (kg/hr)	39,066	60,613	19.2
Molecular weight	44.4	19.9	18.0
Mass density (kg/m3)	516	70.6	1,026

Table 6-7 Properties of streams leaving the dehydration vessel

The properties of the streams leaving the dehydration vessel are shown in Table 6-7 and the outlet streams in Table 6-8.

Composition	Condensate	Dry Gas	Water
Methane	30.7%	80.7%	46ppb
Ethane	18.7%	12.4%	0
Propane	20.3%	5.0%	0
i-Butane	2.7%	0.33%	0
n-Butane	10.0%	0.91%	0
i-Pentane	1.6%	0.07%	0
n-Pentane	3.2%	0.12%	0
n-Hexane	3.1%	0.05%	0
n-Heptane	2.9%	0.02%	0
n-Octane	2.6%	0.01%	0
n-Nonane	2.3%	0.00%	0
n-Decane	1.7%	0.00%	0
Carbon dioxide	0.2%	0.19%	67ppm
Nitrogen	0.0%	0.17%	2.1ppm
Water	141ppm	149ppm	99.99%

Table 6-8 Compositions of streams leaving the dehydration vessel

6.2.4.3 Insulation requirements

The operating temperature of the dehydration vessel will be lower than the seawater temperature so to ensure maximum thermal performance of the dehydration vessel it will need to be suitably insulated. Polyurethane foam insulation was used successfully with the experimental vessel and being already widely used for insulation in subsea environments, it would likely be an appropriate choice of material for the dehydration vessel.

The thermal design in the region of the proposed hydrate management system will need to be reviewed after testing of the proposed solution is completed.

6.2.4.4 System start up

On start-up from ambient conditions the experimental system took several hours of operation to establish a stabilised dehydration process prior to which gas at high water saturation

levels passed out of the dehydration vessel. In a production system sending gas with a high water saturation into a pipeline is likely to be unacceptable so some special start-up processes will be required.

Possible techniques that could be utilised include:

- Pre-chilling the dehydration vessel using the proposed hydrate management system and encouraging hydrates to pre-establish on the walls of the dehydration vessel
- Passing the gas leaving the dehydration vessel through a membrane to remove additional water until the required dewpoint of the outlet stream is established
- Reinjection of gas to a suitable formation until the required dewpoint is established.

6.2.4.5 Nozzle operation

After system shut-in and subsequent cold start the first gas passing to the dehydration vessel will be at close to the temperature of the surrounding seawater. At these low gas inlet temperatures experience from the experimental runs tells us that it is highly likely that on commencement of cooling operations that hydrates will form and will block the nozzle. To prevent hydrate build-up in the nozzle from occurring the ability to heat the nozzle will be required.

As found during the experimentation phase, nozzle heating and inlet gas temperature control are both applicable methods of ensuring constant gas flow and optimum cooling within the dehydration vessel. Gas temperature control with the inlet heat exchangers has a much slower response time than a nozzle heater with good thermal design. As a consequence of its fast response time, the heated nozzle facility may be beneficial to reliable system operations, particularly if sudden changes to gas stream properties occur.

Operating conditions	
Inlet temperature	25 C
Inlet flow rate	8,774 kg/hr
Inlet pressure	15 MPa
Molecular weight of gas	25.43
Specific heat ratio	2.068
Calculated nozzle parameters	
Orifice diameter	30.7 mm

Table 6-9 Estimated nozzle sizing for production dehydration vessel

Using the production scenario parameters the nozzle can be sized. The results are shown in Table 6-9.

See Appendix B.1.2 for the detailed calculation.

6.2.4.6 Hydrate management – capture system

Hydrate build up on the dehydration vessel walls is critical to ensuring gas hydrate contact and the depression of the gas stream water contact.

A possible approach to control the temperature environment within the dehydration reactor is to use solid-state Peltier devices together with control circuits. Peltier devices are layered heat pump devices that can transfer heat from one external face to the opposite external face. The direction of heat transfer is controlled by the direction of current flow, so in a fixed configuration a face can be made to cool or heat relative to the other face simply by controlling the current flow. See appendix F for more information on Peltier devices.

Peltier controlled plates fitted inside the dehydration reactor could be used to alternately cool then heat the faces to first encourage hydrate formation and then to remove the hydrate sheet from the face for dissociation in the bottom of the reactor vessel.

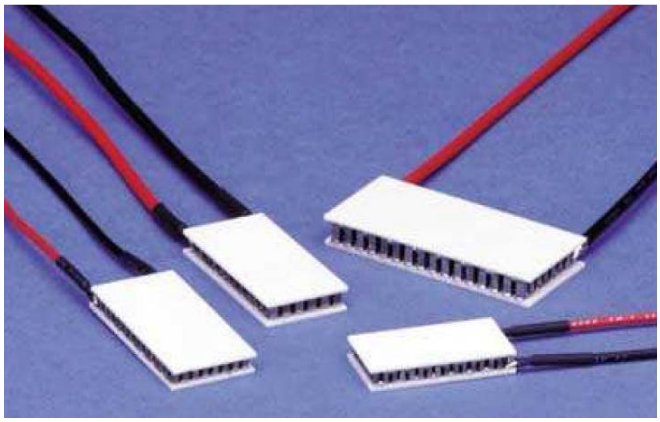

Figure 6-7 Peltier modules

Multiple Peltier based cooling plates could be fitted around the internal face of the reactor as shown in the vessel cross-sectional illustration shown in Figure 6-8.

Each module would be a subassembly comprising the two heat transfer plates with a number of Peltier devices sandwiched between them. To provide mechanical strength and thermal insulation a strong insulting material such as polycarbonate will be used between the plates.

The subassemblies would be attached to the inside face of the dehydration vessel using suitable heat transfer compounds to ensure good thermal contact from cooling plate to

vessel skin. An insulator or physical gap will be between the cooling modules to allow independent operation.

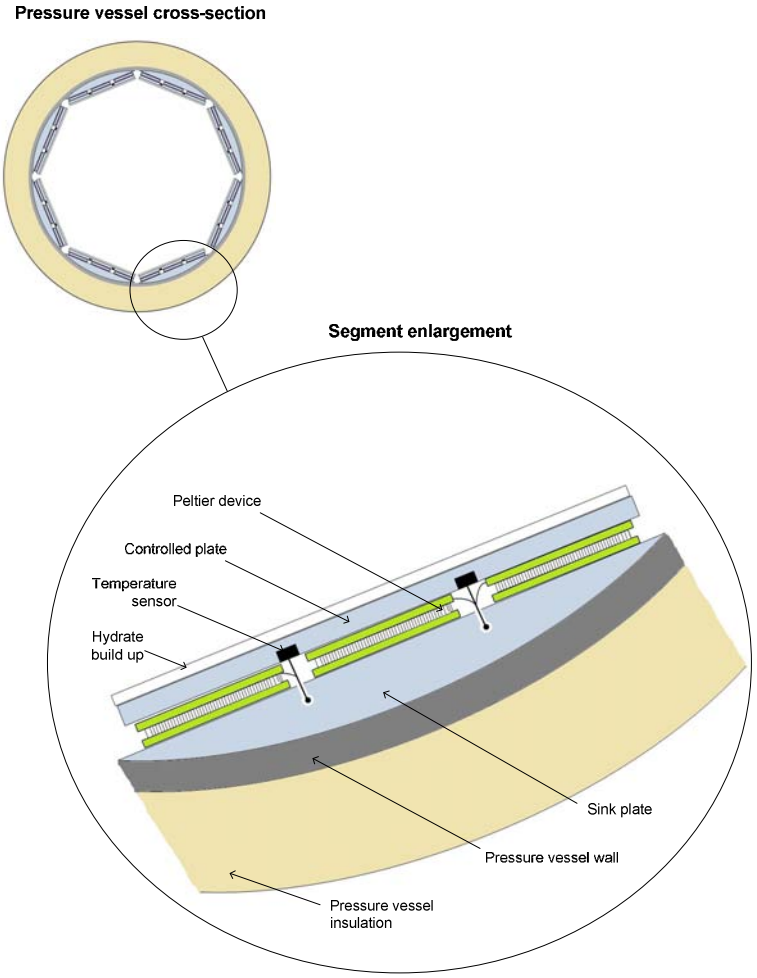

Figure 6-8 Hydrate management - controlled capture system

Control electronics would be required to control the operation of each cooling module. The expected operational cycle would be:

1. At system start-up, all modules will be placed in cooling mode some time before gas flow commences and allowed to stabilize at a temperature low enough to allow fast initiation of hydrate formation.

2. Gas flow commences and hydrates will build up on the controlled plate of the cooling modules.

3. At regular intervals a proportion of the cooling modules are switched to heating mode. The cooling face heats up and the hydrates on the surface of the plate will dissociate. With the release of gas from dissociation and the formation of a water

film the sheet of hydrates on the cooling module will fall under gravity to the bottom of the dehydration vessel. Once the hydrate sheet is released the cooling module reverts to cooling mode. The dehydration vessel will only be exposed to cooling plates at above hydrate dissociation temperature for a short time.

The cycle time for cooling/heating will need to be determined experimentally. It is anticipated that the cooling time will be significantly longer than heating times. With only a proportion of modules in heating mode at any one time the dehydrating ability of the vessel should not be compromised.

The functions of the control electronics will be:

1. Monitor temperatures of module faces (accurate temperature sensors will be built into the cooling modules controlled plate)

2. Control direction and level of module operating current to allow cooling and heating at determined levels to be applied.

3. Implement timing protocols to cycle modules through the cooling/heating cycles.

4. Monitor operational capability of cooling modules

The implementation can include significant system redundancy to ensure that the operational life of the dehydration system is not compromised by failure of an electronic component.

The solution requires no moving parts and has the potential to provide long operating life in the harsh deep sea operating environment.

6.2.4.6.1 *Thermal design considerations*

Considering the thermal design of the proposed solution, there are two states of particular interest that need to be analysed, the point at which the hydrate build-up has reached the desired thickness for the removal process to commence and the state once the hydrate has dropped from the plate. These are illustrated in Figure 6-9 .

With a temperature sensor fitted close to the inside face of the metal plate we can measure the temperature of the steel-hydrate interface. The thermal conductivity of hydrate is approximately 100 times less than that of carbon steel (0.5 W/m.K[76] versus ~54 W/m.K) so even with a small heat flow the temperature of the interface will change markedly as the hydrate layer thickens. Temperatures measured from the various system plates should also assist with identifying when a plate is ready to be cleansed of hydrate.

When the hydrate has reached a predetermined thickness the process of removing it by adding heat with the Peltier devices will commence. The temperature of the steel-hydrate

interface must be raised to above the hydrate formation temperature at the vessel pressure to cause the hydrate at the interface to dissociate. Using the hydrate program, CSMGem developed by Sloan[86] a prediction for the hydrate formation temperature at the vessel pressure of 6 MPa can be determined. Using the gas composition entering the dehydration vessel, at a dehydration vessel pressure of 6 MPa SII type hydrate is predicted to form at 18.4 C.

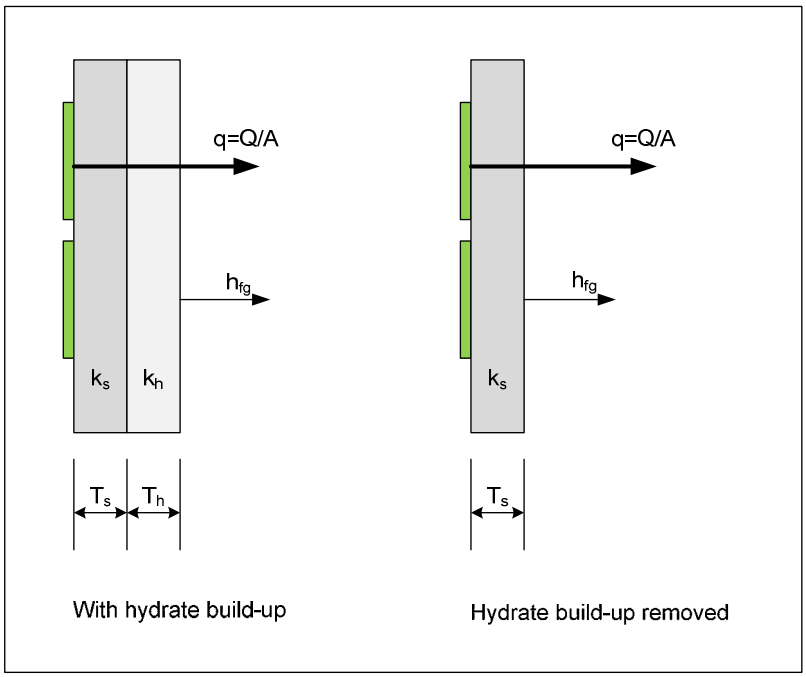

Figure 6-9 Thermal layers within dehydration vessel

As heat is applied, a temperature gradient will establish across the plate and hydrate according to the thermal conductivities of the materials. The low thermal conductivity of the hydrate causes it to act like an insulator so the steel-hydrate interface will heat up quickly with minimal heat transfer through the hydrate to the gas in the vessel. When the plate-hydrate interface exceeds 18.4 C the hydrate at the interface will dissociate and release the trapped gas at high pressure. This high pressure gas should assist in the removal of the hydrate from the steel plate.

Looking at the thermal characteristics, while the hydrate is present on the plate the overall thermal coefficient is calculated to be around 25 $W/m^2.K$ and when it has been removed this doubles to 50 $W/m^2.K$. As the heating power will be kept constant this change in the thermal coefficient will cause a large drop in the temperature differential between the plate and the gas. This will provide an excellent marker to the control electronics to stop heating and start chilling the plate.

To remove the hydrates from the plates, power will be required to heat up the plate and to provide sufficient heat to melt a thin layer of the hydrate at the steel-hydrate interface. Assuming a plate thickness of 10 mm, the heat required to warm the plate from an estimated ambient temperature of 2.6 C to the hydrate dissociation temperature will be 585 kJ per square metre of plate. The hydrate heat of formation is 500 kJ/kg[86]. If a typical plate was 100 mm wide by 200 mm high and 1 mm of hydrate has to be melted for the hydrate sheet to detach itself from the plate a total of 23 KJ of energy will be required. On a plate of these dimensions, Peltier devices capable of providing 300 W of heat could easily be fitted. The time then taken for these devices to provide the required energy to remove the hydrate sheets is less than 2 minutes.

In the worked scenario the inlet gas stream entering the dehydration vessel will be saturated with water. At a pressure of 15 MPa and temperature of 25 C the saturated gas stream contains 421 ppmv of water vapour. At the dehydration vessel exit conditions of 6 MPa and 2.6 C the predicted water content will be 149 ppmv so a total of 272 ppmv of water will be removed from the gas stream within the dehydration vessel. For the scenario flow rate at the dehydration vessel of 3,920 kgmol/hr, the total water capture is 19.2 l/hr.

Some of this captured water will be collected as water droplets falling by gravity to the bottom of the vessel and some as hydrate build-up on the walls of the vessel. How much is captured by each mechanism is presently unknown. When we consider the upward velocity of the gas in the dehydration vessel, calculated to be 5 cm/sec, small condensed droplets will be entrained in the gas stream (refer to section 3.4.3.2) and collection by gravity will rely on the aggregation of droplets as they flow up the vessel.

If we assume the production vessel has the same dimensional scale as the experimental system the total area of capture plates will be around 75 m^2. If 90% of the water is captured on these plates as Hydrate the capture rate will be around 24.5 litres per hour. The time to capture a uniform 1 cm thick layer of Hydrate across the area of plates in the dehydration will be 31 hours. The likelihood of uniform capture is small but this calculation illustrates the slow rate of hydrate build up compared to the rate at which it can be efficiently removed. Details on the calculation are provided in Appendix B.4.

From a thermal design perspective the proposed method looks plausible.

6.2.4.7 Hydrate management – dissociation system

With the described hydrate capture mechanism, periodic cycling of the capture plates will result in sheets of hydrate detaching from the plates and falling to the bottom of the dehydration vessel.

The described dehydration vessel has a horizontal separator at the bottom filled with some warmed condensate. The temperature of the condensate would be controlled to be just

above the dissociation temperature of the hydrate. The hydrate sheet has a higher density than the condensate so will sink into the condensate layer and will dissociate. As it dissociates the released water will sink to the bottom of the separator and the gas will bubble through the condensate to the top of the vessel where it will rejoin the gas stream.

Level controls would be fitted in the separator to control the levels of the condensate and water.

6.2.5 Power requirements and generation

Only thermodynamic processes are proposed to be used to cool the gas stream from the well, no power is proposed to be used for continuous refrigeration. A major consequence of this is that the power requirements of the process are relatively small. Power is needed in the system for the following functions:

- to remove the hydrate from the capture plates through electrically generated heat using the Peltier heat pumps (see section 6.2.4.6.1)
- to cool the capture plates once the hydrate sheets have been dropped
- to warm the condensate bath where the hydrates dissociate.
- nozzle heating at start-up and also potentially for short periods during operations as required.
- for the monitoring and control systems including valve actuators on the heat exchangers and dehydration vessel

Subsea power may be obtained through an umbilical or may be generated subsea. Significant previous work has been performed at Curtin University of Technology by K. Sorani and Dr. D. Pack on potential subsea generation schemes, including an Ocean Thermal Energy Convertor (OTEC) which may be an appropriate technology for this system. Refer to the thesis of K. Sorani for more information.[129]

6.3 Summary of system for production operations

This section has presented a potential implementation scenario for a medium sized gas-condensate well. The complexity of the solution is low, making use of components that are already industrially proven and many that are already in use subsea.

- Subsea separators similar to those already in operation should be applicable
- The heat exchanger uses moderate lengths of pipe and a standard tube-shell component.

- The dehydration vessel is a pressure vessel similar to a separator with an internal hydrate management system that uses proven solid state components. It has no moving parts.

- Existing techniques can be used for power generation and effluent disposal.

There is still a significant amount of research work that needs to be performed to fully confirm the viability of the proposed approach but the calculations presented suggest strongly that the approach is likely to be a practical approach to exploiting some sub-sea gas fields that cannot justify a platform installation.

It is important to note that the solution requires a significant drop in wellhead pressure to obtain the required cooling. This may for some wells drop the pressure to levels where subsea compression will be required to make the pipeline economically viable. This shortcoming may be acceptable for many gas fields whilst making the solution undesirable in others.

7 Conclusions and recommendations

7.1 Summary of the research

The aim of the research was to review the current status of subsea technology and investigate a possible technique for implementing a dehydration process that could be operated in the harsh environment found at depth in the oceans. The technology has been patented[130, 131].

It was determined that most currently used dehydration techniques do not adapt well for subsea operation and a simple technique utilising Joule-Thomson cooling together with hydrate depression of water content could meet the system constraints dictated by subsea operations.

During the system development phase of the research many different system components were tested in particular; dehydration vessel insulation, heated nozzle adaptors, nozzle designs and positioning of the nozzle within the vessel.

Ultimately through this modification and testing process a dehydration system configuration resulted that allowed us to consistently demonstrate dehydration performance for a continuous process that was as good as has previously been obtained by other researchers for batch processes. Whereas the batch processes involved keeping small samples in equilibrium with hydrates for hours, our new process was continuous and only required the gas to be resident in the dehydration vessel for a few minutes.

It is interesting to compare the experimental results of the subsea process with the field results obtained by the above-ground system trialled by Cool Energy.[132] A direct comparison is not possible as the dehydration vessel temperatures established in the field trial were significantly lower than was possible in the subsea system experiments and the field experiments were typically performed at higher vessel pressures. In the field trial at vessel conditions of 6.6 MPa and -4.7 C water contents of 67 ppmv were achieved. Using the Chapoy correlation the predicted water content in equilibrium with hydrates is around 77 ppmv. The experimental results from the subsea experiments also demonstrated water contents lower than that predicted by the Chapoy correlation. If a full scale test of the subsea experimental system is performed it is reasonable to expect similar results to the above-ground system.

7.2 Scaling of the system to a production

Taking the lesson learnt from the experimental process a production scenario was worked for a medium sized gas-condensate well and major system components were sized to meet the functional and flow requirements. A method for managing the hydrate build-up within the dehydration using solid state heat pumps was presented together with a theoretical analysis that demonstrated the process viability.

The production scenario of a well producing 89 MMSCFD of gas and 8,300 bpd of condensate suggested a dehydration vessel 10.5m high and 2.4 m diameter and a mass of around 160 tons, well within the limits for normal subsea deployment

7.3 Advantages of the technology

The solution described has many advantages on other dehydration technologies:

- It can comfortably meet the pipeline gas water content requirement to ensure no condensation occurs within the pipeline
- It will have high reliability due to its simplicity and the lack of moving parts
- It is not prone to problems during shut-ins
- The solid-state hydrate management system can easily be built with significant redundancy to ensure long reliable operation.
- The solution only requires a small amount of electrical power to operate, within that which could be generated subsea.
- It is scalable to production volumes
- It utilises proven components many of which are already used in subsea environments

7.4 Conclusions

Based on the experimental results a number of conclusions were made:

- Thorough insulation of the dehydration vessel allowed the establishment of the lowest vessel temperatures for a given pressure drop.
- The positioning of the nozzle was critical for efficient operation of the system. If not fitted correctly water carry over from the vessel significantly affected the

dehydration performance. A nozzle installed in the centre of the vessel with the gas flow downwards provided the best results.

- The best method for preventing formation of hydrate blockages of the nozzle was through the control of the inlet gas temperature rather than the use of heated nozzle adaptors.

- The dehydration performance of the system was dependent on both reaching the lowest possible vessel temperature and the build-up of Hydrate within the vessel to ensure sufficient gas-hydrate contact time.

- The spraying of cold hydrocarbon liquids in the proximity of the gas exiting the nozzle had no effect on the dehydration performance of the system solution.

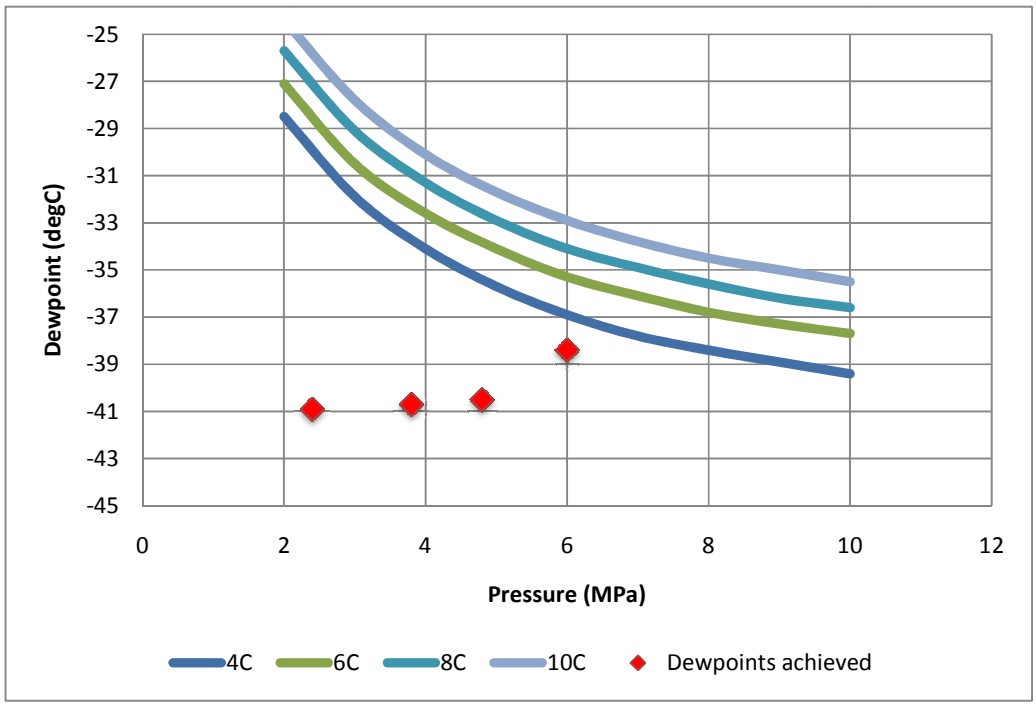

Figure 7-1 Achieved dewpoints versus pipeline requirements

Figure 7-1 shows a plot of the experimentally achieved dewpoints versus the required pipeline dewpoints for different seawater temperatures.

From the measured dewpoint data it is clear that the resultant water content of the gas stream leaving the dehydration vessel is low enough to ensure that no condensation of water will occur as the gas passes through the pipeline.

The study of the production scenario concluded that it was entirely feasible to implement a subsea dehydration based on that tested by this research

7.5 Recommendations

With the small scale experimental plant implemented the combination of Joule-Thomson cooling and the controlled presence of hydrates has been demonstrated as a viable method for subsea dehydration.

To progress the process further towards a production implementation it is recommended that an amount of further work be performed:

1. System tests will need to be performed at higher inlet pressures that will allow typical pipeline pressure to be set as the outlet pressure.

2. Future system should support higher flow rates to allow larger and more optimum nozzle designs

3. It is suggested that future test systems have the facility to perform long run times to ensure that a maximum build-up of hydrates occurs and minimum dewpoints are achieved.

4. To optimally size a production vessel a detailed understanding of gas residence times and the amount of gas-hydrate contact will be required. Optimisation experiments will need to be performed on the dehydration vessel volume and geometry to gain this understanding.

5. A trial of the proposed hydrate management process is undertaken.

8 References

Every reasonable effort has been made to acknowledge the owners of copyright material. I would be pleased to hear from any copyright owner who has been omitted or incorrectly acknowledged.

1. Rivero, M. and E. Nakagawa, *Platform-Free Fields for Stranded Gas Development: Science or Fiction?*, in *SPE Annual Technical Conference and Exhibition*. 2005, SPE: Dallas, Texas, USA.
2. Verghese, J.T., *Options for Exploiting Stranded Gas - An Overview of Issues, Opportunities and Solutions*, in *SPE Annual Technical Conference and Exhibition*. 2003: Denver, Colorado, USA.
3. Bai, Y. and Q. Bai, *Part III Flow Assurance*, in *Subsea Pipelines and Risers*. 2005.
4. Parshall, J., *Evolving Subsea Technology Tackles Huge New Risks of Today's Projects.* JPT, 2008(May 2008): p. 40-47.
5. Moore, E.C. *Subsea Systems move into the Ultra-deep*. 2008; Oct 2, 2008:[Available from: http://www.epmag.com/Magazine/2008/10/item12209.php.
6. Vu, V.K., et al., *Comparison of Subsea Separation Systems*, in *2009 Offshore Technology Conference*. 2009: Houston, Texas, USA.
7. Johansen, O. and E. Leporcher, *Deepwater Separation: What Could be the use of it?*, in *SPE Annual Technical Conference and Exhibition*. 2001: New Orleans,Louisiana, U.S.A.
8. Riviere, L., *Pazflor Applies World's First Large-Scale Subsea Separation System.* Offshore, 2009. **69**(5).
9. Baker, A.C. and J.H. Entress, *The VASPS Subsea Separation and Pumping System Applied to Marginal Fied Developments*, in *Offshore Europe Conference*. 1991, SPE: Aberdeen, Scotland.
10. Peixoto, G.A., et al., *VASPS Prototype in Mirimba Field - Workover and Re-Start*, in *SPE Latin American and Caribbean Petroleum Engineering Conference*. 2005: Rio de Janeiro, Brazil.
11. Rach, N.M., *Shell Installs World's Deepest Production Spar at Perdido.* Oil & Gas Journal, 2008. **106**(34).
12. Kliewer, G., *Tordis becomes World's first Subsea Processing Installation.* Offshore 2007(67).
13. Gedde, H., et al., *Ormen Lange Long Step-Out Power Supply*, in *Offshore Technology Conference*. 2009: Houston, Texas, USA.
14. Stavropoulos, M., et al., *Subsea Electrical Power Generation for Localised Subsea Applications*, in *Offshore Technology Conference*. 2003: Houston, Texas, USA.
15. Cermelli, C.A., D.G. Roddier, and A. Aubault, *Remote power generation for deployment of subsea technologies in deepwater marginal fields.* Offshore, 2008. **68**(1).
16. Ayers, R.C. and M. Parker, *Offshore Produced Waste Water Management*. 2001, Canadian Association of Petroleum Producers.
17. Cobby, G.L., *Produced Water Regulatory Requirements Offshore Australia*, in *Seventh SPE International Conference on Health, Safety and Environment*. 2004: Calgary, Alberta, Canada.
18. Fox, T.J., G.L. Van Houtven, and C.D. Randall, *Economic Analysis of Air Pollution Regulations: Oil and Natural Gas Production*, U.S. EPA.

19. Nazhat, D.H.B.M., *Developing a Water Treatment System for Subsea Gas Processing Plant*, in *Woodside Research Facility*. 2006, Curtin University: Perth.

20. Tronvoll, J., et al., *The Tools of Sand Management*, in *SPE Annual Technical Conference and Exhibition*. 2001, SPE: New Orleans, Louisiana, U.S.A.

21. Stecki, J.S., Prof., *Production Control Systems - An Introduction.* Exploration & Production: The Oil & Gas Review 2003, 2003.

22. Theobald, M.C., *SPARCS Autonomous Control System.* Subsea Control and Data Acquisition, 1994. **32**: p. 155-170.

23. Byrne, S., J. J.P., and P. Dubourdieu, *APAC Concept - A New Umbilical-Less Subsea Control System.* Subsea Control and Data Acquisition, 1998: p. 115-136.

24. Mullen, K., *The Virtual Control Buoy*, in *Deep Offshore Technology International, Asia Pacific*. 2008: Perth Western Australia.

25. Yates, P. and D.M. Jones, *Umbilical-Less Integrated Control System.* Subsea Control and Data Acquisition, 1994. **32**: p. 135-153.

26. Casey, M.D. and C.D.F. Lawlor, *Development and Testing of a Novel Subsea Production System and Control Buoy for the East Spar Field Development, Offshore Western Australia*, in *SPE Asia Pacific Oil and Gas Conference*. 1996: Adelaide, South Australia.

27. Heng, E.I., B.F. Ronalds, and T.J. Edwards, *The Deepwater Subsea Tieback Option for Future Oil and Gas Production in Australia*, in *SPE Asia Pacific Oil and Gas Conference*. 2000: Brisbane, Australia.

28. *Review of Gas Specification for the Dampier to Bunbury Pipeline & Determination of an Appropriate Gas Composition For Design of Stage 5 Expansion*. 2006, M. J. Kimber Consultants Pty. Ltd.

29. Kane, M., A. Singh, and R. Hanssen, *Hydrate Blockage Experience in a Deep Water Subsea Dry Gas Pipeline: Lessons Learned*, in *2008 Offshore Technology Conference*. 2008: Houston, Texas, USA.

30. Nexans, *Subsea Umbilicals, Carpet Trenching and Spider Dredging, Direct Electrical Heating on Subsea Flowlines.* Offshore Technology, 2010.

31. Rasin Tek, M., et al., *Temperature and Pressure Gradients in Gas Wells*, in *SPE 53rd Annual Fall Technical Conference and Exhibition*. 1978: Houston, Texas, USA.

32. McKetta, J.J. and A.H. Wehe, *Use this Chart for Water Content of Natural Gases.* Petroleum Refiner (Hydrocarbon Processing), 1958. **37**(8): p. 153.

33. Kidnay, A.J. and W.R. Parrish, *Fundamentals of Natural Gas Processing*. 2006: CRC Taylor and Francis.

34. Huffmaster, M.A., *Gas Dehydration Fundamentals Introduction*, in *Laurance Reid Gas Conditioning Conference*. 2004: University of Oklahoma.

35. Baker, R.W. and K. Lokhandwala, *Natural Gas Processing with Membranes: An Overview.* Industrial & Engineering Chemistry Research, 2008. **47**(7): p. 2109-2121.

36. Manning, F.S. and R.E. Thompson, *Oil Field Processing of Petroleum*. Vol. 1. 1991: Pennwell Publishing Company, Tulsa, OK, USA.

37. *Reference List - Oil & Gas Treatment Systems, Gas Dehydration and Glycol Regeneration Units*. 2008, ESCHER Process Modules BV. p. 9.

38. Gronner, J. and J. Wermeling, *Sucessful Experience with Vortex Tube Technology at the EPE Cavity Storage of RWE Energy*, in *23rd World Gas Conference*. 2006: Amsterdam, Holland.

39. Lorey, M., J. Steinle, and K. Thomas, *Industrial Application of Vortex Tube Separation Technology Utilizing the Ranque-Hilsch Effect*, in *SPE European Petroleum Conference*. 1998: The Hague, Netherlands. p. 471-479.

40. GPSA, *Engineering Data Book*. 2004, Gas Processors Suppliers Association.

41. Mokhatab, S., W.A. Poe, and J.G. Speight, *Handbook of Natural Gas Transmission and Processing*. 2006: Gulf Professional Publishing.

42. Ungs, R.T. and P.R. Inman, *Conceptual Comparison of On-Platform Versus Onshore Gas Dehydration*, in *Offshore Technology Conference*. 2004: Houston, Texas, USA.

43. Markiewicz, G.S., M.S. Losin, and K.M. Campbell, *The Membrane Alternative for Natural Gas Treating: Two Case Studies*, in *SPE 63rd Annual Technical Conference and Exhibition*. 1988: Houston, Texas, USA.

44. *Advanced PRISM Membranes for Natural Gas Dehydration*. 2002, Air Products and Chemicals Inc.

45. Binci, F., F.E. Ciarapica, and G. Giacchetta, *Natural Gas Dehydration in Offshore Rigs: Comparison between Traditional Glycol Plants and Innovative Membrane Systems*, in *IMSTEC 03*. 2003: UNSW, Sydney, Australia.

46. Minkkinen, A., et al., *Methanol Gas-Treating Scheme Offers Economics, Versatility.* Oil & Gas Journal, 1992. **90**(22).

47. Estebab, A., V. Hernandez, and K. Lunsford, *Exploit the Benefits of Methanol*. 2000, Bryan Research amd Engineering Inc. p. 21.

48. Bloch, H.P. and A. Godse, *Compressors and Modern Process Applications*. 2006. p. 161.

49. Brouwer, J.M. and H.D. Epsom, *Twister Supersonic Gas Conditioning for Unmanned Platforms and Subsea Gas Processing*, in *Offshore Europe*. 2003, SPE: Aberdeen, UK.

50. *Factsheet 5: Twister for Sub-sea Processing*. 2008; Available from: http://www.twisterbv.com/PDF/resources/Twister_for_Sub-sea_Processing.pdf.

51. Tatro, S.R., et al., *Gas Drying using a pass-through Hydrate Crystallizer*, in *2007 SPE International Symposium on Oilfield chemistry*. 2007, SPE: Houston, Texas, U.S.A.

52. Aly, M.A.E.E.M., *Synthetic Hydrate for Natural Gas Dehydration*, in *Department of Petroleum Engineering*. 2004, Curtin University of Technology: Perth, Australia. p. 193.

53. Bradbury, J., *Modular Movement for Subsea Systems.* E&P, 2004.

54. Chetri, A.B. and M.R. Islam, *Problems Associated with Conventional Natural Gas Processing and some Innovative Solutions.* Petroleum Science and Technology, 2008(26): p. 1583-1595.

55. Keyes, D.C. *Toxicity, Ethylene Glycol*. 2009; Available from: http://www.medscape.com/article/814701-overview.

56. Song, K.Y. and R. Kobayashi, *Water Content of CO_2 in Equilibrium with Liquid Water and/or Hydrates.* SPE Formation Evaluation, 1987: p. 500-508.

57. Peng, D.Y. and D.B. Robinson, *A New Two-Constant Equation of State.* Industrial & Engineering Chemistry Fundamentals, 1976. **15**(1): p. 59-64.

58. Fotouh, K. and K. Shukla, *An Improved Peng-Robinson Equation of State with a new Temperature Dependant Attractive Term.* Chemical Engineering Communications, 1997. **159**(1): p. 209 - 229.

59. Lemmon, E.W., M.O. McLinden, and D.G. Friend. *Thermophysical Properties of Fluid Systems*. NIST Chemistry WebBook, NIST Standard Reference Database Number 69 2009; Available from: http://webbook.nist.gov/chemistry/fluid/.

60. Schettler, P.D. and C.R. Parmely, *Gas Composition in Devonian Shales*. SPE Reservoir Engineering, 1989(August 1989): p. 283-287.

61. Campbell, J.H., *Water-Hydrocarbon Phase Behavior*, in *Gas Conditioning and Processing*. 1992.

62. Goff, J.A. and S. Gratch, *Low Pressure Properties of Water from -160 to 212F*, in *52nd Annual meeting of the American Society of Heating and Ventillation Engineers*. 1946: New York, USA.

63. Robinson, D.B., D.Y. Peng, and S.Y.K. Chung, *The Development of the Peng-Robinson Equation and its application to Phase Equilibrium in a system containing Methanol.* Fluid Phase Equilibria, 1985. **24**: p. 25-41.

64. Sloan, E.D., F.M. Khoury, and R. Kobayashi, *Water Content of Methane Gas in Equilibrium with Hydrates*. Industrial & Engineering Chemistry Fundamentals, 1976. **15**(4): p. 318-323.

65. Song, K.Y. and R. Kobayashi, *Measurement and interpretation of the water content of a methane-propane mixture in the gaseous state in equilibrium with hydrate.* Industrial & Engineering Chemistry Fundamentals, 1982. **21**(4): p. 391-395.

66. Chapoy, A., *Phase Behaviour in Water/Hydrocarbon Mixtures involved in Gas Production Systems*, in *Ecole des Mines de Paris*. 2004: Paris, France.

67. Moran, M.J. and H.N. Shapiro, *Fundamentals of Engineering Thermodynamics*. 5th ed. 2006: John Wiley & Sons Inc.

68. Lanzafame, R. and M. Messina, *A New Method for the Calculation of Gases Enthalpy*, in *Energy Conversion Engineering Conference and Exhibit*. 2000: IECEC 35th Intersociety. p. 318-328.

69. Haghighi, B., M.R. Laee, and N.S. Matin, *A Comparison Among Five Equations of State in Predicting the Inversion Curve of some Fluids.* Cryogenics, 2003. **43**: p. 393-398.

70. Geana, D. and V. Feroiu, *Calculation of Joule-Thomson Inversion Curves from a General Cubic Equation of State.* Fluid Phase Equilibria, 1992. **77**: p. 121-132.

71. Lee, B.I. and M.G. Kesler, *A Generalized Thermodynamic Correlation Based on Three-Parameter Corresponding States.* AIChE, 1975. **21**(3): p. 510-527.

72. Brewer, J. and J.M. Geist, *Calculation of Enthalpy of Gaseous Mixtures.* Journal of Chemical & Engineering Data, 1961. **6**(3): p. 405-408.

73. Dilay, G.W. and R.A. Heidemann, *Calculation of Joule-Thomson inversion curves from equations of state.* Industrial & Engineering Chemistry Fundamentals, 1986. **25**(1): p. 152-158.

74. Aspen Technology Inc, C., Massachusetts, USA, *Aspen HYSYS, Version 2006.5 [21.0.0.6924]*. 2003, Aspen Technology Inc.

75. Carroll, J.J., *Natural Gas Hydrates: A Guide for Engineers*. 2003: Gulf Professional Publishing.

76. van der Waal, H.J. and J.C. Platteeuw, *Clathrate Solutions.* Advances in Chemical Physics, 1959. **2**(1).

77. Parrish, W.R. and J.M. Prausnitz, *Dissociation Pressures of Gas Hydrates Formed by Gas Mixtures.* Industrial & Engineering Chemistry Process Design and Development, 1972. **11**(1): p. 26-35.

78. Ng, H.J. and D.B. Robinson, *The Measurement and Prediction of Hydrate Formation in Liquid Hydrocarbon-Water Systems.* Industrial & Engineering Chemistry Fundamentals, 1976. **15**(4): p. 293-298.

79. Ng, H.J. and D.B. Robinson, *The prediction of hydrate formation in condensed systems.* AIChE Journal, 1977. **23**(4): p. 477-482.

80. *Chapter 14: Utilities, Section 12: Hydrate Formation Utility* in *Aspen HYSYS Operations Guide*. 2006, AspenTech. p. 14:100.

81. Mork, M. and J.S. Gudmundsson, Prof., *Rate of Hydrate Formation in Subsea Pipelines, Correlation based on Reactor Experiments*, in *12th International Oil Field Chemistry Symposium*. 2001: Geilo.

82. Sloan, E.D. and C.A. Koh, *Hydrate Formation and Dissociation Processes*, in *Clathrate Hydrates of Natural Gases*. 2008, CRC Press. p. 113.

83. Christiansen, R.L. and E.D. Sloan, *A compact model for hydrate formation*, in *Annual Convention of Gas Processors Association*. 1995: San Antonio, Texas, USA. p. 15.

84. Arjimandi, M., et al., *Is subcooling the right driving force for testing low-dosage hydrate inhibitors?* Chemical Engineering Science, 2005. **60**(5): p. 1313-1321.

85. Sloan, E.D. and C.A. Koh, *Clathrate Hydrates of Natural Gases*. 3rd ed. 2008: CRC Press.

86. Bylov, M. and P. Rasmussen, *The Effects of Impurities on Ethane Hydrate Induction Times.* ACS Fuels, 1997. **42**(2): p. 507-511.

87. Rawlins, C.H. and I.I. Wang, *Design and Installation of a Sand-Separation and Handling System for a Gulf of Mexico Oil Production Facility.* SPE Production and Facilities, 2001(August 2001): p. 134-140.

88. Rosa, E.S., F.A. França, and G.S. Ribeiro, *The cyclone gas-liquid separator: operation and mechanistic modeling.* Journal of Petroleum Science and Engineering, 2001. **32**(2-4): p. 87-101.

89. Wang, B., et al., *Numerical Study of Gas-Solid Flow in a Cyclone Separator*, in *Third International Conference on CFD in the Minerals and Process Industries*. 2003: CSIRO,Melbourne Australia. p. 371-376.

90. Vysniauskas, A. and P.R. Bishnoi, *A kinetic study of methane hydrate formation.* Chemical Engineering Science, 1983. **38**(7): p. 1061-1072.

91. Englezos, P., et al., *Kinetics of Formation of Methane and Ethane Gas Hydrates.* Chemical Engineering Science, 1987. **42**(11): p. 2647-2658.

92. Skovborg, P. and P. Rasmussen, *A mass transport limited model for the growth of methane and ethane gas hydrates.* Chemical Engineering Science, 1994. **49**(8): p. 1131-1143.

93. Herri, J.M., et al., *Methane hydrate crystallization mechanism from "in-situ" particle sizing.* AIChE Journal, 1999. **45**(3): p. 590-602.

94. Gnanendran, N. and R. Amin, *Modeling hydrate formation kinetics of a hydrate promoter-water-natural gas system in a semi-batch spray reactor.* Chemical Engineering Science, 2004. **59**(18): p. 3849-3863.

95. Herri, J.M., et al., *Interest of in situ turbidimetry for the characterization of methane hydrate crystallization: Application to the study of kinetic inhibitors.* Chemical Engineering Science, 1999. **54**(12): p. 1849-1858.

96. Kashchiev, D. and A. Firoozabadi, *Driving Force for Crystallization of Gas Hydrates.* Journal of Crystal Growth, 2002. **241**: p. 220-230.

97. Ribeiro Jr, C.P. and P.L.C. Lage, *Modeling of hydrate formation kinetics: State-of-the-art and future directions.* Chemical Engineering Science, 2008. **63**(8): p. 2007-2034.

98. Dimitrios, A., *An investigation of gas hydrates formation energetics.* AIChE Journal, 2005. **51**(4): p. 1258-1273.

99. Chapoy, A., et al., *Gas Solubility Measurement and Modeling for Methane–Water and Methane–Ethane–n-Butane–Water Systems at Low Temperature Conditions.* Fluid Phase Equilibria, 2004. **220**: p. 113-121.

100. Aoyagi, k., et al. *Improved Measurements aqnd Correlation of the Water Content of Metane Gas in Equilibrium with Hydrate*. in *58th Annual GPA Conference*. 1979. Denver CO.

101. Kobayashi, R. and D.L. Katz, *Metastable Equilibrium in the Dew Point Determination of Natural Gases in the Hydrate Region.* Petroleum Transactions, AIME, 1955. **204**: p. 262-263.

102. Mohammadi, A.H. and D. Richon, *Semiempirical Method for Determining Water Content of Methane-Rich Hydrocarbon Gas in Equilibrium with Gas Hydrates.* Industrial & Engineering Chemistry Research, 2007. **47**(2): p. 451-458.

103. von Stackelberg, M. and H.R. Muller, *Elektrochem.* 1954. **58**(25).

104. Dharmawardhana, P.B., W.R. Parrish, and E.D. Sloan Jr, *Experimental Thermodynamic Parameters for the Prediction of Natural Gas Dissociation Conditions*. Ind. Eng. Chem. Fund., 1980. **19**: p. 410-414.

105. Mohammadi, A.H., *Advances in Estimating Water Content of Natural Gases*, in *85th GPA Annual Conference*. 2006: Grapevine, TX, USA.

106. Daubert, T.E. and R.P. Danner, *DIPPR Data Compilation Tables of Properties of Pure Compounds.* AIChE, 1985.

107. McCain, W.D., *The Properties of Petroleum Fluids*. 2nd ed. 1990, OK., USA: Penwell Publishing Company.

108. Aoyagi, K., *The Water Content of a High Content of Methane in Equilibrium with Hydrates.* GPA Research Report 45, 1980.

109. Song, K.Y., M. Yarrison, and W. Chapman, *Experimental low temperature water content in gaseous methane, liquid ethane, and liquid propane in equilibrium with hydrate at cryogenic conditions.* Fluid Phase Equilibria, 2004. **224**(2): p. 271-277.

110. Sidin, R.S.R., *Droplet size distribution in condensing flow*. 2009, University of Twente: Enschede, Netherlands. p. 207.

111. Melton, P.M. and R.M. Harrison, *The Prediction of Droplet Size and Dispersity from a Hydraulic Hollow Cone Nozzle with Consideration of Physical and Rheological Properties.* Journal of Aerosol Science, 1990. **21 (Supplement 1)**.

112. Luijten, C.C.M., *Nucleation and Droplet Growth at High Pressure*. 1998, Technische Universiteit Eindhoven: Eindhoven.

113. Peeters, P., *Nucleation and Condensation in Gas-Vapor Mixtures of Alkanes and Water*. 2002, Technische Universiteit Eindhoven.

114. Souders, M. and G.G. Brown, *Design of Fractionating Columns I. Entrainment and Capacity.* Industrial & Engineering Chemistry, 1934. **26**(1): p. 98-103.

115. Foss, M.M., *Interstate Natural Gas - Quality Specification & Interchangeability.* Centre for Energy Economics, 2004: p. 52.

116. Low, T.B. and R. List, *Collision, Coalescence and Breakup of Raindrops. Part I: Experimentally Established Coalescence Efficiencies and Fragment Size Distributions.* Journal of Atmospheric Sciences, 1982. **39**: p. 1591-1606.

117. Fabian, P., et al., *Demystifying the Selection of Mist Eliminators Part 2: The Applications.* Chemical Engineering, 1993. **100**(12): p. 106-111.

118. Donaldson. *Filter Housing HD High Pressure*. 23 Nov 2009]; Available from: http://www.odms.net.au/files/organise/donaldsonfilters/data_library/HD%20High%20Pressure%20Filters.pdf.

119. Dawar, S., *Microscale Study of Drop Migration on Fibers in Coalescing Filters*. 2007, The University of Akron. p. 229.

120. Schick, R.J., *Spray Technology Reference Guide: Understanding Drop Size*, S.A.a.R. Services, Editor. 2008: Wheaton, IL., USA.

121. Nuyttens, D., *Effect of Nozzle Type, Size and Pressure on Spray Droplet Characteristics.* Biosystems Engineering, 1997. **97**: p. 333-345.

122. Wark, K., *Thermodynamics for Engineers*. 1994.

123. Incropera, F.P. and D.P. De Witt, *Fundamentals of Heat and Mass Transfer*. 2nd ed. 1985: John Wiley & Sons.

124. Tatel, Y. and A.E. Dukler, *A model for predicting flow regime transitions in horizontal and near horizontal gas-liquid flow.* AIChE Journal, 1976. **22**(1): p. 47-55.

125. Valberg, T., *Temperature Calculations in Production and Injection Wells*, N.F.o.E.S.a. Technology, Editor. 2005.

126. Swindell, G.S., *Reserves and Performance of Canyon Sand Gas Wells, 1970-1994*, in *Permian Basin Oil and Gas Recovery Conference*. 1996: Midland, TX, USA.

127. Patni, S. and J. Davalath, *Subsea HIPPS offers High-Pressure Field Development Option.* Offshore, 2005. **65**(6).

128. *Steel Pipe Catalog*, OneSteel, Editor. 2010.

129. Sorani, K., *Selection of a Standalone Power Generation System for a Novel Remote Sub-sea Gas Processing Facility*, in *Scool of Electrical and Computer Engineering*. 2008, Curtin University of Technology: Perth, Australia.

130. Amin, R.P. and C.K. Groothuis, *Removing Contaminants from Natural Gas*, U.P.a.T. Office, Editor: US Patent and Trademark Office.

131. Amin, R., *Dehydration of a Natural Gas in an Underwater Environment*, A.P. Office, Editor. 2006, Woodside Energy Limited.

132. Kavanagh, N.J., J. Inman, and M. Melaxos, *West Australian Gas Technology Trial - Benefits of a Local Partnership*, in *2008 SPE Asia Pacific Oil & Gas Conference*. 2008: Perth, Australia.

133. Cook, J.G. and D.G. Least, *An Exloratory Study of the Thermal Conductivity of Methane Hydrate.* Geophys. Res. Lett., 1983. **10**(5): p. 397-399.

134. *GP2 Foam Technical Data*, Kirkside, Editor. 2007: Osborne Park, Australia.

135. Bowers, P.J., *NRP and NSL Data File for Insulation*.

136. *Thermal Conductivity of some common Materials*. Available from: http://www.engineerngtoolbox.com/thermal-conducivity-d_429.html.

137. Walker, R.W., *Iterferometer Study on theEffect of Reduced Pressure on Free Convection from a Vertical Plate*, A.F.I.o. Technology, Editor. 1962: Ohio, USA.

Appendix A Papers

1. Gas pipeline preferential site selection occurrence for particle formation / deposition. D.W. Parks, D.J. Pack and A.B. Chesnoy (submitted to SPE for publication – currently under review)
2. Novel subsea Gas Dehydration Process Part 1: the Process Plant and Dehydration Performance, David Parks and Robert Amin (submitted to Journal of Petroleum Science and Engineering for publication)
3. Novel subsea Gas Dehydration Process Part 2: a Modelled Implementation, David Parks and Robert Amin (Awaiting approval to publish)

Appendix B Calculations

B.1 Nozzle sizing

B.1.1 Experimental dehydration vessel nozzle

Equation

$$\dot{m} = \frac{AP_1}{\sqrt{T_1}}\sqrt{\frac{\gamma}{R^*}}\left(\frac{\gamma+1}{2}\right)^{-\left(\frac{\gamma+1}{2(\gamma-1)}\right)}$$

Parameters

Specific heat ratio	1.73	
R universal	8.3145	J/mol.K
Molecular weight	0.01825	kg/mol
Inlet pressure	10	MPa
Inlet temperature	25	C
Gas flow rate	560	sl/min
Gas mass rate	0.0076	kg/s

Calculations

R^*	455.59	J/kg.K
Nozzle area A	0.38	mm^2
Nozzle diameter	**0.70**	**mm**

B.1.2 Example production system nozzle

Equation

$$\dot{m} = \frac{AP_1}{\sqrt{T_1}}\sqrt{\frac{\gamma}{R^*}}\left(\frac{\gamma+1}{2}\right)^{-\left(\frac{\gamma+1}{2(\gamma-1)}\right)}$$

Parameters

Specific heat ratio	2.068			
R universal	8.3145	J/mol.K		
Molecular weight	0.02543	kg/mol		
Inlet pressure	15	MPa		
Inlet temperature	25	C		
Gas mass rate	99,700	kg/hr	27.7	Kg/s

Calculations

R^*	326.96	J/kg.K
Nozzle area A	741.1	mm^2
Nozzle diameter	**30.7**	**mm**

B.1.3 Average size of a droplet grown through condensation

Flow conditions:		
Gas flow rate of experiment	560	sl/min
Molar flow rate of gas	0.42	mol/sec
Inlet gas temperature	25	C
Inlet gas pressure	10.5	MPa
Using HYSYS (Peng Robinson and Alinta gas composition)		
Inlet gas water content	497	ppmv
Water vapour flow rate at input	2.1E-04	mol/sec
Dehydration vessel conditions:		
Dehydration vessel pressure	4	MPa
Using HYSYS (Peng Robinson and Alinta gas composition)		
Dehydration vessel temperature	-8.4	C
Dehydration gas water vapour content	101	ppmv
Water super saturation S is then	4.9	
Assuming water leaves dehydration vessel at equilibrium		
Water vapour flow rate at outlet	4.2E-05	mol/sec
Water captured in dehydration vessel	1.7E-04	mol/sec
Assuming water density of 1cc/g and water molecular weight of 18		
Water volume capture rate	3.0E-03	ml/sec
Looking at the nucleation in the gas flow at vessel conditions		
Nucleation rate	2.0E+13	clusters/m^3.s
Gas flow rate	2.3E-04	m^3/s
Number of nucleation in gas flow	4.7E+09	clusters
Assuming that all nucleated water droplets grow at the same rate and use up all the available water		
Average volume of each water droplet	6.4E-13	ml
Average radius of water droplet	5.3E-05	cm
Average diameter of water droplet	**1.1**	**microns**

B.2 Heat flux for insulated dehydration vessel

Environmental conditions	**Celsius**
Dehydration vessel temp.	-4
Water bath temperature	4
Ambient air temperature	22

Thermal flux of cylinders

Equation

$$q_r = \frac{T_{\infty,1} - T_{\infty,n}}{\frac{1}{2\pi r_1 L h_1} + \frac{\ln(r_2/r_1)}{2\pi k_A L} + \ldots + \frac{\ln(r_n/r_{n-1})}{2\pi k_N L} + \frac{1}{2\pi r_n L h_n}}$$

Large cylinder

Cylinder length 0.7 m

Material	**Radius min**	**Radius max**
	mm	**mm**
Hydrate	72	73
Steel	73	85
Polyurethane	85	292
Polyethylene	292	300

Denominator terms	**Ambient air**	**Water bath**
Methane convection	0.06	0.06
Hydrate conduction	0.01	0.01
Steel conduction	0.001	0.001
Polyurethane conduction	14.32	14.32
Polyethylene conduction	0.03	0.03
Air convection	0.07	
water convection		0.02
Sum (Denominator)	14.49	14.41
	Watts	**Watts**
Heat flux for large cylinder	**1.79**	**0.56**

Small cylinder

Cylinder length 0.06 m

Material	**Radius min**	**Radius max**
	mm	**mm**
Hydrate	72	73
Steel	73	192
	192	300

Denominator terms	**Ambient air**	**Water bath**
Methane convection	0.70	0.70
Hydrate conduction	0.08	0.08
Steel conduction	0.042	0.042
Polystyrene conduction	31.99	31.99
Air convection	0.84	
water convection		0.21
Sum (Denominator)	33.66	32.82
	Watts	**Watts**
Heat flux for small cylinder	**0.77**	**0.24**

Thermal flux of plates

Equation

$$q_x = \frac{T_{\infty,1} - T_{\infty,n}}{\frac{1}{h_1 A} + \frac{L_A}{k_A A} + \ldots + \frac{L_N}{k_N A} + \frac{1}{h_n A}}$$

Top plate

Plate radius 0.073 m

Area 0.017 m^2

Material	Radius min mm	Radius max mm
Hydrate	72	73
Steel	73	131
Polystyrene	131	231

Denominator terms	Ambient air	Water bath
Methane convection	1.14	1.14
Hydrate conduction	0.13	0.13
Steel conduction	0.057	0.057
Polystyrene conduction	161.44	161.44
Air convection	5.69	
water convection		1.42
Sum (Denominator)	168.45	162.76

	Watts	Watts
Heat flux for top plate	**0.15**	**0.05**

Bottom plate

Plate radius	0.073	m
Area	0.017	m^2

Material	Radius min mm	Radius max mm
Hydrate	72	73
Steel	73	131
Polyurethane	131	231
Polyethylene	231	239
Steel tank	239	245

Denominator terms	Tank base
Methane convection	1.14
Hydrate conduction	0.13
Steel conduction	0.057
Polyurethane conduction	304.75
Polyethylene conduction	14.05
Steel tank conduction	0.01
Sum (Denominator)	320.14

	Watts
Heat flux for bottom plate	**0.08**

Calculated heat flux for dehydration vessel in given conditions

	Ambient air	Water bath
Large cylinder	1.79	0.56
Small cylinder	0.77	0.24
Top plate	0.154	0.049
Bottom plate	0.081	0.081
Total heat flux	**2.80**	**0.93**

The values of the thermal coefficients used are given below.

Material	Conductivity (W/m.K)
Methane hydrate (Type SI)	0.45 [133]
Carbon steel	60.5 [123]
Polyurethane foam (GP2)	0.0196 [134]
Polyethylene foam (foil covered)	0.034 [135]
Polystyrene (density - 15kg/m^3)	0.037 [135]
Fluid (unforced convection)	**Convection (W/m^2.K)**
Water	42
Air	10.5
Natural gas at 2.5MPa	52.5

The values taken for convection coefficients of air and water were mid range values reported in the Engineering toolbox website[136]. The value for methane assumed the same coefficient as air at atmospheric conditions and modified the value according to a property of convection coefficients reported by Walker[137]. This report noted that theoretically the convection coefficient was proportional to 0.5 power of the pressure.

Assuming a vessel pressure of 2.5MPa (~25 atmospheres) the convection coefficient used for methane is then 52.5.

The contribution of the convection terms is very small compared to conduction terms so any error in the selection of the coefficients is also small.

B.3 Convection coefficient 'h' for the heat exchanger

Physical parameters				
Internal pipe radius	245	mm		
Internal pipe diameter	0.49	m		
Pipe area	0.189	m^2		
Calculated parameters (HYSYS)				
Gas flow rate to heat exchanger	642	m^3/hr	0.178	m^3/s
Kinematic viscosity	0.1257	cSt	1.26E-07	m^2/s
Dynamic viscosity	0.0240	cP	2.40E-05	Ns/m^2
Specific heat	3,342	J/kg.K		
Thermal conductivity	0.0584	J/s.m.K		
Reynolds number	3,682,717		(flow is turbulent)	
Prandtl number	1.37			
Nusselt number	4,572			
Heat transfer coefficient - gas in pipe	544	J/s.m^2.K		

B.4 Build up of hydrates in production dehydration vessel

Data from HYSYS and CSMHyd program

Pressure 6 MPa
Temperature 18 C
Composition: Dehydration vessel vapour composition from HYSYS

Composition	Mole fraction
Methane	0.8070
Ethane	0.1240
Propane	0.0500
i-Butane	0.0032
n-Butane	0.0091
i-Pentane	0.0007
n-Pentane	0.0012
n-Hexane	0.0005
n-Heptane	0.0002
n-Octane	0.0001
N-Nonane	0.0000
n-Decane	0.0000
Carbon dioxide	0.0019
Nitrogen	0.0017

CSMHyd Hydrate prediction:

Hydrate structure	Type II	
Structure II cages	16 small	8 large
Number water mols	136	

Fractional occupancy of cages:

Component	Small	Large
Methane	81.85%	5.57%
Ethane	0.00%	12.67%
Propane	0.00%	73.23%
i-Butane	0.00%	6.28%
n-Butane	0.00%	1.93%
Nitrogen	0.06%	0.00%
Carbon dioxide	0.09%	0.02%

Calculation of Hydrate molar mass = Mass of molecules/Number of molecules

$$M = \frac{N_W M_W + \sum_{j=1}^{c}\sum_{i=1}^{n} Y_{ij} v_i M_j}{N_W + \sum_{j=1}^{c}\sum_{i=1}^{n} Y_{ij} v_i} \qquad [76] \qquad ...81$$

Component	Molecular weight	Small Mass	Large Mass		Small number	Large number
Methane	16	209.5	0.45		13.096	0.45
Ethane	30	0	2.0		0	1.01
Propane	44	0	17.6		0	5.86
i-Butane	58	0	2.0		0	0.50
n-Butane	58	0	0.62		0	0.15
Nitrogen	28	0.27	0		0.0096	0
Carbon dioxide	44	0.63	0		0.0144	0.0016
Sub totals		210.4	22.7		13.1	8.0
Water	18	2448			136	

Totals **Mass:** **2681** **Molecules:** **157.1**

Molar mass of hydrate **17.07** **g/mol**

Mass hydrate/Mass water 1.10

Volume of water collected 19.2 l/hr
Density of water 1,026 Kg/m^3
Mass of water collected 19.7 Kg/hr
Percentage of water captured as hydrate 90%

Mass of hydrate formed **19.4** **Kg/hr**

Volume of hydrate captured
Density = Mass of molecules/volume of mol of hydrate

$$\rho = \frac{N_W M_W + \sum_{j=1}^{c}\sum_{i=1}^{n} Y_{ij} v_i M_j}{N_A V_{cell}} \quad [76] \quad ...82$$

Volume Structure II cell 5.178E-27
Avogadro's number 6.023E+23
Volume 1 mol of hydrate 3.119E-03 m^3

Density **8.597E+05** **g/m^3**
0.860 **g/cc**

Rate of hydrate growth **22.6** **l/hr**

Average time to grow hydrates to 1cm on plates
Area of plates 75 m^2
Hydrate thickness 0.01 m
Hydrate volume 0.75 m^3

Time to grow **33.2** **hours**

Appendix C Gas compositions

C.1 Alinta mains supplied gas

Component	Day 1	Day 2	Average
Methane	86.82	87.06	86.9
Ethane	6.57	6.42	6.5
Propane	1.45	1.02	1.3
i-Butane	0.08	0.05	0.07
n-Butane	0.10	0.05	0.07
i-Heptane	0.01	0.00	0.005
n-Heptane	0.01	0.00	0.003
Hexane	0.00	0.00	0.002
Nitrogen	1.56	1.62	1.55
Carbon Dioxide	3.41	3.77	3.6

C.2 Macedon

Northern Carnarvon Basin, Western Australia

Component	Mol %
Methane	93.85
Ethane	0.41
Propane	0.01
Octane plus	0.01
Nitrogen	5.34
Carbon Dioxide	0.38

C.3 Gorgon

Northern Carnarvon Basin, Western Australia

Component	Mol %
Methane	77.45
Ethane	3.23
Propane	0.89
i-Butane	0.1
n-Butane	0.2
i-Pentane	0.13
Nitrogen	3
Carbon Dioxide	15

C.4 Jansz

Northern Carnarvon Basin, Western Australia

Component	Mol %
Methane	91.5
Ethane	3.75
Propane	1.06
i-Butane	0.2
n-Butane	0.21
i-Pentane	0.63
Nitrogen	0.3
Carbon Dioxide	2.35

C.5 Bass Strait

Gippsland Basin, Southern Australia

Component	Mol %
Methane	82.14
Ethane	6.92
Propane	4.4
i-Butane	0.87
n-Butane	1.44
i-Pentane	0.56
n-Pentane	0.46
Hexane plus	0.31
Nitrogen	0.7
Carbon Dioxide	2.2

Appendix D Illustrations

D.1 Dehydration Vessel

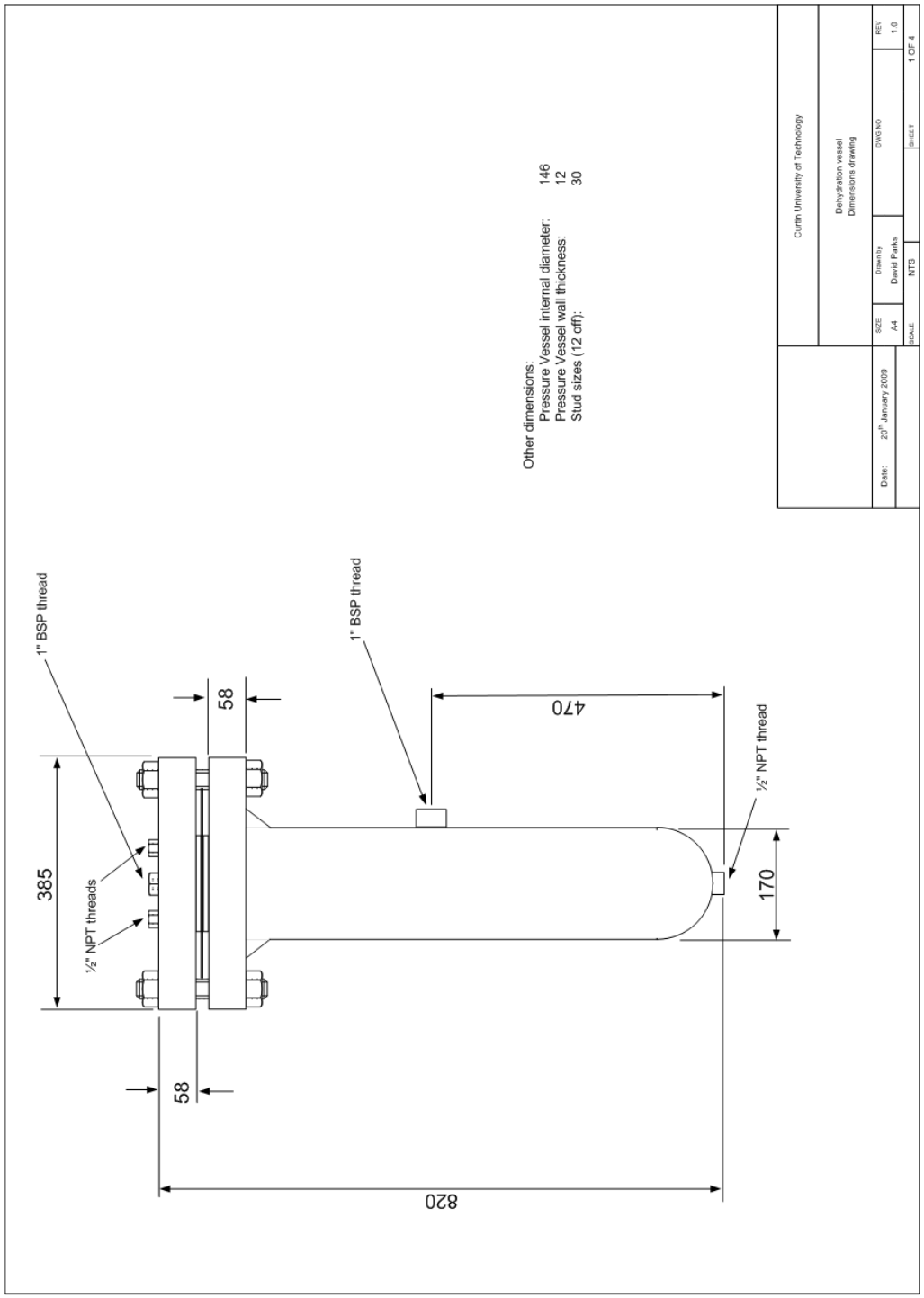

D.2 Heated nozzle system

D.2.1 Nozzle adaptor drawing – version 1

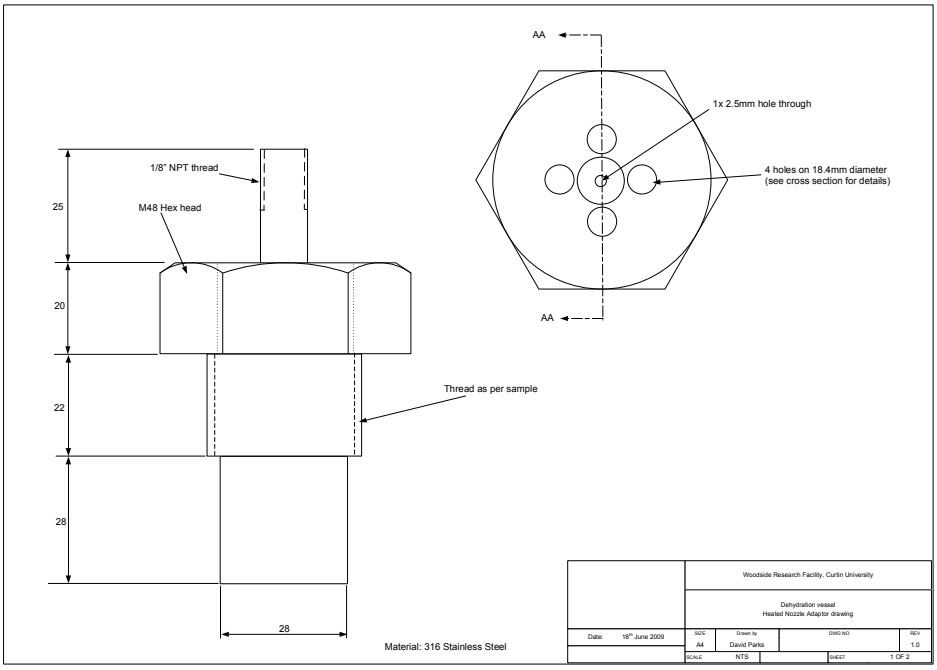

D.2.2 Nozzle adaptor drawing – version 2

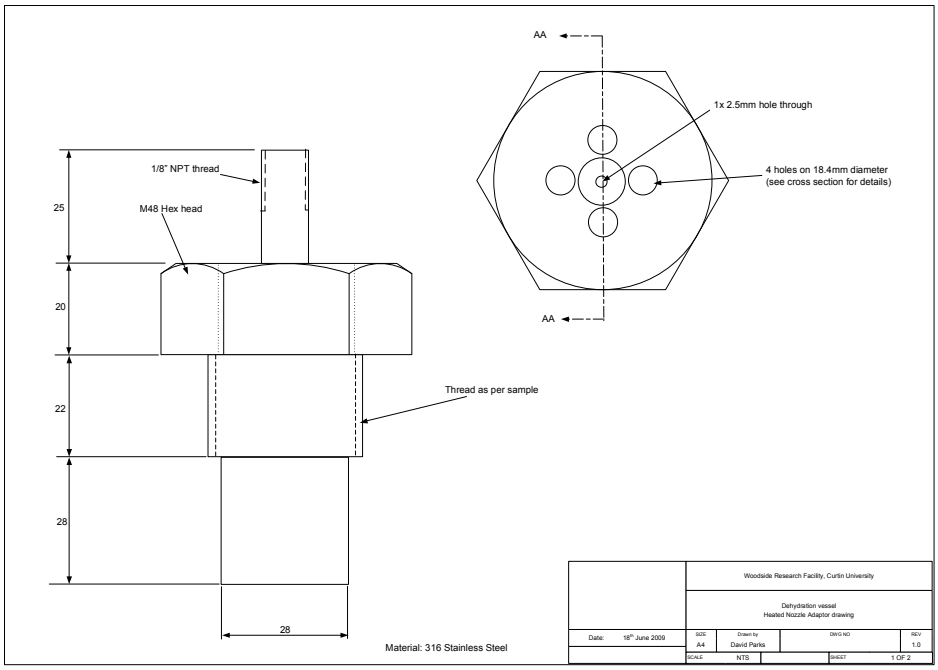

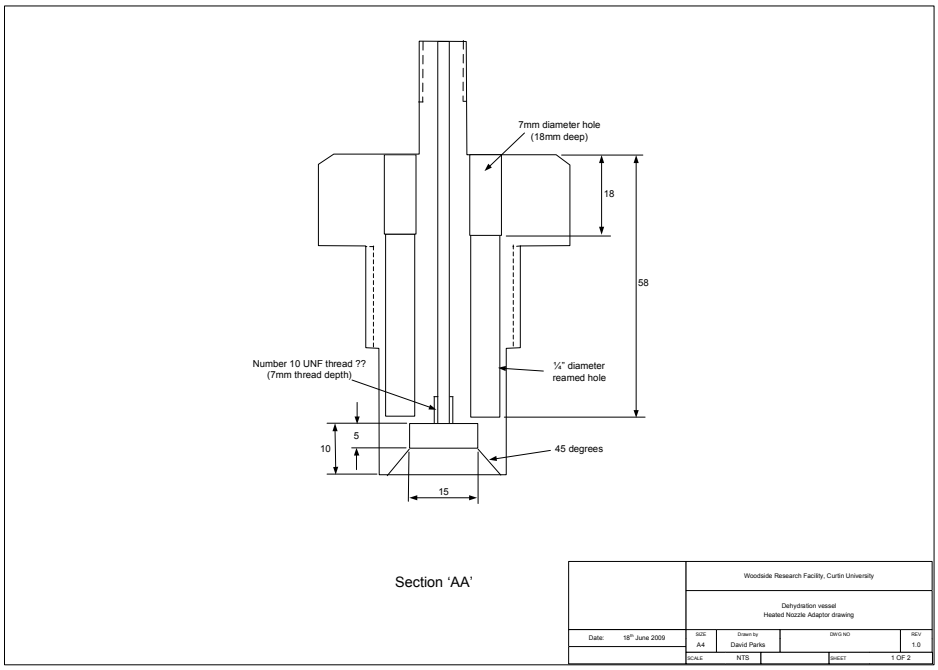

D.3 Bottom injection system

D.3.1 Separator weir assembly

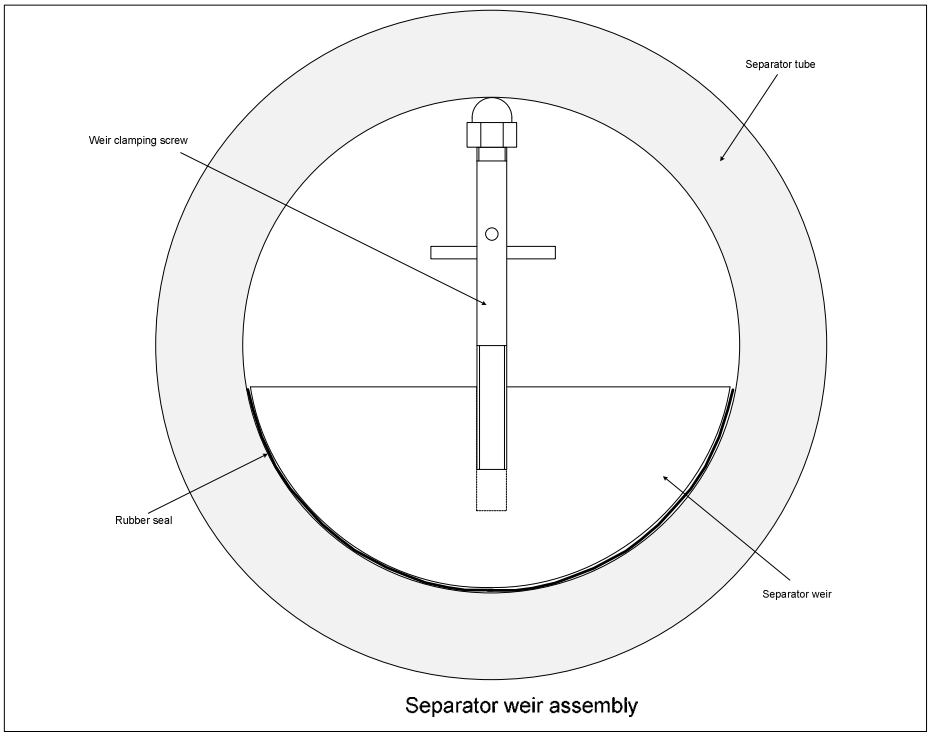

D.3.2 Separator parts

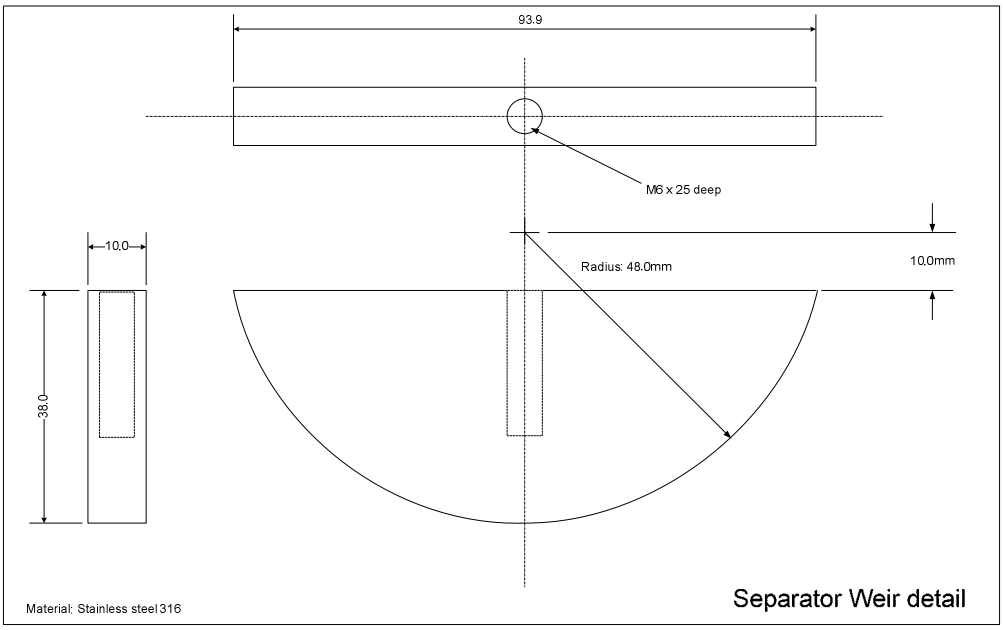

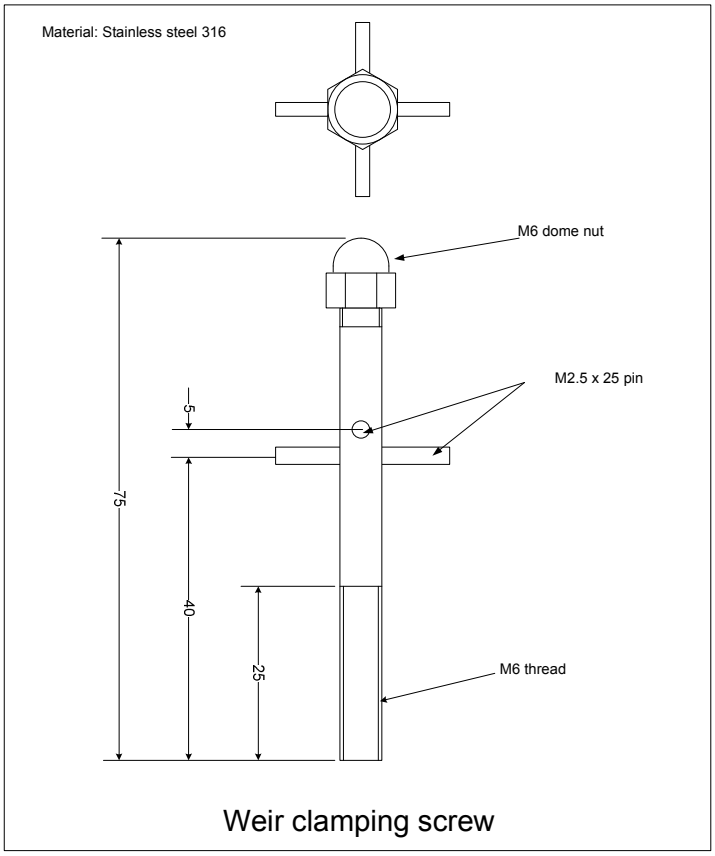

D.3.3 Bottom injection system assembly

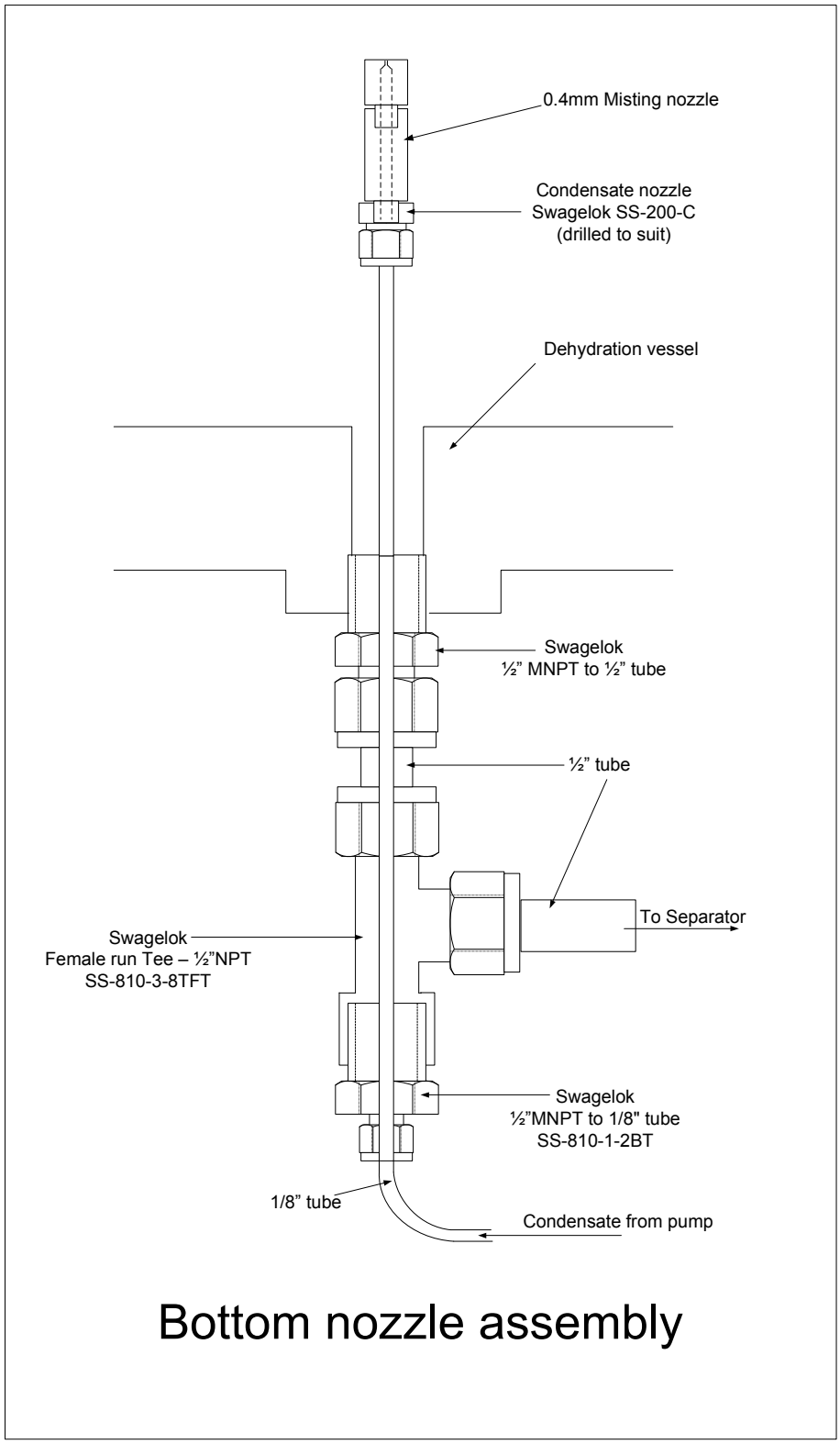

D.3.4 Heptane injector adaptor

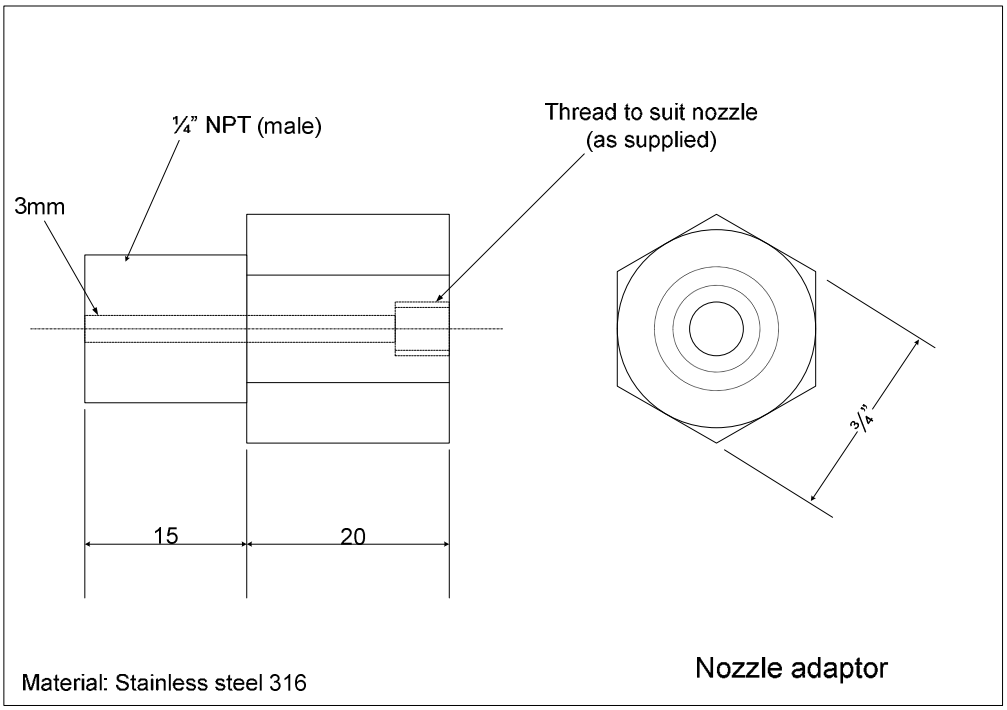

D.3.5 Top gas injection nozzle assembly

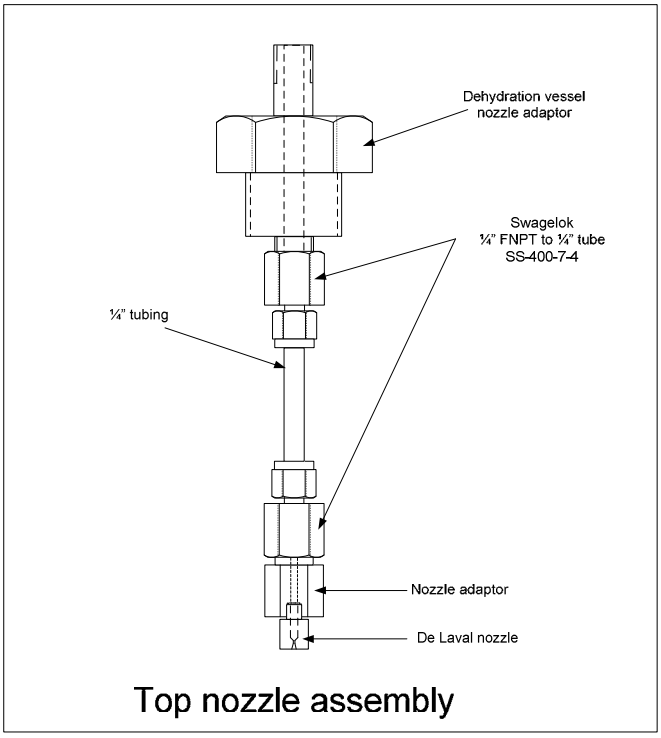

D.4 System PIDs

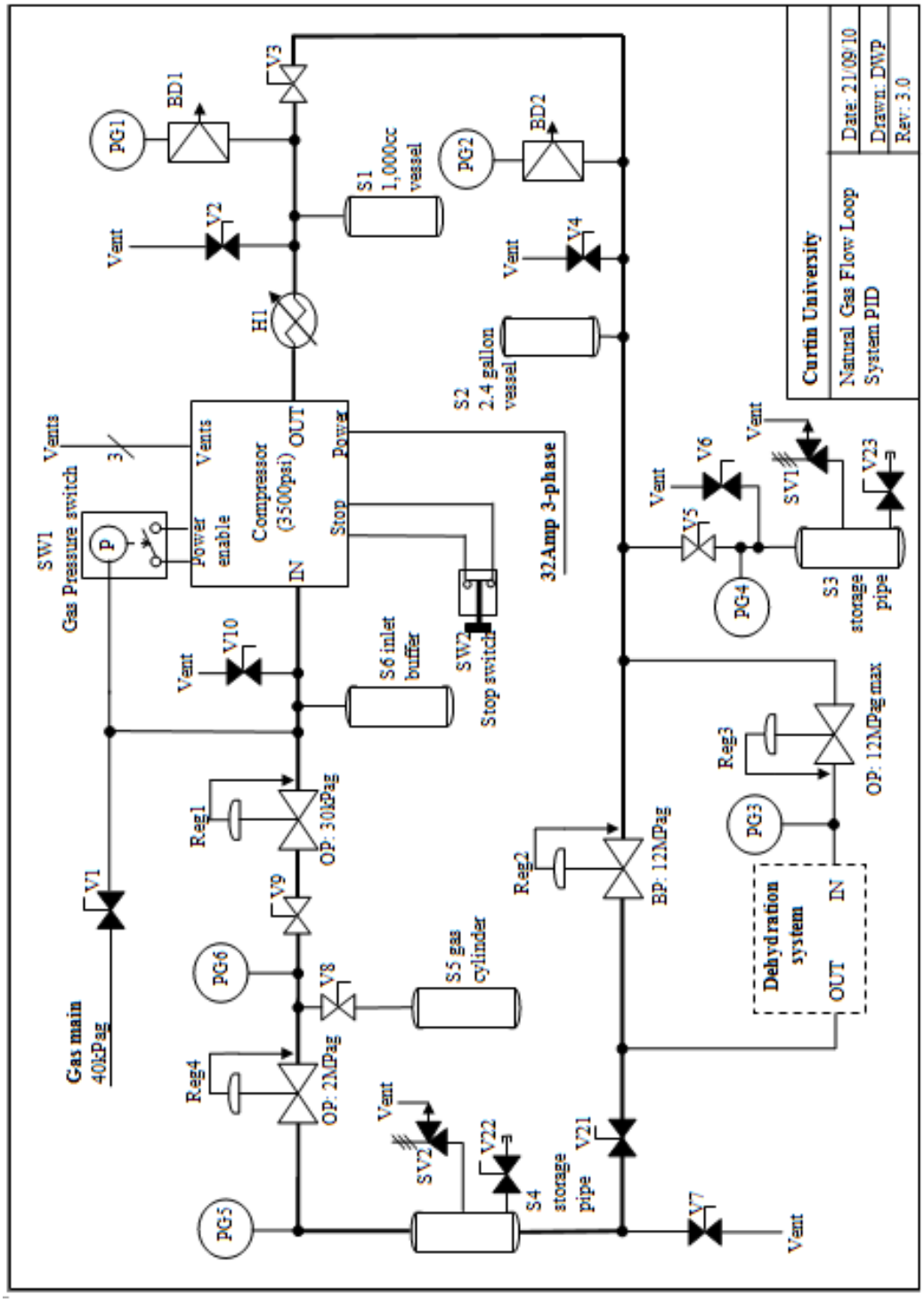

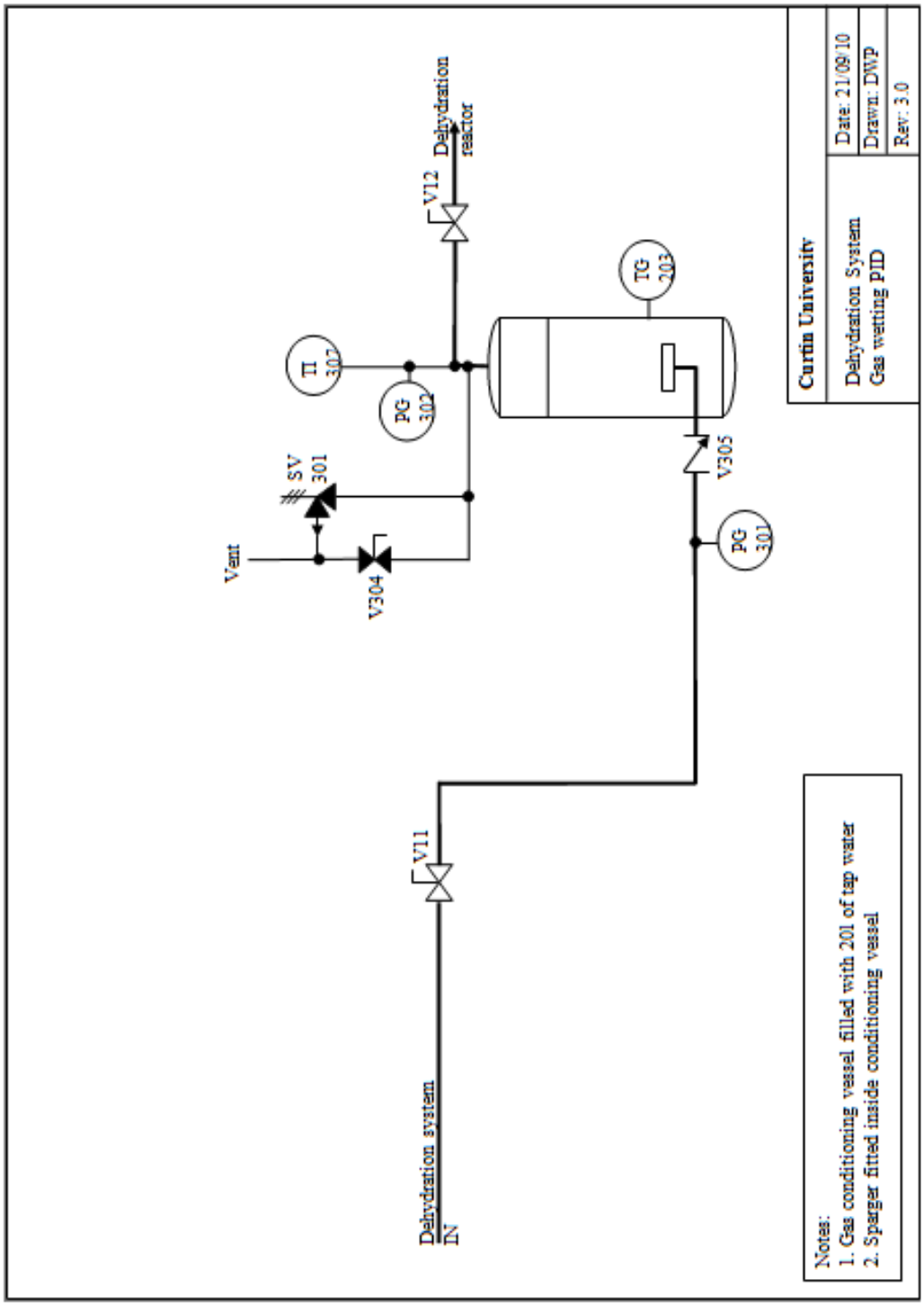
Curtin University
Dehydration System
Gas wetting PID
Date: 21/09/10
Drawn: DWP
Rev: 3.0
Notes:
1. Gas conditioning vessel filled with 20l of tap water
2. Sparger fitted inside conditioning vessel
Dehydration system IN
V11
V12
Dehydration reactor
TG 203
PG 301
V305
PG 302
TI 302
SV 301
V304
Vent

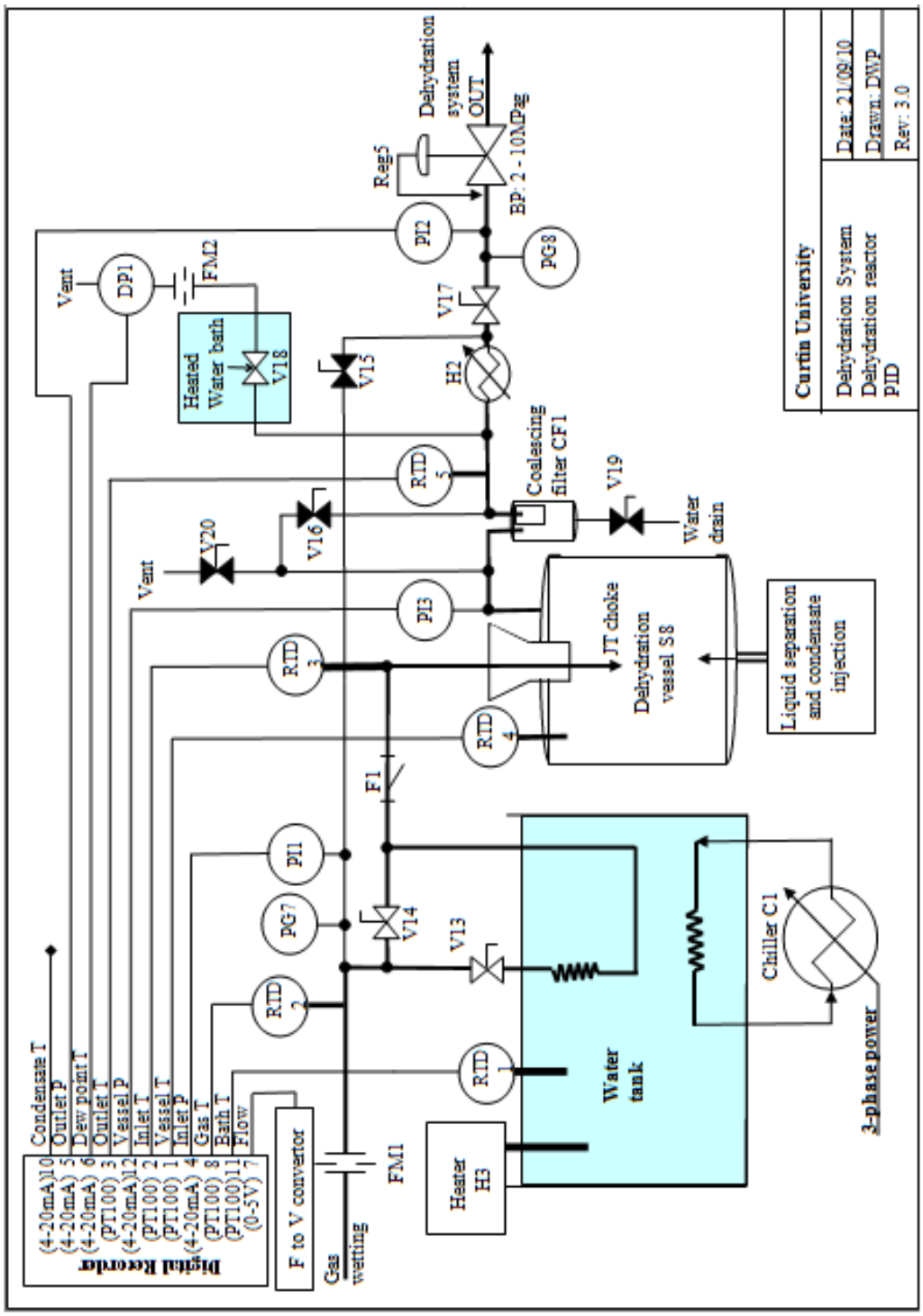
Curtin University
Dehydration System
Dehydration reactor
PID
Date: 21/09/10
Drawn: DWP
Rev: 3.0
Digital Recorder
(4-20mA)10 Condensate T
(4-20mA) 5 Outlet P
(4-20mA) 6 Dew point T
(PT100) 3 Outlet T
(4-20mA)12 Vessel P
(PT100) 2 Inlet T
(PT100) 1 Vessel T
(4-20mA) 4 Inlet P
(PT100) 8 Gas T
(PT100)11 Bath T
(0-5V) 7 Flow
F to V convertor
Gas wetting
FM1
Heater H3
Water tank
RTD 1
RTD 2
RTD 3
RTD 4
RTD 5
PG7
PI1
V14
V13
F1
PI3
V20
Vent
V16
V15
Heated Water bath
V18
Vent
DP1
FM2
H2
V17
PI2
PG8
Reg5
Dehydration system OUT
BP: 2 - 10MPag
Coalescing filter CF1
V19
Water drain
JT choke
Dehydration vessel S8
Liquid separation and condensate injection
Chiller C1
3-phase power

Safety Notes:

1. The maximum gas loop operating pressure as seen at PG2 is 12MPa
2. The maximum dehydration system pressure as seen at PG3 is 10MPa
3. Prior to pressurizing the system or part of the system with Natural Gas suitable purging of Oxygen from the system shall be performed.
4. Prior to venting of a Natural Gas volume, a warning sign shall be erected by the lunch room and permission obtained from a responsible person
5. The compressor shall only be run after a responsible person has been notified that experiments are to be performed.

Operating notes

1. The compressor will only start when sufficient gas pressure is available at the inlet. Switch SW1 must be manually reset after a low pressure event.
2. Valves V1 and V9 must never be open at the same time

Refer to Operating Instructions for more information

Key:

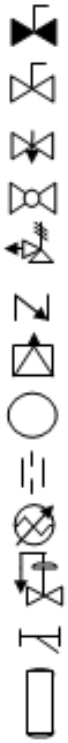

Plug valve – normally closed

Plug valve – normally open

Needle valve

Ball valve

Safety valve

Check Valve

Burst Disc

Gauge or Indicator

Flow meter

Chiller/Heater

Regulator

Filter

Storage vessel

Curtin University	
Dehydration System Notes and Key	Date: 21/09/10
	Drawn: DWP
	Rev: 3.0

D.5 Instrumentation wiring diagrams

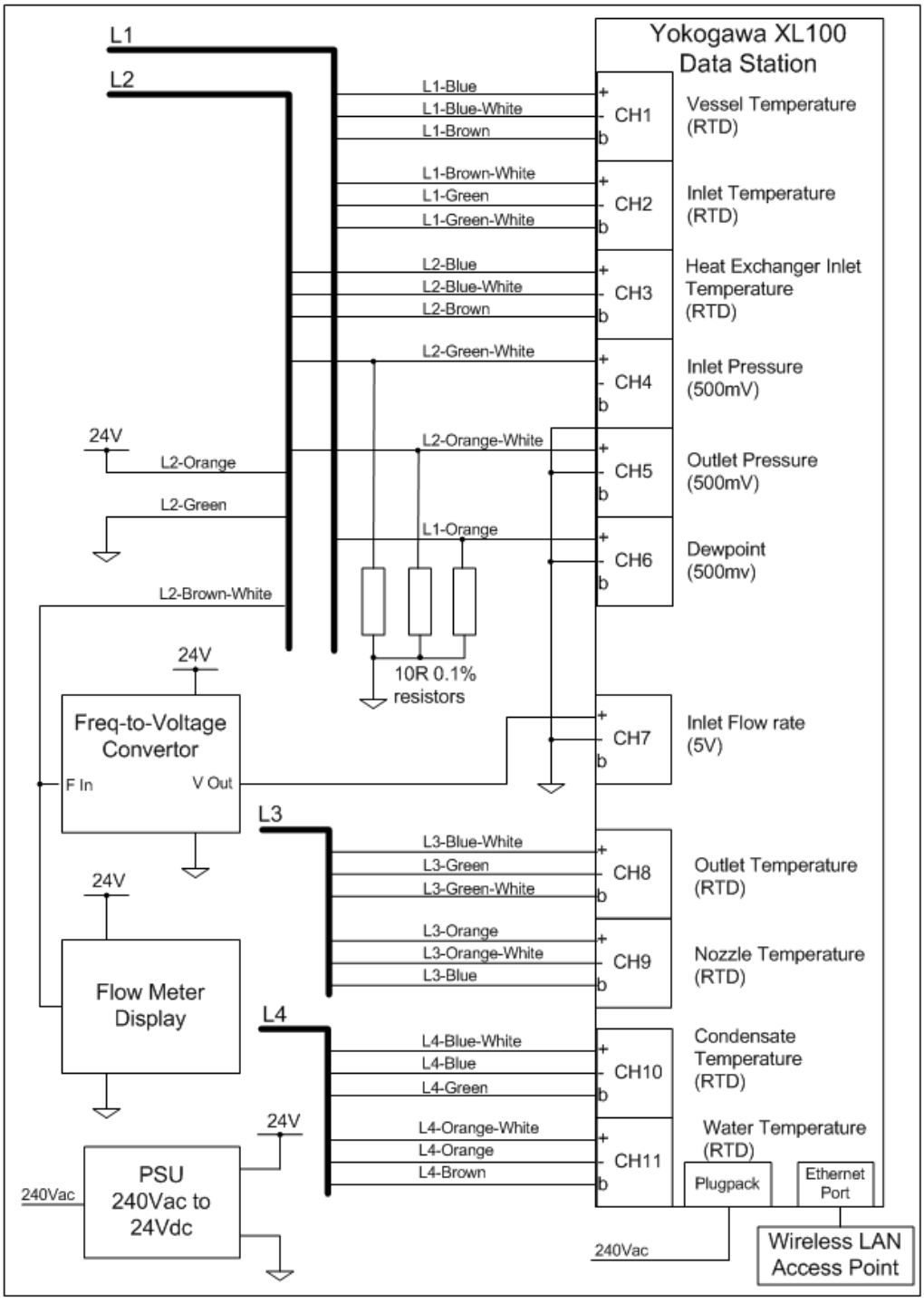

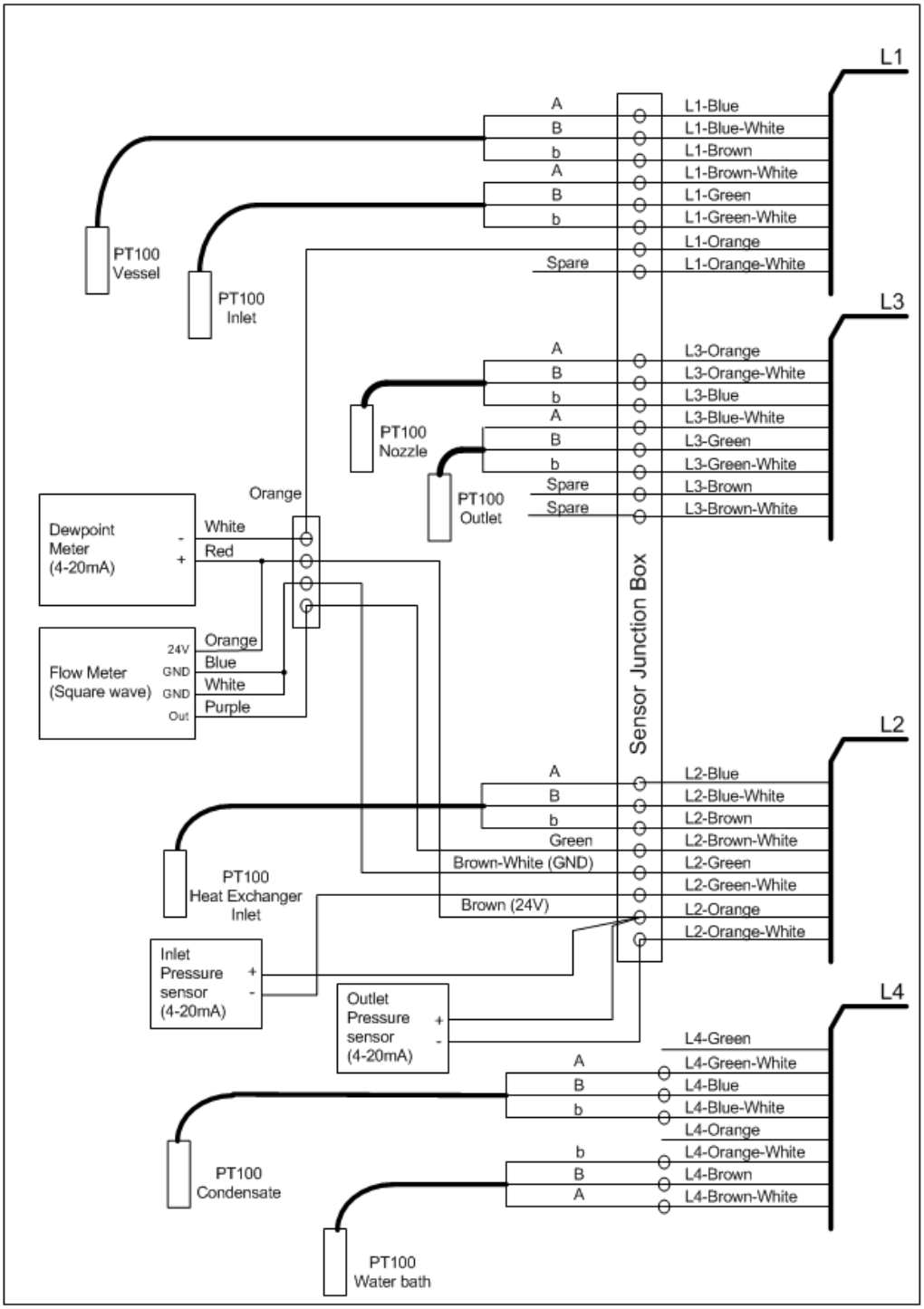
L1
A
B
b
A
B
b
Spare
L1-Blue
L1-Blue-White
L1-Brown
L1-Brown-White
L1-Green
L1-Green-White
L1-Orange
L1-Orange-White
PT100
Vessel
PT100
Inlet
L3
A
B
b
A
B
b
Spare
Spare
L3-Orange
L3-Orange-White
L3-Blue
L3-Blue-White
L3-Green
L3-Green-White
L3-Brown
L3-Brown-White
PT100
Nozzle
PT100
Outlet
Orange
Dewpoint
Meter
(4-20mA)
-
+
White
Red
Flow Meter
(Square wave)
24V
GND
GND
Out
Orange
Blue
White
Purple
Sensor Junction Box
L2
A
B
b
Green
Brown-White (GND)
Brown (24V)
L2-Blue
L2-Blue-White
L2-Brown
L2-Brown-White
L2-Green
L2-Green-White
L2-Orange
L2-Orange-White
PT100
Heat Exchanger
Inlet
Inlet
Pressure
sensor
(4-20mA)
+
-
Outlet
Pressure
sensor
(4-20mA)
+
-
L4
A
B
b
b
B
A
L4-Green
L4-Green-White
L4-Blue
L4-Blue-White
L4-Orange
L4-Orange-White
L4-Brown
L4-Brown-White
PT100
Condensate
PT100
Water bath

D.6 Pictures of experimental equipment

Conditioning vessel (left-hand unit)

Underwater tank and high pressure storage loops

Heptane injection system and separator

Insulated dehydration vessel and inlet heat exchanger

D.7 Dehydration data capture plots

On all plots:

- channel CH01 is the dehydration vessel temperature
- channel CH05 is the dehydration vessel pressure
- channel CH06 is the dewpoint measured at the data recorder (there was a problem in the 4-20 milliamp measurement circuit causing a reading error of between 2 and 2.5 C at the data recorder compared to the value reported at the sensor. For all the dewpoint measurements reported, the value at the dewpoint meter was taken to be correct and recorded data was adjusted accordingly. The plots below show the raw uncorrected data measured at the data recorder)
- channel CH07 is the gas flow rate

Dehydration test runs with increasing inlet temperature

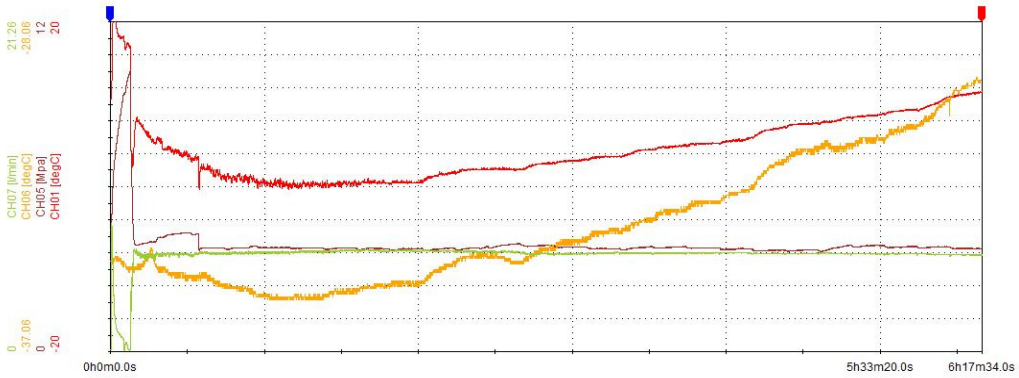

Data plot of run performed on 2/08/10

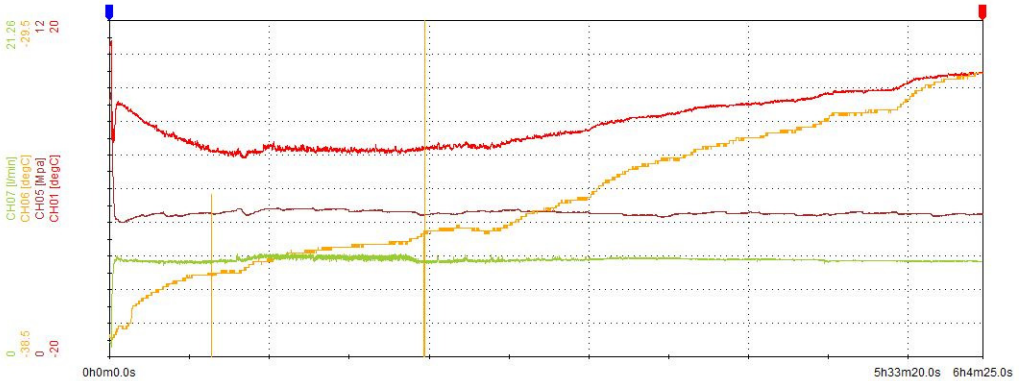

Data plot of run performed on 3/08/10

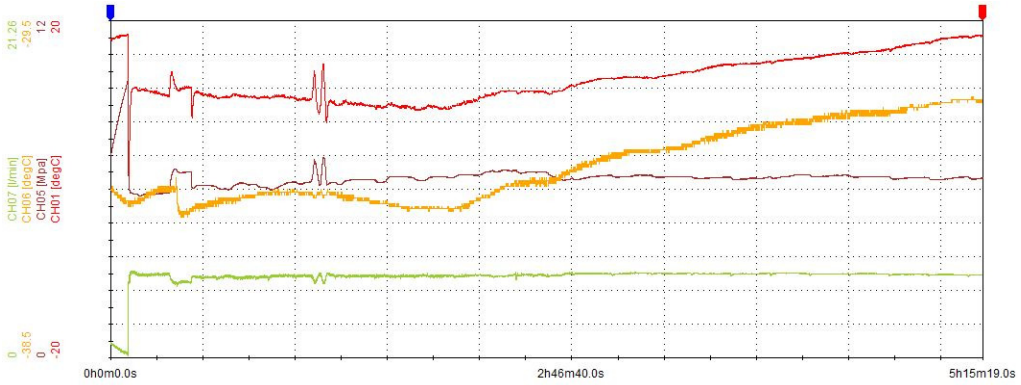

Data plot of run performed on 6/08/10

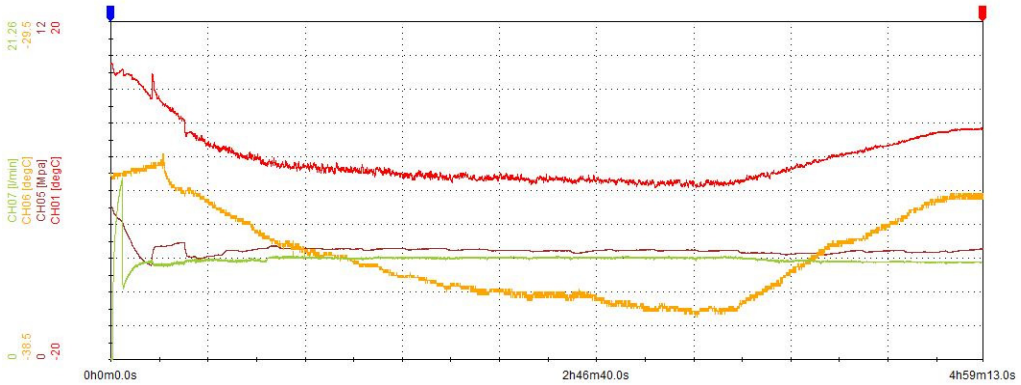

Data plot of run performed on 11/08/10

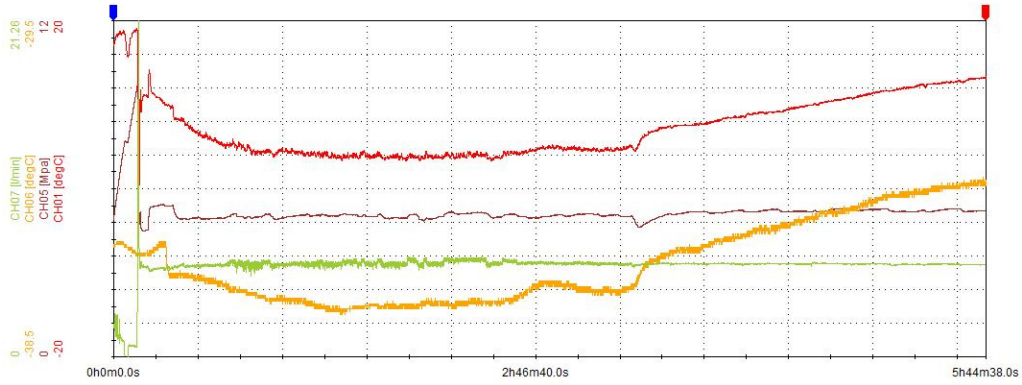

Data plot of run performed on 13/08/10

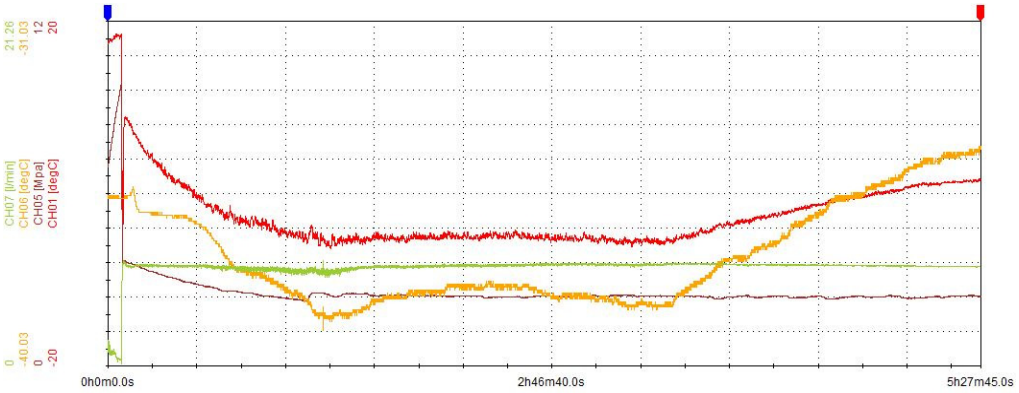

Data plot of run performed on 16/08/10

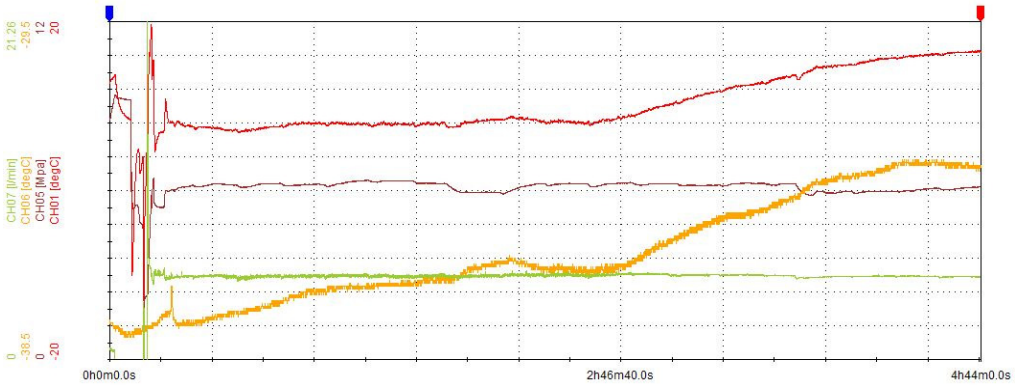

Data plot of run performed on 17/08/10

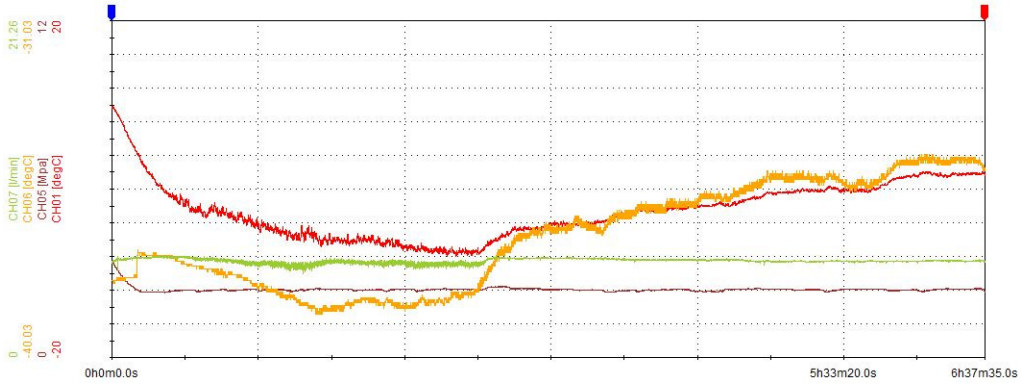

Data plot of run performed on 20/08/10

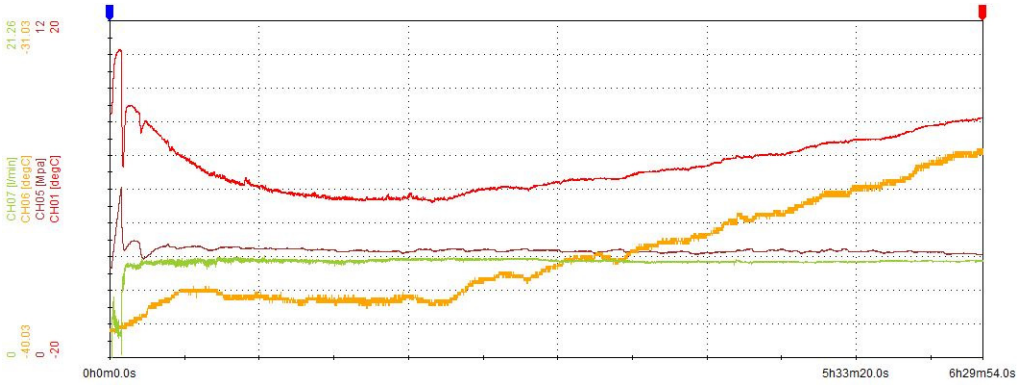

Data plot of run performed on 23/08/10

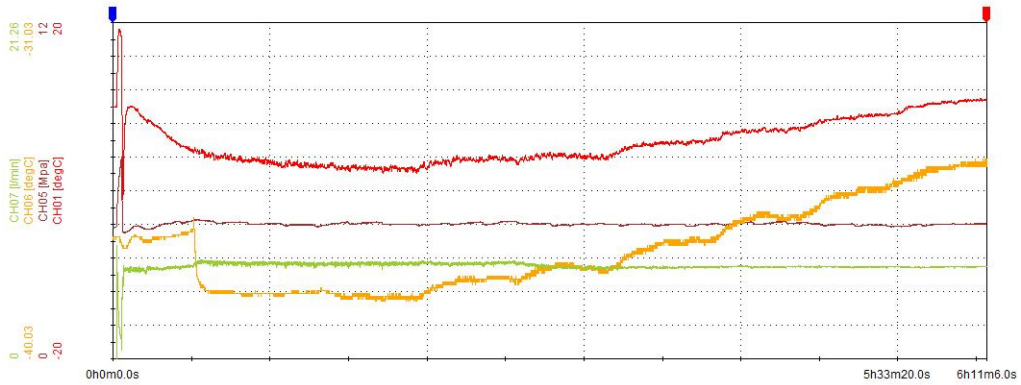

Data plot of run performed on 24/08/10

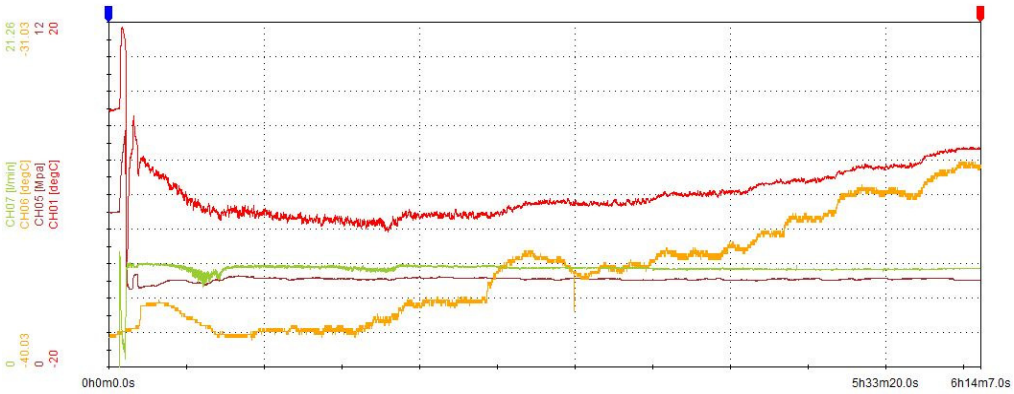

Data plot of run performed on 25/08/10

Dehydration test runs with fixed points

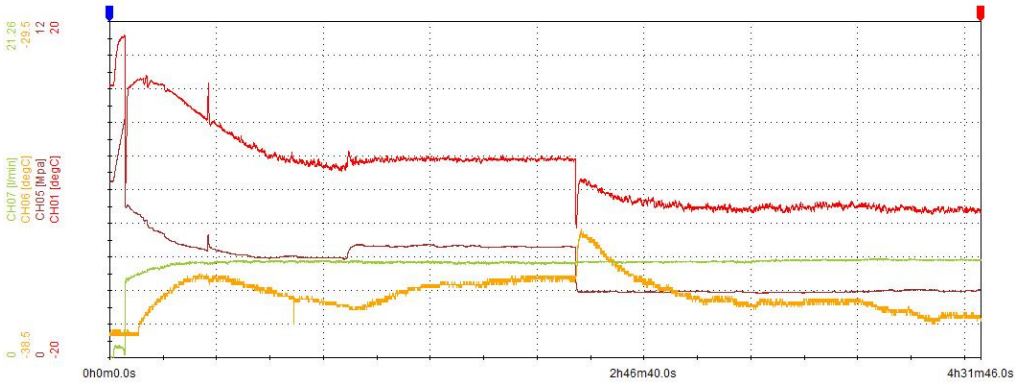

Data plot of run performed on 18/08/10

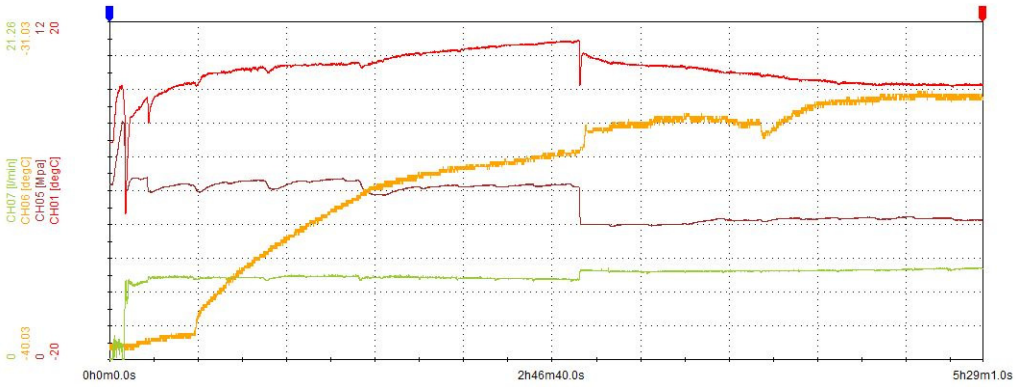

Data plot of run performed on 19/08/10

Appendix E Frequency to voltage convertor

The flow meter used to measure inlet gas flow provided a 10V pulse output of 114,000 pulses/actual cubic foot. This was incompatible with the data recorder so a conversion circuit was designed, built and tested.

E.1 Circuit diagram

The circuit diagram of the frequency to voltage convertor is shown below:

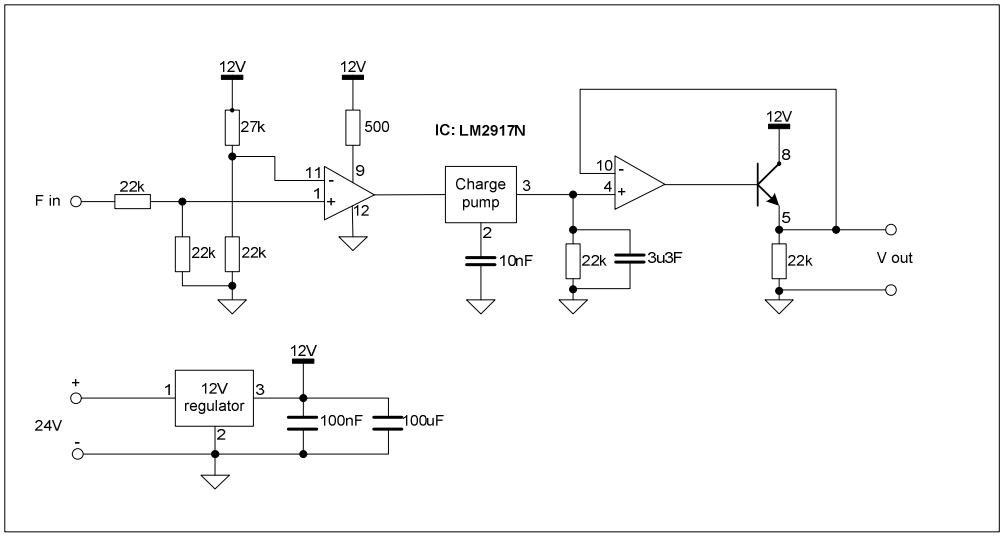

E.2 Linearity tests

Linearity tests on the Frequency to Voltage convertor were performed using a frequency generating circuit and an accurate frequency counter and volt meter.

The results of the linearity test were excellent and are shown plotted below:

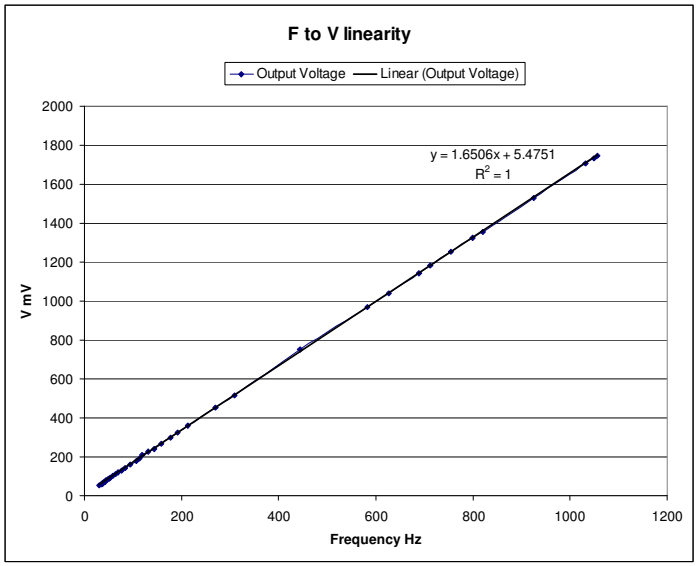

The calculated conversion equation, Voltage (mV) = 1.65606 x Frequency (Hz) + 5.4751 was used with the frequency to flow rate parameter of the flow meter to program the data recorder so that accurate flow rate could be displayed and recorded.

Appendix F Peltier devices

Peltier devices are Thermoelectric modules that are available in a wide range of sizes (typically 2.5 to 50 mm square and 2.5 to 5mm in height) and electrical characteristics. The devices are constructed from arrays of thermocouples made of high performance crystalline semiconductor material.

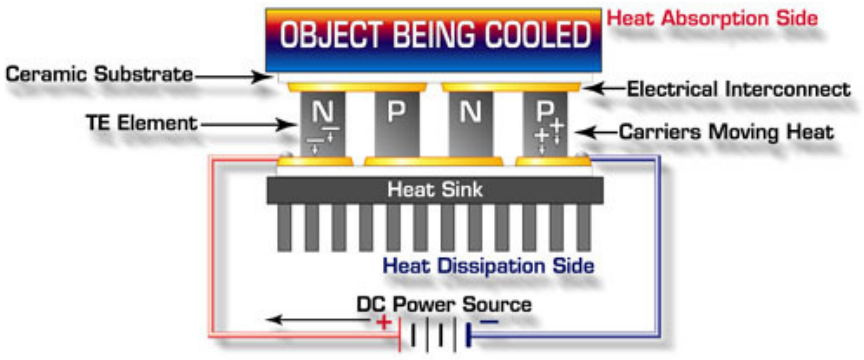

Passing a current through the device generates a temperature differential across the thermocouples thereby implementing a solid state heat pump. Temperature differential of over 70°C can be achieved. Reversing the current flow reverses the heat flow allowing the top surface (labelled 'Heat Absorption Side' above) to either cool or heat the object. Cooling capacity (heat actively pumped through the thermoelectric module) is proportional to the magnitude of the applied DC electric current and the thermal conditions on each side of the module. By varying the input current from zero to the device maximum rating, it is possible to regulate the heat flow and control the surface temperature.

Thermoelectric modules offer many advantages including:

- No moving parts
- Small and lightweight
- Maintenance-free
- Acoustically silent and electrically "quiet"
- Heating and cooling with the same module (including temperature cycling)
- Wide operating temperature range
- Highly precise temperature control (to within 0.1°C)
- Operation in any orientation, zero gravity and high G-levels

- Environmentally friendly
- Sub-ambient cooling
- Cooling to very low temperatures (-80°C)

The Peltier principal was discovered in the early 1800's and commercial devices have been available since around 1960. Devices of various power handling capabilities are available with a typical 62mm x 62mm standard device able to handle over 120W. Devices are extremely reliable with expected lifetimes of over 10 years. Temperature cycling does not impact the reliability of the device.

Peltier devices have been used industrially for over 40 years in many harsh environments including space and remote outdoor locations, and have proven to be extremely reliable.

Appendix G Xentaur LPDT Dewpoint Transmitter

Loop-Powered Dewpoint Transmitter
Model LPDT

Xentaur

Fully Functional Instrument

Xentaur's model LPDT is the world's smallest loop powered (2-wire) dewpoint transmitter.

The LPDT is also a fully functional instrument, featuring the well proven easy to use user interface of all other Xentaur dewpoint instruments, by now familiar to many. Set-up functions, result display of dewpoint, temperature and optionally pressure are accommodated by a miniature custom LCD display and three programming buttons.

The LPDT is also the world's only loop-powered dewpoint transmitter featuring both, analog as as well as digital outputs.

Analog Output Loop

4 - 20 mA is drawn by the instrument from the power supply, with the current being linear to the selected engineering units. The range of the output is programmable. The output resolution is 0.1°C(dp)

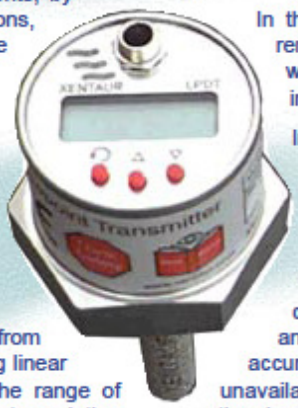

Digital Output Loop

The instrument can supply digital output by modulating the 4 - 20 mA loop line. The timing and format of the data conforms to RS-232, and the output can be interfaced to a PC or other RS-232 devices with an optional adapter.

In the digital mode, the LPDT can be remotely operated and dewpoint as well as temperature (and pressure if installed) can be read.

In the digital mode, multiple units can operate on the same loop cable as a multi-channel instrument.

HTF High Capacitance Aluminum Oxide Sensor

The LPDT uses a Xentaur HTF high capacitance aluminum oxide sensor and therefore provides a degree of accuracy, speed of response and stability unavailable from instruments using conventional sensors.

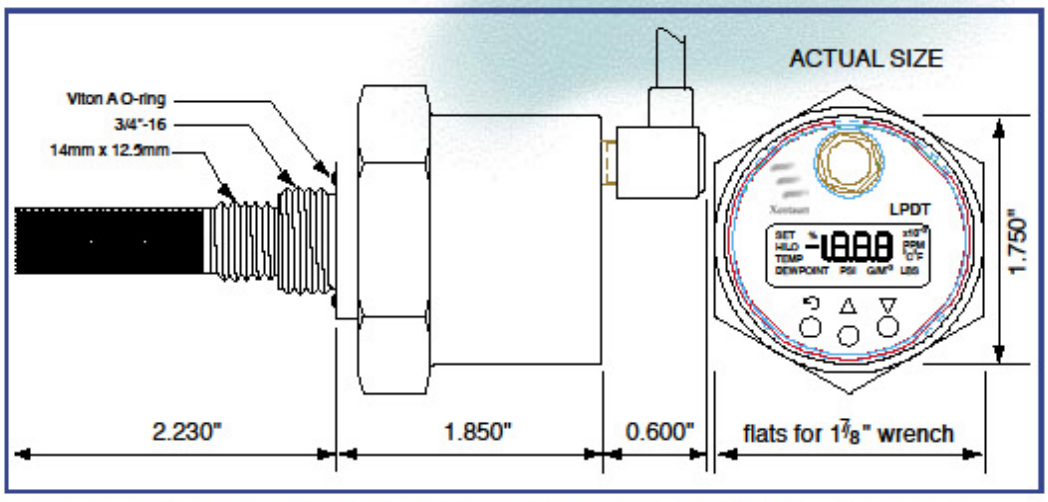

Xentaur Corp., 84 Horseblock Rd., Unit F, Yaphank, NY 11980 (631)345-3434 Fax: (631) 345-5349 email: xentaur@xentaur.com

Specifications:

Dewpoint Sensor Element

Type	Hyper Thin Film high capacitance Al_2O_3
Dewpoint range:	
XTR-100:	-148°F to +68°F (-100°C to +20°C)
XTR-65	-85°F to +68°F (-65°C to +20°C)
Capacitance:	15nF to 200nF
Accuracy:	±5.5°F (±3°C)
Repeatability:	±0.9°F(±0.5°C
Temperature Range:	-14°F-158°F (-10°C to +70°C)
Sample flow range:	
(linear vel. @ 1atm):	Static to 100 m/s
Storage temperature:	-40°F to +176°F (-40°C to +80°C)
Calibration method:	Autocal, sensor saturates at dewpoint above +68°F (+20°C). NIST/NPL traceable factory multipoint calibration available optionally

Temperature and Pressure Measurement

The instrument measures the sample temperature with a precision integrated circuit sensor. Units may be optionally fitted with a pressure sensor.

Electronics

Input resolution:	0.1°C(dp)
Indicators:	3.5 digit LCD with custom legends
Engineering units:	°C, °F, PPM, LBS H_2O/mm scf, gm H_2O/M^3
Controls	3 push buttons, all settings stored in EPROM
Outputs:	Analog: 4 - 20mA
	Digital: RS-232 (bi-directional)
Alarms:	The 4 - 20mA or the digital output may be used by an external device to operate relays
Isolation	Sensor and case are isolated from the current loop and shunted with 33V transorbs.

Mechanical

Enclosure	Stainless Steel
	Weatherproof cover optionally available
Pressure operating range:	Standard: 500 PSI (34 bar)
	Optional: 5,000 PSI (340 bar)
Electrical connections:	2.1 mm power jack with retainer
Mechanical connections:	14 mm x 1.25 mm and 3/4" x 16 threads
Cable:	Two conductor cable
Power requirements:	10 to 33 VDC, the instrument draws 4-20mA depending on measured dewpoint.

Warranty: .....1 year

http://www.xentaur.com

Methods of Using and Interfacing the LPDT:

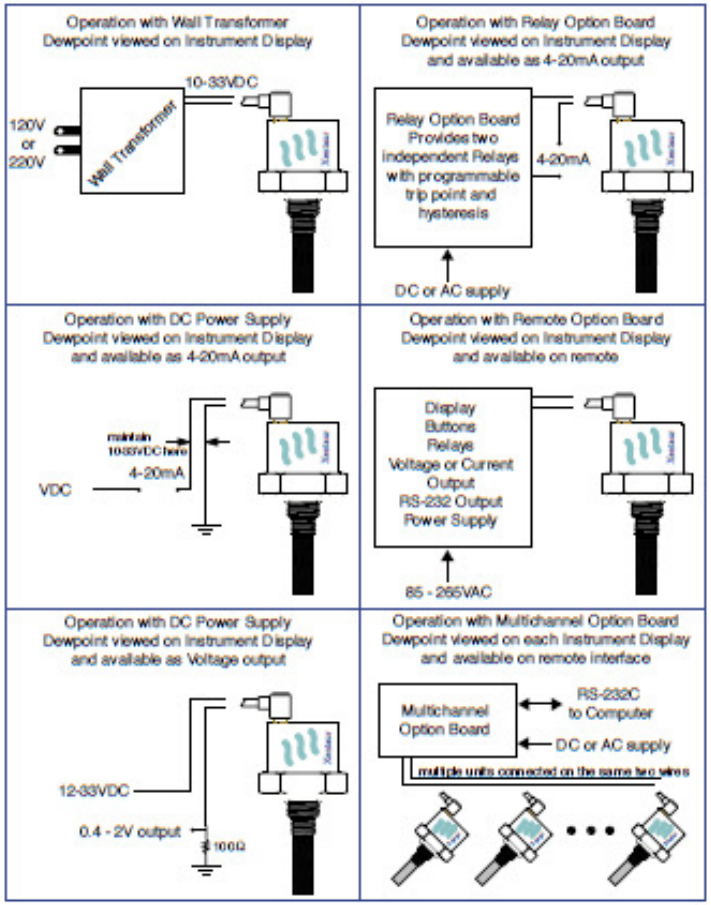

Xentaur Corp., 84 Horseblock Rd., Unit F, Yaphank, NY 11980
(631)345-3434 Fax: (631) 345-5349 email: xentaur@xentaur.com

Appendix H Test run summary

Date	Test Description	Conditions	Comments	Nozzle	System modifications
14/01/09	Pressure testing of system using air	Test pressure up to 12.5MPa	Some leaks identified and repaired	-	
15/01/09	Pressure testing of system using air	Soak test at 12.2MPa	No change in pressure after 2 hours	-	
22/01/09	Nozzle sizing tests	To utilise full output of compressor	1mm too large, 0.6mm too small	various	Nozzle adaptor fitted
27/01/09	Pressure sensor testing	Tested up to 9MPa	Sensors require calibration	0.835mm	Pressure sensors fitted, nozzle opened up
28/01/09	Pressure testing of system using air	Tested to 9.3MPa	Minor leaks repaired	0.835mm	Dehydration vessel installed in water tank
29/01/09	Flow test with air, vessel in air	Pressures- in 8.2MPa, out 2.1MPa	Max temp drop inlet/outlet of 7.2C	0.835mm	
30/01/09	Flow test with air, vessel in air	Pressures- in 8.2MPa, out 2.2MPa	Max temp drop inlet/outlet of 6C	0.835mm	Chart recorder installed
30/01/09	Flow test with air, vessel in water	Pressures- in 8.2MPa, out 2.2MPa	Lower drop 3C when submerged in water	0.835mm	Dehydration vessel submerged in water
2/02/09	Flow test with air, vessel in water	Pressures- in 8.2MPa, out 2.2MPa	Compressor overheating and cut out	0.835mm	
3/02/09	Flow test with air, vessel in water	Pressures- in 8.2MPa, out 2.2MPa	Temperature drop of 2C measured	0.835mm	
4/02/09	Testing of water cooler	Cool water tank to 4C	3hrs to cool from 6.6C to 4.4C	-	Installed cooler system
6/02/09	Flow test with air, vessel in cold water	P in/out 8.2/2.2MPa, water 4C	Vessel temp ~ water temp, T drop 12C	0.835mm	
6/02/09	Flow test with cold air, vessel in cold water	P in/out 8.2/2.2MPa, water 5C	Vessel temp 1C, Temp drop only 4.5C	0.835mm	Installed inlet gas coil into water tank
10/02/09	Test effectiveness of insulation	P in/out 8.2/2.2MPa, water 6C	Temp drop of 5.8C, 1.3C improvement		Dehydration vessel insulated with foam/foil
13/02/09	Calibration of pressure sensors	Calibrated over range 0 - 12MPa			

Date	Test Description	Conditions	Comments	Nozzle	System modifications
26/02/09	Testing of flow meter and Freq-V convertor	Flow rates up to 6.6 litres/min at 8.6MPa	Flow on chart calibrated successfully	0.835mm	Flow meter installed with F-V convertor
5/03/09	Testing of dewpoint meter and data recorder	P in/out 8.6/2.2MPa, water 20C	All sensors operating	0.835mm	Dewpoint meter and new data recorder fitted
11/03/09	First test with natural gas (bottled)	P in/out 10/6.5MPa, water 7C	Blockage of nozzle within 4 mins	0.835mm	Natural gas bottle connected to conditioning vessel, compressor disconnected
29/05/09	Testing of nozzle heater		Half nozzle power provided a 10C increase in temperature at adaptor		Installed heated nozzle assembly
3/06/09	Approval of gas connection to compressor		MILESTONE		Installation to compressor formally approved
10/06/09	Pressure testing with natural gas	Tested to 4.5MPa	Icing at compressor output, Regulator sticking		Hazop system modifications implemented
15/06/09	Gas loop testing	Test to 5MPa	Loop operating fine		Added heat exchanger to compressor output
15/06/09	Nozzle heater tests	Inlet P 5MPa	Early blockage cleared with heater	0.835mm	
16/06/09	Flow test	Pressure in/out 9/6.5MPa, heater on full	Irregular flow then blockage	0.835mm	Added heat exchanger to vessel output
17/06/09	Flow test	Pressure in/out 10/6MPa, heater on full	Irregular flow then blockage	0.95mm	New nozzle fitted closer to adaptor
22/06/09	Test of conditioning vessel performance	Pressures between 2.5 and 4.5MPa	Dewpoints to low, poor pressure regulation		
21/07/09	Test of conditioning vessel performance		Dewpoints still too low, icing at control valve		Vessel outlet heat exchanger design improved
29/07/09	Test of sparger and dewpoint system change	Pressure 4.5MPa, gas T 14.4C	Dewpoint meter failure - sent for repair		Sparger added to conditioning vessel, added water bath to dewpoint measuring system
31/08/09	Test of new nozzle heating adaptor	Water filled tank	Earth leakage detected at one heater		New heated nozzle assembly fitted

Date	Test Description	Conditions	Comments	Nozzle	System modifications
1/09/09	Nozzle heater tests	Low water level	Validating data from previous run	0.8mm	Leaking heater removed from circuit
2/09/09	Nozzle heater tests	Vessel submerged		0.8mm	
3/09/09	Input heat exchager tests			0.8mm	
4/09/09	Start-up approach tests	Start with high input and output pressure	Hydrate blockage at nozzle at start of run	0.8mm	
7/09/09	Start-up approach tests	Start with low input and output pressure		0.8mm	
8/09/09	DPM tests	Fixed input and output pressure		0.8mm	DPM fitted by BP regulator
9/09/09	DPM tests	Fixed input and output pressure	Run failed due to earth leakage in nozzle heater	0.8mm	
15/09/09	Measure DP with varying output pressure	Fixed input pressure 10MPa	Run failed due to blockage at nozzle	0.8mm	Replaced faulty heater cartridge
16/09/09	Measure DP with varying output pressure	Fixed input pressure 10MPa	Run failed due to heater failure	0.8mm	
16/09/09	Measure DP with varying output pressure	Fixed input pressure 6MPa		0.8mm	
17/09/09	Measure DP with varying output pressure	Fixed input pressure 6MPa	Validating data from previous run	0.8mm	
18/09/09	Measure DP with varying output pressure	Fixed input pressure 6MPa	Validating data from previous run	0.8mm	
21/09/09	Measure DP at outlet pressure of 4MPa	Fixed input and output pressure	Run failed due to cold inlet gas temp	0.8mm	
23/09/09	Measure DP at outlet pressure of 4MPa	Fixed input and output pressure	Run failed due to heater failure	0.8mm	
28/09/09	Measure DP at outlet pressure of 4MPa	Fixed input and output pressure		0.6mm	Nozzle changed to 0.6mm, heaters replaced
30/09/09	Measure DP at outlet pressure of 4MPa	Fixed input and output pressure	Run failed due to hydrate blockage at filter	0.6mm	
6/10/09	Measure DP at outlet pressure of 4MPa	Fixed input and output pressure	DP higher than expected	0.6mm	Dehydration vessel insulation improved, Nozzle assembly moved to top of vessel

Date	Test Description	Conditions	Comments	Nozzle	System modifications
7/10/09	Measure DP at outlet pressure of 4MPa	Fixed input and output pressure		0.6mm	DPM moved to vessel output
8/10/09	Measure DP with varying output pressure	Fixed input pressure 10MPa	15.7C inlet gas temp	0.6mm	
12/10/09	Measure DP with varying output pressure	Fixed input pressure 10MPa	13.5C inlet gas temp	0.6mm	
14/10/09	Test to measure gas outlet temperature	Fixed input pressure 10MPa	Outlet gas temp too high	0.6mm	BP heat exchanger repaired, Fitted outlet gas temp sensor
14/10/09	Test to measure gas outlet temperature	Fixed input pressure 10MPa	Output gas temp measurement OK	0.6mm	Improved gas contact at outlet temp sensor
16/10/09	Measure DP with varying output pressure	Fixed nozzle temp, input pressure	Run failed due to variable flow rate at DPM	0.6mm	
19/10/09	Measure DP with varying output pressure	Fixed nozzle temp, input pressure	Run failed due to nozzle heater failure	0.6mm	Flow meter and water bath at DPM
19/10/09	Measure DP with varying output pressure	Fixed nozzle temp, input pressure	Run failed due to low starting nozzle temp	0.6mm	Nozzle heater controller upgraded
20/10/09	Measure DP with varying output pressure	Fixed nozzle temp, input pressure	Increasing output pressure	0.6mm	
21/10/09	Measure DP with varying output pressure	Fixed nozzle temp, input pressure	Decreasing output pressure	0.6mm	
22/10/09	Measure DP with varying nozzle temp	Fixed input and output pressure -2.5MPa	at 16.5 C and 25.3C input gas temp	0.6mm	
27/10/09	Measure DP with varying nozzle temp	Fixed input and output pressure -2.5MPa	at 18.6 C and 27.3C input gas temp	0.6mm	
28/10/09	Measure DP with varying nozzle temp	Fixed input and output pressure -3.5MPa	at 18.6 C and 27.3C input gas temp	0.6mm	
30/10/09	Measure DP with varying nozzle temp	Fixed input and output pressure -2.5MPa	at 18.6 C and 27.3C input gas temp	0.8mm	One heater failed - earth leakage
9/11/09	Top integration test with water	P in/out 10/2.5MPa, T in 27.3C	Dewpoint increased, no water collected	0.8mm	Top injection system installed

Date	Test Description	Conditions	Comments	Nozzle	System modifications
10/11/09	Top integration test with condensate	P in/out 10/2.5MPa, T in 25.3C	Dewpoint reading high, residual water found	0.8mm	
10/11/09	Top integration test with condensate	P in/out 10/2.5MPa, T in 28C	Odd behaviour of vessel temperature sensor	0.8mm	
11/11/09	Top integration test with cool condensate	P in/out 10/2.5MPa, T in 23.6C	Dewpoint drop followed vessel temp drop	0.8mm	Vessel temperature sensor relocated
12/11/09	Top integration test with cool condensate	P in/out 10/4MPa, T in 23.6C	No apparent benefit of condensate injection	0.8mm	
17/11/09	Top integration test with cold condensate	P in/out 10/2.5MPa, Cond T -8C	No apparent benefit of condensate injection	0.8mm	Methanol/dry ice bath added to cool condensate
20/11/09	Top integration test with very cold condensate	P in/out 10/2.5MPa, Cond T -38C	No apparent benefit of condensate injection	0.8mm	
14/12/09	Tests with modified gas path in vessel	P in/out 10/2.5MPa, T in 28.3C	No apparent benefit of modified gas flow	0.8mm	Added cowling around gas inlet to change gas path
15/12/09	Tests with modified gas path in vessel	P in/out 10/4.7MPa, T in 2.6C	No apparent benefit of modified gas flow	0.8mm	
12/01/10	Test effect of coalescing filter	P in/out 10/2.1MPa, T in 26.7C	No apparent benefit of coalescing filter	0.8mm	Added coalescing filter to dehydration vessel outlet
13/01/10	Test effect of coalescing filter	P in/out 10/2.7MPa, T in 27.8	No apparent benefit of coalescing filter	0.8mm	
14/01/10	See if water captured by filter	P in/out 10/2.7MPa, T in 30.5	No water collected immediately after run, 1ml after 1hr at ambient temp.	0.8mm	
15/01/10	See if water captured by filter, longer warm up	P in/out 10/3MPa, T in 28.5	1.8ml captured from filter	0.8mm	
18/01/10	Test for hydrates in dehydration vessel	P in/out 10/2.2MPa, T in 24.1C	Evidence of dewpoint suppression - hydrate capture in vessel confirmed - 117ml	0.8mm	
19/01/10	Test for hydrates in dehydration vessel	P in/out 10/2.2MPa, T in 24.5C	Repeat of 18Jan test with same results	0.8mm	

Date	Test Description	Conditions	Comments	Nozzle	System modifications
20/01/10	Test for hydrates in dehydration vessel	P in/out 10/2.2MPa, T in 24.9C	Repeat of 18Jan test with same results	0.8mm	
9/02/10	Test of 0.8/1.6 de Laval nozzle	P in/out 10/2.2MPa, T in 28.5C	Irregular flow, much poorer dewpoint reached	0.8/1.6mm	Changed nozzle design to De Laval design
10/02/10	Test of 0.8/1.6 de Laval nozzle	P in/out 10/2.2MPa, T in 24.7C	Blockage of nozzle soon after start	0.8/1.6mm	
2/03/10	System test post addition of bottom injectors	P in/out 10/2.2MPa, T in 27.8C	Higher dewpoint measured than previous runs	0.8mm	Removed de Laval nozzle fitted bottom injection system and relocated nozzle down into vessel
3/03/10	Repeat system test	P in/out 10/2.2MPa, T in 26.5C	Higher dewpoint measured than previous runs	0.8mm	
4/03/10	Test of bottom injection of C7 - 60ml/min	P in/out 10/2.2MPa, T in 27.2C	C7 run for 3hrs - no apparent benefit	0.8mm	
8/03/10	Test of bottom injection of C7 - >100ml/min	P in/out 10/2.2MPa, T in 26.7C	C7 run for 4hrs - no apparent benefit	0.8mm	
9/03/10	Test limits of inlet gas temperature	P in/out 10/4MPa, T in 22.7C	Inlet gas temp of 23C sustainable	0.8mm	
11/03/10	Test of bottom injection of chilled C7	P in/out 10/4MPa, T in 22.7C	Injection pump failed	0.8mm	Methanol/dry ice bath added to cool C7
12/03/10	Test of bottom injection of chilled C7	P in/out 10/2MPa, T in 25.6C	Dewpoint changes consistent with vessel temperature change	0.8mm	Injection pump seals replaced
15/03/10	Test of bottom injection of chilled C7	P in/out 10/2MPa, T in 26.4C	Repeat of 12Mar test with same results	0.8mm	
16/03/10	Test of bottom injection of chilled C7	P in/out 10/4.5MPa, T in 24.6C	Dewpoint changes consistent with vessel temperature change	0.8mm	
17/03/10	Pressure test		Dewpoint meter readings too low - faulty	0.8mm	Internal cowling removed, nozzle repositioned lower
10/05/10	Water bath heater tests		2kW heater performed well	0.85mm	Fitted new nozzle, inlet water bath heater fitted

Date	Test Description	Conditions	Comments	Nozzle	System modifications
27/07/10	General system test		All sensors operating	0.85mm	Fitted repaired dewpoint meter, added coalescing filter bypass and vessel outlet pressure sensor
28/07/10	Dehydration test run	P in/out 9.3/2.6MPa, T in 26C	Dewpoint of -36.8C	0.85mm	
30/07/10	Dehydration test - constant P vary inlet T	P in/out 9.5/2.2MPa	Nozzle blockage at 25C inlet temp	0.85mm	
2/08/10	Dehydration test - constant P vary inlet T	P in/out 9.4/3.8MPa		0.85mm	
3/08/10	Dehydration test - constant P vary inlet T	P in/out 9.8/5.1MPa		0.85mm	
4/08/10	Dehydration test - constant P vary inlet T	P in/out 10/6.2MPa	Failure of water bath heater - nozzle blockage	0.85mm	
5/08/10	Dehydration test - constant P vary inlet T	P in/out 9.7/6.2MPa	Irregular BP control – heat exchanger failure	0.85mm	Fuse replaced in heater
6/08/10	Dehydration test - constant P vary inlet T	P in/out 9.7/6.4MPa	No water capture at coalescing filter	0.85mm	Heat exchanger repaired
9/08/10	Dehydration test - constant P vary inlet T	P in/out 9.7/2.5MPa		0.85mm	
10/08/10	Dehydration test - constant P vary inlet T	P in/out 10/6.2MPa		0.85mm	
11/08/10	Dehydration test - constant P vary inlet T	P in/out 9.4/3.9MPa		0.85mm	
13/08/10	Dehydration test - constant P vary inlet T	P in/out 10/5MPa		0.85mm	
16/08/10	Dehydration test - constant P vary inlet T	P in/out 9.5/2.4MPa		0.85mm	
17/08/10	Dehydration test - constant P vary inlet T	P in/out 10/6.2MPa		0.85mm	
18/08/10	Dehydration test - fixed point	P in/out 9.8/4.0 and 2.4MPa	Confirmed validity of above test method	0.85mm	
19/08/10	Dehydration test - fixed point	P in/out 9.7/6.0 and 5.0MPa	Confirmed validity of above test method	0.85mm	

Date	Test Description	Conditions	Comments	Nozzle	System modifications
20/08/10	Dehydration test - constant P vary inlet T	P in/out 9.5/2.4MPa		0.85mm	
23/08/10	Dehydration test - constant P vary inlet T	P in/out 9.7/3.8MPa		0.85mm	
24/08/10	Dehydration test - constant P vary inlet T	P in/out 10/4.8MPa		0.85mm	
25/08/10	Dehydration test - constant P vary inlet T	P in/out 9.8/3MPa		0.85mm	
1/09/10	Injection system tests		Blockage at separator input	0.85mm	Recommissioned bottom injection system
2/09/10	Injection system tests		Injection pump failed	0.85mm	
10/09/10	Bottom injection with C7	P in/out 9.6/4MPa	No apparent benefit of condensate injection	0.85mm	Fitted non-return valve to outlet of injection pump
13/09/10	Bottom injection with C7 - chilled	P in/out 9.6/3.8MPa	Blockage at C7 injector	0.85mm	
14/09/10	Bottom injection with C7 - chilled	P in/out 9.6/2.8MPa	Dewpoint changes consistent with vessel temperature change	0.85mm	Nozzle assembly removed and cleaned
15/09/10	Bottom injection with C7 - chilled	P in/out 9.6/4.4MPa	Blockage at C7 injector	0.85mm	
16/09/10	Bottom injection with C7 - chilled	P in/out 9.7/4.7MPa	Dewpoint changes consistent with vessel temperature change	0.85mm	Nozzle assembly removed and cleaned

H.1 JT coefficients for experimental runs

Date	Inlet pressure (MPa)	Inlet temperature (C)	Outlet Pressure (MPa)	Outlet temperature (C)	Pressure drop (MPa)	Temperature change (C)	JT coefficient (K/MPa)	Calculated outlet temp. (degC)	Calculated JT coefficient (K/MPa)	JT error
22/10/09	9.8	25.3	2.8	-5.6	7	30.9	4.41	-9.6	4.99	0.57
27/10/09	9.7	26.8	2.5	-3.9	7.2	30.7	4.26	-9.2	5.00	0.74
7/11/10	9.9	27.7	2.25	-6	7.65	33.7	4.41	-10.6	5.01	0.60
11/11/09	9.72	22.9	3	-6.9	6.72	29.8	4.43	-11	5.04	0.61
12/11/09	10.47	26	4.18	-2.3	6.29	28.3	4.50	-3	4.61	0.11
17/11/09	10.3	26.4	2.61	-8.4	7.69	34.8	4.53	-11.8	4.97	0.44
20/11/09	10.52	24.1	2.64	-10.3	7.88	34.4	4.37	-15.6	5.04	0.67
12/01/10	10.14	30.3	2.07	-4.4	8.07	34.7	4.30	-9.4	4.92	0.62
13/01/10	9.86	33.8	2.97	4.6	6.89	29.2	4.24	2.1	4.60	0.36
14/01/10	10.07	35.4	2.78	3.9	7.29	31.5	4.32	2.1	4.57	0.25
15/01/10	10.32	31.1	2.98	1.1	7.34	30	4.09	-3.3	4.69	0.60
18/01/10	9.7	24	2.26	-8.7	7.44	32.7	4.40	-14.5	5.17	0.78
19/01/10	10.09	24.6	2.24	-8.9	7.85	33.5	4.27	-15.7	5.13	0.87
20/01/10	10.29	25.9	2.2	-7.8	8.09	33.7	4.17	-15.2	5.08	0.91
9/02/10	10.47	28.2	2.02	-7	8.45	35.2	4.17	-14.1	5.01	0.84
2/03/10	9.85	27	2.33	-4.3	7.52	31.3	4.16	-10.8	5.03	0.86
3/03/10	10.28	27.6	2.2	-5.7	8.08	33.3	4.12	-12.8	5.00	0.88
4/03/10	10.82	27.5	2.34	-5	8.48	32.5	3.83	-14.5	4.95	1.12
28/07/10	9.16	26.2	2.56	-3.7	6.6	29.9	4.53	-7	5.03	0.50
30/07/10	9.32	27.7	2.2	-4.7	7.12	32.4	4.55	-8.2	5.04	0.49
2/08/10	9.18	25	3.73	0.4	5.45	24.6	4.51	-1.3	4.83	0.31
3/08/10	9.73	23.8	5.18	4.5	4.55	19.3	4.24	3.2	4.53	0.29
6/08/10	9.94	24	6.43	9.7	3.51	14.3	4.07	9.1	4.25	0.17
9/08/10	9.78	25.7	2.44	-4	7.34	29.7	4.05	-11.4	5.05	1.01
10/08/10	10.11	25.1	6.25	8.3	3.86	16.8	4.35	8.8	4.22	-0.13

Date	Inlet pressure (MPa)	Inlet temperature (C)	Outlet Pressure (MPa)	Outlet temperature (C)	Pressure drop (MPa)	Temperature change (C)	JT coefficient (K/MPa)	Calculated outlet temp. (degC)	Calculated JT coefficient (K/MPa)	JT error
11/08/10	9.34	25.1	3.84	1	5.5	24.1	4.38	-1.2	4.78	0.40
13/08/10	10.04	24.9	5.14	4.2	4.9	20.7	4.22	3	4.47	0.24
16/08/10	9.52	26.8	2.41	-5.4	7.11	32.2	4.53	-8.9	5.02	0.49
17/08/10	10.53	25.1	6.24	8.1	4.29	17	3.96	7.1	4.20	0.23
18/08/10	9.37	29	2.39	-2.7	6.98	31.7	4.54	-5.5	4.94	0.40
	9.77	29	3.99	3.6	5.78	25.4	4.39	2.5	4.58	0.19
19/08/10	9.53	33.7	6.2	17.6	3.33	16.1	4.83	20.3	4.02	-0.81
	9.88	33.7	4.9	12.5	4.98	21.2	4.26	12.6	4.24	-0.02
20/08/10	9.78	26.5	2.36	-7	7.42	33.5	4.51	-10.9	5.04	0.53
23/08/10	9.46	25.2	3.81	-1.1	5.65	26.3	4.65	-1.8	4.78	0.12
24/08/10	9.74	24.7	4.81	2.7	4.93	22	4.46	2.2	4.56	0.10
25/08/10	9.79	26.4	3.06	-4	6.73	30.4	4.52	-6.5	4.89	0.37
31/08/10	9.56	26.7	3.33	-2.1	6.23	28.8	4.62	-3.4	4.83	0.21
1/09/10	9.68	27.3	3.26	-1.8	6.42	29.1	4.53	-3.6	4.81	0.28
6/09/10	9.52	27.1	2.78	-3.9	6.74	31	4.60	-6.1	4.93	0.33
7/09/10	9.46	26.8	3.03	-2.5	6.43	29.3	4.56	-4.6	4.88	0.33
8/09/10	9.73	28.1	2.22	-7.3	7.51	35.4	4.71	-9.5	5.01	0.29
10/09/10	9.77	27.2	4.06	1.7	5.71	25.5	4.47	0.7	4.64	0.18
13/09/10	9.58	27.3	3.71	0.6	5.87	26.7	4.55	-0.4	4.72	0.17
14/09/10	9.33	27.4	2.95	-1.6	6.38	29	4.55	-3.8	4.89	0.34
16/09/10	9.8	27.6	4.58	5.1	5.22	22.5	4.31	4	4.52	0.21
						Averages	**4.38**		**4.79**	**0.41**